

REPUBLIQUE DU CAMEROUN

Paix-Travail-Patrie

\*\*\*\*\*

UNIVERSITE DE YAOUNDE I

\*\*\*\*\*

FACULTE DES SCIENCES

\*\*\*\*\*

CENTRE DE RECHERCHE ET DE FORMATION  
DOCTORALE EN SCIENCES, TECHNOLOGIES  
ET GEOSCIENCES

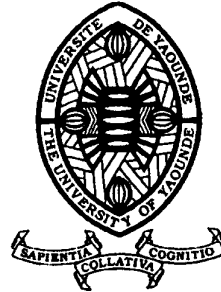
\*\*\*\*\*

UNITE DE RECHERCHE ET DE FORMATION  
DOCTORALE PHYSIQUE ET APPLICATIONS

\*\*\*\*\*

B.P: 812 Yaoundé

Email: crfd\_stg@uy1.uninet.cm



REPUBLIC OF CAMEROON

Peace-Work-Fatherland

\*\*\*\*\*

THE UNIVERSITY OF YAOUNDE I

\*\*\*\*\*

FACULTY OF SCIENCE

\*\*\*\*\*

POSTGRADUATE SCHOOL OF SCIENCE,  
TECHNOLOGY AND GEOSCIENCES

\*\*\*\*\*

RESEARCH AND POSTGRADUATE TRAINING  
UNIT FOR PHYSICS AND APPLICATIONS

\*\*\*\*\*

P.O. Box: 812 Yaoundé

Email: crfd\_stg@uy1.uninet.cm

LABORATOIRE D'ENERGIE ET SYSTEMES ELECTRIQUES ET ELECTRONIQUES  
*ENERGY-ELECTRIC AND ELECTRONIC SYSTEMS LABORATORY*

## LEAPFROGGING OSCILLATIONS, AMPLIFICATION AND DAMPING OF ELECTRICAL PULSES IN NONLINEAR TRANSMISSION LINES

*Thesis submitted and defended publicly in fulfillment of the requirements for the  
Award of a Doctor of Philosophy/PhD degree in Physics*

*Specialty: Energy, Electronics and Electrical Systems*

*Option: Electronic and Electrical Systems*

By

**Nkongho Achere AKEM**

Registration Number: **08W1158**

Master of Science in Physics

Under the Supervision of

**DIKANDE Alain Moïse**

Professor

University of Buea

and

**ESSIMBI ZOBO Bernard**

Professor

University of Yaoundé I



Year 2021



**DEPARTEMENT DE PHYSIQUE**  
DEPARTMENT OF PHYSICS

**ATTESTATION DE CORRECTION DE LA THESE DE**  
**DOCTORAT/PhD**

Nous, Professeurs NDJAKA Jean-Marie Bienvenu, FOTSIN Hilaire Bertrand, BIYA MOTTO Frédéric et Professeur WOAFU Paul, respectivement Examineurs et Président du Jury de la thèse de Doctorat/PhD de Monsieur NKONGHO Achere AKEM Matricule 08W1158, préparée sous la direction du Professeur ESSIMBI ZOBO Bernard, intitulée: « LEAPFROGGING OSCILLATIONS, AMPLIFICATION AND DAMPING OF ELECTRICAL PULSES IN NONLINEAR TRANSMISSION LINES », soutenue le Vendredi, 10 Décembre 2021, en vue de l'obtention du grade de Docteur/Ph.D en Physique, Spécialité Systèmes Electriques et Electroniques, attestons que toutes les corrections demandées par le Jury de soutenance ont été effectuées.

En foi de quoi, la présente attestation lui est délivrée pour servir et valoir ce que de droit.

Fait à Yaoundé le **14 MAR 2022** .....

Le Président du Jury

WOAFU Paul, Pr ;

Les Examineurs

NDJAKA Jean-Marie Bienvenu, Pr ;

BIYA MOTTO Frédéric, MC ;



Chef de Département de Physique

*NDjaka Jean-Marie Bienvenu*  
Professeur

**The University of Yaoundé I**

**Faculty of Science**

**Department of Physics**

**LEAPFROGGING OSCILLATIONS, AMPLIFICATION AND  
DAMPING OF ELECTRICAL PULSES IN NONLINEAR  
TRANSMISSION LINES**

Thesis submitted and defended publicly in fulfillment of the requirements for the  
Award of a Doctor of Philosophy/PhD degree in Physics

**Specialty:** Energy, Electronics and Electrical Systems

**Option:** Electronic and Electrical Systems

By

**Nkongho Achere AKEM**

Registration Number: **08W1158**

Master of Science in Physics

Under the Supervision of

**DIKANDE Alain Moïse**

Professor

University of Buea

and

**ESSIMBI ZOBO Bernard**

Professor

University of Yaoundé I

Year 2021

**Laboratory of Energy, Electronics and Electrical Systems**

---

---

# Dedication

---

This thesis is dedicated to GOD Almighty, and also to the entire AKEM'S family.

*And be not conformed to this world: but be ye transformed by the renewing of your mind, that ye may prove what is that good, and acceptable, and perfect, will of God.*

*Romans 12:2*

---

---

# Acknowledgements

---

I would like to express my sincere gratitude to Professor ESSIMBI ZOBO Bernard, for accepting to undertake this PhD project under his supervision in the laboratory of Energy, Electronics and Electrical Systems, Department of Physics of the University of Yaoundé 1. I am forever grateful to him.

I wish to thank my director Professor DIKANDE Alain Moise for both putting me out on a limb, and for making sure that I did not fall. Through his many roles as an advisor, a mentor, a father, and above all, as a friend, he has a tremendous all round impact on both my profession as a scientist and personal development. His guidance, encouragement, and friendship made this reserach project a success. I look forward to us exploring many more ideas.

My sincere gratitude also goes to the members of the jury of this thesis for all they did to make it a success for me. Thank you all for your suggestions that have greatly improved this thesis.

I wish to express my sincere gratitude also to the staff of the Department of Physics of the University of Yaoundé 1 and most especially to: Professor KOFANE Timoléon Crépin, Professor WOAFU Paul, Professor NDJAKA Jean Marie Bienvenu (HOD), Professor TCHAWOUA Clément, whom in one way or another have greatly shaped my scientific mind in the way I think about research problems and life in general.

The friendly atmosphere and productive research environment of the Department of Physics, University of Buea have made my experiences as a staff and graduate student both challenging and rewarding. I wish to extend my sincere gratitude to all my colleagues in the Department of Physics, University of Buea, and most especially to: Professor DIKANDE Alain Moise (HOD), Professor Moukam Kakmeni F. M., Dr. Mborong V. B., Dr. Ebobenow J., Dr. Mkam Tchouobiap, Dr. Atoneche F. and Dr. Ndifon I., for many years of friendship and thought provoking discussions on the subject matter of this thesis and related issues.

I am also grateful to the Laboratory of Research on Advanced Materials and Nonlinear Sciences (LaRAMaNS) for useful discussions, seminars and friendly atmosphere of the lab and its members. I am especially grateful to Mr. Akong Ngate for useful scientific contributions to this research work.

Finally, I would like to thank my parents, Mr. Achere Akem T. and Mrs. Arreytabot B. Oben for their love and support and for being my very first teachers. Many thanks to my uncle, Mr. Akem Ndip Ashu-Ebob for his all forms of endless support that has made this work a big success. Also, thanks to my siblings and most importantly, thanks to my wife, Mrs. Nkongho Akem née Etoh Jocelyne Mbong, for her unending love and encouragement.

# Contents

<b>Dedication</b>	<b>i</b>
<b>Acknowledgements</b>	<b>ii</b>
<b>Table of Contents</b>	<b>iv</b>
<b>List of Figures</b>	<b>vii</b>
<b>List of Abbreviations</b>	<b>x</b>
<b>List of Symbols</b>	<b>xii</b>
<b>Abstract</b>	<b>xiii</b>
<b>Résumé</b>	<b>xiv</b>
<b>General Introduction</b>	<b>1</b>
<b>Chapter I Literature Review on NLTs</b>	<b>12</b>
I.1 Introduction . . . . .	12
I.2 Survey Research on NLTs . . . . .	13
I.3 Transmission Lines . . . . .	23
I.3.1 General considerations . . . . .	23
I.3.2 The Four Terminal Model . . . . .	27
I.4 Types of Transmission Lines . . . . .	29
I.4.1 Balanced Two Wire Line . . . . .	29
I.4.2 Coaxial Cable . . . . .	30
I.4.3 Microstrip line . . . . .	31
I.4.4 Stripline . . . . .	33
I.4.5 Slot Line . . . . .	33
I.4.6 Coplanar Waveguide . . . . .	34
I.5 Theory of Nonlinear Transmission Lines . . . . .	35

I.5.1	NLTLS Developed from Nonlinear Dielectric Materials . . . . .	38
I.5.2	NLTLS Developed from Semiconductor Materials . . . . .	42
I.5.3	NLTLS Developed from Ferrite Magnetic Materials . . . . .	45
I.5.4	Constraints of NLTLS . . . . .	49
I.6	Conclusion . . . . .	51
<b>Chapter II</b>	<b>Materials and Methods</b>	<b>52</b>
II.1	Introduction . . . . .	52
II.2	Nonlinear Model Reduction Methods . . . . .	53
II.2.1	Nonlinear Reduction Based on Taylor Series . . . . .	53
II.3	Perturbation Theory and the Reductive Perturbation Method . . . . .	55
II.3.1	Reductive Perturbation Method . . . . .	57
II.3.2	The Method of Multiple Scales . . . . .	59
II.3.3	Nonlinear Evolution Equations . . . . .	60
II.4	The Runge Kutta Method . . . . .	61
II.5	Models and Theoretical Analysis . . . . .	64
II.5.1	Coupled NLTLS with Coupling Shunt by Resistor . . . . .	64
II.5.2	Coupled RLC NLTLS . . . . .	71
II.5.3	Coupled LC NLTLS . . . . .	76
II.5.4	NLTL with Voltage-Terminal Modules . . . . .	79
II.6	Conclusion . . . . .	82
<b>Chapter III</b>	<b>Results and Discussions</b>	<b>83</b>
III.1	Introduction . . . . .	83
III.2	Dynamics of Soliton-pair Leapfrogging in Two RC-Coupled Nonlinear Electrical Transmission Lines . . . . .	83
III.2.1	Adiabatic equations of soliton-pair motion . . . . .	83
III.2.2	Numerical Results . . . . .	88
III.3	Leapfrogging of Electrical Solitons in Coupled Nonlinear Transmission Lines: Effect of an Imperfect Varactor . . . . .	97
III.3.1	Analysis of Leapfrogging for Coupled RLC NLTLS . . . . .	97
III.3.2	Analysis of Leapfrogging for Coupled LC NLTLS with Impurity . . . . .	106
III.4	Pulse Amplification and Damping in Lossy Nonlinear Transmission lines with Voltage-Terminals . . . . .	112
III.4.1	Adiabatic equation of soliton motion . . . . .	112
III.4.2	Numerical Simulations of Discrete Line Equations . . . . .	113
III.5	Conclusion . . . . .	118



**General Conclusion**

**119**

**Bibliography**

**125**

**List of Publications**

**140**

# List of Figures

<b>Figure 1</b>	Two-port model of a transmission line. . . . .	24
<b>Figure 2</b>	Different types of transmission lines. . . . .	24
<b>Figure 3</b>	Two port Network . . . . .	27
<b>Figure 4</b>	Equivalent Circuit model of one section of an NLTL . . . . .	36
<b>Figure 5</b>	Illustration of a monolithic GaAs NLTL[97]: (a) circuit diagram, (b) equivalent circuit. . . . .	44
<b>Figure 6</b>	Layout of a monolithic NLTL constructed with finline structure periodically loaded with HBV diodes [88] . . . . .	45
<b>Figure 7</b>	Equivalent representation of two nonlinear $LC$ transmission lines, coupled by capacitor $C_m$ with a resistance $R_m$ in its shunt branch. . . . .	64
<b>Figure 8</b>	Equivalent representation of two nonlinear RLC transmission lines with Schottky-type in-line varactor $C(V_n)$ coupled by linear capacitors $C_m$ . . . . .	71
<b>Figure 9</b>	Equivalent circuit model of coupled NLTLs. The capacitance at the $n$ th cell is given by $C(V_n)$ . . . . .	76
<b>Figure 10</b>	Equivalent circuit model of a Schottky-type lossy NLTL, with a voltage terminal connected to each elementary electric cell. . . . .	79
<b>Figure 11</b>	Temporal evolutions of $\lambda_1$ and $\lambda_2$ for $D_1 = 0.23$ and $\kappa = 0.6$ . The solid, dashed and dotted curves corresponds respectively to $D_2 = 0.001, 0.005$ and $0.009$ . . . . .	88
<b>Figure 12</b>	Leapfrogging dynamics of $\lambda_1$ (solid curve) and $\lambda_2$ (dashed curve) . . . . .	89
<b>Figure 13</b>	Suppression of leapfrogging for large initial values of $\lambda_1(= 0.1)$ and $\lambda_1(= 0.2)$ , with $D_1 = 0.25, D_2 = 0.0005$ and $\kappa = 0.5$ . . . . .	89
<b>Figure 14</b>	Temporal oscillations of the amplitude difference $\Delta\lambda$ and phase difference $\Delta\zeta$ for $D_1 = 0.25$ and $D_2 = 0.005$ . . . . .	90
<b>Figure 15</b>	Oscillating amplitude and phase differences for increasing resis- tance. The top, middle and bottom set of curves are for $D_2 = 0.01,$ $0.05$ and $0.09$ respectively. Here $D_1 = 0.25$ and $\kappa = 0.63$ . Leapfrog- ging ceases in the last set of curves due to very high value of resistance. . . . .	91

<b>Figure 16</b>	Influence of the resistance on the leapfrogging frequency for different values of $\kappa$ . $D_1 = 0.25$ . . . . .	95
<b>Figure 17</b>	Anharmonic oscillations of $\lambda_1$ (solid curves) and $\lambda_2$ (dashed curves), for large initial values: <b>(a)</b> $R_1 = 5 \times 10^{-10}$ , <b>(b)</b> $R_1 = 5 \times 10^{-8}$ , <b>(c)</b> $R_1 = 5 \times 10^{-6}$ , <b>(d)</b> $R_1 = 5 \times 10^{-4}$ . . . . .	96
<b>Figure 18</b>	Phase-space representation of the leapfrogging dynamics. Here, $D_1 = 0.001$ , $D_2 = 0.23$ and $\kappa = 0.6$ . . . . .	96
<b>Figure 19</b>	Time variations of $\lambda_1$ (downward from $T = 0$ ) and $\lambda_2$ (upward from $T = 0$ ) for $\kappa = 2$ , $M = 0.2$ and from top to bottom $N = 0.0, 0.001, 0.01, 0.1$ . . . . .	101
<b>Figure 20</b>	Time variations of amplitude difference $\Delta\lambda$ , initial values are $\lambda_1 = 0.25, \lambda_2 = 0.2, \theta_1 = 0.25, \theta_2 = 0.2$ . Also $\kappa = 2, M = 0.2$ and from top to bottom $N = 0.0, 0.001, 0.01, 0.1$ . . . . .	102
<b>Figure 21</b>	Left column: Time variations of $\lambda_1$ (downward from $T = 0$ ) and $\lambda_2$ (upward from $T = 0$ ). Right column: Time variations of amplitude difference $\Delta\lambda$ , initial values are $\lambda_1 = 0.3, \lambda_2 = 0.1, \theta_1 = 0.28, \theta_2 = 0.1$ . Parameter values are $\kappa = 2, M = 0.2$ . From top to bottom rows: $N = 0.0, 0.001, 0.1$ . . . . .	103
<b>Figure 22</b>	Left column: Time variations of $\lambda_1$ (downward from $T = 0$ ) and $\lambda_2$ (upward from $T = 0$ ). Right column: Time variations of amplitude difference $\Delta\lambda$ , initial values are $\lambda_1 = 0.30076, \lambda_2 = 0.1, \theta_1 = 0.28, \theta_2 = 0.1$ . Parameter values are $\kappa = 2, M = 0.2$ . From top to bottom rows: $N = 0.0, 0.01$ . . . . .	104
<b>Figure 23</b>	Left column: Time variations of $\lambda_1$ (downward from $T = 0$ ) and $\lambda_2$ (upward from $T = 0$ ). Right column: Time variations of amplitude difference $\Delta\lambda$ , initial values are $\lambda_1 = 0.301, \lambda_2 = 0.1, \theta_1 = 0.28, \theta_2 = 0.1$ . Parameter values are $\kappa = 2, M = 0.2, N = 0.0$ . . . . .	104
<b>Figure 24</b>	Time variations of $\lambda_1$ (downward from $T = 0$ ) and $\lambda_2$ (upward from $T = 0$ ) for $\lambda_1 = 0.25, \lambda_2 = 0.2, \theta_1 = 0.25, \theta_2 = 0.2$ with parameter values $\kappa = 2, M = 0.2, u_o = 0.3$ and from top to bottom $N = 0.0, 0.001, 0.01$ . . . . .	109
<b>Figure 25</b>	Time variations of $\Delta\lambda$ for $\lambda_1 = 0.25, \lambda_2 = 0.2, \theta_1 = 0.25, \theta_2 = 0.2$ with parameter values $\kappa = 2, M = 0.2, u_o = 0.3$ and from top to bottom $N = 0.0, 0.001, 0.01$ . . . . .	110
<b>Figure 26</b>	(Color online) space-time evolution of the voltage signal along the NLTL, in the absence of voltage terminal (i.e. $\phi_0 = 0$ ) and for different values of the resistance $R$ . Top graphs: $R = 0.0005$ (left), $R = 0.01$ (right). Bottom graphs: $R = 0.05$ (left), $R = 0.1$ (right). . . . .	115

<b>Figure 27</b>	(Color online) space-time evolution of the voltage signal along the NLTL, for $\phi_0 = 0.5$ and for different values of the resistance $R$ . Top graphs: $R = 0.0005$ (left), $R = 0.01$ (right). Bottom graphs: $R = 0.05$ (left), $R = 0.1$ (right). . . . .	116
<b>Figure 28</b>	(Color online) space-time evolution of the voltage signal along the NLTL, for $\phi_0 = 1.5$ and for different values of the resistance $R$ . Top graphs: $R = 0.0005$ (left), $R = 0.01$ (right). Bottom graphs: $R = 0.05$ (left), $R = 0.1$ (right). . . . .	117
<b>Figure 29</b>	Equivalent circuit model of a coupled NLTLs with voltage terminal modules . . . . .	123
<b>Figure 30</b>	Equivalent circuit model of NLTL with monoinductance in parallel with capacitance $C_1$ . . . . .	124

---

# List of Abbreviations

---

<b>1D</b>	:	<b>One Dimensional</b>
<b>2D</b>	:	<b>Two Dimensional</b>
<b>a.c.</b>	:	<b>alternating current</b>
<b>BAE</b>	:	<b>British Aircraft Corporation</b>
<b>COTS</b>	:	<b>Commercial Of The Shelf</b>
<b>CPW</b>	:	<b>Coplanar Waveguide</b>
<b>CW</b>	:	<b>Continuous Wave</b>
<b>DC</b>	:	<b>Direct Current</b>
<b>EM</b>	:	<b>Electromagnetic</b>
<b>FD</b>	:	<b>Fully Distributed</b>
<b>HBVs</b>	:	<b>Heterostructure-Barrier Varactors</b>
<b>HF</b>	:	<b>High Frequency</b>
<b>KCL</b>	:	<b>Kirchhoff's Current Law</b>
<b>KdV</b>	:	<b>Korteweg de Vries</b>
<b>KP</b>	:	<b>Kadomtsev Petviashvili</b>
<b>KVL</b>	:	<b>Kirchhoff's Voltage Law</b>
<b>LH</b>	:	<b>Left Handed</b>
<b>LHM</b>	:	<b>Left Handed Materials</b>
<b>MMIC</b>	:	<b>Monolithic Microwave Integrated Circuit</b>
<b>MMS</b>	:	<b>Method of Multiple Scale</b>
<b>NDB</b>	:	<b>Nonlinear Diffusion Burger</b>
<b>NL-LH-TL</b>	:	<b>Nonlinear Left Handed Transmission Line</b>
<b>NLR</b>	:	<b>Nonlinear Resistance</b>

<b>NLS</b>	:	<b>Non-Linear Schrödinger</b>
<b>NLTls</b>	:	<b>Nonlinear Transmission Lines</b>
<b>PCB</b>	:	<b>Printed Circuit Board</b>
<b>PL</b>	:	<b>Periodically Loaded</b>
<b>PMD</b>	:	<b>Polarisation Mode Dispersion</b>
<b>QDA</b>	:	<b>Quasi Discreteness Approximation</b>
<b>RF</b>	:	<b>Radio Frequency</b>
<b>RPM</b>	:	<b>Reductive Perturbation Method</b>
<b>SG</b>	:	<b>Sine Gordon</b>
<b>TEM</b>	:	<b>Transverse Electromagnetic</b>
<b>TL</b>	:	<b>Transmission Line</b>
<b>UHF</b>	:	<b>Ultra High Frequency</b>
<b>VHF</b>	:	<b>Very High Frequency</b>
<b>ZK</b>	:	<b>Zakharov Kuznetsov</b>

---

# List of Symbols

---

$V_J$	:	Junction potential
$C_o$	:	Zero bias junction capacitance
$m$	:	Grading coefficient
$V_b$	:	Bias voltage
$C_m$	:	Coupling capacitance
$\lambda_i$	:	Amplitude of signal on line $i$
$\Delta\lambda$	:	Change in amplitude of signals
$\zeta_i, \theta_i$	:	Phases of signal in line $i$
$\Delta\zeta, \Delta\theta$	:	Change in phases of signals
$D_1$	:	Capacitive coupling parameter
$D_2$	:	Resistive coupling parameter
$\omega_{lf}$	:	Leapfrogging frequency
$M$	:	Capacitive coefficient parameter
$N$	:	Resistive coefficient parameter
$\phi_0$	:	Voltage terminal module constant

---

# Abstract

---

In this thesis we are interested in the dynamics of electrical pulses in weakly coupled nonlinear transmission lines, with emphasis on two contexts of pulse dynamics: first the context of leapfrogging dynamics, characterized by periodic opposite-phase oscillations of two pulses on two distinct transmission lines one with respect to the other. The second context deals with pulse propagation in nonlinear transmission lines in the presence of inhomogeneities, such as capacitive impurity and resistances both in the main and the shunt branches. It is well established that the presence of such inhomogeneities can cause pulse amplification or damping. We first consider a setup consisting of two  $LC$  nonlinear transmission lines, coupled via a linear capacitance shunted with a linear resistance. Using mathematical analysis we showed that nonlinear excitations of the two coupled NLTLs can be described by two perturbed KdV equations, in the long-wavelength and small-amplitude regimes. We examined the effect of adding the resistive shunt on the soliton leapfrogging, and obtained the analytical expression of the leapfrogging frequency. In the second case we considered two  $RLC$  nonlinear transmission lines coupled by a linear capacitance, and in the third case we examined the effects of a localized impurity on the soliton leapfrogging in the context of pulses propagating in the model studied by Koichi Narahara. In these two last cases we carefully examined the soliton leapfrogging and its stability under variations of relevant characteristic parameters of the models.

Then we examined a model of nonlinear electrical transmission line, which mimics a ladder circuit periodically loaded with Schottky varactors having a resistance in their shunt branches and connected to voltage-terminal modules. Analytical treatment reduces to the perturbed KdV equation which establishes that pulse-shaped electrical solitons can propagate in the nonlinear transmission line while experiencing amplification due to the voltage terminals, but also a damping caused by the resistance. Numerical simulations bring out a novel process namely a possible disintegration of the single pulse into two or more pulses upon propagation in the nonlinear transmission line, resulting from the competition between amplification and damping.

**Keywords:** NLTLs; capacitive impurity; leapfrogging, amplification, damping.



---

# Résumé

---

Dans cette thèse, nous nous intéressons à la dynamique des impulsions électriques dans les lignes de transmission non linéaires faiblement couplées, en mettant l'accent sur deux contextes de dynamique d'impulsion: d'abord le contexte de la dynamique dite "leapfrogging" ou (saute-mouton), caractérisée par des oscillations périodiques et en opposition de phases de deux impulsions se propageant chacune sur une ligne de transmission. Le second contexte traite de la propagation des impulsions dans les lignes de transmission non linéaires, en présence des inhomogénéités telles que les impuretés capacitatives et les résistances dans les branches principale et de shunt. Il est bien établi que la présence de telles inhomogénéités peuvent provoquer une amplification ou un amortissement des impulsions. Nous considérons d'abord une configuration composée de deux lignes de transmission  $LC$  non linéaires, couplées via une capacité linéaire shuntée par une résistance linéaire. En utilisant l'analyse mathématique, nous avons montré que les excitations non linéaires des deux lignes de transmissions non linéaires couplés peuvent être décrites par deux équations de KdV perturbées, en régimes de grande longueur d'onde et de petite amplitude. Nous avons examiné l'effet de l'ajout d'un shunt résistif sur la dynamique "saute-mouton" du soliton, et obtenu l'expression analytique de la fréquence de ce type particulier de mouvement. Dans le second cas, nous avons considéré deux lignes de transmission non linéaires  $RLC$  couplées par une capacité linéaire, et dans le troisième cas nous avons examiné les effets d'une impureté localisée sur le mouvement "saute-mouton" des solitons dans le contexte des impulsions se propageant dans un modèle étudié par Koichi dans un précédent travail. Dans ces deux derniers cas, nous avons soigneusement examiné la dynamique "saute-mouton" de la paire de solitons et sa stabilité sous les variations des paramètres caractéristiques pertinents des modèles.

Ensuite, nous avons examiné un modèle de ligne de transmission électrique non linéaire, qui imite un circuit en échelle chargé périodiquement de varactors type "Schottky" ayant une résistance dans leurs branches shunt et connectés à des modules de bornes de tension. Le traitement analytique se réduit à l'équation KdV perturbée qui établit que les solitons électriques, qui sont des pulses, peuvent se propager dans la ligne de

transmission non linéaire tout en subissant une amplification due aux bornes de tension, mais également un amortissement causé par la résistance. Des simulations numériques mettent en évidence un nouveau phénomène physique caractéristique des lignes de transmissions non linéaires couplées, à savoir une désintégration possible des solitons à un pulse sur les lignes de transmission, en deux ou plusieurs impulsions au cours de leur propagation dans la ligne de transmission non linéaire, résultant de la compétition entre l'amplification et l'amortissement.

**Mots clés:** lignes de transmission non linéaires; impureté capacitive; "leapfrogging", amplification, amortissement.

---

# General Introduction

---

The study of nonlinear phenomena has become very popular in science, most especially in Physics. Nonlinearity is a fascinating feature of nature whose importance has been thought of for many years when considering large amplitude wave motions observed in various fields ranging from fluids and plasma to solid state, biological and chemical systems.

One particular aspect of nonlinear science that has attracted a lot of attention is that of solitons. Solitons are a special class of pulse-shaped waves that propagate without changing their shape in nonlinear dispersive media. A balancing mechanism between nonlinearity and dispersion is responsible for the appearance of soliton phenomena.

In electronics, nonlinear transmission lines (NLTLs) serve as nonlinear dispersive media where electrical signals can propagate in the form of voltage waves. NLTLs are constructed by periodically loading normal transmission lines with nonlinear capacitors and/or nonlinear inductors. The NLTL can be modeled as a typical  $LC$  ladder network[1] where the series inductors are connected to ground by a shunt capacitor. The nonlinear capacitors are simply reverse biased p-n junction diodes whose capacitance is a function of its terminal voltage and decreases with increasing voltage. This model retains most of the physics of the NLTL. An inductor  $L$  and a capacitance  $C(V)$  model each section of the transmission line. This model is accurate enough as long as the minimum wavelength of the propagating signal is longer than the distance between nonlinear capacitances.

If the nonlinearity of the NLTL comes from the inductors then the inductance is defined as a function of the current through it. The inductance value will decrease as the current through the inductor increases. Nonlinear magnetic materials receive the most considerations for nonlinear inductors. A majority of nonlinear magnetic materials

used today are a type of soft ferrites which are typically characterized at low frequencies ( $\simeq 10$  kHz). A major problem with these ferrites is that they have a wide range of permeability; saturation flux and resistivity values and are relatively inexpensive. An  $LC$  ladder network with both nonlinear capacitors and nonlinear inductors is called the nonlinear hybrid line or simply hybrid line.

The fundamental reason nonlinear materials allow the creation of solitons is that the wave velocity is a function of the electric and magnetic field strengths. Specifically, the wave velocity in a transmission line is given by  $v = \frac{1}{\sqrt{\mu\epsilon}}$ , where  $\mu$  and  $\epsilon$  are respectively, the permeability and the permittivity of the material. Both permeability and permittivity decrease with increasing field strengths. Therefore the portion of the wave having a relatively large field strength propagates rapidly and the lower field strength portion at a reduced velocity thereby sharpening broad pulses into shorter duration pulses that usually have a larger peak value.

Quantitatively, the origin of solitons in NLTLs is explained by the balance between the effect of dispersion (due to the periodic location of capacitors in the NLTL) and nonlinearity (due to the voltage dependence of the capacitance). A soliton is a localized waveform that travels along the system with constant velocity and undeformed shape. This means that due to nonlinearity, points closer to the peak of the current or voltage signal will have a faster propagation velocity and produce a shock wavefront. Conversely, dispersion due to discreteness of the NLTL causes the signal to spread out. It is well known that in transmission media supporting solitons, any input pulse with a duration greater than soliton width tends to dissolve into a superposition of solitons. In this regard, a sinusoidal signal fed to the NLTL will progressively decompose into multiple solitons per cycle, and harmonics of the input frequency will be obtained at the output. When the nonlinearities are large over the signal amplitudes, the problem does not always admit analytical solutions. Rather, one must resort to numerical or graphical methods. But when nonlinearities are small, we can make use of conventional perturbation techniques to obtain analytical results.

Although much of the work related to nonlinear lumped  $LC$  networks has been

done with the Toda lattice (and its particular C-V characteristics), a discrete Korteweg de Vries (KdV) equation, sometimes referred to as the nonlinear ladder equation, has been also studied and experimentally implemented[2]. In accordance to fabricated NLTL prototypes, previous theoretical works are mainly based on Schottky diodes as the nonlinear device. Since these diodes need to be reverse biased, the use of small signal conditions around a DC value is fairly justified. Heterostructure-barrier-varactors (HBVs) have been proposed as the nonlinear candidates for harmonic generation in NLTLs. HBVs have a key advantage: only odd order harmonics of the input frequency are proposed due to the symmetric C-V characteristics of the HBV[3].

NLTLs have also become increasingly popular as a way of developing very high frequency, wideband waveforms that offer extremely fast rise time usually unobtainable by any other method. The applications of NLTLs range from very wideband telecommunication systems to high energy physics. An electrical NLTL[4] is undoubtedly one of the best platforms for all electrical short pulse generation. When a pulse is input to an NLTL such that the nonlinearity of the Schottky varactors compensate for dispersion, the line generates multiple solitonic pulses, where widths are generally smaller than that of the input. By extracting the largest, an NLTL operates as a good short pulse generator[5]. Moreover when a step pulse is input to an NLTL such that both nonlinearity and dispersion sharpen the edge, the edge finally results in a shock, by which a sub-picosecond temporal transient is observed[6]. An NLTL is useful for more than just short pulse generation. By applying a short pulse supported by a step-like wave to an NLTL enables a short pulse amplification[7]. In the linear regime, NLTLs can be used as phase shifters phase antennas arrays where time delay can be controlled by means of DC bias applied to Schottky diodes acting as variable reactance. Under large signal conditions, NLTLs can serve as pulse compressors or frequency multipliers[8].

The interest in monolithic NLTLs has ground[9, 10] due to their ability to give acceptable power efficiencies at terahertz frequencies by harmonic multiplication. The multiplicative process in NLTLs is understood as a direct consequence of soliton-like propagation in this medium. Due to technological progress in fast integrated Schottky

diodes, practical NLTLs with excellent performance have been realized in the past two decades. In almost all published work on NLTLs, a periodically loaded NLTL approach has been used, i.e., a linear transmission line is periodically loaded by nonlinear devices, either varactors or HBVs. The structure of a transmission line can be either continuous (fully distributed (FD)) or discrete (periodically loaded (PL)). Continuous transmission lines are typically wave guide-based while discrete transmission lines usually consist of repeated identical subcircuits made up of lumped elements (e.g. resistors, capacitors, inductors, etc.), any one of which can be voltage dependent.

NLTLs are good examples of a few systems where solitons are easily and directly observed in controlled laboratory experiments. The development in NLTLs has demonstrated its capacity to work as signal processing tools [12, 13, 14]. To cite only a few examples, it has been demonstrated that the nonlinear uniform electrical line can be used for:

1. extremely wideband signal shaping applications [15].
2. waveform equalizer in the compensation scheme for signal distortion caused by optical fibre polarization dispersion mode [16].
3. doubling repetition rate of incident pulse streams [17] and the delay of ultrashort pulses through the coupled propagation of the solitonic and dispersive parts, which is important in that it enables the characterization of high-speed electronic devices and raises the possibility of establishing future ultra-high signal processing technology [18].

## **Review on Leapfrogging in Nonlinear Dynamics**

Leapfrogging of soliton pairs in the past three decades had been proposed to describe the particular motion of two weakly interacting solitons characterized by their anti-phase oscillations and oppositely varying amplitudes [19]. In fluid dynamics the leapfrogging of co-propagating KdV pulses have been widely discussed, and shown to provide an

interesting configuration of the system dynamics in which solitons in the pair oscillate periodically one with respect to the other such as to mutually sustain their propagation at very small velocity [20]. This concept was recently extended to nonlinear electrical transmission lines by Koichi Narahara [21], who considered two capacitively coupled nonlinear transmission lines and determined characteristic properties for the leapfrogging motion of electrical soliton pairs.

Leapfrogging of solitary waves has also been observed in pycnoclines. Pycnocline is a region between two fluids of different densities. Pycnoclines support internal waves which are dispersive, and can be nonlinear even for modest amplitudes. Eckart discussed the linear internal-wave problem for two well-separated pycnoclines, and showed the resonant transfer of energy between waves in each of the pycnoclines. This energy transfer is also possible between solitary waves, each on its own pycnocline. This situation was treated by Liu *et al.* [22], in which they derived two coupled equations for the evolution of the wave amplitudes of single-mode waves propagating along each pycnocline with nearly equal speeds, and investigated the interactions numerically. They noticed that after initial transients there appear clearly time-periodic solitary waves, which alternate their relative phase relationship as a result of the oscillation of wave amplitudes. That is the solitary waves are leapfrogging over each other as they propagate. In Liu, Pereira and Ko [23], weak coupling between nonlinear internal solitary waves on neighbouring pycnoclines was seen to allow resonant energy exchange. The lagging wave increases its energy and speed at the expense of the front-running wave, so that the waves leapfrog about an average position. Their analytical estimates for this process agreed with the wave-tank experiments described by Wiedman and Johnson [24].

Leapfrog oscillations of two-mode solitary waves were first realized in the laboratory experiments performed by Wiedman and Johnson (referred to as WJ). These experiments were performed in a 10m channel in which the initial two-pycnoclines stratification was constructed using saline water. Under the gravitational collapse of two uniformly mixed regions at one end of the tank, two-mode waves formed, travelled down the tank and reflected at the endwall resulting in as many as five visible hops. Measurements of

solitary wave amplitudes and positions were taken after an initial adjustment period in which dispersive waves were shed, exhibited the leapfrog dynamics.

In a couple of instances in the WJ experiments, two solitary waves ordered in amplitude evolved along each pycnocline from the collapsed mixed regions. In one such realization, a lead and trailing wave on one pycnocline interacted with the lead wave on the neighbouring pycnocline, the remaining trailing wave having been left behind. This resulted in a three-wave interaction which combines both *upstream* and *downstream* energy transfer. Again, dissipation precluded evaluation of the long-time behaviour of this curious interaction. Wiedman and Johnson conjectured that the ideal (inviscid) three-wave interaction is not one of simple resonance since the time scale for forward energy transfer between waves traveling along the given pycnocline is faster than the rearward energy transfer between waves on neighbouring pycnoclines. As a result it was postulated that the motion is either a Fermi-Pasta-Ulam recurrence phenomenon or chaotic. By using simple averages and the assumption that the waves can be described by Joseph solitons, Wiedman and Johnson obtained reasonably good agreement with the predicted oscillations frequency reported in Liu *et. al* companion paper, even for relatively long-amplitude waves.

Following the publication of the WJ experiments, there have appeared other studies of leapfrogging KdV solitary waves. First and foremost is the work of Gear and Grimshaw who derived a set of amplitude equations for the interaction of weakly nonlinear internal gravity waves on pycnoclines not widely separated,  $H/\lambda \ll 1$ . The equations describing this system are both nonlinearly and dispersively coupled. Integrations for realistic Brunt Väisälä frequencies reveal that the upper and lower disturbances evolve, after an initial adjustment, into a completely phase-locked non-oscillatory solitary wave system. When the coefficients of the nonlinear terms are set to zero, on the other hand, the system evolves into a quasi-periodic state with upper and lower amplitudes continually exchanging energy, closely resembling the leapfrog results found in [22]. However, Gear and Grimshaw carefully noted that complete periodicity is not attained, as some trailing radiation is continually being formed. Should this occur for  $H/\lambda = 0(1)$ , an asymptotic



periodic leapfrog behaviour of the Liu, Kubota and Ko (referred to as LKK) system would not be possible.

Malomed in [20] also studied the LKK equations coupled only through dispersion. Using the adiabatic approximation, he found *inter alia*:

1. An estimate of the frequency of small oscillations in the vicinity of equilibrium.
2. The power radiated in the form of small-amplitude quasilinear waves from leapfrogging solitons.

Not surprisingly, he found that the frequency of radiation coincides with the frequency of soliton oscillation. No mention was made of the possible long-time behaviour of the system.

Wright and Scheel [25] analyse the linear stability of a coupled pair of evolution equations which include those of Gear and Grimshaw as special case. They found that the system is linearly unstable and concluded that the slowly growing oscillatory instability is the origin of the leapfrogging behaviour described in previous literatures. As a numerical example, they integrated a pair of equations coupled only nonlinearly through parameter  $\epsilon$ . For  $\epsilon < 0$  leapfrog oscillations are found with waves radiating behind the travelling wave system. When the integration is carried out to long times the amplitudes decrease, the spatial oscillations grow and eventually the interaction ceases at which point the waves separate as individual solitary waves. Thus leapfrogging is a transient behaviour for the KdV equations coupled only through nonlinearity.

In Nitsche *et al.* [26], the phenomenon of leapfrogging internal solitary waves located on separate pycnoclines was revisited to explore the behaviour of the near resonance phenomenon. They presented a numerical study of two-mode solitary waves travelling on neighbouring pycnoclines to determine the range of parameters for which leapfrogging occurs and their ultimate long-time behaviour. Their work was motivated by the original numerical discovery of leapfrog oscillations by Liu *et al.* [22] for an inviscid fluid and by the laboratory experiments of Wiedman and Johnson who observed highly damped leapfrog behaviour in a viscous fluid.

Koichi Narahara in [21] studied the characterization of leapfrogging solitary waves in coupled NLTLs. In his study, he clarified how the leapfrogging frequency depends on the physical parameters of the coupled NLTLs using a numerical model validated through measuring test lines. He also demonstrated the relaxation of leapfrogging. In addition, coupled KdV equations are derived by applying the reductive perturbation method to the transmission equations of coupled NLTLs. Leapfrogging pulses were detected and were well modelled by the numerical calculations.

Nonlinear electrical networks composed of two coupled NLTLs have been considered in the studies of simultaneous propagation of two electrical solitons obeying two coupled KdV equations [27, 28]. Previous theoretical and experimental works on electrical line networks have provided a consistent amount of knowledge about fundamental properties and the complex dynamics of soliton structures propagating along such structures. In particular there have been recent experimental and theoretical evidences of a rich and complex dynamics in the case when a pair of electrical solitons propagate on two coupled lines at nearly equal velocities.

In [21] it was observed experimentally that when the difference in velocity of the two pulses is very small, their interaction is optimized, thus favouring a bound state in which electrical energy will be alternately transferred from a leading soliton to a trailing soliton. To be more explicit, when one of the solitons in the bound state is at its maximum amplitude it leads the pair motion, while the second, trailing soliton, is at its minimum amplitude. As the energy leaves the leading soliton to the trailing soliton, the amplitude of the leading soliton dies down while the amplitude of the trailing soliton grows. Given that by definition the velocity of the KdV soliton increases with amplitude, the trailing soliton is expected to speed up and to eventually overtake the leading soliton, such that the direction of energy transfer is reversed. Under certain conditions, this overtaking will occur repeatedly giving rise to relative oscillations in amplitudes and phases in which the two solitons in the bound states continuously leap over each other periodically. Such motion is called "leapfrogging". It is worthwhile noting that the leapfrogging dynamics of electrical solitons offers the possibility to quasi-resonantly transfer energy between

coupled ladder lines in distributed electrical networks. Remarkably such process would be of great interest for space/time multiplexed ultrafast electronics.

There has been recent interest in the possibility for short-pulse amplification using NLTLs, for possible applications in high-resolution measurements and high-speed communication systems [12, 29]. Thus, considering the Hirota-Suzuki line and envisaging connection of elementary circuits to voltage-terminal modules (or voltage edges), it was shown that the propagation of a KdV pulse could result into pulse amplification by the voltage terminal. Quite remarkably the author established that while pulse amplification was of a universal exponential law, the amplification rate was dependent on the specific characteristic properties of the Schottky varactor loaded in the line. In the general context of studies of soliton propagation in NLTLs, it is well known that although pulses possess robust shape by virtue of their soliton features, resistive components which are almost always present in the line cause pulse energy to be dissipated as it propagates. Given that within the framework of the adiabatic perturbation theory, the amplitude damping in this later case too follows an exponential law, it is useful to examine the competition between the amplification due to voltage terminals and the damping related to a resistive component.

The work carried out in this thesis was motivated by the works of Koichi [7, 21, 40]. In [21], Koichi studied the characterization of leapfrogging solitary waves in lossless coupled NLTLs. As an extension to his model, we formulated three models. Two of which are gotten by adding a shunt resistance to the coupling capacitor in one model and in the other we added an intraline resistance. In the third model we studied the lossless coupled NLTLs in [21] in the case where one of the varactors in one line is defective. In these three models we studied the leapfrogging dynamics of electrical pulses as they travel down the weakly coupled NLTLs. Finally our fourth and last model is also an extension to the model studied by Koichi in [40]. In this last model we added shunt resistances to the varactors. In this final model we studied how amplification and damping of electrical pulses is moderated by the balance between voltage terminal modules and varactor shunt resistances.

## Objectives of Thesis

In this thesis, we present models used to study leapfrogging dynamics, amplification and damping of soliton signals in NLTLs. In this connection, we will investigate certain scenarios, as follows:

Firstly, we seek to investigate the leapfrogging of a pair of electrical pulses propagating each along a nonlinear  $LC$  line, both weakly interacting via a coupling branch composed of a constant capacitor shunted by a linear resistance. In this case our study rest on the analysis of the time evolution of the amplitudes and phases of two electrical pulses, within the framework of the adiabatic perturbation theory based on exact solution to the KdV equation.

Secondly we investigate the leapfrogging dynamics of a pair of KdV solitons in two nonlinear transmission lines, weakly coupled by a linear capacitance. To do this, we explore two different configurations: the first comprising of two  $RLC$  lines with intraline resistances, and the second is two coupled  $LC$  lines one of which is the host of a localized capacitive impurity.

Finally, we consider a nonlinear electrical transmission line periodically loaded with Schottky varactors having a resistance in their shunt branches and connected to voltage terminal modules. Using multiple-scale expansion and the adiabatic perturbation theory, we seek to investigate that pulse-shaped electrical solitons can propagate in the NLTL while experiencing amplification due to the voltage terminals, and also a damping caused by resistive elements in the line.

## Outline of Thesis

There are altogether three chapters in this thesis. The thesis begins with general introduction which gives the general description of soliton propagation in NLTLs.

Chapter 1 presents the in-depth literature review of signal propagation in NLTLs, leapfrogging dynamics and amplification of signals in NLTLs.

Chapter 2 presents the various nonlinear model reduction methods that we deemed relevant to the research work of this thesis. This is followed by the explicit sixth order Runge-Kutta method used in our numerical simulations. Next we present all the models under study and their various mathematical analysis.

In chapter 3, we present the results and discussions of this thesis. First we discuss the effects of a resistive component shunting a coupling capacitor on the leapfrogging dynamics of a pair of electrical pulse solitons, propagating along two weakly coupled NLTLs. Secondly we investigate the leapfrogging dynamics of a pair of KdV solitons in two nonlinear transmission lines, weakly coupled by a linear capacitance. Two different physical configurations of coupled nonlinear transmission lines are considered: the first configuration was two *RLC* lines with intraline Schottky varactors and the second configuration had two coupled *LC* lines one of which had a localized capacitive impurity. Lastly we investigate the competition between amplification and damping effects of pulse-shaped electrical solitons in NLTLs connected to voltage-terminal modules.

And finally, this dissertation ends with a general conclusion on all work carried out in this thesis. We also present some perspectives of future works on signal propagation in NLTLs.

---

# LITERATURE REVIEW ON NLTLs

---

## I.1 Introduction

The interest in waves propagating through a nonlinear and dispersive media was kindled over a century and half ago by Scott-Russell who observed that disturbances could propagate over long distances in a channel of water. Scott's classical treatise was among the first to treat the physics of transmission lines. Scott showed that the KdV equation describes weakly nonlinear waves in the uniform NLTL. If the nonlinearity is moved from the capacitor parallel to the shunt branch of the line to a capacitor parallel to the series branch, the NLS equation is obtained instead.

A lot of research on NLTLs has been carried out for the past seven decades. In recent years, considerable interest has been shown in problems associated with the propagation of EM waves in nonlinear media in order to effectively utilize the nonlinear effects in both the radio and the optical range. When losses in the medium are small, shock wave formation is possible. Thus, transmission lines with nonlinear propagation media can be used for sharpening wavefronts and consequently for harmonic generation and parametric amplification of EM signals. Mullick in 1967 published a theoretical investigation of signals in transmission lines whose nonlinear parameters are distributed capacitance and conductance. He carried out his analysis by conventional perturbation theory, where nonlinearity and dispersion were assumed to be small. Using perturbation technique, they solved the problem of propagation of signals in NLTLs with weak nonlinearity in its distributed capacitance and small nonlinear shunt loss. They derived the condition for the formation of shock waves, and that for sinusoidal inputs, the presence of nonlinearity in the shunt loss makes possible the formation of shock waves

at a smaller amplitude than when the nonlinearity is absent. For step-like inputs, this critical amplitude either increases or decreases depending on the sign of the nonlinearity and the polarity of the step.

In 1895, Korteweg and de Vries were able to derive an equation now called the Korteweg de Vries (KdV) equation, in which they were able to explain the observed phenomena of Scott-Russell. With the advent of numerical techniques and higher speed computers, several problems which have their origin in studying wave propagation in nonlinear dispersive media have been examined. An extensive review article on these nonlinear equations, their properties, and techniques of solutions has been written by Scott et. *al.*. By 1970's, only two experiments had been reported which described some properties associated with solitary-wave propagation in electrical networks. The first was constructed by Hirota and Suzuki [4].

## I.2 Survey Research on NLTs

The theoretical study of soliton propagation in nonlinear  $LC$  networks has been carried out with much attention devoted to two equations: The Toda lattice equation and the KdV equation. In 1973, Hirota and Suzuki demonstrated that the  $LC$  ladder network with a nonlinear shunt capacitance given by the expression

$$C(V) = \frac{C_o V_o}{(V - V_o)}, \quad (1)$$

where  $V_o$  is constant, is equivalent to the Toda lattice, for which soliton solutions are well known. They even reported experimental results for the transmission of solitons in  $LC$  networks by using varactor diodes with nonlinearity given by  $C(V) \simeq 27(V - V_o)^{-0.48}$  pF. Singer and Oppenheim [2] proposed a new hardware implementation of the Hirota and Suzuki capacitor, providing a more accurate experimental implementation of the Toda lattice with electrical circuits.

Wave propagation on nonlinear dispersive transmission lines leads to the generation

of harmonics, each of which travels at its own characteristic velocity. If nonlinearity and dispersion are just "balanced" a dynamic steady state propagation of waves with permanent profile occurs, similar to the behaviour of solitons which are today discovered in a lot of areas in physics. Lumped electrical networks have been used very often to study nonlinear dispersive wave propagation in which some fundamental properties, like the generation of solitary waves and soliton interactions and the recurrence phenomena have been confirmed.

Nagashima and Amagishi also obtained a quantitative method to analyse the nonlinear  $LC$  circuit equivalent to the Toda lattice and pointed out that the difference from the analysis of Hirota and Suzuki came from the definition of the nonlinear charge. With the use of this quantitative method, the energy of a soliton were calculated and compared with experimental results. When the amplitude of a soliton is small, the width of a soliton becomes large and as a results the continuum approximation of the circuit holds. In this limit, the circuit equation reduces to the KdV equation.

Many equations for lines that combine nonuniformity, nonlinearity, and resistive loss have been derived, but these models were not analyzed and the possible applications of a nonuniform NLTL were not explored. In other works, numerics and experiments indicated that a nonuniform NLTL could be used for "temporal contraction" of pulses. For the description of long waves in a  $2D$  lattice consisting of  $1D$  lines coupled together by capacitors, one obtains a modified ZK equation [30]. When a small transverse perturbation is added to the KdV equation, one obtains a Kadomtsev-Petviashvili (KP) model equation. Dinkel et al. [31] carried out this procedure for a uniform nonlinear  $2D$  lattice, and mentioned that the circuit maybe useful for "mixing" purposes. The classification of the effects of discreteness, nonuniformity and nonlinearity in the theory of  $1D$  transmission lines is reviewed in [15]. Also in [15] Afshari et al. showed analytically that a linear nonuniform transmission line, with constant delay but exponentially tapered impedance, can be used for combination of signals. The speed and amplitude of outgoing signals are analyzed directly from the continuum model. Also they showed numerically that introducing weak nonlinearities causes outgoing pulses to assume a solitonlike shape.



The notion of transmission was generalized to a  $2D$  transmission lattice, in which case, they applied the reductive perturbative method and showed that a modified KP equation describes the weakly nonlinear wave propagation in the lattice.

Extending the transmission line model to higher dimensions has proven difficult, both theoretically and experimentally. There have been particular applications of versions of the KdV equation. Experiments have been performed on cylindrical solitons using a  $2D$  transmission line. Resonances of a  $2D$  transmission line have also been examined. However, with the rapid developments in integrated circuit technology, we believe that soliton propagation in higher dimensional transmission lines will be a topic that will continue to receive attention. In [31], they were able to model distributed electrical transmission lines containing common linear and nonlinear electrical elements and to transform the  $1D$  and  $2D$  nonlinear equations into the KdV and the KP equations respectively. They suggested that the critical resonance angle and the amplitude enhancement found in the KP equation may have a practical application. For example, in a "mixing" application for small signal detection of a soliton B, they suggested that an idler soliton propagation on path A would always be present at an interaction region. If soliton B is also incident at the interaction region simultaneously, a soliton whose amplitude is four times as large would be created. This amplitude enhancement may be sufficient to keep it out of the background noise in a communication system or even to bring a low-level signal out of the background noise in a detection system.

Based on the lumped element equivalent circuit of the NLTL, a numerical model[32] was presented to study soliton behaviour in NLTLs. The main advantage of this model over previous model is that it allows us to obtain soliton waveforms regardless of the considered nonlinear capacitance. Their model can be used to predict soliton propagation in fabricated NLTLs and is especially useful in studying the influence of nonlinear device on soliton characteristics, since  $C - V$  curves experimentally obtained on nonlinear loading devices can be introduced in the formation. However, for strong lumped solitons, or to study soliton propagation in nonlinear  $LC$  networks with arbitrary  $C(V)$  nonlinearity, a KdV approach cannot generally be applied. Also in [32], a new procedure

to obtain soliton solutions in NLTLs described by its lumped element equivalent circuit is presented and applied to structures with HBV-like nonlinear devices. By considering model parameters of typical HBV-like NLTL structures, soliton waveforms for different propagation delays were numerically obtained. It was found that the resulting voltage pulses are stable and maintain shape and speed after interaction. These results validated their model for use in studying soliton behaviour in NLTLs.

NLTLs have evolved from large-scale prototypes using discrete components and producing nanosecond edges into integrated circuits capable of pico- and sub-picosecond outputs. These circuits are interesting not only because of their intrinsic ultrafast physics but also for their applications in measuring other high-speed or broadband phenomena, such as in spectroscopy or device characterization. In [33], it is shown that electrical circuits can reach well into the femtosecond regime by using the NLTL concept with a  $\delta$ -doped epitaxial profile to achieve large  $C(V)$  nonlinearities and low capacitance diodes on the same substrate. Similar benefits could be realized for other harmonic generation and mixing integrated circuits. In [34], the study of soliton propagation characteristics in NLTLs loaded with HBVs was investigated. A simple equation, valid for any nonlinear device, was presented to directly determine the relationship between soliton amplitude and per-second propagation delay. By means of a simple approximation, an analytical expression for the complete description of the solitaries was presented. Their results clearly justified the utility of our approach for the study of moderate to high voltage solitons in actual NLTLs. Their model helps in the understanding of soliton-like harmonic generation in NLTLs loaded with HBVs for terahertz frequency multipliers. In [35], a discrete NLTL with nonlinear intersite resistance exhibiting pulse signal voltages with compact shape was introduced and investigated. More precisely, they first showed that shunting the linear inductor in each cell of the basic  $LC$  electrical transmission line by a nonlinear resistance(NLR) induces a nonlinear diffusion term in the circuit equations. Next their study was completed by the investigation of losses of circuit components on the compacton propagation where they showed that the Tanaka's perturbation method can be satisfactorily applied to the NDB equation which admits a solitary wave with

compact shape.

The integration of nonlinearity and periodicity has brought to electronics engineering, as well as many other fields in Physics, plenty of interesting topics [6]. The gap soliton is a typical product of such an integration [36]. Moreover, interest has been shown in the role solitons play in communications. In [37], Essimbi showed that localized solitary signals in the form of kinks (antikinks) waves with eigenfrequencies lying inside the nonlinearity-induced gap can propagate with a remarkable stability on the nonlinear  $LC$  circuit, where the nonlinear capacitor is supposed to be a quadratic function of voltage. Also in [38], Essimbi studied nonlinear localized excitation in a model of an electric circuit. Based on a QDA, he analytically showed that the amplitude equation derived in an NLS equation can give in a unified way non-propagating gap solitons as well as an intrinsic localized mode for the whole Brillouin zone of the CW spectrum, except at the Brillouin zone upper edge. Finally he noticed that when the shunt circuit is regarded as a stray parasite component of a nonlinear capacitor, the circuit is equivalent to an electrical Toda lattice, which can support upper cut off localized modes.

In [16], Koichi et al. proposed a new polarisation mode dispersion (PMD) compensation scheme that uses an NLTL as its key device. When the number of eigenvalues corresponding to the input pulse shape is unique, the device can equalize the input pulses distorted by many factors other than PMD, which includes attenuation in metallic cables. The proposed schemes succeeds in compensating for the distortions whose PMD delay causes the interference with distinct polarization mode pulses corresponding to the same bit. Again in [39], a new type of retimer which employs an NLTL coupled to a linear transmission line is proposed. For the retimer, the data and the clock are applied at the same ends of the NLTL and the linear line respectively. The clock signal couples with the solitonic data to achieve synchronization, and is continuously modulated with a fixed propagation velocity. This modulation causes the solitonic data to be pinned by the clock. The retimer does not have any feedback and is designed in a fully distributed or a traveling-wave manner. Therefore, it has the potential to achieve ultrahigh-speed signal retiming, which cannot be attained by the lumped transistor-based retimer. In [40],

a method of short pulse amplification with NLTL is proposed. The pulse propagation on an NLTL is perturbatively treated to find that the nonlinear coupling of the solitonic part with an edge establishes the amplification. Koichi numerically obtained results that explicitly show the process of pulse amplification. The growth rate of the pulse is linearly dependent on the line inductance and the gradient of the edge. He also believe that the property of an NLTL to control the height of a short pulse may provide many beneficial functions in high-speed electronics.

The optical fiber is another example of a nonlinear dispersive medium where optical solitons are observed. optical solitons with higher order dispersion are subject of wide mathematical interest and development of methods for their analytical and numerical solutions [41].

Artificial materials with simultaneously negative permeability and permittivity are sometimes called left-handed materials (LHMs). LHMs use arrays of metallic wires and arrays of split-ring resonators or planar transmission line periodically loaded with series capacitors and shunt connected inductors [42]. Most studies on LHMs have been performed in linear regime of wave propagation. However, combination of nonlinearity and anomalous dispersion of LHMs may give rise to many new and interesting phenomena and applications. Some nonlinear wave phenomena that occur during propagation of the wave along the boundary between right-hand medium and left-hand medium, when one or both of them are nonlinear, have been considered in [43, 44, 45, 46]. Soliton propagation in left-handed (LH) NLTL with series varactors has also been examined [47]. At microwave frequencies, a number of transmission lines with LH characteristics have been proposed [42, 48].

In [49], the characteristics of nonlinear left-handed transmission lines (NL-LH-TLs) were discussed for the first time. An NL-LH-TL was analyzed, and shown to exhibit anomalous frequency dispersion and negative nonlinearity. It's voltage-wave partial differential equation was derived and its harmonic/pulse responses were described. They also suggested potential applications of the NL-LH-TLs such as pulse shaping for Ultra-Wide Band (UWB) and radar systems. In [50], Kozyrev et al. introduced

NLTLs based on LH media and simulated third harmonic generation in a material that in  $2D$  could also focus microwaves. Their simulations demonstrated efficient harmonic generation along LH NLTLs. Harmonic generation is possible over a significantly wider operating frequency range and at relatively higher frequencies in comparison with dual conventional low-pass filter type NLTL. Extending their results for  $1D$  LH NLTL media with focusing, due to the negative refractive index of  $2D$  LH transmission line media, leading to the development of highly efficient powerful frequency multipliers.

LH transmission lines are compact systems showing regimes of backward wave propagation similar to negative-index metamaterials. They have been applied to a number of engineering applications, including the study of leaky wave antennas, compact resonators, and dual band couplers [51]. In a number of these applications, nonlinear elements have been introduced to create tunable structures [52, 53] and, in addition, they have been used as a platform for the study of nonlinear wave propagation in the system supporting the propagation of backward waves [54, 55, 56]. Parametric gain is a nonlinear process whereby a high-energy pump wave exchanges energy with a weaker signal wave through modulation of the material or circuit parameters, thus amplifying it. This effect is commonly used in optical systems, and it has been proposed as a way to mitigate the losses in negative-index metamaterials [57]. In [58], David et *al.* experimentally studied the parametric amplification and generation in nonlinear LH transmission lines. By utilising the complex dispersion characteristics of this system, they demonstrated that the amplification of a weak signal in the three different regimes: with the signal in the LH propagation band, with the signal in the stop band, and with the signal at a defect frequency. Their results show that substantial gain can be achieved in nonlinear systems exhibiting backward wave propagation, and they confirmed that parametric processes are promising candidates for mitigating the losses found in artificial backward wave media, including negative-index metamaterials. In [59], modeling of a LH NLTL loaded periodically with nonlinear series capacitors and linear shunt inductors is presented. In this article it is shown that the spatial derivative of the voltage across the transmission line satisfies a NLS equation. The coefficients of the obtained NLS equation show that the

dispersion coefficient (Q) is always positive, but the sign of the nonlinearity coefficient (P) is determined by the characteristics of the varactor. Depending on the sign of the product  $PQ$ , the proposed LH NLTL can generate either bright or dark solitons. The condition for which this LH NLTL can exhibit modulational instability was studied in [60].

There have been reports of applying NLTL to pulsed power generator [61, 62]. With the development in electronics and semiconductor technology there is also increase need for short pulses for testing and measuring of electrical equipment. Commercially available pulse generators are nowadays quite capable, but sometimes the properties of the generators are inadequate to create short-time pulses with suitable waveforms. In [63], Kuusela et al. proposed the nonlinear electric transmission line as a solution to this problem. It is a simple device that is added to a conventional signal generator to enable the generation of burst of most faster pulses. They showed that NLTLs offer a practical tool to generate short-time voltage pulses for various pulses. Wilson et al. proposed the utilization of ferroelectric ceramic capacitors as nonlinear capacitors, and used  $BaTiO_3$  ceramic capacitors that were manufactured specially for nonlinear capacitors. They proposed pulse sharpening effect of the NLTL to generate short rise-time high voltage pulses. In [61], Fairlie proposed utilization of electrical solitons to generate short pulse width high voltage pulses. However, the voltage amplification effect of the NLTL attracted no attention at that time. In [63], they developed a new pulse generator which generates a large- amplitude and short pulse width voltage pulses at a high repetitive frequency. This generator utilizes the voltage amplification effect of the head-on collision of two solitons in the NLTLs containing nonlinear capacitors.

Electrical NLTL [4], is undoubtedly one of the best platforms for all electrical short pulse generation. When a pulse is input to an NLTL such that the nonlinearity of the Schottky varactors compensates for dispersion, the line generates multiple solitonic pulses, whose widths are generally smaller than that of the input. By extracting the largest pulse, an NLTL operates as a good short pulse generator [5]. Moreover when a step pulse is input to an NLTL such that both the nonlinearity and dispersion sharpen the

edge, the edge finally results in a shock, by which a sub-picosecond temporal transient is observed [6]. An NLTL is useful for more than just short pulse generation, it is found that applying a short pulse supported by a step-like wave to an NLTL enables a short amplification [7]. Nowadays there has been a great interest in the study of nonlinear lumped transmission lines for high power RF generation. This has been motivated by two scientific advances. Seddon et al. [64] in the first advance obtained from BAE systems, was development of a saturated ferrite core transmission line that is capable of generating RF power peaks of about 20 MW with efficiency of 20% at 1.0 GHz. The other one was the experimental work developed by Smith [65] at Oxford involving nonlinear lumped transmission lines made of barium or strontium titanate ceramic tiles, which provided 60 MW RF power at frequencies between 100-300 MHz. In [66], they showed that the principle of soliton generation in nonlinear lumped transmission lines. They checked that there is a minimum rise time for the input pulse to excite the high frequency solitons at the output of the line. They also reported that there is great prospect for hybrid lines to produce solitons with frequency of the order of 800 MHz operating close to the saturation region.

There have been many investigations on the dynamics of solitons in coupled nonlinear systems including both weakly and strongly dispersive ones, governed by the coupled KdV equations [67, 68, 69, 70, 71] and NLS equation [72] respectively. Yoshinaga and Kakutani considered a coupled transmission line which consists of two *LC* ladder lines connected by identical intermediary capacitors, and showed that weakly nonlinear long waves on this line simulate long gravity waves on a two-layer fluid. In [27], Essimbi et al. investigated the class localized electrical signal voltages near the gap of continuous spectrum of two weakly coupled nonlinear *LC* transmission lines. They found that in all cases such excitations are asymmetric envelope solitons, undergoing periodic modulations in time at frequencies lying in the continuous spectrum but close to the point  $\omega(q = \pi/2)$ , where  $\omega$  is the frequency of linear waves, and  $q$  is their wave vector.

By assuming the  $C - V$  characteristics be of the form

$$C = \frac{C_o}{1 + \left(\frac{V}{V_o}\right)^p}, \quad (2)$$

where  $V$  is the voltage of the transmission line,  $C_o$ ,  $V_o$ , and  $p$  are all constants, Dinkel et al. have studied the nonlinear wave on the coupled NLTL [31]. They found that, in the continuum limit, the voltage for the transmission line is described by a modified  $ZK$  equation. The exact cut off frequencies of the growth rate of the solitary waves for the transverse perturbation were obtained. In [73], coupled NLTLs are studied for which  $C - V$  characteristics is of the form

$$C = C_o(1 + k_1V + k_2V^2 + \dots), \quad (3)$$

where  $C_o$ ,  $k_1$ , and  $k_2$  are constants and  $V$  is the perturbation voltage in the transmission line. Only the case where  $V$  is small enough compared to the equilibrium voltage is considered. He found in his analysis that there is instability to the transverse perturbations with the wave number  $k$  such that  $0 < k < k_c$  where  $k_c$  is the critical wave number for a coupled  $ZK$  equation. In addition if there are higher order perturbations in the transverse direction, the solitary wave is unstable if the wave number,  $k$ , of the transverse perturbation satisfies  $0 < k < k_c$  with  $k_c$  numerically given in the article.

In [74], he considered a weakly dispersive coupled NLTLs in order to develop baseband pulses governed by the KdV equation and proposed a method of double repetition rate of pulse stream input to the line. The dispersive distortions are well compensated for by nonlinearity for both  $c-$  and  $\pi-$ mode pulses.  $c-$  and  $\pi-$ modes are two different propagation modes on linear coupled NLTLs. The properties of the nonlinear pulses carried by the  $c-$  and  $\pi-$ modes are quantified based on the reductive perturbation method. The double repetition rate was successfully confirmed by the numerical evaluation. Koichi in [21], studied leapfrogging solitary waves characterized in two capacitively coupled NLTLs. In this work Koichi considered the case when two coupled, nonlinear, weakly dispersive systems are almost symmetrical, so that their dispersion allows two baseband modes with almost coincident velocity. The closed form formula of the leapfrogging



frequency was obtained via the perturbative approach, which simulated the properties well for the pulse amplitude uniquely specified by the coupling strength. Koichi also in [28] investigated two capacitively coupled NLTLs. The asymmetrical pulses developed in these lines were analyzed on the basis of numerical calculations. The closed-form formula of the minimum spatial separation between two pulses interacting repulsively was obtained via reduction theory, which simulated the properties quantitatively well in order to determine the dependence on the pulse velocity and mutual capacitance. The repulsive collision between pulses with different polarities could be effectively used to amplify short electrical pulses.

Recently in [75], a review of the three main topologies for NLTLs was carried out. In these topologies, lumped element and nonlinear material designs are promising for HPM applications, while SRR designs are more applicable for lower power systems and antenna applications. NLTLs are a promising technology for providing high power ( $> 100MW$ ), high frequency ( $> 1GHz$ ), and high repetition rate ( $> 1kHz$ ) solutions in a solid state package, while greatly decreasing the need for auxiliary systems required compared to traditional HPM technology. Current research demonstrates the feasibility of increasing the frequency of nonlinear capacitor-based lines simultaneously with increasing power output and efficiency.

## **I.3 Transmission Lines**

### **I.3.1 General considerations**

A transmission line is a two-port network used to connect a generator or transmitter signal to a receiving load over a distance as shown in figure (1).

A transmission line is also a device designed to guide electrical energy from one point to another. That is a transmission line is a guided structure used to direct the propagation of energy from the source to the load. It is used, for example, to transfer the output RF energy of a transmitter to an antenna. Transmission lines are used mainly in transmitting

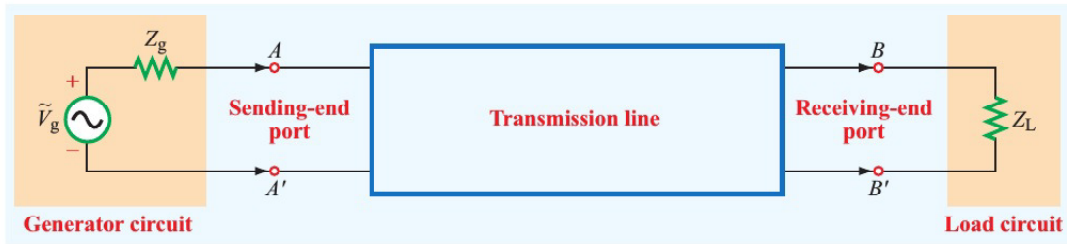


Figure 1: Two-port model of a transmission line.

power at low frequencies and in communications at high frequencies. Transmission lines may be a coaxial line, two-wire line, parallel plate, planar line and microstrip line. Common examples of transmission lines in our lives are twisted wire pairs which are used in computer networks and coaxial cables which are used in TVs. Figure (2) shows a cross section of different types of transmission line.

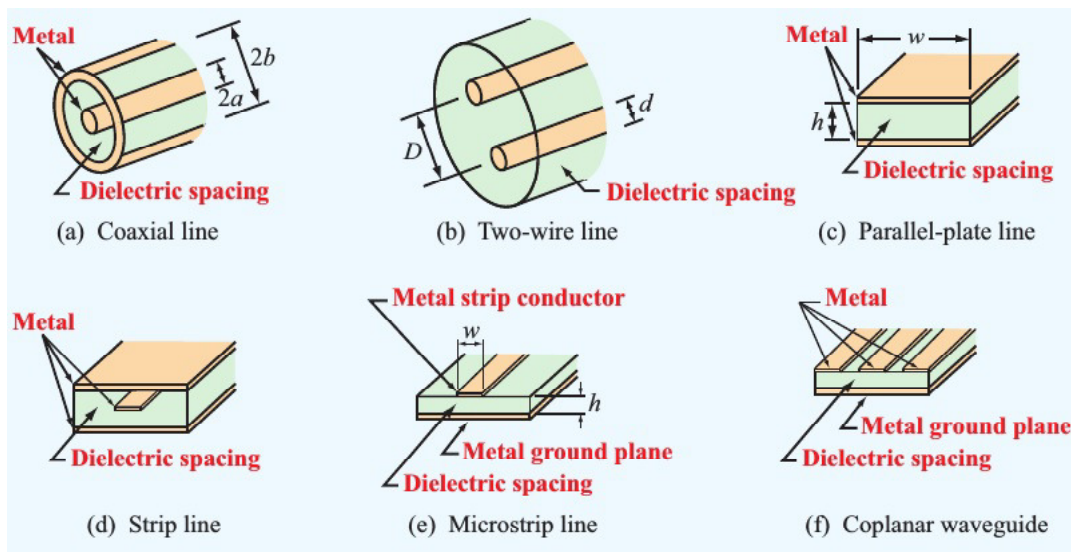


Figure 2: Different types of transmission lines.

A transmission line stores electric and magnetic energy distributed in space and alternating between the two forms in time. That is, at any point along the line the energy is stored in a combination of electric and magnetic forms. As such, a transmission line has a circuit form that combines inductors, capacitors, resistors, whose values are dependent on the geometry of the line and the properties of the materials comprising the line. The transmission lines considered here are systems of two or more closely spaced parallel

conductors <sup>1</sup>. Most of the discussions in this section is restricted to just two parallel conductors, with the distance between the two conductors being substantially smaller than the wavelengths of the signals on the line. With this the structure maybe satisfactorily analyzed on the basis of voltages and currents. By considering a transmission line where electrically small transverse line dimensions (say, less than 1/20 of the wavelength) prevail, a number of useful results are obtained on a voltage and current basis.

In low frequency analog and digital circuits, transmission lines are often referred to as interconnects and can be viewed simply as wires, and provided that the wire has sufficiently low resistance, the interconnect can be largely ignored. However, if transmission must be over a nonnegligible distance compared to the wavelength, then the interconnect must be considered as part of the circuit.

The earliest fundamental understanding of signal transmission led to telegraphy over distances. The critical theoretical step that enabled transmission over more than short distances to be achieved was the development of an understanding of signal transmission on lines using phasor analysis. A phasor is a complex number that combines the amplitude and phase of a sinewave. With transmission line equations, the introduction of phasors eliminates time dependence from the equations and the dimensionality of the equations is reduced by one. When phasors are used in circuit analysis, differential equations in time become algebraic equations. Also no information on frequency is retained when phasors are used.

In electronics and communications engineering, a transmission line is a specialized cable or other structure designed to conduct alternating current of radio frequency. Transmission lines are used for purposes such as connecting radio transmitters and receivers with their antennas, distributing cable television signals, trunkline routing calls between telephones switching centers, computer network connections and high speed computer data buses. Ordinary electrical cables suffice to carry low frequency a.c., such as mains power and audio signals. However, they cannot be used to carry current in the

---

<sup>1</sup> Rectangular waveguide is a transmission line that has just one conductor. Dielectric line can have no conductor.

radio frequency range, i.e. above 30 kHz, because the energy tends to radiate off the cable as radio waves, causing power losses. Radio frequency currents also tend to reflect from discontinuities in the cable such as joints and connectors, and travel back down the cable toward the source [76, 77]. These reflections act as bottlenecks, preventing the signal power from reaching the destination. Transmission lines use specialized constructions and impedance matching, to carry EM signals with minimal reflections and power losses. The distinguishing feature of most transmission lines is that they have uniform cross sectional dimensions along their length, giving them a uniform impedance, called the characteristic impedance [77, 78] to prevent reflections.

At microwave frequencies and above, power losses in transmission lines become excessive, and waveguides are used instead, which functions as "pipes" to confine and guide the EM waves. At even higher frequencies, in the terahertz, infrared and visible ranges, waveguides in turn become lossy, and optical methods, are used to guide EM waves [79]. Mathematical analysis of the behavior of electrical transmission lines grew out of the work of James Clerk Maxwell, Lord Kelvin and Oliver Heaviside. In 1885 Lord Kelvin formulated a diffusion model of the current in a submarine cable. The model correctly predicted poor performance of the 1858 trans-atlantic submarine telegraph cable. In 1885 Heaviside published the first papers that described his analysis of propagation in cables and the modern form of the telegraph equation.

In many electric circuits, the length of the wires connecting the components can for the most part be ignored. That is, the voltage on the wire at a given time can be assumed to be same at all points. However, when the voltage changes in a time interval comparable to the time it takes for the signal to travel down the wire, the length becomes important and the wire is important and the wire must be treated as a transmission line. That is, the length of the wire is important when the signal includes frequency components with corresponding wavelength comparable to or less than the length of the wire. A common rule of thumb is that the cable or wire should be treated as a transmission line if the length is greater than 1/10 of the wavelength. At this length the phase delay and the interference of any reflections on the line become important and can lead to unpredictable behavior

in systems which have not been carefully designed using transmission line theory.

### I.3.2 The Four Terminal Model

For the purposes of analysis, an electrical transmission line can be modeled as a two port network as shown in figure (3). A two port network is an electrical network with two separate ports for input and output.

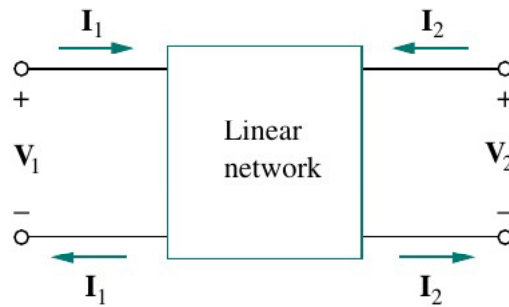


Figure 3: Two port Network

The two port network model is a popular modeling technique used to characterize the electrical transmission line. A two port network may be voltage-driven or current-driven. To characterize a two port network requires that we relate the terminal quantities  $V_1$ ,  $V_2$ ,  $I_1$ , and  $I_2$  in figure (3), out of which two are independent. The various terms that relate these voltages and currents are called *parameters*. These parameters are impedance ( $z$ -), admittance ( $y$ -), hybrid ( $h$ -), and transmission ( $ABCD$ -) parameters.

Among the various approaches in two port modeling, the two port impedance ( $z$ -) model reproduces the system behavior by exciting the model with currents. As illustrated in figure (3), the model is excited by supplying input port and output port with currents  $I_1$  and  $I_2$  respectively. The responses to the excitation are obtained as the input port and output port voltages  $V_1$  and  $V_2$ , respectively. The input-output behavior of the transmission line can now be easily characterized by the four variables  $V_1$ ,  $V_2$ ,  $I_1$ , and  $I_2$ , and mathematically represented using the excitation-response variables and coefficients,

called the  $z$ - parameters. The terminal voltages are related to the terminal currents as;

$$\begin{pmatrix} V_1 \\ V_2 \end{pmatrix} = \begin{pmatrix} z_{11} & z_{12} \\ z_{21} & z_{22} \end{pmatrix} \begin{pmatrix} I_1 \\ I_2 \end{pmatrix} = [\mathbf{z}] \begin{pmatrix} I_1 \\ I_2 \end{pmatrix}, \quad (4)$$

where the  $\mathbf{z}$  terms are called the impedance parameters, and have units of ohms. These  $z$ - parameters are obtained by open-circuiting the input or output port.  $z_{11}$  and  $z_{22}$  are the input and output impedances while  $z_{12}$  and  $z_{21}$  are the forward and reverse transfer impedances.

In the simplest case, the network is assumed to be linear, and the two ports are assumed to be interchangeable. If the transmission line is uniform along its length, then its behavior is largely described by its characteristic impedance,  $Z_o$ .  $Z_o$  is the ratio of the complex voltage of a given wave to the complex current of the same wave at any point on the line. Typical values of  $Z_o$  are  $50\Omega$  or  $75\Omega$  for a coaxial cable, about  $100\Omega$  for a twisted pair of wires. When sending power down a transmission line, it is usually desirable that as much power as possible will be absorbed by the load and as little as possible will be reflected back to the source. This can be ensured by making the load impedance equal to characteristic impedance  $Z_o$ , in which case the transmission line is said to be matched. Some of the power fed into a transmission line is lost because of resistance. This in effect is called ohmic or resistive loss. At high frequencies, another effect called dielectric loss becomes significant, adding to the losses caused by resistance. Dielectric loss is caused when the insulating material inside the transmission line absorbs energy from the alternating electric field and converts it to heat. The total loss of power in a transmission line is often specified in decibels per meter (dB/m), and usually depends on the frequency of the signal. A loss of 3 dB corresponds approximately to a halving of the power.

## **I.4 Types of Transmission Lines**

In what follows in this subsection of this thesis, the following types of transmission lines; balanced two wire, coaxial cable, microstrip line, strip line, slot line and coplanar waveguides will be discussed.

### **I.4.1 Balanced Two Wire Line**

A balanced line is a transmission line consisting of two conductors of the same type, and equal impedance to ground and other circuits. There are many subtypes of balanced lines, amongst which the most common are twisted pairs, star quad and twin-lead.

#### **1. Twisted Pairs:**

In this transmission line the rubber piping is used in circular or square shape. The two conducting wires are kept inside the rubber at opposite sides of the piping. These conducting wires run through the construction and remains parallel to each other. Twisted pair lines are commonly used for terrestrial telephone communication. In such cables, many pairs are grouped together in a single cable, from two to several thousand. Twisted pairs are also used for data network distribution inside buildings, but the cable is more expensive because the transmission line parameters are highly controlled.

#### **2. Star Quad:**

Star quad is a four-conductor cable in which all four conductors are twisted together around the cable axis. It is sometimes used for two circuits, such as 4-wire telephony and other telecommunication application. In this configuration each pair uses two non-adjacent conductors. When used for a single line, such as audio applications and 2-wire telephony, two non-adjacent conductors are terminated together at both ends of the cable. The disadvantage of star quad is that, in combining two conductors, doubles

the capacitance. High capacitance causes increasing distortion and greater loss of high frequencies as distances increases.

### **3. Twin-Lead:**

Twin-lead consist of a pair of conductors held apart by a continuous insulator. By holding the conductors a known distance apart, the geometry is fixed and the line characteristics are reliably consistent. This line has a lower loss than coaxial cable because the wave propagates mostly in the air rather than in the thin dielectric. However, it is more susceptible to interference.

Twin-lead transmission lines have the property that the EM wave propagating down the line extends into space surrounding the parallel wires. these lines have low loss, but also have undesirable characteristics. They cannot be bent, tightly twisted, or otherwise shaped without changing their characteristic impedance, causing reflection of the signal back toward the source. They also cannot be burried or run along or attached to anything conductive, as the extended fields will induce currents in the nearby conductors causing unwanted radiation and detuning of the line. Coaxial lines largely solve this problem.

Other balanced lines include Lecher lines. They are a form of parallel conductor that can be used at UHF for creating resonant circuits. They are also a convenient practical line that fills the gap between lumped components (used at HF/VHF) and resonant cavities (used at UHF/SHF). The cost of two wire lines is very low compared to other types of transmission lines. Their design is quite simple and easy too. In addition to these, they are capable of handling high power.

### **I.4.2 Coaxial Cable**

A coaxial line is the quintessential transmission line, as it is one of the few transmission line structures that can be described exactly from first principles when there is no loss. A realistic coaxial line is considered with conductors having a small amount of loss, a structure that does not have an exact solution.



A coaxial line is a type of transmission line that has an inner conductor surrounded by a tabular insulating layer, surrounded by a tabular conducting shield. The term coaxial comes from the inner conductor and the outer shield sharing a geometric axis. Coaxial lines were invented by Oliver Heaviside, who patented the design in 1880. Coaxial lines conduct electrical signals using an inner conductor surrounded by an insulating layer and all enclosed by a shield, typically one to four layers of woven metallic braids and metallic tape. The line is protected by an outer insulating jacket.

When a positive voltage pulse is applied to the center conductor of the coaxial line, an electric field results that is essentially directed from the center conductor to the outer conductor. A much smaller component of the electric field will also be directed along the line. The direction of the electric field is the direction in which a positive charge would move if it was released into the field. The component of the field that is directed along the shortest path from the center conductor to the outer conductor is denoted  $E_T$ , and the component directed along the line is denoted  $E_L$ . The subscripts  $T$  and  $L$  denote transverse and longitudinal components respectively. Thus, while  $E_L \ll E_T$ , it is necessary to accelerate electrons on the conductors and give rise to current flow, and hence the movement of the pulse along the line.

The advantage of coaxial design is that electric and magnetic fields are restricted to the dielectric with little leakage outside the shield. Conversely, electric and magnetic fields outside the cable are largely kept from interfering with signals inside the cable. The characteristic impedance of a coaxial line is determined by the dielectric constant of the inner insulator and the radii of the inner and outer conductors. Common applications of coaxial line include video, RF and microwave transmission, and computer and instrumentation data connections.

### **I.4.3 Microstrip line**

Microstrip lines have a very simple geometric structure but the EM fields involved are actually complex. However, simple approaches to quasi-TEM mode calculations

with frequency dependent expressions yield quite acceptable design accuracy for many applications. Microstrip line was developed by Grieg and Engelmann at ITT laboratories. Microstrip line is a type of electrical transmission line which can be fabricated using printed circuit board (PCB) technology, and is used to convey microwave frequency signals. It consists of a conducting strip separated from a ground plane by a dielectric layer known as the substrate. Microwave components such as antennas, couplers, filters, power dividers etc. can be formed from microstrip, with the entire device existing as the pattern of metallization on the substrate. Microstrip is thus less expensive than traditional waveguide technology, as well as being far lighter and more compact.

Microstrips have been developed for many years and is the most popular transmission line configuration for MMIC applications due to several reasons. Firstly, passive and active elements are easily inserted in series in microstrip structure; also, the metalized ground plane on the back of the substrate can be used both as the mounting surface and the heat sink for heat generated by active devices on the surface. Moreover, a large amount of theoretical and experimental data has been developed for microstrip applications and most of the EM software packages are designed for this type of structure. However, we cannot deny the difficulty of connecting elements in shunt to ground due to the non-coplanar geometry as well as the thinned substrate for making via holes which is fragile and increases fabrication cost. Furthermore, the parasitic inductance associated with the via holes would degrade the performance at high frequency [80].

Microstrip lines are also used in high-speed digital PCB designs, where signals need to be routed from one part of the assembly to another with minimal distortion, and avoiding high cross-talk and radiation. Microstrip are generally associated with lower power handling capacity, and higher losses. Also, unlike waveguides, microstrip is not enclosed, and is therefore susceptible to cross-talk and unintentional radiation.

#### **I.4.4 Stripline**

A stripline is a symmetrical structure somewhat like a coaxial line completely flattened out so that the center conductor is a rectangular metal strip and the outer grounded metal is simply a rectangular box. The entire structure is 100% filled with dielectric, and therefore transmission is TEM and dependent upon the relative permittivity explicitly. therefore the wavelength is simply the free space value divided by the square root of the permittivity. Stripline is a transverse electromagnetic (TEM) transmission line medium invented by Robert M. Barrett of the Air Force Cambridge Research Center in 1955. This means that striplines are nondispersive and have very high cut-off frequency. Striplines offer better isolation between adjacent traces than the microstrip simply because the upper ground plane prevents the electric fields to expand to wide area.

A stripline circuit uses a flat strip of metal which is sandwiched between two parallel ground planes. The insulating material of the substrate forms a dielectric. The width of the strip, the thickness of the substrate and the relative permittivity of the substrate determine the characteristic impedance of the strip. In general, the dielectric material maybe different above and below the central conductor.

To prevent the propagation of unwanted modes, the two ground planes must be shorted together. This is commonly achieved by a row of vias running parallel to the strip on each side. The disadvantage of stripline is that the fabrication is more complicated and expensive. Lumped elements either have to be buried between the ground planes or be transferred to microstrip structure to get the components onto the top of the substrate. Moreover, because of the existence of the second ground plane, the strip width of a stripline is much narrower for a given impedance and dielectric thickness than that of microstrip.

#### **I.4.5 Slot Line**

Slot line is one of the basic instruments used in radio frequency test and measurement at microwave frequencies. It consist of a precision transmission line, usually coaxial but

waveguide implementations are also used, with a movable insulated probe inserted into a longitudinal slot cut into the line. Slot line was first introduced in 1968 as an alternative transmission line for integrated circuits. Due to its property of radiation, it is normally used in broadband antenna.

Slot lines are relatively cheap and can perform many of the measurements done by more expensive equipment such as network analyzers. Slot lines are able to obtain a characteristic impedance of  $50\Omega$  with a similar geometry size as those of microstrip line. It is also the advantage in achieving higher theoretical impedance levels than with microstrip for the same dielectric substrate. However, slot line support non-TEM mode of propagation and therefore is quite dispersive and lossy. They have also difficulties to connect devices in series therefore do not allow a great del of versatility in the circuit layout.

#### **I.4.6 Coplanar Waveguide**

Coplanar waveguides are a type of electrical planar transmission line which was invented in 1969 by Cheng P. Wen, primarily as a means by which non-reciprocal components such as gyrators and isolators could be incorporated in planar transmission line circuits.

Coplanar waveguides have a coplanar geometry with a central conductive strip and two adjacent ground planes on the same surface of the substrate. The effective dielectric constant and characteristic impedance are determined by the dimensions of the center strip width, the gap, the thickness and permittivity of the dielectric substrate. For coplanar waveguides, devices and components can be grounded without via holes, which means it is not necessary to thin down the substrate and the fabrication cost can be reduced. It also suffers much less dispersion loss than microstrip line. Packing density can be increased because the ground lines provide shielding between adjacent signal lines. Coplanar waveguides have the advantage of small radiation at discontinuities [80].

The EM wave carried by a coplanar waveguide exists partly in the dielectric substrate, and partly in the air above it. In general, the dielectric constant of the substrate will be

different (and greater) than that of the air, so that the wave is traveling in an inhomogeneous medium. In consequence, coplanar waveguides will not support a true TEM wave; at nonzero frequencies, both the electric and magnetic fields will have longitudinal components.

Low characteristic impedance of conventional coplanar waveguides is achieved by increasing the central strip width and decreasing the slot width. This will cause the dimension size inconvenient for fabrication and any small variation of geometries would lead to unpredictable behavior. Another disadvantage of coplanar waveguides is that because of the ground, conductors are on each side of the signal line with small separation distances and this will result in most of the electric field concentrated on the edge of the signal line causing the current crowding phenomenon [81, 82]. The crowded current on the edge of the transmission line will not only increase the dissipation loss but also produce more heat which may damage the surrounding active devices.

## **I.5 Theory of Nonlinear Transmission Lines**

NLTLs comprise of transmission lines periodically loaded with nonlinear varactors and/or nonlinear inductors. In the case of nonlinear varactors the nonlinearity arises from the variable depletion layer width of the varactor, which depends both on the DC bias voltage and on the AC voltage of the propagating signal. NLTLs have been the subject of several studies that have investigated their performance by means of mathematical analysis [83, 84, 85], computer simulation, and practical experiments that have shown their suitability for application in high speed and wide bandwidth systems. These applications involve techniques for pulse forming and sharpening which are applied in signal processing such as pulse compressor [86, 87], frequency multiplier [88], etc. An NLTL in general is two wires through which a signal is transmitted. The behavior of a pulse propagating on the NLTL is dependent on the nature of the wires, and the nature of the pulse. The study of these various effects make up the NLTL theory.

The generation of solitons can be obtained with three different types of NLTLs:

1. in a line where there is a balance between nonlinearity and dispersion;
2. through the effect of damped procession motion of magnetic dipoles moment in a line buit with ferrimagnetic materials that are polarized with external magnetic field
3. in a line that exhibits anomalous dispersion and nonlinearity.

A lumped NLTL is an LC right-handed line where each section consists of a capacitor and an inductor. A single section of NLTL is shown in figure (4)

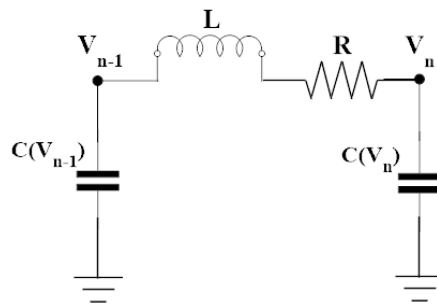


Figure 4: Equivalent Circuit model of one section of an NLTL

A discrete NLTL consists of a nonlinear dispersive medium where electrical solitons propagate in the form of voltage waves with constant shape and velocity. Dispersion in the line arises from the periodic nature of the elements while the nonlinearity is introduced by nonlinear dielectric materials, such as voltage-dependent capacitors, and/or nonlinear ferrimagnetic materials, such as current-dependent inductors, which are arranged in a series of LC section low-pass filters. The NLTL is called capacitive when it employs capacitors as nonlinear devices, inductive when nonlinear inductors are used, or hybrid with the simultaneous use of nonlinear capacitors and inductors in the line section.

Consider the NLTL if figure (4), there are three basic equations for describing the discrete LC ladder network, namely: the phase velocity  $v_p$ , the characteristic impedance  $Z_o$ , and the cutoff frequency  $f_c$ , also called the Bragg frequency because of the similarity to Bragg diffraction in optics, which corresponds to a phase shift of  $180^\circ$  per stage. These

equations are:

$$v_p = \frac{1}{\sqrt{[L(I)C(V)]}}, \quad (5)$$

$$Z_o = \sqrt{\frac{L(I)}{C(V)}}, \quad (6)$$

$$f_c = \frac{1}{\pi\sqrt{[L(I)C(V)]}}, \quad (7)$$

where  $L(I)$  is the inductance as a function of current and  $C(V)$  is the capacitance as a function of voltage. If we consider a capacitive line, then as  $C$  decreases with the applied voltage, the propagation velocity will increase with increasing voltage. Thus, the portion of the pulse with higher voltage amplitude will travel faster than the lower initial amplitude, and the pulse peak will catch up the low-voltage amplitude, forming an output shock wavefront with a very fast rise time [89].

Another parameter in the NLTL characterization is the voltage modulation depth (VMD). It is defined for the first three cycles, given as [90]

$$VMD = V_{ave} = \frac{\sum_{j=1}^3 (V_{pt})_j}{3}, \quad (8)$$

where  $j$  is the oscillation cycle number and  $V_{pt}$  is the peak-to-trough load voltage.

For varactor diodes, the voltage dependence of the diode capacitance can be modeled from the  $C(V)$  curve given by [89]

$$C(V) = C_o \left(1 + \frac{V}{V_j}\right)^{-m}, \quad (9)$$

where  $V$  is the applied voltage,  $V_j$  is the junction potential,  $C_o$  is the initial capacitance, and  $m$  is a grading coefficient determined by the doping profile of the varactors. Also the time charging function  $Q(V)$  is calculated as the integral of the variable capacitance  $C(V)$  with respect to  $V$  as

$$Q(V) = \int_o^V C(V) dV. \quad (10)$$

Thus substituting equation (9) in (10) we get

$$Q(V) = \left( \frac{C_o}{1-m} \right) \cdot \left[ \left( \frac{V}{V_j} + 1 \right)^{(1-m)} \right]. \quad (11)$$

In the case of a nonlinear inductive line where we have a constant capacitance and a nonlinear inductor, we adopt from [66] an equation modified so as to have a smoothly varying inductance function that approaches an asymptotic value as the current increases. This equation is given by

$$L(I) = (L_o - L_s) \left[ 1 - \tanh^2 \left( \frac{I}{I_s} \right) \right] + L_s, \quad (12)$$

where  $L_o$  is the initial inductance (at zero current),  $L_s$  is the asymptotic inductance with current increase,  $I$  is the current flowing through inductor and  $I_s$  is the inductive nonlinear factor.

### I.5.1 NLTLs Developed from Nonlinear Dielectric Materials

It is well known that the thickness of the reverse-biased diodes depletion layer increases with increasing voltage. This results in a junction capacitance which decreases as the reverse bias voltage increases. Because this effect was well known, this approach was employed for the first demonstrations of NLTLs. Indeed, this nonlinear capacitance can be very large because it is not limited by molecular relaxation. The greatest limitation is the device resistance which appears in series with the junction capacitance and the breakdown voltage. Schottky diodes suitable for high frequencies are limited to low voltages, but this approach has been used in NLTL shocklines to produce some of the fastest electrical pulses with even sub-ps rise times being achievable.

Nonlinear dielectrics have been incorporated into transmission lines for over thirty years [91, 92]. Using various dielectrics and geometries gave a broad range of shock forming lines, NLTLs for pulse sharpening, or RF sources. Ferrite loaded coaxial lines were used to produce sub-ns high voltage pulses through magnetic compression. Early



research examined issues with various geometries for NLTL design. Since coaxial geometry generates nonuniform fields, some researchers decided to use a parallel plate geometry for a shock forming line. Several NLTLs studies have evaluated the effectiveness of ferroelectric materials on NLTLs. As an example, [85] proposed invalid material constraints since it was not bound by the laws of electrostatics. But some models [83] were physics-based and did not violate basic laws.

When the nonlinear components are made of a ferroelectric dielectric giving rise to a capacitance that is dependent on applied voltage, we end up with a nonlinear capacitive transmission line. Ferroelectric materials are found in some ceramic capacitors that exhibit a capacitance change when subjected to a great variation of voltage. Ideally, NLTLs are simply made from nonlinear materials. Characterizing the physical behaviour of these materials and designing effective manufacturing processes is challenging. A few published articles [93, 94, 95] have also reported the use of ceramic blocks specially manufactured to use as a nonlinear dielectric in NLTLs, which also require the application of higher input voltages in the range of several kilovolts.

Ferroelectric materials are characterized with two phases: paraelectric (or nonpolar) and ferroelectric (or polar). In the first, the polarization of the material has a linear behavior when subjected to an external electric field and the oriented dipoles return to their original states when the field is removed. In addition to being nonlinear, in the ferroelectric phase there is a spontaneous electric polarization that can be reversed by the application of a strong external electric field and, as a result, the relative permittivity (dielectric constant) in the ferroelectric phase can vary by the application of an external electric field. These materials usually present high values of electric permittivity which are temperature dependent due to the well-known structural phase transition at the Curie temperature.

Dielectric losses in ferroelectric materials arise from conduction losses, that is ohmic conductivity, hysteresis losses and relaxation losses due to reorientation of the electric dipoles in response to an alternating electric field. Dielectric losses cause the degradation in the performance of an NLTL by reducing its conversion efficiency and limiting its

operating frequency.

The nonlinear characteristic of ferroelectric materials finds application in the construction of NLTLs but requires the control of several factors that effectively enable the access of the nonlinearity of ferroelectric materials. Some of these factors include:

1. The Curie temperature of the compound should be near the operating room temperature to allow operation of the dielectric in its paraelectric phase, where depending on the material it can present a strong nonlinearity.
2. The breakdown voltage should be high enough to allow achieving higher nonlinearity of the dielectric, that is, to obtain the required variation of the capacitance across the range of applied voltage.
3. Low dielectric losses in the radio frequency range at least at a repetition pulse rate in the tens of hertz without external cooling.

It is worth mentioning that reports on the investigation of dispersive NLTLs using a nonlinear dielectric in a parallel-plate design with ceramic blocks made of ferroelectric compounds such as barium and strontium titanate [93, 94], or lead magnesium niobate [95], which present an extremely high relative permittivity. To maximize the nonlinearity of these ferroelectric materials, they should be used near to the Curie temperature (around 120 C barium titanate) and to be exposed to an electric field variation of the order of kilovolts.

The ferroelectric ceramics used in the construction of discrete NLTLs consist of commercially available ceramic capacitors that exhibit nonlinear capacitance when a voltage is applied. The reduction of capacitance with increasing voltage is not a property of all capacitors, but only applies to capacitors made of ferroelectric dielectrics like barium titanate constructed without the addition of dopants to control thermal stability and, as a result, their capacitance has both strong temperature and voltage dependences.

The generation of high-power pulsed signals with fast rise times is the main application of NLTLs using commercial ceramic capacitor as a nonlinear element and requires

the use of high-voltage input signals to effectively obtain the desired nonlinear behavior. The following setbacks are observed With the use of ceramic capacitors:

1. The nonlinearity is achieved with capacitors with large temperature dependence, and the heat generation by the hysteresis losses must be considered.
2. The commercial ceramic capacitors are normally limited up to  $5kV$  rated voltages and have self-resonant frequencies, that is a frequency at which the capacitor starts behaving like an inductor, in the hundreds of megahertz range. This is a limiting factor for high-power and high-frequency applications.
3. The phenomenon of aging in ceramic capacitors is well known, and the manufacturers usually quote an aging rate in terms of the reduction of the value of a capacitance as a logarithmic function of time, and this process tends to be accelerated when they are subjected to a high level of electric stress that is required to produce the nonlinear response.

In [96] experimental results with high-voltage NLTLs were presented showing the generation of pulsed RF waveforms at tens of kilovolts and frequencies from around 10 to  $90MHz$ . These NLTLs were built using obsolete ceramic capacitors that had an excellent capacitance ratio and were stacked to improve their voltage rating. Single pulses around  $30kV$  were generated to supply these lines. The whole assembly operated submerged in insulating oil.

Other ceramic and organic materials may well prove to be better materials for NLTL sources, but we must be aware that heavy ions, such as barium and lead, can give high dielectric constant but naturally increase the molecular relaxation time which is detrimental to our application. Any new materials to be considered for use in NLTLs must be screened for microwave absorption frequency peaks and suitable Curie temperature range from the onset.

## 1.5.2 NTLs Developed from Semiconductor Materials

The nonlinearity of semiconductor devices as the nonlinear element in NTLs arises from the junction capacitance under a reverse bias. Typically, the operating voltage of these devices ranges from few volts for silicon varactors diode and can reach the value of  $3.3kV$  for carbide silicon Schottky diodes. Therefore, by using these diodes in stacked configuration, an upper bound above  $3.3kV$  can be reached in high-voltage NTLs. Besides the lumped lines, these capacitive NTLs can be constructed with compact dimensions using different forms of planar transmission lines such as microstrip line, slot line, CPW, and finline.

The construction of capacitive NTLs using three different types of diodes that exhibit nonlinear capacitance with reverse applied voltage, which are varactor diodes, HBVs, and Schottky diodes. These devices have different characteristics due to their different construction and materials employed. A capacitive NTL built with these diodes would have its performance directly influenced by the diode reverse breakdown voltage, the cutoff frequency, and the capacitance ratio.

In a diode, the depletion region, which is formed at the p-n junction under a reverse voltage polarization, gives rise to a junction capacitance. All diodes exhibit this variable junction capacitance, but varactors are manufactured to exploit this effect and to increase the capacitance variation. Unfortunately, as diode doping profile is made more abrupt the cutoff frequency also decreases. Varactor diodes are used to construct low voltage capacitive NTLs.

A Schottky diode is a semiconductor diode formed by the junction of a semiconductor with a metal. This diode presents a higher power handling capability, low power loss, low forward voltage drop, and a very fast switching action.

HBV diodes exhibit symmetric capacitancevoltage and asymmetric currentvoltage characteristics. This leads to the generation of only odd harmonics of an applied signal since the even harmonics are canceled due to the symmetric nature of the nonlinearity, so they are used to build NTLs that operate as frequency multipliers [88].

Besides the voltage-capacitance relation of equation (9), another important equation of a varactor is the cutoff frequency ( $f_c$ ) which is described by [98]

$$f_c = \frac{S_{\max} - S_{\min}}{2\pi R_s}, \quad (13)$$

where  $S_{\max}$  and  $S_{\min}$  are the maximum and minimum differential elastances (inverse of capacitance), respectively, during a pump cycle and  $R_s$  is the parasitic series resistance. For high efficiency, any varactor diode must exhibit low series resistance  $R_s$  and must accommodate a large elastance swing, that is, a high  $S_{\max}/S_{\min}$  ratio.

The cutoff frequency is defined as the frequency at which the capacitive reactance is equal to the series resistance. It is also a function of voltage, achieving its maximum value at the breakdown voltage, being an important consideration in diode selection. Ultimately, the minimum pulsewidth which may be generated on an NLTL is limited by the diode cutoff frequency and the total line loss [99].

The oscillation depth and total number of solitons generated can be increased by varying the nonlinearity and the total number of stages; however, the conductive and dielectric losses will dissipate much of the energy of the oscillations. This can significantly reduce the overall efficiency of the lines with many stages [100].

The investigation of parameters that affect the performance of low-voltage NLTLs using varactors is now possible since the test equipment needed to perform these experiments are easily found in electronics labs. The experimental results with low-voltage NLTLs were presented in [96], reporting the generation of pulse bursts at frequencies ranging from a few megahertz to  $250\text{MHz}$ . These lines were constructed using varactors diodes (BB212) and specially manufactured inductors. The results of research on low-voltage capacitive NLTLs built with varactors and inductors assembled on PCBs reported the generation of pulses on the order of  $100\text{V}$  with a rise time of  $10\text{ns}$  [101]. This 48-section NLTL employed inductors of  $1\text{H}$  and low-voltage varactors (1N5822). The diodes presented a capacitance variation between  $400$  and  $70\text{pF}$ , when subjected to voltage pulses of the order of  $40\text{V}$ .

Several research have reported the construction of monolithic NLTLs, which enables the construction of very compact NLTLs structures loaded with Schottky or HBV diodes that are fabricated in a semiconductor substrate. These semiconductors have very high cutoff frequency (THz) but have a breakdown voltage of less than  $10V$ , allowing the construction of low-voltage NLTLs. In [97], the authors reported the construction of a monolithic NLTL built with a CPW structure loaded by reverse-biased gallium arsenide (GaAs) Schottky diodes at spacing  $d$ , as shown in figure (5).

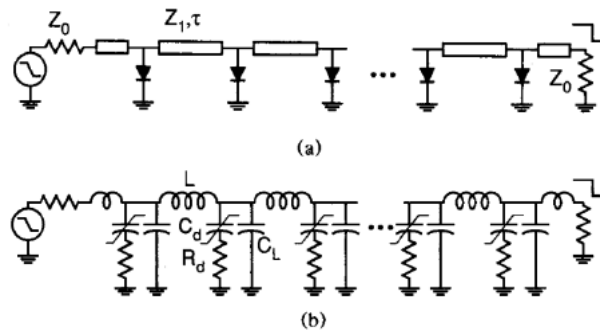


Figure 5: Illustration of a monolithic GaAs NLTL[97]:  
(a) circuit diagram,  
(b) equivalent circuit.

The experiments generated electrical step functions of about  $5V$  magnitude and with less than  $1.4ps$  of fall time, which allowed for the development of sampling circuits with bandwidth around  $300GHz$ . The authors pointed that in a CPW structure the circuit layout introduces a parasitic series inductance and shunt capacitance at the diode locations. However, CPW skin loss is a major parasitic parameter that must be minimized.

The construction of a monolithic NLTL was presented in [88]. In it the NLTL consists of 15 discrete GaAs-based HBV diodes periodically soldered across a finline transmission line with tapered slot couplers at the input and output as shown in figure (6). The HBV diodes presented a capacitance variation of 74% ( $6.8pF/26pF$ ).

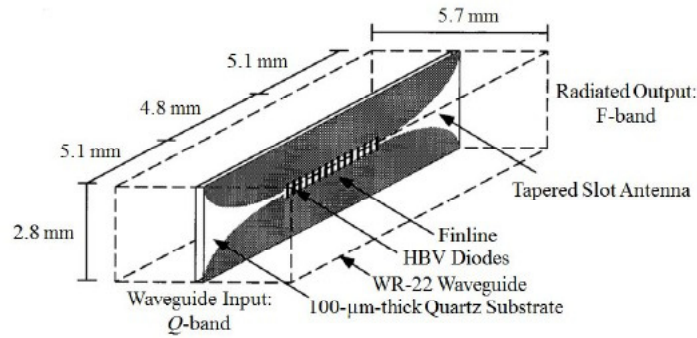


Figure 6: Layout of a monolithic NLTL constructed with finline structure periodically loaded with HBV diodes [88]

Using diodes with variable capacitance in embedded coplanar or microstrip line, it is possible to achieve frequency in the GHz range, but with extremely low power. For very high Bragg frequencies, diode areas and spacing become impractically small, and parasitic effects can dominate the cell. Dissipation is also an issue for very high Bragg frequency lines since waveguide dimensions must become very small [102].

### I.5.3 NLTLs Developed from Ferrite Magnetic Materials

The first nonlinear pulse compression scheme used magnetic material in the form of laminated metallic strips wound to form a toroidal core. More recent high frequency shocklines and particularly the dispersive NLTL employed by the BAE source, use high resistance ferrite material.

The construction of coaxial-based NLTLs loaded with ferrimagnetic materials make use of ferrites beads and inductors made of windings in ferrite cores. The gyromagnetic properties of ferrites induce high-frequency oscillations which are reinforced by the nonlinearity in synchronous wave and gyromagnetic NLTLs.

The macroscopic magnetic properties of a magnetic material are a consequence of interactions between an external magnetic field and the magnetic dipole moments of the constituent atoms. The relative magnetic permeability ( $\mu$ ) is defined as the ratio of magnetic flux density (B) to magnetic field intensity (H) obtained from the slope of the  $B - H$  curve.

Hysteresis in magnetic materials means lagging of the magnetization behind the magnetizing field and represents the losses when the material subjected to an alternating magnetic field. These losses arise due to the limit of magnetization switching frequency. In the  $B - H$  curve, the area of the hysteresis loop is associated with core losses, which increase in direct proportion to frequency, since each cycle traverses the hysteresis loop. Another contribution to losses is the eddy currents which are induced in the core material by the time-varying magnetic flux; these currents, in turn, induce flux in opposition to the initial flux. Due to the high resistivity characteristic in the ferrimagnetic materials, eddy current losses in the core are usually much less than those due to hysteresis.

Ferrimagnetic materials are characterized by the temperature dependence of the magnetic properties. Above the Curie temperature, the ferrimagnetic materials undergo a phase transition and become paramagnetic, giving rise to a sharp change in magnetic properties due to the random orientation of magnetic moments.

Investigation on synchronous wave NLTLs using axially biased ferrite and capacitive crosslinks has been reported as a feasible technique to improve the performance of capacitive NLTLs, which present the decay of the amplitude of the oscillations, caused by losses, and wide frequency spectrum [103]. These lines are usually built with coaxial transmission line configurations, providing simple means of axial biasing and increased voltage handling capability.

In [64], the authors presented the experimental results of a synchronous NLTL, which produced 20MW peak power with center frequencies from 200MHz to 2GHz that could be electronically tuned by adjusting the circuit parameters ( $L, C, C$ ) and feeding a continuous dc bias current through the NLTL, which allows for the control of the initial state of the nonlinear inductors. Another type of synchronous NLTL reported the construction of a line in a coaxial oil-insulated geometry [104] that generated RF with tunable frequency in the range of 0.9 to 1.5GHz and instantaneous peak power on the order of 100MW. This NLTL used an axial bias to control the shock speed and spatially dispersive geometric structure to provide a broad tuning range.

Recent research reports the generation of high-power RF using gyromagnetic NLTLs.



These lines consist of a uniform coaxial line whose center conductor is encapsulated by ferrite beads. The biasing field can be provided by a solenoid wrapped around the NLTL or even by permanent magnets. The operational frequency can be controlled by varying the dimensions of the ferrimagnetic material, which affects the azimuthal magnetic field and material losses, or by varying the bias field strength.

The experimental results of two gyromagnetic NLTLs built with NiZn ferrite rings distributed with a step of  $9\text{cm}$  and length of  $41$  and  $77\text{cm}$  is reported in [105]. The experimental setup consists of two uniform sections filled with transformer oil and the NLTL between them. The NLTL was filled with transformer oil for increasing the electric strength. The maximum amplitude of the input voltage pulse was  $295\text{kV}$ . The performance of these lines was evaluated with the ferrites in both unsaturated and saturated condition. The saturated condition was achieved with the application of an external magnetic field ( $H_0 \leq 80\text{kA/m}$ ) generated by a dc solenoid.

In [106], Romanchenko *et al.* reported the development of a gyromagnetic NLTL source used in biological research. This line produced RF pulses at frequencies from  $0.6$  to  $1\text{GHz}$ , with the ability to change the peak amplitude by about 400 times ( $52\text{dB}$ ), reaching a maximum value of nearly  $40\text{kV/cm}$  and decreasing to tens of  $\text{V/cm}$ . The experiments were performed using nickel zinc ferrite beads with saturation field  $B_{sat} = 0.35\text{T}$  and coercivity  $H_c = 410\text{A/m}$ . This NLTL was built in an air-filled waveguide and was fed by a driver which produced pulses with  $9\text{ns}$  width whose amplitude can be varied from  $150$  to  $270\text{kV}$  and optimal bias magnetic field of about  $50\text{kA/m}$ . The approximate length of this NLTL was about  $1\text{m}$ .

In [107], their investigation presented the construction of gyromagnetic NLTLs loaded with NiZn and MnZn ferrites. Due to the large electric fields found inside the NLTL, a fully encapsulating dielectric medium (SF6 pressurized to  $680\text{kPa}$ ) was used as an insulator to prevent breakdown. A secondary dc power supply provided the necessary current through a solenoid wrapped around the outer conductor of the NLTL to produce the axially directed, magnetic biasing field. By altering the bias magnitude, length of bias, and ferrite, the NLTL could be actively tuned for specific delay times. These NLTLs

were fed by a single shot pulse around  $30kV$ . The line built with MnZn ferrite proved to be too lossy and did not produce microwaves, while the lines built with NiZn ferrites produced RF power of  $4.8MW$  with pulse lengths ranging from 1 to  $5ns$  and tuning frequency in the range of 2 to  $4GHz$ . The NiZn ferrites had different compositions; however, oscillations with higher amplitudes were achieved with ferrites that have relative permeabilities in the upper hundreds and saturation magnetizations around  $3500G$ . Chadwick *et al.* [108] reported the construction of fully solid-state high-power microwave source that was built using a semiconductor opening switch diode as a pulse generator and a gyromagnetic NLTL. This structure produced peak output power about  $90MW$  and frequencies between  $700MHz$  and  $1GHz$ . The suitability of yttrium iron garnet ferrites for use in gyromagnetic NLTLs was reported in [109]. The generation of microwave oscillations with peak power up to  $200kW$  was noted for an input signal of less than  $6kV$  with sub-nanosecond rise time. The resulting output of this NLTL was radiated, and field levels exceeding  $1kV/m$  at a target distance of  $3m$  at frequencies between 1.7 and  $1.8GHz$  were observed.

In [110], Bragg *et al.* reported the temperature dependence of a ferrimagnetic-based NLTL that had been tested under the temperature range of  $20^{\circ}C$  up to  $150^{\circ}C$ . This temperature range covered a wide range of potential operating temperature and provided some insight into operational performance above the Curie temperature. The experiments were conducted with a single shot operation and the NLTL consisted of a coaxial line with toroidal ferrites loaded on the inner conductor. The experiments showed an increase of 50% in peak power relative to room temperature and a significant decrease of the frequency between  $0^{\circ}C$  and  $100^{\circ}C$ . This paper concluded that the exact mechanisms responsible for power and frequency changes are not fully understood, and therefore, further experiments are needed to know the behavior of permeability, relaxation time, and switching time versus temperature. The excellent result obtained with a gyromagnetic NLTL capable of producing RF pulses with estimated peak power of  $260MW$  at frequencies around  $1GHz$  with  $100Hz$  pulse repetition rate is described in [111]. The synchronized operation of four gyromagnetic NLTLs based on the parallel arrangement

and loaded onto conical helix antennas is reported in [112]. The experiments showed that the radiation power density of synchronous four-channel operation is higher than for one-channel operation for 16 times.

The behavior of ferrite magnetic material is much more complicated than that of nonlinear dielectrics in that the ferrite material stores significant energy in both magnetic and electric fields. That is, the value of permittivity is generally much larger than one and is typically nonlinear with the applied electric field. The low frequency hysteresis provided by the manufacturers does not accurately reflect the performance of the material under fast pulsed saturation.

#### **I.5.4 Constraints of NLTLS**

NLTLS built in CPW structures produced higher frequency oscillations, however, the miniaturized design showed a low-power handling capability. The Schottky diodes used to build this line provided very low values of capacitance providing oscillations around  $240GHz$ . To achieve higher frequencies, the dimensional reduction of the diode junction capacitance is required, but this is limited by the capability of the technological process of manufacture. Moreover, the low reverse breakdown voltage of the Schottky diodes determined power level limitation. This line showed losses due to skin effect in the semiconductor and layout parasitic impedances associated with the high-frequency operation. The capacitive NLTLS assembled in a PCB using varactor diodes have their performance limited by the maximum reverse breakdown voltage of the varactor. The operating frequency defined in equation (7) is related to the minimum capacitance value provided by the varactor. The maximum frequency is around  $300MHz$ , since the stray impedances of the PCB is of order of several pF for a minimum capacitance value provided by the commercial available varactors (pF) and of tens of nH for a minimum inductance provided by the inductors formed on the PCB track layers [113].

The use of ferroelectric ceramic materials to build high-voltage NLTLS has been studied in [93, 94, 95, 114, 96], showing that the operational frequency is limited to

400MHz. The best result achieved for RF generation using NLTLs built with nonlinear dielectric ceramics was reported in [93] using ceramics blocks based on barium and strontium titanate. These surveys have demonstrated that:

1. high-voltage values needed to access the nonlinear behavior of the relative permittivity;
2. the intrinsic temperature dependence behavior of the relative permittivity is a critical parameter;
3. the dielectric loss was the main constraint for ferroelectric materials, since it can prevent the RF generation.

Furthermore, the difficulty of coupling the RF pulse from the nonlinear lines efficiently into a linear resistive load is well known and is caused, primarily, by the voltage dependence of the line impedance [114]. The analysis of the results obtained with capacitive NLTLs built with ferroelectric ceramics indicates the need of new research on ferroelectric materials to find materials with low dielectric losses at frequencies above 400MHz. Considering that chemically different perovskites display very different ferroelectric behavior, Benedek and Fennie [115] and Mulder *et al.* [116] reported the connection between structural distortions and the ferroelectricity in perovskite oxides. Since prototypical ferroelectrics, such as  $BaTiO_3$  and  $PbTiO_3$ , do not have structures with octahedral rotation distortions, the authors suggested that the design of new ferroelectric materials should pay attention to the structural stability in such a way to avoid the ferroelectricity suppression caused by octahedral rotation distortions. Using this approach, the research on different ferroelectric compositions could reveal useful materials to build NLTLs.

The efficiency of gyromagnetic NLTLs is strongly related to magnetic losses of the ferrite materials. The parallel arrangement of four gyromagnetic NLTLs was reported in [112] as a way to improve the device efficiency. This research also investigated the connection between the efficiency and the physical dimension of the ferrite geometry, concluding that the efficiency could be maximized by an optimal arrangement of ferrite

dimensions, bias magnetic field and the amplitude of the incident pulse. Due to high-voltage oscillations, gyromagnetic NLTLs require the use of electric insulation to prevent breakdown. The efficiency of the gyromagnetic lines is affected by the insulator due to its dielectric properties [106]. The temperature-dependent behavior of gyromagnetic NLTLs performance was reported in [110]. The unstable behavior of the magnetic properties of the ferrites is responsible for the variation in the oscillations (amplitude and frequency). Gyromagnetic NLTLs are also subject to the temperature rise caused by heat dissipation due to resistive and magnetic switching losses in the ferrites operating under pulsed repetition mode.

## I.6 Conclusion

In this chapter we have exhausted most of the literature on soliton propagation in NLTLs as well as in coupled NLTLs. We also explored notions on the theory of NLTLs. The performance of NLTLs is strongly related to the properties of nonlinear ferroelectric and ferrimagnetic materials that are employed. The improvement of the performance of NLTLs is still hampered by the lack of materials that present simultaneously nonlinear behavior, low losses, and thermal stability.

---

# MATERIALS AND METHODS

---

## II.1 Introduction

Almost every realistic physical system is nonlinear in nature. Nonlinear models can be derived in many areas of physics from the propagation of water waves to the macroscopic theory of superconductivity and superfluidity and to general relativity. Moreover one can say all *chaos theory* originated from the study of nonlinear dynamics. A great number of models of physical situations, called integrable models, exhibit features as regularity, stability and predictability of the motion. For example the KdV equation for a real function  $u(x, t)$  arises in the propagation of shallow water surface waves when weakly nonlinear restoring forces are present, of long internal waves in a density stratified ocean, of ion-acoustic waves in a plasma and acoustic waves on a crystal lattice.

The modeling of nonlinear phenomena always resolves to nonlinear differential equations whose mathematical difficulties are numerous and solutions sometimes are not direct. To overcome these shortcomings in the mathematics, physics has made use, in an almost symmetrical way, of reduction methods that allow us to replace the initial nonlinear and not solvable problem by another one that is linear and solvable.

For systems for which spectral, symmetry or other algebraic methods are not of great help or at disposal, a great help comes from perturbative techniques. In general, perturbation theory is a collection of iterative methods for the systematic analysis of the behavior of solutions to differential and difference equations.

## II.2 Nonlinear Model Reduction Methods

The methods for nonlinear model reduction are much less developed and are by far more challenging to develop and analyze. The problem of nonlinear model reduction deals with approximations of the systems in the form of a nonlinear ordinary differential equation. The goal of nonlinear model reduction methods, broadly speaking, is to reduce costs of simulation of such systems. It involves not only reducing the dimensionality of the state vector, say  $x$ , but also finding ways to efficiently calculate the right-hand and left-hand sides of our ordinary differential equation.

The problem of nonlinear model reduction consists of the following two sub problems:

- Reducing the dimensionality of the state vector.
- Finding representations of the reduced nonlinear functions such that the values and derivatives can be computed efficiently.

Addressing either one of these issues leads to computational gains. Algorithms which address both of these issues are usually much more beneficial. Up till now, the only practical developed nonlinear dimensionality reduction methods are based on projections. The reduction technique can be further refined by integrating the order-estimation algorithm with the proper-orthogonal decomposition reduction model to increase efficiency and decrease computational cost [117].

While analytic models and simulations of lumped element NLTLs are valuable for system design, they must ultimately be compared to experimental results. Several studies have constructed NLTLs using COTS components such as nonlinear capacitors, nonlinear inductors, and hybrid lines. Experiments with COTS nonlinear capacitors agreed well with lumped element models [90].

### II.2.1 Nonlinear Reduction Based on Taylor Series

Circuit equations in NLTLs can be simplified from a partial differential equation to an ordinary differential equation using Taylor series expansions and appropriate simplifi-

cations [15, 86]. This technique can model NLTLs with nonlinear capacitors made from metal oxide semiconductor varactors.

Taylor series expansion of a function in a nonlinear equation is applicable to either quadratic or weakly nonlinear systems. The very first practical approaches to nonlinear model reduction were based on using Taylor series expansion [118, 119, 120, 121].

Lets consider the folowing nonlinear ordinary differential equations [122]:

$$\dot{x}(t) = f(x(t), u(t)), \quad x(t) \in \mathbb{R} \quad (14)$$

$$y(t) = g(x(t), u(t)), \quad (15)$$

where the time-dependent vector  $x(t)$  called the *state* summarizes all the past inputs  $u(x, t)$  needed to evaluate future outputs  $y(t)$  of the system. Such descriptions arise, for example, from simulation of electrical circuits with nonlinear capacitors and/or nonlinear inductors. Lets assume that we performed a Taylor series expansion of the function  $f$  in the state-space model of equation (14) around some nominal  $x_o$  and input  $u_o$ :

$$\begin{aligned} \dot{x} \approx f(x_o, u_o) &+ \frac{\partial f}{\partial x}(x - x_o) + \frac{\partial f}{\partial u}(u - u_o) + \frac{1}{2} \frac{\partial^2 f}{\partial x^2}(x - x_o) \otimes (x - x_o) + \\ &+ \frac{\partial^2 f}{\partial x \partial u}(x - x_o) \otimes (u - u_o) + \frac{\partial^2 f}{\partial u^2}(u - u_o) \otimes (u - u_o) + \dots, \end{aligned} \quad (16)$$

where all derivatives of  $f$  are taken at the expansion point  $(x_o, u_o)$ . We assume that our Taylor series, truncated upto a certain order, can approximate the original monlinear ordinary differential equation describing our system in equation (14) with sufficient accuracy.

We now represent  $x \approx Uz, z \in \mathbb{R}^q$  and project our series in equation (16) onto the rowspan of matrix  $V$ , assuming it is biorthogonal to  $U$ :

$$\begin{aligned} \dot{z} = V^T f(Uz_o, u_o) &+ V^T \frac{\partial f}{\partial x} U(z - z_o) + V^T \frac{\partial f}{\partial u}(u - u_o) + \\ &\frac{1}{2} \left( V^T \frac{\partial^2 f}{\partial^2 x} U \otimes U \right) (z - z_o) \otimes (z - z_o) + \dots, \end{aligned} \quad (17)$$



Observe that this expansion in equation (17) is equivalent to the Taylor series expansion of the function given as follows:

$$f^r(z, u) \equiv V^T f(Uz, u), \quad (18)$$

with respect to reduced state  $z$  and input  $u$  upto some order as in equation (16). In the cases treated in this thesis we carried out a Taylor series expansion of our voltage signals  $V(x, t)$  and  $W(x, t)$  up to the fourth order.

Nonlinear reduction based on Taylor series has the following advantages and limitations:

- The use of Taylor series limits the applicability of the reduction to only weakly nonlinear dynamical systems. It is directly applicable to quadratic systems.
- Quite often in this method the original system's Jacobian and higher-order derivatives are sparse. Consequently, memory and computational cost impose severe constraints on the reduced order of the system, making large reduced models not practical.
- There is no global guarantee of stability of the reduced system. In general, that is no error bounds are guaranteed. Local stability can be established based on the linearization around equilibrium.

## II.3 Perturbation Theory and the Reductive Perturbation Method

The KdV, NLS and SG equations and several others are exactly integrable nonlinear equations that play an outstanding role in physical problems. These equations are so important because they furnish universal mathematical models for some very general physical phenomena.

All perturbations can be naturally divided into two classes: Hamiltonian and dissipative. If a Hamiltonian perturbation does not depend explicitly on time and spatial coordinates, the perturbed equations conserve energy and momentum.

In most perturbations, the perturbing terms are assumed to be small. The corresponding perturbed equations are called nearly integrable systems. We will spend most of what follows discussing the effects produced by small integrable perturbations added to integrable equations, principally the KdV equation. We will recall that the most remarkable property of exact integrable equations is the presence of exact solitonic solutions. The existence of a one-soliton solution is not itself a specific property of integrable partial differential equations; many nonintegrable equations also possess simple localized solutions that may be called one-solitonic. In most cases many solitons solutions describe purely elastic interactions between individual solitons.

Perturbation induced effects are of interest mainly because they represent physical phenomena that cannot be comprised by exactly integrable models. In this connection, nearly integrable systems are of special concern, as perturbation-induced effects in those systems may be treated analytically.

Perturbation methods in nonlinear dynamics had been developed since the 19<sup>th</sup> century. Several perturbation schemes have been suggested in the problem of nonlinearities. These methods are now considered to be standard tools for the analytical investigations of dynamical systems. In such methods expansion of the system variables in terms of small parameter  $\epsilon$  as  $P = P_0 + \epsilon P_1 + \epsilon^2 P_2 + \dots$ , is used, where  $P_0$  is the unperturbed quantity for a variable  $P$ . Gardner and Morikawa introduced some scale transformations in terms of  $\epsilon$ , whereby Reductive Perturbation Method (RPM) is developed. Such perturbation method has been used continuously over the last several decades to derive popularly famous evolution equations like the KdV equation, NLS equation, KdV-Burger's equation, ZK equations etc.

Direct perturbation theory was first developed by Ostrovskii et al.. A basis for the application of direct perturbation theory to the perturbed SG equation has been long elaborated by Fogel et al.. The most powerful perturbative technique is based on the

IST. This technique requires the unperturbed equation to be exactly solvable by the IST, which restrict the range of applications, but enables one to solve the most sophisticated dynamical problems.

The general procedure of perturbation theory is to identify a parameter  $\epsilon$  such that the solution of the given problem is constructed as a power series of  $\epsilon$  around  $\epsilon_0$  value at which limit the problem becomes solvable, i.e., very often the system is reduced to an integrable system. The perturbation theory results are useful in the study of solutions in all the situations when the spectral problem is not turnable into an algebraic one. Conversely, certain features of the dynamics of integrable and nonintegrable systems need not an explicit solution to be enlightened as they appear only in specific asymptotic regimes. The description of these regimes is the subject of the so called reductive perturbation method, a method which reduces the system under study to a more tractable and solvable system.

### II.3.1 Reductive Perturbation Method

The RPM method is a very important way of deriving simplified models describing nonlinear wave propagation and interaction. This method is intimately related to plasma wave theory. The RPM method has been applied in [123, 124] and many others. The RPM method is mostly applied to small amplitudes nonlinear waves.

To apply this method, the stretched variables  $\xi$  and  $\tau$  are introduced as follows:

$$\xi = \epsilon^\alpha(x - \nu t), \quad (19)$$

$$\tau = \epsilon^{\alpha+1}t, \quad (20)$$

where  $\epsilon (\ll 1)$  is the small parameter characterizing the strength of the nonlinearity,  $\nu$  is the phase velocity of the soliton signal and  $\alpha$  is an integer. Along with the stretching, expansion of the flow variables in terms of  $\epsilon$  is given by

$$P = P_0 + \epsilon P_1 + \epsilon^2 P_2 + \dots, \quad (21)$$

where  $P_o$  is the unperturbed quantity for a flow variable  $P$ . If we consider upto 2nd order perturbation terms, the complete nonlinearity is not incorporated in this method.

We will use a very simple one dimensional ion acoustic plasma wave mode to explain the RPM method. For ions we have

$$\frac{\partial n_i}{\partial t} + \frac{\partial}{\partial x}(n_i v_i) = 0, \quad (22)$$

$$\frac{\partial n_i}{\partial t} + v_i \frac{\partial n_i}{\partial x} = -\frac{\partial \phi}{\partial x}, \quad (23)$$

where  $n_i$ ,  $n_e$ , and  $v_i$  are ion density, electron density and velocity of ions respectively. For electrons,  $n_e = e^\phi$ , and the Poisson equation

$$\frac{\partial^2 \phi}{\partial x^2} = n_e - n_i, \quad (24)$$

is used to close the model of plasma wave. Our perturbation scheme for  $n_i$ ,  $v_i$  and  $\phi$  are defined as follows:

$$\begin{aligned} n_i &= 1 + \epsilon n_{i,1} + \epsilon^2 n_{i,2} + \epsilon^3 n_{i,3} + \dots \\ v_i &= \epsilon v_{i,1} + \epsilon^2 v_{i,2} + \epsilon^3 v_{i,3} + \dots \\ \phi_i &= \epsilon \phi_{i,1} + \epsilon^2 \phi_{i,2} + \epsilon^3 \phi_{i,3} + \dots, \end{aligned} \quad (25)$$

By using the stretched coordinates;  $\xi = x - \nu t$ ,  $\tau = \epsilon \nu t$ , where  $\nu$  is the phase velocity of the soliton and substituting equation (25) into equations (22), (23), and (24), the lowest order equations in  $\epsilon$  are obtained as:

$$\begin{aligned} n_{i,1} &= \phi_1, & \frac{\partial n_{i,1}}{\partial \xi} &= \frac{\partial v_{i,1}}{\partial \xi}, & \frac{\partial v_{i,1}}{\partial \xi} &= \frac{\partial \phi_1}{\partial \xi}, \\ \Rightarrow n_{i,1} &= \phi_1 = v_{i,1}. \end{aligned} \quad (26)$$

Next,  $\mathcal{O}(\epsilon^2)$ , gives the following equations:

$$\begin{aligned}\frac{\partial n_{i,2}}{\partial \xi} &= \frac{\partial}{\partial \xi}(n_{i,1}v_{i,1}) + \frac{\partial n_{i,1}}{\partial \tau} + \frac{\partial v_{i,2}}{\partial \xi}, \\ \frac{\partial v_{i,2}}{\partial \xi} &= v_{i,1}\frac{\partial v_{i,1}}{\partial \xi} + \frac{\partial v_{i,1}}{\partial \tau} + \frac{\partial \phi_2}{\partial \xi}, \\ \frac{\partial^2 \phi_1}{\partial \xi^2} &= \phi_2 + \frac{\phi_1^2}{2} - n_{i,2}.\end{aligned}\tag{27}$$

By eliminating  $n_{i,2}, v_{i,2}$  from equation (27) and making use of equation (26), we finally get the KdV equation:

$$\frac{\partial \phi_1}{\partial \tau} + B\phi_1\frac{\partial \phi_1}{\partial \xi} + A\frac{\partial^3 \phi_1}{\partial \xi^3} = 0,\tag{28}$$

where  $A$  and  $B$  are nonzero real values,  $\phi_1$  is the dependent variable and  $\tau, \epsilon$  are the independent variables.

### II.3.2 The Method of Multiple Scales

Some natural processes have more than one characteristic length or time scales associated with them, for example, the turbulent flow consist of various length scales of the turbulent eddies along with the length scales of the objects over which the fluid flows. The failure to recognize a dependence on more than one space/time scale is a common source of nonuniformity in perturbation expansions.

The MMS method was proposed by Zakharov and Kuznetsov to reduce the KdV equation into the NLS equation and apply to a class of nonlinear evolution equations. They showed that using this method, conventionally employed in the theory of nonlinear waves, integrable systems are reduced to other integrable systems. If the initial system is nonintegrable, the result can be either integrable or nonintegrable. But if we treat an integrable system properly, we must always get an integrable system as a result of our analysis. This is the main purpose in the application of the method to integrable systems.

A first close link between multiscale expansions and integrable equations comes from the physical situations in which the latter arise. Let us consider the KdV equation in hydrodynamics: the formation of solitons assumes relations to be satisfied between the

amplitude of the solitary waves, their lengths, the canal depth and the propagation distance. All these quantities are lengths, whose order of magnitude differ, but are no way arbitrary. From the physical nature of this phenomenon itself, we have multiple scales. The formation of a soliton occurs only if some relations are satisfied between these orders of magnitude, and between them and that of the wave amplitude.

The MMS method comprises techniques used to construct uniformly valid approximations to the solutions of perturbation problems in which the solutions depend simultaneously on widely different scales. This is done by introducing fast-scale and slow-scale variables for an independent variable, and subsequently treating these variables, fast and slow, as if they are independent. The MMS method is a more general approach that involves two key tricks. The first is the idea of introducing scaled space and time coordinates to capture the slow modulations of the pattern, and treating these as separate variables in addition to the original variables that must be retained to describe the pattern state itself. The second is the use of what are known as solvability conditions in the formal derivation.

The formalization of the multiple scales involves the introduction of small perturbation parameter  $\epsilon$ , so that the orders of magnitude of the various effects are determined by means of their order in an expansion in a series of powers of  $\epsilon$ . This induces homogeneity properties of the mathematical expressions considered. Therefore, the model equations which are derived this way must satisfy these homogeneity properties: the number of possible equations is hence small. Consequently, a few equations are shown to account for analogous phenomena in many very different domains of physics.

### **II.3.3 Nonlinear Evolution Equations**

The Method of Multiple Scales (MMS) or its cousin called the Reductive Perturbation Method (RPM) are commonly used to derive nonlinear evolution equations. Precisely the MMS allows a perturbation solution to a problem by addressing the problem on appropriate time and distance scales. In this framework the relevant dispersive and

nonlinear effects become apparent. MMS derivation for propagation of signals in optical fibres can be found in [125].

Boyd in, said that these methods are justification for inverse scattering in the sense that, so many physical systems reducible to either KdV and NLS equations would be mathematically curios. Such is the universality of the KdV and NLS equations, Leroy wrote two companion papers entitled "Nonlinear Evolution Equations without Magic", to dispel the almost "magical" way they appear in many problems. The number of different applications of these equations is testament to the fact that nonlinear dispersive systems all behave in a similar manner, regardless of the particular physical manifestation.

Note that the KdV and NLS equations are not complete descriptions of any real system, but multiple scales and reductive perturbations are convenient ways of reducing complex nonlinear problems to equations which are ideally soluble.

## II.4 The Runge Kutta Method

Numerical techniques, such as the Bulirsch-Stoer or Runge-Kutta methods [126, 127], have been used to solve the wave equation for the nonlinear circuits. The Runge-Kutta method is more efficient than the Bulirsch-Stoer method for very sharp rise times due to its simpler step calculation.

Runge-Kutta methods are single-step methods with multiple stages per step. They are motivated by the dependence of the Taylor methods on the specific initial value problem. Runge-Kutta methods are among the most popular ordinary differential equation solvers. They were first studied by Carle Runge and Martin Kutta around 1900. Modern developments are mostly due to John Butcher in the 1960s.

The Runge-Kutta method treats every step in a sequence of steps in identical manner. Prior behavior of a solution is not used in its propagation. This is mathematically proper, since any point along the trajectory of an ordinary differential equation can serve as an initial point. The fact that all steps are treated identically also makes it easy to incorporate Runge-Kutta into relatively simple "driver" schemes.

Lets consider the following system of ordinary differential equations:

$$\frac{dy}{dx} = f(x, y), \quad y(x_o) = y_o, \quad (29)$$

where  $y(x)$  and  $f(x, y)$  are vector-valued functions given by

$$y(x) = (y_1(x), y_2(x), \dots, y_m(x)), \quad (30)$$

$$f(x, y) = (f_1(x, y), f_1(x, y), \dots, f_m(x, y)). \quad (31)$$

This means we now have  $m$  simultaneous first-order equations. By Runge-Kutta process we mean numerically solving the differential equation (29) at the point  $x = x_o + h$ , where  $h$  is the stepsize of our solution. The equations defining a  $\nu$  stage Runge-Kutta process are given by:

$$\begin{aligned} g_1 &= f(x_o, y_o), \\ g_2 &= F(x_o + c_2h, y_o + ha_{21}g_1), \\ g_3 &= F(x_o + c_3h, y_o + h(a_{31}g_1 + a_{32}g_2)), \\ &\vdots \quad \quad \quad \vdots \\ g_\nu &= F(x_o + c_\nu h, y_o + h(a_{\nu 1}g_1 + a_{\nu 2}g_2 + \dots + a_{\nu, \nu-1}g_{\nu-1})), \end{aligned} \quad (32)$$

where

$$\begin{aligned} c_2 &= a_{21}, \\ c_3 &= a_{31} + a_{32}, \\ &\vdots \quad \quad \quad \vdots \\ c_\nu &= a_{\nu 1} + a_{\nu 2} + \dots + a_{\nu, \nu-1}, \end{aligned} \quad (33)$$

and  $a_{21}, a_{31}, a_{32}, \dots, a_{\nu, \nu-1}, b_1, b_2, \dots, b_\nu$  are a set of parameters which characterize the process [128].



For the interval  $[x_n, x_n + h]$ , Lobatto quadrature points leading to a remainder of order eight are [137]:

$$x_n, \quad x_n + h/2, \quad x_n + (7 - (21)^{1/2})h/14, \quad (7 - (21)^{1/2})h/14, \quad x_n + h. \quad (34)$$

The Runge-Kutta formulas related to these quadrature point for  $\nu = 1$  are:

$$k_1 = hf(x_n, y_n), \quad (35)$$

$$k_2 = hf(x_n + h, y_n + k_1), \quad (36)$$

$$k_3 = hf(x_n + h/2, y_n + \{3k_1 + k_2\}/8), \quad (37)$$

$$k_4 = hf(x_n + 2h/3, y_n + \{8k_1 + 2k_2 + 8k_3\}/27), \quad (38)$$

$$k_5 = hf(x_n + (7 - (21)^{1/2})h/14, y_n + \{3(3(21)^{1/2} - 7)k_1 - 8(7 - (21)^{1/2})k_2 + 48(7 - (21)^{1/2})k_3 - 3(21 - (21)^{1/2})k_4\}/392), \quad (39)$$

$$k_6 = hf(x_n + (7 + (21)^{1/2})h/14, y_n + \{-5(231 + 51(21)^{1/2})k_1 - 40(7 + (21)^{1/2})k_2 - 320(21)^{1/2}k_3 + 3(21 + 121(21)^{1/2})k_4 + 392(6 + (21)^{1/2})k_5\}/1960), \quad (40)$$

$$k_7 = hf(x_n + h, y_n + \{15(22 + 7(21)^{1/2})k_1 + 120k_2 + 40(7(21)^{1/2} - 5)k_3 - 63(3(21)^{1/2} - 2)k_4 - 14(49 + 9(21)^{1/2})k_5 + 70(7 - (21)^{1/2})k_6\}/180), \quad (41)$$

and therefore

$$y_{n+1} = y_n + \{9k_1 + 64k_3 + 49k_5 + 49k_6 + 9k_7\}/180. \quad (42)$$

This sixth-order Runge-Kutta method is what we used in our numerical analysis in

this thesis.

## II.5 Models and Theoretical Analysis

NLTLs can be modeled with lumped elements by making the standard transmission line capacitance and inductance functions of voltage and current, respectively. The KdV equation may be solved numerically for NLTLs comprised of nonlinear capacitors with linear inductors [90], nonlinear inductors with linear capacitors [129], and hybrid line configuration with nonlinear capacitors and nonlinear inductors [130, 131]. The output of nonlinear capacitive transmission lines use a decoupling capacitor to extract the AC signal, which is then applied to a load to allow for direct extraction [90].

### II.5.1 Coupled NLTLs with Coupling Shunt by Resistor

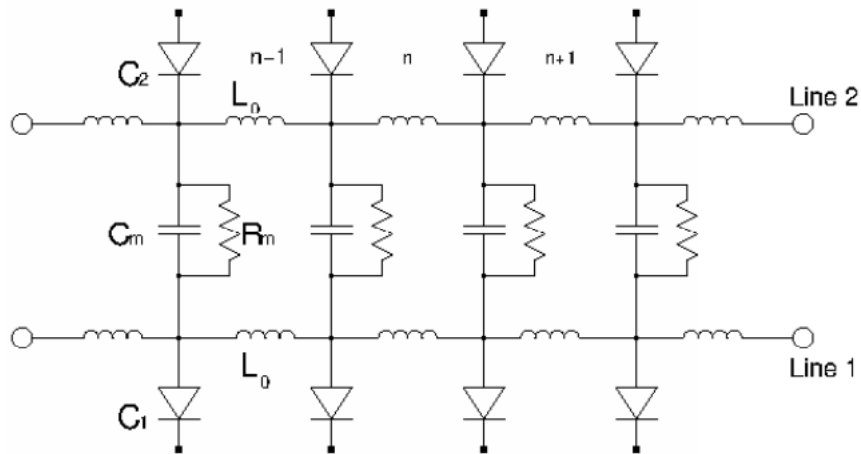


Figure 7: Equivalent representation of two nonlinear  $LC$  transmission lines, coupled by capacitor  $C_m$  with a resistance  $R_m$  in its shunt branch.

The electrical network formed by the two NLTLs considered in this study is depicted in figure (7). The two lines consist of periodic arrangements of identical  $LC$  circuit units, and corresponding sections in lines 1 and 2 are connected by intermediary linear capacitors  $C_m$  shunted by linear resistors  $R_m$ . Dispersion in this coupled NLTLs is achieved by the discrete nature of the lines, while nonlinearity is achieved by making use of the

conductive nonlinearity of varactors [132]. In reverse bias, varactors have a variable capacitance that depends on the applied reverse voltage. In our study we shall consider the case when the varactors in the two lines are connected with opposite polarities.

Let  $V_n$  and  $I_n$  denote the voltage and current respectively at node  $n$  of line 1, and  $W_n$  and  $J_n$  denote the voltage and current respectively at node  $n$  for line 2. The bias voltages in lines 1 and 2 are  $-V_b < 0$  and  $V_b$  respectively, reflecting the opposite polarities of the varactor diodes on the two lines. The capacitance-voltage characteristics for lines 1 and 2 shall assume the relations [21, 133]:

$$C_1(x) = C_o \left(1 - \frac{x}{V_J}\right)^{-m}, \quad (43)$$

$$C_2(x) = C_o \left(1 + \frac{x}{V_J}\right)^{-m}, \quad (44)$$

where  $C_o$  represents the zero bias junction capacitance,  $V_J$  is the junction potential, and  $m$  is a grading coefficient determined by the doping profile of the varactors [132, 133]. We note that except for the opposite polarities of the varactors the lines are symmetrical, this near symmetry turns out to be relevant, for it favours electrical pulses at almost equal velocities to travel on the lines as a bound state.

Applying KVL in the  $n$ th cell of lines 1 and 2, we have:

$$L_o \frac{dI_n}{dt} = V_{n-1} - V_n, \quad (45)$$

$$L_o \frac{dJ_n}{dt} = W_{n-1} - W_n. \quad (46)$$

Similarly applying KVL in the  $(n + 1)$ th cell of lines 1 and 2 and comparing the equations obtained to equations (45) and (46) gives

$$L_o \frac{d}{dt}(I_n - I_{n+1}) = V_{n-1} - 2V_n + V_{n+1}, \quad (47)$$

$$L_o \frac{d}{dt}(J_n - J_{n+1}) = W_{n-1} - 2W_n + W_{n+1}. \quad (48)$$

KCL applied to node  $n$  of lines 1 and 2 results in the following two coupled transmission line equations:

$$I_n - I_{n+1} = C_1(V_n - V_b) \frac{dV_n}{dt} + C_m \frac{d}{dt}(V_n - W_n) + \frac{1}{R_m}(V_n - W_n), \quad (49)$$

$$J_n - J_{n+1} = C_2(W_n + V_b) \frac{dW_n}{dt} + C_m \frac{d}{dt}(W_n - V_n) + \frac{1}{R_m}(W_n - V_n). \quad (50)$$

By substituting equation (47) into equation (49) and equation (48) into equation (50) respectively we get:

$$\frac{d}{dt} \left[ C_1(V_n - V_b) \frac{dV_n}{dt} \right] + C_m \frac{d^2}{dt^2}(V_n - W_n) + \frac{1}{R_m} \frac{d}{dt}(V_n - W_n) = \frac{1}{L_o}(V_{n-1} - 2V_n + V_{n+1}), \quad (51)$$

$$\frac{d}{dt} \left[ C_2(W_n + V_b) \frac{dW_n}{dt} \right] + C_m \frac{d^2}{dt^2}(W_n - V_n) + \frac{1}{R_m} \frac{d}{dt}(W_n - V_n) = \frac{1}{L_o}(W_{n-1} - 2W_n + W_{n+1}). \quad (52)$$

For convenience, we define

$$C_b \equiv C_o \left( 1 + \frac{V_b}{V_J} \right)^{-m}. \quad (53)$$

A Lagrangian  $L_a$  for equations (45) to (52) can be given by [21]:

$$\begin{aligned} L_a = \sum_n \left[ \frac{L_o}{2} (\dot{Q}_{1,n}^2 + \dot{Q}_{2,n}^2) + \int^{\dot{P}_{1,n}^2} dx \int^x dy C_1(y - V_b) + \right. \\ \left. + \int^{\dot{P}_{2,n}^2} dx \int^x dy C_2(-y + V_b) + \frac{C_m}{2} (\dot{P}_{1,n} - \dot{P}_{2,n})^2 + \right. \\ \left. + \dot{Q}_{1,n}(P_{1,n} - P_{1,n-1}) + \dot{Q}_{2,n}(P_{2,n} - P_{2,n-1}) + \right], \quad (54) \end{aligned}$$

where

$$\dot{P}_{j,n} \left( \equiv \frac{dP_{j,n}}{dt} \right) \quad \text{and} \quad \dot{Q}_{j,n} \left( \equiv \frac{dQ_{j,n}}{dt} \right),$$

represents the voltage and current at the  $n$ th cell of line  $j$ , respectively.

In the long-wavelength limit, when wave phenomena associated with voltage and current propagation along the two lines are dominated by wave structures of wavelengths far larger than the size  $h$  of an electric cell, we can readily approximate the discrete position  $n$  by a continuous position variable  $x = nh$ . In this continuous regime, the discrete voltages transform as  $V_n(t) \rightarrow V(x, t)$  and  $W_n(t) \rightarrow W(x, t)$  such that we can carry out a continuous-limit expansion in powers of  $h$ , for the two quantities  $V_{n\pm 1}(t) = V(x \pm h, t)$  and  $W_{n\pm 1}(t) = W(x \pm h, t)$ . To the fourth order in  $h$  the expansion yields:

$$V_{n\pm 1}(t) = V(x, t) \pm h \frac{\partial V}{\partial x} + \frac{h^2}{2!} \frac{\partial^2 V}{\partial x^2} \pm \frac{h^3}{3!} \frac{\partial^3 V}{\partial x^3} + \frac{h^4}{4!} \frac{\partial^4 V}{\partial x^4} + \mathcal{O}(h^5), \quad (55)$$

$$W_{n\pm 1}(t) = W(x, t) \pm h \frac{\partial W}{\partial x} + \frac{h^2}{2!} \frac{\partial^2 W}{\partial x^2} \pm \frac{h^3}{3!} \frac{\partial^3 W}{\partial x^3} + \frac{h^4}{4!} \frac{\partial^4 W}{\partial x^4} + \mathcal{O}(h^5). \quad (56)$$

Setting  $h \equiv 1$  for simplicity, equations (51) and (52) becomes:

$$\begin{aligned} C_1(V) \frac{\partial^2 V}{\partial t^2} + C_m \frac{\partial^2}{\partial t^2} (V - W) + \frac{1}{R_m} \frac{\partial}{\partial t} (V - W) + \frac{dC_1(V)}{dV} \left( \frac{\partial V}{\partial t} \right)^2 = \\ = \frac{1}{L_o} \left( \frac{\partial^2 V}{\partial x^2} + \frac{\partial^4 V}{\partial x^4} \right), \end{aligned} \quad (57)$$

$$\begin{aligned} C_2(W) \frac{\partial^2 W}{\partial t^2} + C_m \frac{\partial^2}{\partial t^2} (W - V) + \frac{1}{R_m} \frac{\partial}{\partial t} (W - V) + \frac{dC_2(W)}{dW} \left( \frac{\partial W}{\partial t} \right)^2 = \\ = \frac{1}{L_o} \left( \frac{\partial^2 W}{\partial x^2} + \frac{\partial^4 W}{\partial x^4} \right). \end{aligned} \quad (58)$$

As we are interested in localized electrical solitons with a pulse shape, we follow a standard approach by applying the Reductive Perturbation Methodology [19] in order

to obtain coupled KdV equations governing their spatiotemporal evolutions. We now introduce a small parameter  $\epsilon$  and define new variables:

$$s = \epsilon^{1/2}(x - \eta_1 t), \quad (59)$$

$$\tau = \epsilon^{3/2}t, \quad (60)$$

with  $\eta_1^{-2} = L_o C_b$ , and  $C_b = C(-V_b)$ . The voltages  $V$  and  $W$  are expressed as perturbation series in powers of  $\epsilon$  as :

$$V(s, \tau) = -V_b + \sum_{i=1}^{\infty} \epsilon^i V_i(s, \tau), \quad (61)$$

$$W(s, \tau) = V_b + \sum_{i=1}^{\infty} \epsilon^i W_i(s, \tau). \quad (62)$$

To conform to the weak-coupling assumption for the two coupled lines, the coupling capacitance  $C_m$  and resistance  $R_m$  must be of the order of  $\epsilon$ , and define as:

$$C_m = \epsilon C, \quad (63)$$

$$R_m = \epsilon^{-3/2} R. \quad (64)$$

By using equations (59), (60), (61), (62), (63) and (64) we get the following expression for the terms in equation (57).

$$C_1(V) \frac{\partial^2 V}{\partial t^2} = \alpha_1 C_o \left( \epsilon^2 \eta_1^2 \frac{\partial^2 V_1}{\partial s^2} + \epsilon^3 \eta_1^2 \frac{\partial^2 V_2}{\partial s^2} - 2\epsilon^3 \eta_1 \frac{\partial^2 V_1}{\partial s \partial \tau} \right) + \alpha C_o \epsilon^3 \eta_1^2 V_1 \frac{\partial^2 V_1}{\partial s^2}, \quad (65)$$

$$\left( \frac{\partial V}{\partial t} \right)^2 = \epsilon^3 \eta_1^2 \left( \frac{\partial V_1}{\partial s} \right)^2, \quad (66)$$

$$C_m \frac{\partial^2}{\partial t^2} (V - W) = \epsilon^3 \eta_1^2 C \frac{\partial^2}{\partial s^2} (V_1 - W_1), \quad (67)$$

$$\frac{1}{R_m} \frac{\partial}{\partial t} (V - W) = -\frac{1}{R_1} \epsilon^3 \eta_1 \frac{\partial}{\partial s} (V_1 - W_1), \quad (68)$$

where  $\alpha = m/V_J$ ,  $\alpha_1 = (1 - \alpha V_b)$ . The corresponding equations for expressions in equation (58) are gotten by replacing  $V$  with  $W$  and  $W$  with  $V$  in equations (65), (66), (67) and (68). Substituting equations (65)-(68) into equations (57) and (58) and keeping only terms of order  $\epsilon^3$ , for which nonlinearity balances dispersion, we obtain the following equations:

$$-2\eta_1 \alpha_1 C_o \frac{\partial^2 V_1}{\partial s \partial \tau} + \alpha C_o \eta_1^2 \frac{\partial}{\partial s} \left( V_1 \frac{\partial V_1}{\partial s} \right) + \eta_1^2 C \frac{\partial^2}{\partial s^2} (V_1 - W_1) - \frac{\eta_1}{R_1} \frac{\partial}{\partial s} (V_1 - W_1) - \frac{1}{12L_o} \frac{\partial^4 V_1}{\partial s^4} = 0, \quad (69)$$

and

$$-2\eta_1 \alpha_1 C_o \frac{\partial^2 W_1}{\partial s \partial \tau} + \alpha C_o \eta_1^2 \frac{\partial}{\partial s} \left( W_1 \frac{\partial W_1}{\partial s} \right) + \eta_1^2 C \frac{\partial^2}{\partial s^2} (W_1 - V_1) - \frac{\eta_1}{R_1} \frac{\partial}{\partial s} (W_1 - V_1) - \frac{1}{12L_o} \frac{\partial^4 W_1}{\partial s^4} = 0. \quad (70)$$

Integrating equations (69) and (70) once with respect to  $s$  we gets

$$-2\eta_1 \alpha_1 \frac{\partial V_1}{\partial \tau} - \alpha \eta_1^2 V_1 \frac{\partial V_1}{\partial s} + \frac{1}{12C_o L_o} \frac{\partial^3 V_1}{\partial s^3} = \frac{\eta_1^2 C}{C_o} \frac{\partial}{\partial s} (V_1 - W_1) - \frac{\eta_1}{R_1 C_o} (V_1 - W_1), \quad (71)$$

and

$$-2\eta_1 \alpha_1 \frac{\partial W_1}{\partial \tau} - \alpha \eta_1^2 W_1 \frac{\partial W_1}{\partial s} + \frac{1}{12C_o L_o} \frac{\partial^3 W_1}{\partial s^3} = \frac{\eta_1^2 C}{C_o} \frac{\partial}{\partial s} (W_1 - V_1) - \frac{\eta_1}{R_1 C_o} (W_1 - V_1). \quad (72)$$

We now carry out a rescaling of the variables  $s$ ,  $\tau$ ,  $V_1$  and  $W_1$  in equations (71) and (72) as follows:

$$\tau' = \frac{1}{2\eta_1\alpha_1}\tau, \quad (73)$$

$$s' = \sqrt[3]{12C_oL_o}s, \quad (74)$$

$$V' = \frac{1}{6}\alpha\eta_1^2\sqrt[3]{12C_oL_o}V_1, \quad (75)$$

$$W' = -\frac{1}{6}\alpha\eta_1^2\sqrt[3]{12C_oL_o}W_1, \quad (76)$$

we obtain the following coupled KdV equations:

$$\frac{\partial V'}{\partial \tau'} - 6V' \frac{\partial V'}{\partial s'} + \frac{\partial^3 V'}{\partial s'^3} = D_1 \frac{\partial}{\partial s'}(V' + W') - D_2(V' + W'), \quad (77)$$

and

$$\frac{\partial W'}{\partial \tau'} - 6W' \frac{\partial W'}{\partial s'} + \frac{\partial^3 W'}{\partial s'^3} = D_1 \frac{\partial}{\partial s'}(W' + V') - D_2(W' + V'), \quad (78)$$

where

$$D_1 = \frac{\eta_1^2 C}{C_o} \sqrt[3]{12C_oL_o}, \quad (79)$$

and

$$D_2 = \frac{\eta_1}{R_1 C_o}. \quad (80)$$



## II.5.2 Coupled RLC NLTLS

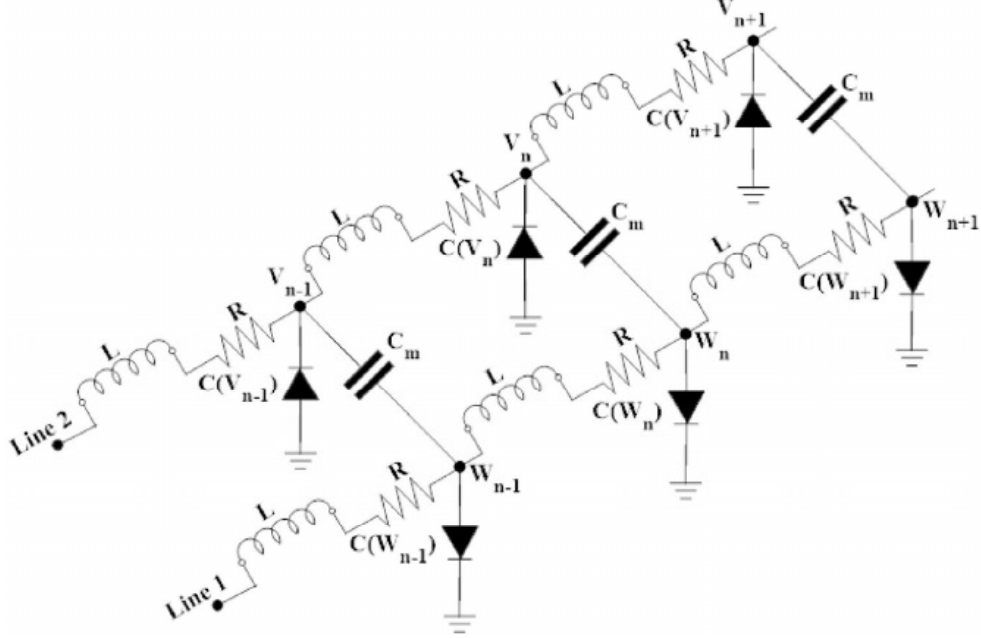


Figure 8: Equivalent representation of two nonlinear RLC transmission lines with Schottky-type in-line varactor  $C(V_n)$  coupled by linear capacitors  $C_m$ .

Consider the coupled NLTLS as shown in figure (8), where each elementary unit of a NLTLS consists of a linear inductor  $L$  in parallel with a nonlinear capacitor of capacitance  $C = C(V)$ . The two lines are coupled by means of linear capacitor  $C_m$  mode. The nonlinear capacitors are varactor diodes, and except for their opposite polarities in our study we shall use a common type of varactor diode with a Schottky barrier for both lines [21, 134]. Therefore our Schottky varactors can be defined by the same capacitance-voltage characteristics as in equations (43) and (44)

We assume that the bias voltages in lines 1 and 2 are  $-V_b$  and  $V_b$  respectively, reflecting the opposite polarities of the varactor diodes loaded on the two lines. For convenience we define:

$$C_b = C_o \left(1 + \frac{V_b}{V_J}\right)^{-m}, \quad (81)$$

an effective zero-bias capacitance which below turns out to be a relevant characteristic parameter.

## Line Equations and Coupled Dissipative KdV Equations

Applying Kirchhoff's rules on the two coupled electrical ladder circuits, we obtain the following sets of discrete transmission line equations:

$$L \frac{d}{dt}(J_{n-1} - J_n) + R(J_{n-1} - J_n) = W_{n-1} - 2W_n + W_{n+1}, \quad (82)$$

$$L \frac{d}{dt}(I_{n-1} - I_n) + R(I_{n-1} - I_n) = V_{n-1} - 2V_n + V_{n+1}, \quad (83)$$

$$J_{n-1} - J_n = \frac{dQ_n}{dt} + Cm \frac{d}{dt}(W_n - V_n), \quad (84)$$

$$I_{n-1} - I_n = \frac{dq_n}{dt} + Cm \frac{d}{dt}(V_n - W_n). \quad (85)$$

In equations (82) to (85),  $W_n$  and  $J_n$  are respectively the voltage and current of the  $n$ th section in line 1, while  $V_n$  and  $I_n$  are respectively the voltage and current of the  $n$ th section in line 2. In the continuum limit, when the size of the elementary sections in the circuits are very small compared to the length of the transmission lines, the right hand sides of equations (82) and (83) can readily be approximated with partial derivatives with respect to a continuum variable  $x = nl$ . This, more exactly, corresponds to the long-wavelength approximation which consists in Taylor expanding the discrete variables  $W_{n\pm 1}$  and  $V_{n\pm 1}$ , i.e.:

$$W_{n\pm 1} = W_n \pm \frac{\partial W}{\partial x} + \frac{1}{2} \frac{\partial^2 W}{\partial x^2} \pm \frac{1}{6} \frac{\partial^3 W}{\partial x^3} + \frac{1}{24} \frac{\partial^4 W}{\partial x^4} + \dots, \quad (86)$$

$$V_{n\pm 1} = V_n \pm \frac{\partial V}{\partial x} + \frac{1}{2} \frac{\partial^2 V}{\partial x^2} \pm \frac{1}{6} \frac{\partial^3 V}{\partial x^3} + \frac{1}{24} \frac{\partial^4 V}{\partial x^4} + \dots. \quad (87)$$

Also, from the definition

$$dQ_n = C(W_n)dW_n \quad \text{and} \quad dq_n = C(V_n)dV_n, \quad (88)$$

and setting  $\alpha_o = m/V_J$ , equations (82) to (85) now becomes:

$$LC_o \left( \frac{\partial^2 W}{\partial t^2} + \frac{\alpha_o}{2} \frac{\partial^2 W^2}{\partial t^2} \right) + LC_m \frac{\partial^2}{\partial t^2} (W - V) + RC_m \frac{\partial}{\partial t^2} (W - V) + \\ + RC_o \left( \frac{\partial W}{\partial t} + \frac{\alpha_o}{2} \frac{\partial W^2}{\partial t} \right) = \frac{\partial^2 W}{\partial x^2} + \frac{1}{12} \frac{\partial^4 W}{\partial x^4}, \quad (89)$$

$$LC_o \left( \frac{\partial^2 V}{\partial t^2} - \frac{\alpha_o}{2} \frac{\partial^2 V^2}{\partial t^2} \right) + LC_m \frac{\partial^2}{\partial t^2} (V - W) + RC_m \frac{\partial}{\partial t^2} (V - W) + \\ + RC_o \left( \frac{\partial V}{\partial t} - \frac{\alpha_o}{2} \frac{\partial V^2}{\partial t} \right) = \frac{\partial^2 V}{\partial x^2} + \frac{1}{12} \frac{\partial^4 V}{\partial x^4}. \quad (90)$$

Since we are interested in voltage signals with localized wave profile in space and time, it is useful to find approximate equations reproducing such structures. It is in this light that we choose the reductive perturbation method, in which the voltage variables  $W$  and  $V$  can be expanded in series according to:

$$W(x, t) = -V_b + \sum_{i=1}^n \epsilon^i W_i(x, t), \quad (91)$$

$$V(x, t) = V_b + \sum_{i=1}^n \epsilon^i V_i(x, t). \quad (92)$$

In addition to equations (91) and (92), we apply the following new transformations on the space and time variables, as well as on the resistance coefficient  $R$ :

$$z = \epsilon^{\frac{1}{2}} (x - \eta t), \quad (93)$$

$$\tau = \epsilon^{\frac{3}{2}} t, \quad (94)$$

$$R = \epsilon^{\frac{3}{2}} R_1, \quad (95)$$

where  $\eta = (LC_b)^{-1/2}$  with  $C_b$  defined as in equation (81). Furthermore, the coupling capacitance  $C_m$  must be of the order  $\epsilon$  [134], i.e. we should define  $C_m = \epsilon C$ . Substituting equations (91) to (95) into equations (89) and (90) and using the above transformation of

coupling capacitance, we obtain the following equations to the order  $\mathcal{O}(\epsilon^3)$ :

$$-\frac{2}{\eta} \frac{\partial^2 W_1}{\partial z \partial \tau} + \frac{\alpha_o C_o}{2C_b} \frac{\partial^2 W_1^2}{\partial z^2} + \frac{C}{C_b} \frac{\partial^2}{\partial z^2} (W_1 - V_1) - R_1 C_b \eta \frac{\partial W_1}{\partial z} = \frac{1}{12} \frac{\partial^4 W_1}{\partial z^4}, \quad (96)$$

$$-\frac{2}{\eta} \frac{\partial^2 V_1}{\partial z \partial \tau} - \frac{\alpha_o C_o}{2C_b} \frac{\partial^2 V_1^2}{\partial z^2} + \frac{C}{C_b} \frac{\partial^2}{\partial z^2} (V_1 - W_1) - R_1 C_b \eta \frac{\partial V_1}{\partial z} = \frac{1}{12} \frac{\partial^4 V_1}{\partial z^4}, \quad (97)$$

with  $\alpha_o = \alpha$ , which was defined earlier in section II.5.1.

By integration of equations (96) and (97) once with respect to  $z$ , and scaling  $W_1, V_1, \tau$ , and  $z$  as

$$W_1 = \frac{6\gamma C_b}{\alpha_o C_o} \psi, \quad (98)$$

$$V_1 = -\frac{6\gamma C_b}{\alpha_o C_o} \phi, \quad (99)$$

$$\tau = \frac{2}{\eta} T, \quad (100)$$

$$z = \gamma u, \quad (101)$$

where  $\gamma = 1/\sqrt[3]{12}$ , we find that

$$\frac{\partial \psi}{\partial T} - 6\psi \frac{\partial \psi}{\partial u} + \frac{\partial^3 \psi}{\partial u^3} = P_1(u, T), \quad (102)$$

$$\frac{\partial \phi}{\partial T} - 6\phi \frac{\partial \phi}{\partial u} + \frac{\partial^3 \phi}{\partial u^3} = P_2(u, T). \quad (103)$$

Equations (102) and (103) describes two coupled KdV equations, in which the quantities  $P_i(u, T)$ ,  $i = 1, 2$  grouping the coupling and the resistive terms play roles of perturbations, and are defined as:

$$P_1(u, T) = \frac{C}{\gamma C_b} \frac{\partial}{\partial u} (\psi + \phi) - R_1 C_b \eta \psi, \quad (104)$$

$$P_2(u, T) = \frac{C}{\gamma C_b} \frac{\partial}{\partial u} (\phi + \psi) - R_1 C_b \eta \phi. \quad (105)$$

When  $P_i(u, T) = 0$ ,  $i = 1, 2$  our equations (102) and (103) reduces to two homogeneous

KdV equations of the form:

$$\frac{\partial \psi}{\partial T} - 6\psi \frac{\partial \psi}{\partial u} + \frac{\partial^3 \psi}{\partial u^3} = 0, \quad (106)$$

$$\frac{\partial \phi}{\partial T} - 6\phi \frac{\partial \phi}{\partial u} + \frac{\partial^3 \phi}{\partial u^3} = 0. \quad (107)$$

Equations (106) and (107) admit the following one-soliton solutions:

$$\psi = -2\kappa_1^2 \operatorname{sech}^2 y_1, \quad (108)$$

$$\phi = -2\kappa_2^2 \operatorname{sech}^2 y_2, \quad (109)$$

where

$$y_1 = \kappa_1(u - \theta_1), \quad \theta_1 = 4\kappa_1^2 T, \quad (110)$$

$$y_2 = \kappa_2(u - \theta_2), \quad \theta_2 = 4\kappa_2^2 T. \quad (111)$$

In the original coordinates the one-soliton solution in equations (108) and (109) can be written as:

$$W(x, t) = -\frac{3D_1(V_J + mV_b)}{\sqrt[3]{12m}} \operatorname{sech}^2 \left( \sqrt{\frac{D_1}{4\gamma^2}} (x - \eta(1 + \frac{1}{2}\gamma D_1)t) \right), \quad (112)$$

$$V(x, t) = \frac{3D_2(V_J + mV_b)}{\sqrt[3]{12m}} \operatorname{sech}^2 \left( \sqrt{\frac{D_2}{4\gamma^2}} (x - \eta(1 + \frac{1}{2}\gamma D_2)t) \right), \quad (113)$$

with  $D_1 = 4\epsilon\kappa_1^2$  and  $D_2 = 4\epsilon\kappa_2^2$ .

### II.5.3 Coupled LC NLTLs

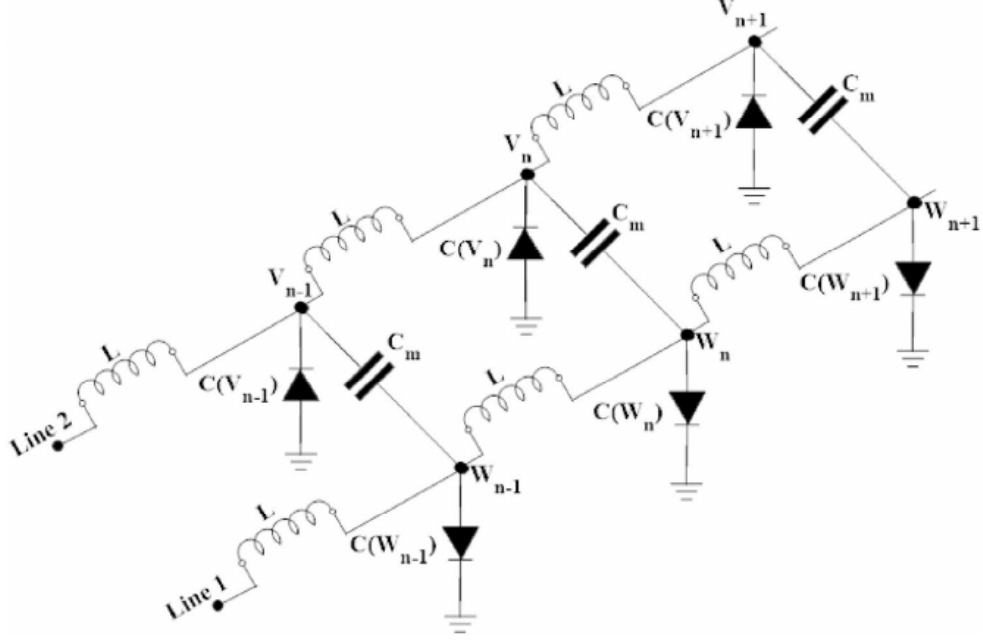


Figure 9: Equivalent circuit model of coupled NLTLs. The capacitance at the  $n$ th cell is given by  $C(V_n)$ .

We will now consider two coupled NLTLs without intraline resistance as depicted in figure (9). This model was studied in [21], with emphasis on conditions under which soliton leapfrogging is expected.

In this model we are interested in the evolution of leapfrogging solitons in the electrical transmission network of figure (9), when one Schottky diode in line 1 is defective. Mathematically, we model the defect by an impurity in the feedback part of the diode localized at position  $x = x_o$  on the NLTL 1. Using a  $\delta$  function to represent the localized impurity, the capacitances of the two varactors can be expressed as:

$$C_1(W) = C_o \left( 1 - \frac{1}{V_J} (1 - \beta \delta(x - x_o) W) \right)^{-m}, \quad (114)$$

$$C_2(V) = C_o \left( 1 + \frac{1}{V_J} V \right)^{-m}, \quad (115)$$

where the impurity rate  $\beta$  is assumed positive and  $0 \leq \beta \leq 1$ . For convenience, we have

set the bias voltage  $V_b$  to zero and hence  $C_b = C_o$ . Also let

$$\alpha_1 = \frac{\alpha_o}{2}(1 - \beta\delta(x - x_o)). \quad (116)$$

### Line Equations and Coupled KdV equations

Applying Kirchhoff's rules on the two coupled electrical ladder circuits, we obtained the following sets of discrete transmission line equations:

$$L \frac{d}{dt}(J_{n-1} - J_n) = W_{n-1} - 2W_n + W_{n+1}, \quad (117)$$

$$L \frac{d}{dt}(I_{n-1} - I_n) = V_{n-1} - 2V_n + V_{n+1}, \quad (118)$$

$$J_{n-1} - J_n = \frac{dQ_n}{dt} + Cm \frac{d}{dt}(W_n - V_n), \quad (119)$$

$$I_{n-1} - I_n = \frac{dq_n}{dt} + Cm \frac{d}{dt}(V_n - W_n). \quad (120)$$

Again in the continuum limit, the right side of equations (117) and (120) are approximated with partial derivatives with respect to  $x$ . From  $dQ_n = C(W_n)dW_n$  and  $dq_n = C(V_n)dV_n$  equations (117) to (120) reduces to:

$$LC_o \left( \frac{\partial^2 W}{\partial t^2} + \alpha_1 \frac{\partial^2 W^2}{\partial t^2} \right) + LC_m \frac{\partial^2}{\partial t^2}(W - V) = \frac{\partial^2 W}{\partial x^2} + \frac{1}{12} \frac{\partial^4 W}{\partial x^4}, \quad (121)$$

$$LC_o \left( \frac{\partial^2 V}{\partial t^2} - \frac{\alpha_o}{2} \frac{\partial^2 V^2}{\partial t^2} \right) + LC_m \frac{\partial^2}{\partial t^2}(V - W) = \frac{\partial^2 V}{\partial x^2} + \frac{1}{12} \frac{\partial^4 V}{\partial x^4}. \quad (122)$$

We series expand the voltage variables  $W$  and  $V$ , i.e.:

$$W(x, t) = \sum_{i=1}^n \epsilon^i W_i(x, t), \quad (123)$$

$$V(x, t) = \sum_{i=1}^n \epsilon^i V_i(x, t). \quad (124)$$

In addition to transformations introduced in equation (94), we apply the following transformation on the space coordinate:

$$z = \epsilon^{\frac{1}{2}}(x - \eta_o t), \quad (125)$$

where  $\eta_o = (LC_o)^{-1/2}$ . Substituting equations (123) to (125) into equations (121) and (122) and integrating once with respect to  $z$ , we obtain the following equations to the other  $\mathcal{O}(\epsilon^3)$ :

$$\begin{aligned} \frac{2}{\eta} \frac{\partial W_1}{\partial \tau} - \alpha_o W_1 \frac{\partial W_1}{\partial z} + \frac{1}{12} \frac{\partial^3 W_1}{\partial z^3} &= \frac{C}{C_o} \frac{\partial}{\partial z} (W_1 - V_1) - \\ &- \frac{\alpha_o \beta}{2} \int \delta(z - z_o) \frac{\partial^2 W_1^2}{\partial z^2} dz, \end{aligned} \quad (126)$$

$$\frac{2}{\eta} \frac{\partial V_1}{\partial \tau} + \alpha_o V_1 \frac{\partial V_1}{\partial z} + \frac{1}{12} \frac{\partial^3 V_1}{\partial z^3} = \frac{C}{C_o} \frac{\partial}{\partial z} (V_1 - W_1). \quad (127)$$

By scaling  $W_1$ ,  $V_1$ ,  $\tau$ , and  $z$  as in equation (101) gives:

$$W_1 = \frac{6\gamma}{\alpha_o} \psi, \quad (128)$$

$$V_1 = -\frac{6\gamma}{\alpha_o} \phi, \quad (129)$$

$$\tau = \frac{2}{\eta_o} T, \quad (130)$$

where  $\gamma$  is the same as defined in the previous section, (i.e.  $\gamma = 1/\sqrt[3]{12}$ ), we find that:

$$\frac{\partial \psi}{\partial T} - 6\psi \frac{\partial \psi}{\partial u} + \frac{\partial^3 \psi}{\partial u^3} = P_3(u, T), \quad (131)$$

$$\frac{\partial \phi}{\partial T} - 6\phi \frac{\partial \phi}{\partial u} + \frac{\partial^3 \phi}{\partial u^3} = P_4(u, T). \quad (132)$$



The perturbation terms  $P_i(u, T)$ ,  $i = 3, 4$  in this present case are given by:

$$P_3(u, T) = \frac{C}{\gamma C_o} \frac{\partial}{\partial u} (\psi + \phi) - \frac{3\beta}{\gamma} \int \delta(u - u_o) \frac{\partial^2 \psi_1^2}{\partial u^2} du, \quad (133)$$

$$P_4(u, T) = \frac{C}{\gamma C_o} \frac{\partial}{\partial u} (\phi + \psi). \quad (134)$$

In the absence of the perturbations, equations (131) and (132) become two independent KdV equations admitting one-soliton solutions similar to equations (108) and (109).

#### II.5.4 NLTL with Voltage-Terminal Modules

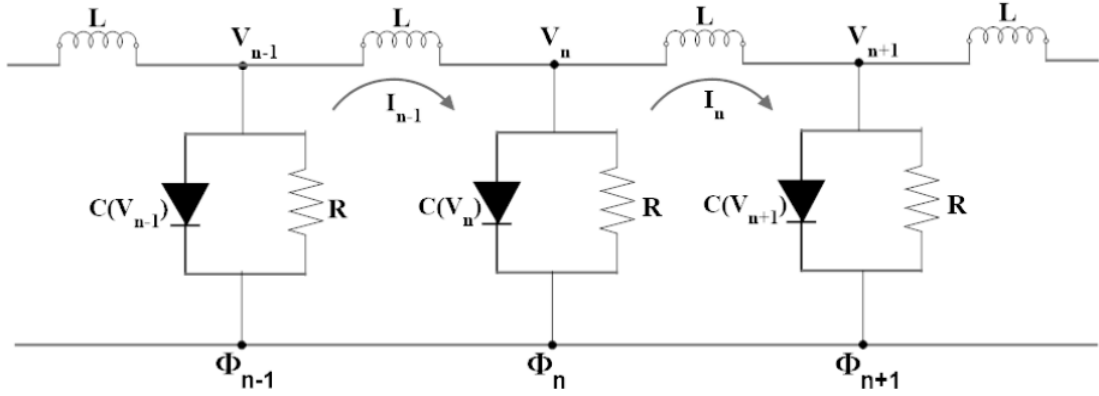


Figure 10: Equivalent circuit model of a Schottky-type lossy NLTL, with a voltage terminal connected to each elementary electric cell.

Consider a NLTL consisting of an homogeneous inductor,  $L$ , and a nonlinear capacitor,  $C$ , shunted by a passive resistance  $R$  in each unit cell as shown in Figure 10. Each unit cell of the NLTL is individually biased by a voltage terminal such that  $V_n$ ,  $I_n$  and  $\Phi_n$  are the voltage, current and bias voltage respectively, in the  $n^{th}$  cell.

The Schottky varactor is a capacitor of a nonlinear capacitance, with a generic  $C(V)$  characteristics [132, 133]:

$$C(V) = \frac{C_0}{\left(1 - \frac{V}{V_J}\right)^m}, \quad (135)$$

where  $V$  is the line voltage. In the above formula  $C_0$ ,  $V_J$  and  $m$  are the zero-bias junction capacitance, the characteristic junction voltage and the grading index respectively. In the

following we shall define a nonlinear coefficient  $b = 1/V_J$ . Also instructive to note, the grading index  $m$  can take distinct values depending on the specific Schottky diode at hand [132, 133]. For most Schottky diodes the grading index will be within the interval  $0 < m \leq 1$  [132, 133].

Applying Kirchhoff's laws in the  $n^{th}$  unit cell, we obtain the following set of equations for the line voltage  $V_n$  and current  $I_n$ :

$$L \frac{dI_{n-1}}{dt} = V_{n-1} - V_n, \quad (136)$$

$$I_{n-1} - I_n = \frac{dQ_n}{dt} + \frac{V_n - \Phi_n}{R}, \quad (137)$$

$$Q_n = C(V_n - \Phi_n) V_n, \quad (138)$$

where  $Q_n$  represents the total charge stored in the Schottky diode embedded within the  $n^{th}$  unit cell. Since sizes of unit cells are usually negligible compared with lengths of the line, electrical signals propagating along the line are expected to spread over many cells such that the discrete spatial coordinate  $n$  can be replaced by a continuous one i.e.  $x$ . For mathematical simplifications we set the size of the unit cells to unity, and a long-wavelength expansion of the voltage variables  $V_{n\pm 1}$  up to the fourth-order terms is carried out as in equation (87).

Eliminating current  $I_n$  from equations (136), (137) and applying the long-wavelength approximation, the continuous evolution equation for the line voltage  $V(x, t)$  is obtained as:

$$L \frac{\partial C(V - \Phi)}{\partial V} \left( \frac{\partial V}{\partial t} \right)^2 + LC(V - \Phi) \frac{\partial^2 V}{\partial t^2} + \frac{L}{R} \frac{\partial(V - \Phi)}{\partial t} = \frac{\partial^2 V}{\partial x^2} + \frac{1}{12} \frac{\partial^4 V}{\partial x^4}. \quad (139)$$

We seek for solutions to equation (139) which are nonlinear waves with pulse shape. To this end, we adopt the reductive perturbation approach by which the continuous variables  $V(x, t)$  and  $\Phi(x, t)$  are series expanded in powers of some perturbation coefficient  $\epsilon$  i.e.:

$$V(x, t) = \sum_{i=1}^n \epsilon^i V_i(x, t), \quad (140)$$

$$\Phi(x, t) = V_0 + \sum_{i=1}^n \epsilon^i \phi_i(x, t), \quad (141)$$

where it is assumed that  $\epsilon \ll 1$ . In addition to equations (140) and (141) we also make use of the space and time variables defined in equations (93) and (94) and rescale the resistance accordingly [135, 136]:

$$R = \epsilon^{-\frac{3}{2}} R_2, \quad (142)$$

where  $\eta_2 = (LC_0)^{-1/2}$ . By evaluating equation (139) at each order of  $\epsilon$ , we can extract equations describing contributions from different orders of the perturbation  $\epsilon$ . Namely, terms of orders  $O(\epsilon)$  and  $O(\epsilon^2)$  give constant contributions whereas terms of order  $O(\epsilon^3)$ , grouped together, introduce nonlinear excitations governed by the following perturbed KdV equation:

$$\begin{aligned} \frac{\partial V_1}{\partial \tau} - \frac{m}{2\sqrt{LC_0}(V_0 + V_J)} V_1 \frac{\partial V_1}{\partial z} + \frac{1}{24\sqrt{LC_0}} \frac{\partial^3 V_1}{\partial z^3} = \\ - \frac{m}{2\sqrt{LC_0}(V_0 + V_J)} \phi_1 \frac{\partial V_1}{\partial z} - \frac{V_J}{2R_2 C_0 (V_0 + V_J)} (V_1 - \phi_1). \end{aligned} \quad (143)$$

Let us rescale  $V_1$ ,  $\tau$  and  $z$  as follows:

$$V_1 = \frac{18(V_0 + V_J)}{m} V, \quad \tau = \frac{1}{9\eta} \tau', \quad z = \frac{1}{6} z'. \quad (144)$$

With these new variables, equation (143) reduces to:

$$\frac{\partial V}{\partial \tau'} - 6V \frac{\partial V}{\partial z'} + \frac{\partial^3 V}{\partial z'^3} = P_5(z', \tau'), \quad (145)$$

$$P_5(z', \tau') = \alpha V - \alpha \gamma \phi_1 - 6\gamma \phi_1 \frac{\partial V}{\partial z'}, \quad (146)$$

where

$$\alpha = \frac{V_J}{18\eta R_2 C_0 (V_0 + V_J)}, \quad (147)$$

$$\gamma = \frac{m}{18(V_0 + V_J)}. \quad (148)$$

In the absence of perturbation i.e. when  $P_5(z', \tau') = 0$ , the KdV equation admits the

following one-soliton solution [19]:

$$V(z', \tau') = -2\kappa_0^2 \text{sech}^2 y, \quad (149)$$

$$y = \kappa_0(z' - \zeta), \quad \zeta = 4\kappa_0^2 \tau', \quad (150)$$

where  $\kappa_0$  is the soliton amplitude. In the original system of coordinates i.e.  $(x, t)$ , the above one-soliton solution becomes:

$$V(x, t) = -\frac{A(V_0 + V_J)}{m} \text{sech}^2 \left[ \sqrt{A} \left( x - \frac{t}{\sqrt{LC_b}} - \frac{At}{6\sqrt{LC_b}} \right) \right], \quad (151)$$

where  $A = 36\epsilon\kappa_0^2$ . To keep the spirit of ref. [135] regarding the effects of voltage terminals on pulse propagation in the NLTL, we shall pick:

$$\begin{aligned} \Phi(x, t) &= V_0 + \epsilon^{\frac{3}{2}} \varphi_0(x - \eta t) \\ &= V_0 + \epsilon \varphi_0 z. \end{aligned} \quad (152)$$

Comparing equation (152) and equation (141) we find that:

$$\phi_1 = \varphi_0 \frac{z'}{6}. \quad (153)$$

## II.6 Conclusion

In this chapter we have explored the background of the materials and methods that will be useful to understand the concepts to be developed in our subsequent chapter. Circuit models have been developed and described for NLTLs. Most especially we have presented models for our NLTLs and also the nonlinear model reduction methods that we applied to our nonlinear differential equations. These models will be used extensively to investigate the leapfrogging, amplification and damping of electric pulses in NLTLs.

---

# RESULTS AND DISCUSSIONS

---

## III.1 Introduction

In this chapter we present and discuss the main results of this thesis obtained from mathematical analysis and numerical simulations. We now carry out numerical analysis on all four models of our NLTs discussed in section II.5. This is done by applying a sixth-order Runge-Kutta scheme adapted from [137] on our adiabatically obtained sets of equations in section II.5.

## III.2 Dynamics of Soliton-pair Leapfrogging in Two RC-Coupled Nonlinear Electrical Transmission Lines

### III.2.1 Adiabatic equations of soliton-pair motion

The two coupled equations (77) and (78) are not tractable analytically, because of the presence of coupling terms on the right hand side of these equations. However, since the two coupling terms are assumed very small, they can be treated as perturbations. Therefore we can rewrite equations (77) and (78) formally with their right hand sides grouped to give a single perturbation function:

$$\epsilon P(V', W') = D_1 \frac{\partial}{\partial s'} (V' + W') - D_2 (W' + V'). \quad (154)$$

Because of the weak coupling assumption, profiles of the two voltage signals will be determined by the two KdV equations represented by the left hand side of equations (77) and (78), while the perturbation  $\epsilon P(V', W')$  is expected to influence only their charac-

teristic parameters, namely the signal's amplitudes, widths and phases. In the absence of perturbation, i.e.  $\epsilon P(V', W') = 0$ , equations (77) and (78) are two independent KdV equations whose single-pulse soliton solutions are [19]:

$$V' = -2\kappa_1^2 \operatorname{sech}^2(z_1), \quad (155)$$

$$W' = -2\kappa_2^2 \operatorname{sech}^2(z_2), \quad (156)$$

where the arguments  $z_1$  and  $z_2$  are given by

$$z_1 = \kappa_1(s' - \zeta_1), \quad (157)$$

$$z_2 = \kappa_2(s' - \zeta_2), \quad (158)$$

connect the pulse amplitudes  $\kappa_1$  and  $\kappa_2$  to their respective phases  $\zeta_1$  and  $\zeta_2$  which are defined as:

$$\zeta_1 = 4\kappa_1^2 \tau', \quad (159)$$

$$\zeta_2 = 4\kappa_2^2 \tau'. \quad (160)$$

To determine the time evolutions of soliton characteristic parameters  $\kappa_i$  and  $\zeta_i$  ( $i = 1, 2$ ) for small  $\epsilon P(V', W')$ , it is useful to start by remarking that although the evolution of bound solitons cannot be strictly periodic because of relative losses, for small perturbations we can disregard the effects of amplitude waves emission by the oscillating soliton-pair. In this small perturbation regime the time evolutions of soliton characteristic parameters can readily be determined by solutions of the following adiabatic equations [19]:

$$\frac{d\kappa_i}{d\tau'} = -\frac{1}{4\kappa_i} \int_{-\infty}^{\infty} \epsilon P(V', W') \operatorname{sech}^2(z_i) dz_i, \quad (161)$$

and

$$\frac{d\zeta_i}{d\tau'} = 4\kappa_i^2 - \frac{1}{4\kappa_i^3} \int_{-\infty}^{\infty} \epsilon P(V', W') \operatorname{sech}^2(z_i) [z_i + \frac{1}{2} \sinh(2z_i)] dz_i, \quad (162)$$

with ( $i = 1, 2$ ). It is worth noting that the interaction between the two solitons will be optimal when their velocities coincide, i.e.,  $\dot{\zeta}_1 = \dot{\zeta}_2$ . In terms of equations (155) and (156), this also traduced by the equality of their amplitudes, i.e.:

$$\kappa_1 = \kappa_2. \quad (163)$$

From a general consideration in the specific context of leapfrogging motion [20, 138], if the amplitudes  $\kappa_i (i = 1, 2)$  are of the same order the stronger-interaction condition of equation (163) implies that  $\kappa_i^2 (i = 1, 2)$  perform only small oscillations mediated by the perturbation  $\epsilon P(V', W')$  around their mean values  $\langle \kappa_i^2 \rangle (i = 1, 2)$ . Since the two lines are assumed identical and symmetric we can set  $\langle \kappa_1^2 \rangle = \langle \kappa_2^2 \rangle = \kappa^2$ , which allows us to define:

$$\kappa_i = \kappa + \lambda_i, \quad (164)$$

with  $i = 1, 2$  and  $\kappa$  is always constant and the variables  $\lambda_i$  are assumed small compared to  $\kappa$ . Similarly the phase difference  $\Delta\zeta = \zeta_1 - \zeta_2$  can be assumed so small that we have:

$$z_2 \simeq z_1 + \kappa\Delta\zeta. \quad (165)$$

From equation (161),  $P(V', W')$  can be expressed as  $P(z_1, \tau')$  for line 1 and  $P(z_2, \tau')$  for line 2. Lets assume  $y = \kappa\Delta\zeta$ , then

$$\begin{aligned} P(z_1, \tau') &= D_1[4\kappa_1^3 \operatorname{sech}^2(z_1) \tanh(z_1) + 4\kappa_2^3 \operatorname{sech}^2(z_1 + y) \tanh(z_1 + y)] + \\ &D_2[2\kappa_1^2 \operatorname{sech}^2(z_1) + 2\kappa_2^2 \operatorname{sech}^2(z_1 + y)], \end{aligned} \quad (166)$$

and

$$\begin{aligned} P(z_1, \tau') \operatorname{sech}^2(z_1) &= D_1[4\kappa_1^3 \operatorname{sech}^4(z_1) \tanh(z_1) + \\ &+ 4\kappa_2^3 \operatorname{sech}^2(z_1 + y) \operatorname{sech}^2(z_1) \tanh(z_1 + y)] + \\ &+ D_2[2\kappa_1^2 \operatorname{sech}^4(z_1) + 2\kappa_2^2 \operatorname{sech}^2(z_1) \operatorname{sech}^2(z_1 + y)]. \end{aligned} \quad (167)$$

Now we linearize and approximate  $\text{sech}^2(z_1 + y)$  and  $\tanh(z_1 + y)$  as follows:

$$\text{sech}^2(z_1 + y) \simeq \text{sech}^2(y)[1 - 2 \tanh(y)\tanh(z_1)] \text{sech}^2(y), \quad (168)$$

$$\tanh(z_1 + y) \simeq (\tanh(y) + \tanh(z_1))[1 - 2 \tanh(y)\tanh(z_1)]. \quad (169)$$

With these, equation (161) for  $i = 1$  then becomes

$$\begin{aligned} \frac{d\kappa_1}{d\tau'} = & - \frac{1}{4\kappa_1} \left[ 4D_1\kappa_1^3 \int_{-\infty}^{\infty} \text{sech}^4(z_1) \tanh(z_1) dz_1 + \right. \\ & + 4D_1\kappa_2^3 \int_{-\infty}^{\infty} \text{sech}^2(z_1 + y) \text{sech}^2(z_1) \tanh(z_1 + y) dz_1 + \\ & \left. + 2D_2\kappa_1^2 \int_{-\infty}^{\infty} \text{sech}^4(z_1) dz_1 + 2D_2\kappa_2^2 \int_{-\infty}^{\infty} \text{sech}^2(z_1) \text{sech}^2(z_1 + y) dz_1 \right], \end{aligned}$$

which reduces to

$$\frac{d\kappa_1}{d\tau'} = 0 - \frac{8D_1\kappa_2^3}{15\kappa_1} \text{sech}^2(y)[\tanh(y) + \tanh^3(y)] - \frac{2D_2\kappa_1^2}{4\kappa_1} \left[ \frac{4}{3} \right] - \frac{2D_2\kappa_2^2}{4\kappa_1} \left[ \frac{4}{3} \text{sech}^2(y) \right]. \quad (170)$$

And using equation (164) we get

$$\frac{d\lambda_1}{d\tau'} = -\frac{8D_1\kappa_2^3}{15\kappa_1} \text{sech}^2(y)[\tanh(y) + \tanh^3(y)] - \frac{2D_2\kappa_1}{3} - \frac{2D_2\kappa_2^2}{3\kappa_1} \text{sech}^2(y). \quad (171)$$

Also for  $i = 2$  we obtain  $\frac{d\lambda_2}{d\tau'}$  from equation (161). Note that in this case  $z_1 \simeq z_2 - y$  is substituted for  $z_1$ . This gives

$$\frac{d\lambda_2}{d\tau'} = \frac{8D_1\kappa_2^3}{15\kappa_1} \text{sech}^2(y)[\tanh(y) + \tanh^3(y)] - \frac{2D_2\kappa_1}{3} - \frac{2D_2\kappa_2^2}{3\kappa_1} \text{sech}^2(y). \quad (172)$$



In a similar way, from equation (162)

$$\begin{aligned}
\frac{d\zeta_1}{d\tau'} &= 4\kappa_1^2 - \frac{1}{4\kappa_1^3} \int_{-\infty}^{\infty} P(z_1, \tau') (z_1 \operatorname{sech}^2(z_1) + \tanh(z_1)) dz_1 \\
&= 4\kappa_1^2 - \frac{1}{4\kappa_1^3} \int_{-\infty}^{\infty} P(z_1, \tau') z_1 \operatorname{sech}^2(z_1) dz_1 - \\
&\quad - \frac{1}{4\kappa_1^3} \int_{-\infty}^{\infty} P(z_1, \tau') \tanh(z_1) dz_1.
\end{aligned} \tag{173}$$

By evaluating the two integrals on the right hand side of equation (173), we obtain:

$$\begin{aligned}
-\frac{1}{4\kappa_1^3} \int_{-\infty}^{\infty} P(z_1, \tau') z_1 \operatorname{sech}^2(z_1) dz_1 &= -\frac{1}{3} D_1 - \frac{D_1 \kappa_2^3}{3\kappa_1^3} \operatorname{sech}^2(y) \left[ 1 - \frac{31}{15} \tanh^2(y) \right] + \\
&\quad + \frac{D_2 \kappa_2^2}{3\kappa_1^3} \operatorname{sech}^2(y) \tanh(y),
\end{aligned} \tag{174}$$

and

$$\begin{aligned}
-\frac{1}{4\kappa_1^3} \int_{-\infty}^{\infty} P(z_1, \tau') \tanh(z_1) dz_1 &= -\frac{2}{3} D_1 - \frac{2D_1 \kappa_2^3}{3\kappa_1^3} \operatorname{sech}^2(y) \left[ 1 - \frac{9}{5} \tanh^2(y) \right] + \\
&\quad + \frac{2D_2 \kappa_2^2}{3\kappa_1^3} \operatorname{sech}^2(y) \tanh(y).
\end{aligned} \tag{175}$$

By substituting equations (174) and (175) into equation (173) we obtain:

$$\frac{d\zeta_1}{d\tau'} = 4\kappa_1^2 - D_1 - \frac{D_1 \kappa_2^3}{\kappa_1^3} \operatorname{sech}^2(y) \left[ 1 - \frac{17}{9} \tanh^2(y) \right] + \frac{D_2 \kappa_2^2}{\kappa_1^3} \operatorname{sech}^2(y) \tanh(y). \tag{176}$$

In a similar way, i.e.  $i = 2$ , we obtain  $\frac{d\zeta_2}{d\tau'}$  from equation (162). Again we note that in this case  $z_1 = z_2 - y$  is substituted for  $z_1$ . This gives

$$\frac{d\zeta_2}{d\tau'} = 4\kappa_2^2 - D_1 - \frac{D_1 \kappa_1^3}{\kappa_2^3} \operatorname{sech}^2(y) \left[ 1 - \frac{17}{9} \tanh^2(y) \right] - \frac{D_2 \kappa_1^2}{\kappa_2^3} \operatorname{sech}^2(y) \tanh(y). \tag{177}$$

Equations (171), (172), (176) and (177) are solved numerically using a sixth-order Runge-Kutta scheme [137] with fixed step, and numerical results are presented in the next section.

### III.2.2 Numerical Results

We applied a sixth-order Runge-Kutta scheme adapted from [137] on the set of equations (171), (172), (176), and (177), with  $\kappa$  fixed to an arbitrary constant but sufficiently large compared to  $\lambda_1$  and  $\lambda_2$  which is consistent with the definition of equation (164). Initial values of  $\lambda_1$ ,  $\lambda_2$ ,  $\zeta_1$  and  $\zeta_2$  were chosen such that the differences  $\lambda_1 - \lambda_2$  and  $\Delta\zeta$  are small enough to ensure their harmonic oscillations from the onset of motion. That is the leapfrogging motion of the two solitons, described as the regime of motion where their amplitudes vary is investigated. This was done by carrying out numerical simulations on the four coupled ordinary differential equations (171), (172), (176), and (177). Since it is also relevant to see what effects the coupling resistance,  $D_2$ , would have on the amplitudes of the individual solitons, we start by plotting the time series of  $\lambda_1$  and  $\lambda_2$  for a fixed value of the capacitive coupling  $D_1$ .

Figures (11a) and (11b) show a time series plot of  $\lambda_1$  and  $\lambda_2$  for a fixed value of the capacitive coupling  $D_1(D_1 = 0.025)$ , for different values of the resistance coupling parameter, i.e.  $D_2 = 0.001, 0.005$  and  $0.009$ . From these plots one sees that the time series of  $\lambda_1$  and  $\lambda_2$  are periodic oscillations with an exponential decrease from their maxima. This exponential damping is more and more pronounced as  $D_2$  increases.

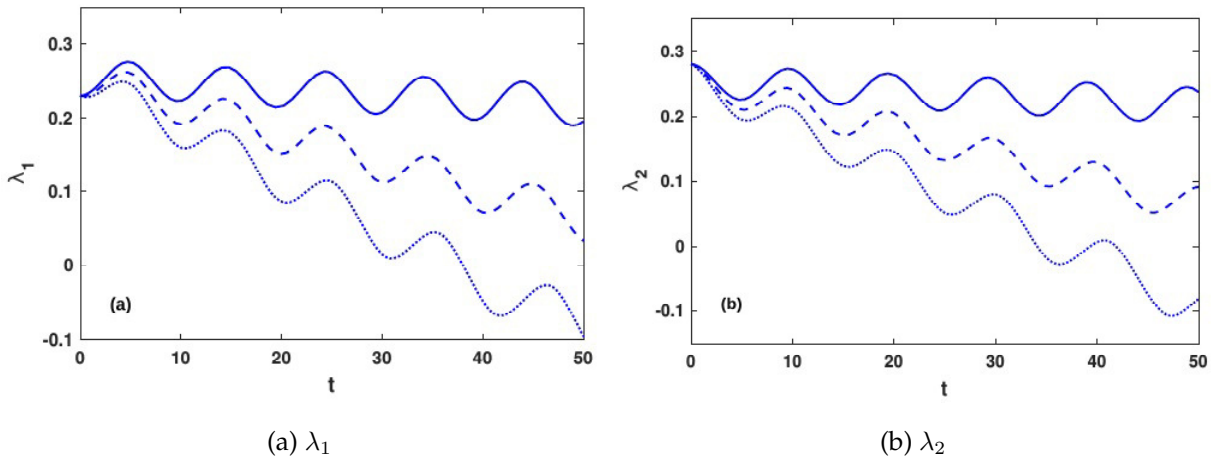


Figure 11: Temporal evolutions of  $\lambda_1$  and  $\lambda_2$  for  $D_1 = 0.23$  and  $\kappa = 0.6$ . The solid, dashed and dotted curves corresponds respectively to  $D_2 = 0.001, 0.005$  and  $0.009$ .

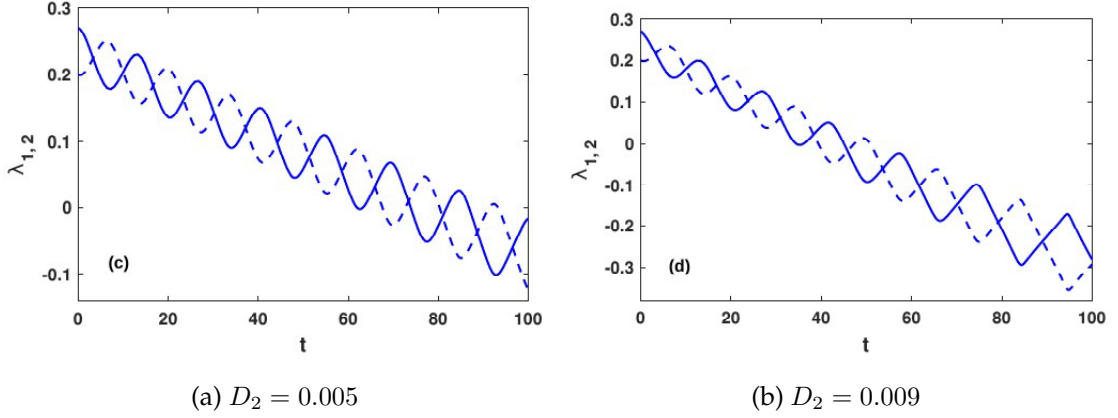


Figure 12: Leapfrogging dynamics of  $\lambda_1$ (solid curve) and  $\lambda_2$ (dashed curve)

To highlight the anti-phase oscillations of the two amplitudes, figures (12a) and (12b) shows plots of  $\lambda_1$  and  $\lambda_2$  on the same graph for large values of  $D_2$  ( $D_2 = 0.005$  and  $D_2 = 0.009$ ) keeping  $D_1 = 0.025$  and  $\kappa = 0.5$ . The leapfrogging motions observed in these curves occur more exactly when initial values of  $\lambda_1$  and  $\lambda_2$  used in the simulations are very close.

Figure (13) illustrates the absence of leapfrogging, when the difference between initial values of the two parameters in the simulations is relatively large.

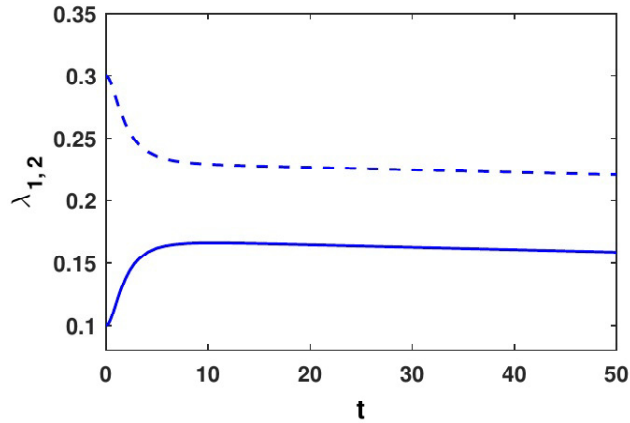


Figure 13: Suppression of leapfrogging for large initial values of  $\lambda_1$ (= 0.1) and  $\lambda_2$ (= 0.2), with  $D_1 = 0.25$ ,  $D_2 = 0.0005$  and  $\kappa = 0.5$ .

The signature of leapfrogging is to be observed both in the oscillating phase difference  $\Delta\zeta = \zeta_1 - \zeta_2$ , and the oscillating amplitude difference  $\Delta\lambda = \lambda_1 - \lambda_2$  of the two solitons. Therefore, to gain a consistent knowledge of this signature in the two parameters, we

solved numerically the amplitude and phase difference equations derived from the coupled sets, equations (171), (172), (176), and (177) by subtracting equation (172) from (171) on the one hand and equation (177) from (176) on the other hand.

Figure (14) suggest a dynamics of the soliton pair which is summarized as follows: initially, that is at  $t = 0$  the amplitude difference of the two solitons is at some finite initial value, while their phase difference is zero. As the two solitons propagate they exchange energy, this causes them to slowly approach each other. Their amplitude difference thus decreases gradually to zero at the time when the two electrical pulses coincide and have equal velocities. After hopping pass each other, their amplitude and phase differences begin to rise again and the cycle continues, for as long as the leapfrogging motion goes on resulting in oscillating amplitude and phase differences.

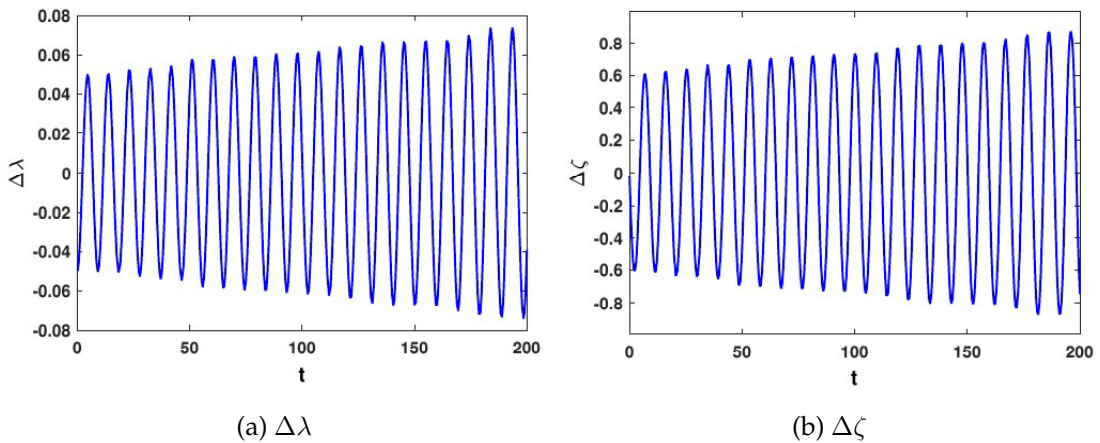


Figure 14: Temporal oscillations of the amplitude difference  $\Delta\lambda$  and phase difference  $\Delta\zeta$  for  $D_1 = 0.25$  and  $D_2 = 0.005$ .

To further emphasize the effects of the resistance on the leapfrogging dynamics of the bound solitons, we plot three sets of curves to illustrate the behaviour of the oscillating amplitude difference and phase difference, with increasing resistance. Using fairly large values for the resistance, the curves clearly show that as the resistance increases, the number of oscillations in  $\Delta\lambda$  and  $\Delta\zeta$  decreases until the leapfrogging motion stops. Since the oscillating evolutions of the amplitude and phase differences are here assumed to characterize the leapfrogging of the soliton-pair, the decrease in the number of oscillations

readily indicates a weakening and eventually a relaxation of the leapfrogging motion. See figure (15).

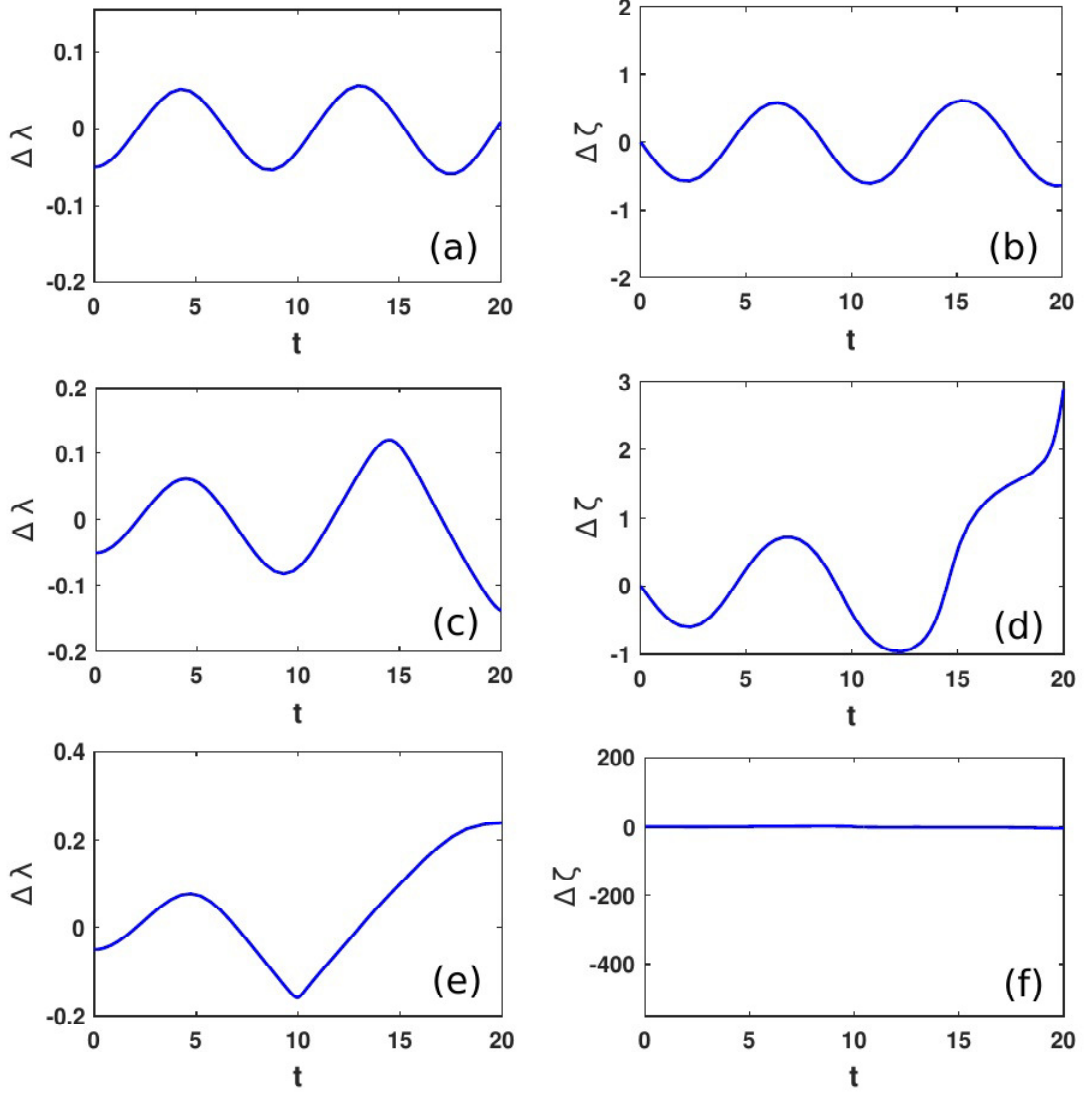


Figure 15: Oscillating amplitude and phase differences for increasing resistance. The top, middle and bottom set of curves are for  $D_2 = 0.01, 0.05$  and  $0.09$  respectively. Here  $D_1 = 0.25$  and  $\kappa = 0.63$ . Leapfrogging ceases in the last set of curves due to very high value of resistance.

To provide an analytical understanding of the origin of the harmonic oscillations observed in numerical solutions to the phase and amplitude difference equations, it is useful to remark that the arguments of the hyperbolic functions in equations (171), (172), (176), and (177) are proportional to  $\Delta\zeta$ . Thus, for leapfrogging to occur in numerical simulations, this latter parameter should remain very small which justifies our choice

of very small initial values for the phase and amplitude differences. Analytically, small amplitude and phase differences imply linearizing equations (171), (172), (176), and (177). Recall that equations (171), (172), (176), and (177) are nonlinear functions of  $\lambda_1, \lambda_2, \zeta_1, \zeta_2$  as well as  $\kappa_1$  and  $\kappa_2$ .  $\kappa_1$  and  $\kappa_2$  are functions of  $\lambda_1$  and  $\lambda_2$ , and to linearize terms involving them we use the following linear approximations:

$$\begin{aligned}
\kappa_i &\simeq \kappa^2 + 2\kappa\lambda_i, \\
\frac{\kappa_1^2}{\kappa_2^3} &\simeq \kappa^{-1} - 3\kappa^{-2}\lambda_2 + 2\kappa^{-2}\lambda_1, \\
\frac{\kappa_2^2}{\kappa_1^3} &\simeq \kappa^{-1} - 3\kappa^{-2}\lambda_1 + 2\kappa^{-2}\lambda_2, \\
\frac{\kappa_1^3}{\kappa_2^3} &\simeq 1 - 3\kappa^{-1}\lambda_2 + 3\kappa^{-1}\lambda_1, \\
\frac{\kappa_2^3}{\kappa_1^3} &\simeq 1 - 3\kappa^{-1}\lambda_1 + 3\kappa^{-1}\lambda_2,
\end{aligned} \tag{178}$$

with ( $i = 1, 2$ ). Also

$$\begin{aligned}
\operatorname{sech}(y) &\simeq 1 - \frac{1}{2}y; & \operatorname{sech}^2(y) &\simeq 1 - y^2, \\
\operatorname{sech}^2(y)\tanh(y) &\simeq y; & \operatorname{sech}^2(y)\tanh^2(y) &\simeq y^2
\end{aligned} \tag{179}$$

At leapfrogging  $\langle \kappa_1^2 \rangle = \langle \kappa_2^2 \rangle = \kappa^2$ , therefore

$$\begin{aligned}
-\frac{2D_2\kappa_1}{3} - \frac{2D_2\kappa_2^2}{3\kappa_1} \operatorname{sech}^2(y) &\simeq -\frac{4D_2}{3}\kappa_2 \\
&= -\frac{4D_2}{3}\kappa - \frac{4D_2}{3}\lambda_2,
\end{aligned} \tag{180}$$

and

$$\begin{aligned}
\frac{8D_1\kappa_2^3}{15\kappa_1} \operatorname{sech}^2(y)[\tanh(y) + \tanh^3(y)] &\simeq \frac{8}{15}y \\
&= \frac{8}{15}\kappa\Delta\zeta.
\end{aligned} \tag{181}$$

Equations (171) and (172) now become

$$\frac{\lambda_1}{d\tau'} = -\frac{8}{15}D_1\kappa^3\Delta\zeta - \frac{4}{3}D_2\kappa - \frac{4}{3}D_2\lambda_2, \quad (182)$$

and

$$\frac{\lambda_2}{d\tau'} = \frac{8}{15}D_1\kappa^3\Delta\zeta - \frac{4}{3}D_2\kappa - \frac{4}{3}D_2\lambda_1. \quad (183)$$

Subtracting equation (183) from equation (182) we obtain:

$$\frac{\lambda_1}{d\tau'} - \frac{\lambda_2}{d\tau'} = -\frac{16}{15}D_1\kappa^3\Delta\zeta. \quad (184)$$

Also equations (176) and (177) reduces to

$$\frac{d\zeta_1}{d\tau'} = 4\kappa_1^2 - D_1 - \frac{D_1\kappa_2^3}{\kappa_1^3} + \frac{D_2\kappa_2^2}{\kappa_1^3}y, \quad (185)$$

$$\frac{d\zeta_2}{d\tau'} = 4\kappa_2^2 - D_1 - \frac{D_1\kappa_1^3}{\kappa_2^3} - \frac{D_2\kappa_1^2}{\kappa_2^3}y. \quad (186)$$

Subtracting equation (186) from equation (185) we obtain:

$$\frac{d\zeta_1}{d\tau'} - \frac{d\zeta_2}{d\tau'} = 4(\kappa_1^2 - \kappa_2^2) - D_1\left(\frac{\kappa_2^3}{\kappa_1^3} - \frac{\kappa_1^3}{\kappa_2^3}\right) + D_2y\left(\frac{\kappa_2^2}{\kappa_1^3} + \frac{\kappa_1^2}{\kappa_2^3}\right),$$

which reduces to

$$\frac{d\Delta\zeta}{d\tau'} = \left(8\kappa + \frac{6D_1}{\kappa}\right)(\lambda_1 - \lambda_2) + \frac{D_2}{\kappa}\left[2\kappa - (\lambda_1 + \lambda_2)\right]. \quad (187)$$

Differentiating equation (187) with respect to  $\tau'$  yields:

$$\frac{d^2\Delta\zeta}{d\tau'^2} = \left(8\kappa + \frac{6D_1}{\kappa}\right)\left(\frac{d\lambda_1}{d\tau'} - \frac{d\lambda_1}{d\tau'}\right) + \frac{D_2}{\kappa}\left[(2\kappa - (\lambda_1 + \lambda_2))\frac{d\Delta\zeta}{d\tau'} - \left(\frac{d\lambda_1}{d\tau'} + \frac{d\lambda_1}{d\tau'}\right)\Delta\zeta\right],$$

and by substituting equation (187) we obtain

$$\frac{d^2\Delta\zeta}{d\tau'^2} = -(8\kappa^2 + 6D_1)\left(\frac{16D_1}{15}\kappa^2\right) + \frac{D_2^2}{\kappa^2}\left[(2\kappa - (\lambda_1 + \lambda_2))^2 + \frac{4\kappa}{3}(2\kappa + (\lambda_1 + \lambda_2))\right] + \frac{D_2}{\kappa^2}\left[(2\kappa - (\lambda_1 + \lambda_2))(8\kappa^2 + 6D_1)(\lambda_1 - \lambda_2)\right]. \quad (188)$$

The variable  $\lambda_1$  and  $\lambda_2$  were assumed to be small compared with  $\kappa$ . So we can conveniently make the following assumption without loss of generality:

$$2\kappa \pm (\lambda_1 + \lambda_2) \simeq 2\kappa. \quad (189)$$

Substituting equation (189) into (188) we get

$$\frac{d^2\Delta\zeta}{d\tau'^2} = -\Gamma_a\Delta\zeta + \Gamma_b, \quad (190)$$

where

$$\Gamma_a = \frac{16}{15}D_1(8\kappa^2 + 6D_1)\kappa^2 - \frac{20}{3}D_2^2, \quad (191)$$

$$\Gamma_b = \frac{2}{\kappa}D_2(8\kappa^2 + 6D_1)(\lambda_1 - \lambda_2). \quad (192)$$

Equation (190) is the equation of motion for an harmonic oscillator, the frequency  $\omega_{lf}$  of which can be gotten considering the following trial solution in equation (190).

$$\Delta\zeta = \Gamma_o e^{i\omega_{lf}\tau'} - \frac{\Gamma_b}{\Gamma_a}. \quad (193)$$

By substituting equation (193) into equation (190) we obtain:

$$\omega_{lf} = \left(\frac{128}{15}D_1\kappa^4 + \frac{96}{15}D_1^2\kappa^2 - \frac{20}{3}D_2^2\right), \quad (194)$$

where  $\omega_{lf}$  is the leapfrogging frequency. Equation (194) shows that the leapfrogging frequency is decreased by the presence of the resistive element in the coupling branch. From this expression of  $\omega_{lf}$  it is also apparent that as the resistance increases, the frequency



can become complex such that the relative amplitude and phase of the two solitons are either exponentially amplified, or exponentially damped with time. This is in agreement with the behaviour observed in figures (11), (12) and (14). A plot of the leapfrogging frequency against the resistance for different values of  $\kappa$  is shown in figure (16).

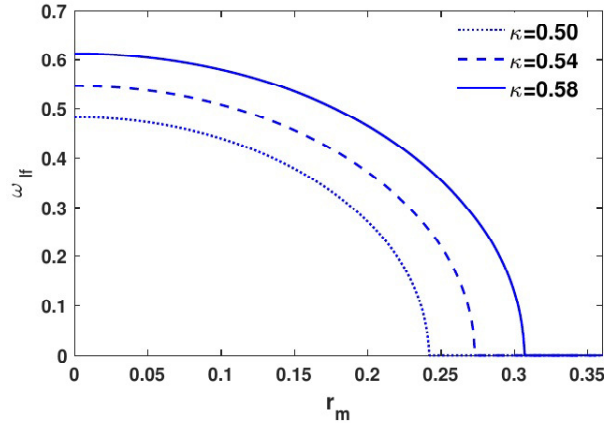


Figure 16: Influence of the resistance on the leapfrogging frequency for different values of  $\kappa$ .  $D_1 = 0.25$ .

In all of our analysis so far, it appeared that our choice of small initial values for the amplitude and phase differences was necessary for the observation of leapfrogging in numerical simulations of the coupled set of equations (171), (172), (176), and (177). A plot of the time series of  $\lambda_1$  and  $\lambda_2$  for relatively large values of the initial phase and amplitude differences, considering different values of  $D_2$  is shown in figure (17). As one can see, the time series of the soliton characteristic parameters are now strongly anharmonic, more generally an enhancement of the anharmonicity by relatively large initial values will cause a relaxation of leapfrogging after a finite propagation time, as observed in the graphs of figure (17).

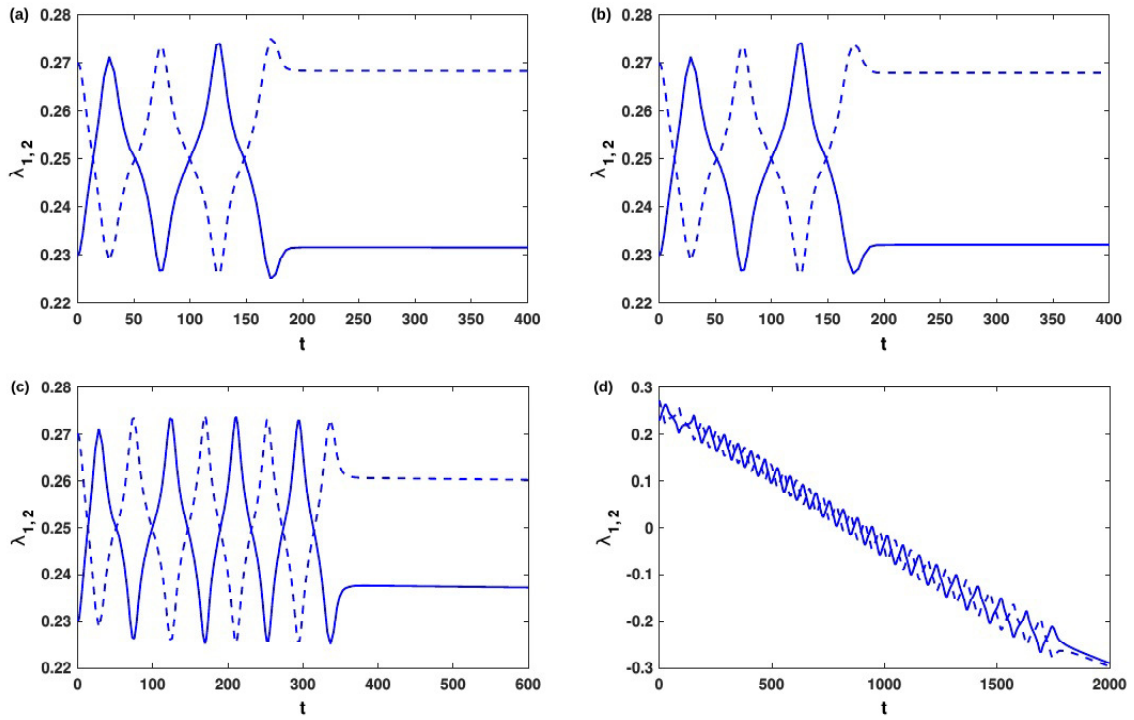


Figure 17: Anharmonic oscillations of  $\lambda_1$ (solid curves) and  $\lambda_2$ (dashed curves), for large initial values: **(a)**  $R_1 = 5 \times 10^{-10}$ , **(b)**  $R_1 = 5 \times 10^{-8}$ , **(c)**  $R_1 = 5 \times 10^{-6}$ , **(d)**  $R_1 = 5 \times 10^{-4}$ .

A graph of  $\lambda_1$  plotted as a function of  $\lambda_2$  is represented in figure (18). This graph shows an explicit picture of the leapfrogging dynamics of the two solitons summarized in the phase-space representation of figure (18).

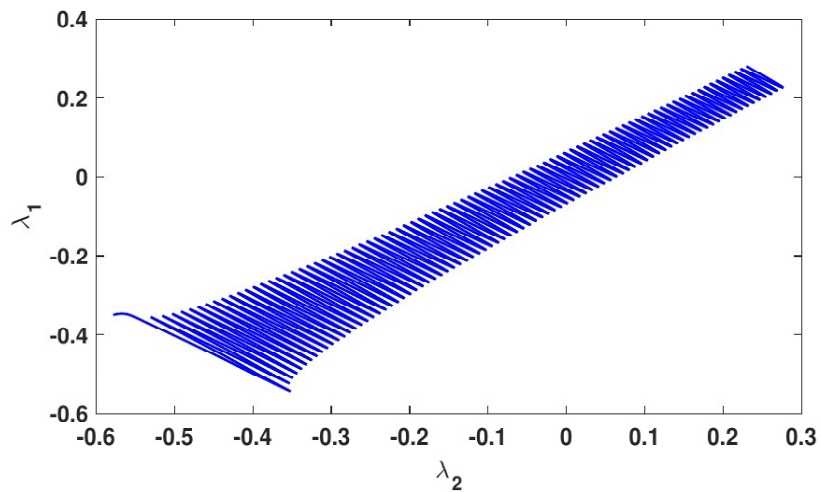


Figure 18: Phase-space representation of the leapfrogging dynamics. Here,  $D_1 = 0.001$ ,  $D_2 = 0.23$  and  $\kappa = 0.6$ .

### III.3 Leapfrogging of Electrical Solitons in Coupled Non-linear Transmission Lines: Effect of an Imperfect Varactor

#### III.3.1 Analysis of Leapfrogging for Coupled RLC NLTs

In our previous study [134] we investigated the leapfrogging dynamics of soliton pairs propagating along two LC NLTs, weakly coupled by a linear capacitance shunted with a linear resistance. Instructively, this coupled model considered was an extension of the study done in [40] where the author addressed the problem considering only the capacitive coupling.

In this section of the thesis, we are interested in the leapfrogging motion of a soliton pair in two distinct physical contexts [136]. First we consider the case of two RLC NLTs coupled via a linear capacitance, and secondly two capacitively coupled LC NLTs one of which contains a defective varactor.

#### Adiabatic equations of soliton-pair motion

Within the framework of the adiabatic perturbation theory [19], the temporal evolutions of the amplitudes  $\kappa_i$  and phases  $\theta_i$  ( $i = 1, 2$ ) of the two pulses described by equations (102) and (103) are determined by solving the following coupled first-order ordinary differential equations:

$$\frac{d\kappa_i}{dT} = -\frac{1}{4\kappa_i} \int_{-\infty}^{\infty} P_i(y_i, T) \operatorname{sech}^2 y_i dy_i, \quad (195)$$

and

$$\frac{d\theta_i}{dT} = 4\kappa_i^2 - \frac{1}{4\kappa_i^3} \int_{-\infty}^{\infty} P_i(y_i, T) [y_i + \frac{1}{2} \sinh(2y_i)] \operatorname{sech}^2 y_i dy_i. \quad (196)$$

To find explicit forms of these variational equations, we must substitute the pulse solutions (112) and (113) into the perturbation parameters  $P_i(u, T)$ . So doing, equations (195)

and (196) burst into the following four coupled first-order ordinary differential equations:

$$\frac{d\kappa_1}{dT} = -\frac{8M}{15}\kappa_2^2 \operatorname{sech}^2 A [\tanh A + \tanh^3 A] - \frac{2}{3}N\kappa_1, \quad (197)$$

$$\frac{d\kappa_2}{dT} = \frac{8M}{15}\kappa_1^2 \operatorname{sech}^2 A [\tanh A + \tanh^3 A] - \frac{2}{3}N\kappa_2, \quad (198)$$

$$\frac{d\theta_1}{dT} = 4\kappa_1^2 - M - \frac{M\kappa_2^3}{\kappa_1^3} \operatorname{sech}^2 A [1 - \frac{17}{9}\tanh^2 A], \quad (199)$$

$$\frac{d\theta_2}{dT} = 4\kappa_2^2 - M - \frac{M\kappa_1^3}{\kappa_2^3} \operatorname{sech}^2 A [1 - \frac{17}{9}\tanh^2 A], \quad (200)$$

where  $M = \frac{C}{\gamma C_b}$ ,  $N = R_1 C_b \eta$ , and  $A = \kappa \Delta\theta$ , with  $\Delta\theta = \theta_1 - \theta_2$  the phase difference.

Leapfrogging of the two interacting solitons corresponds to small oscillations of their amplitudes  $\kappa_i$  around a common average value  $\kappa$ . Consequently we can introduce a small deviation  $\lambda_i$  from the average amplitude  $\kappa$ , in such a way that we can write  $\kappa_i = \kappa + \lambda_i$ . Similarly the phase difference  $\Delta\theta$  must be small. By using the approximation  $y_2 \approx y_1 + A$  and linearizing, equations (197) to (200) become:

$$\frac{d\lambda_1}{dT} = -\frac{8M}{15}\kappa^3 \Delta\theta - \frac{2N}{3}(\kappa + \lambda_1), \quad (201)$$

$$\frac{d\lambda_2}{dT} = \frac{8M}{15}\kappa^3 \Delta\theta - \frac{2N}{3}(\kappa + \lambda_2), \quad (202)$$

$$\frac{d\theta_1}{dT} = 4(\kappa^2 + 2\kappa\lambda_1) - M[2 - 3\kappa^{-1}(\lambda_1 - \lambda_2)], \quad (203)$$

$$\frac{d\theta_2}{dT} = 4(\kappa^2 + 2\kappa\lambda_2) - M[2 + 3\kappa^{-1}(\lambda_1 - \lambda_2)], \quad (204)$$

where  $\Delta\lambda = \lambda_1 - \lambda_2 = \kappa_1 - \kappa_2$ . Subtracting equation (202) from (201) we obtain:

$$\frac{d\lambda_1}{dT} - \frac{d\lambda_2}{dT} = -\frac{16M}{15}\kappa^3 \Delta\theta - \frac{2N}{3}(\lambda_1 - \lambda_2), \quad (205)$$

and also subtracting equation (204) from (203) gives:

$$\frac{d\Delta\theta}{dT} = (8\kappa + 6\kappa^{-1}M)(\Delta\lambda). \quad (206)$$

Taking the second derivative of equation (206), and the fact that  $\frac{d\lambda_1}{dT} - \frac{d\lambda_2}{dT} = \frac{d\Delta\lambda}{dT}$  gives:

$$\frac{d^2\Delta\theta}{dT^2} = (8\kappa + 6\kappa^{-1}M) \frac{d\Delta\lambda}{dT}. \quad (207)$$

From equation (206):

$$\Delta\lambda = \frac{\kappa}{(8\kappa^2 + 6M)} \frac{d\Delta\theta}{dT}, \quad (208)$$

and equation (205) becomes:

$$\frac{d\Delta\lambda}{dT} = -\frac{16M}{15}\kappa^3\Delta\theta - \frac{2N}{3} \frac{\kappa}{(8\kappa^2 + 6M)} \frac{d\Delta\theta}{dT}. \quad (209)$$

Substituting equation (209) into (207) gives:

$$\frac{d^2\Delta\theta}{dT^2} + \frac{2N}{3} \frac{d\Delta\theta}{dT} + \frac{(8\kappa^2 + 6M)}{\kappa} \frac{16M}{15} \kappa^3 \Delta\theta, \quad (210)$$

from which we obtain:

$$\frac{d^2\Delta\theta}{dT^2} + \gamma_d \frac{d\Delta\theta}{dT} + \omega_o^2 \Delta\theta = 0, \quad (211)$$

with

$$\gamma_d = \frac{2N}{3}, \quad (212)$$

$$\omega_o^2 = \frac{16M}{15} \kappa^2 (8\kappa^2 + 6M). \quad (213)$$

Equations (208) and (211) are reminiscent of the motion of a damped harmonic oscillator, where  $\gamma_d$  and  $\omega_o$  are the damping coefficient and resonance frequency respectively. It is remarkable that the damping coefficient,  $\gamma_d$ , is a linear function of the intraline resistance  $R_1$ , while the resonance frequency,  $\omega_o$ , or the frequency of the undamped oscillators, is proportional to the coupling capacitance  $C$ . It is worth noting that the adiabatic perturbation theory is valid only when  $C_m/C_b \ll V_s/V_b$  where

$$V_s = \frac{12\epsilon\kappa^2(V_J + mV_b)}{\sqrt[3]{12m}} \quad (214)$$

is the average voltage amplitude of the incident solitons. Given that the coupling capacitance  $C$  and the intraline resistance  $R_1$  should be very small, consistent with the spirit of the adiabatic perturbation theory, the leapfrogging frequency can only be increased with an increase in the pulse amplitude  $\kappa$ .

### Numerical Simulations of Leapfrogging for the Coupled RLC NLTLs

In [21], an analysis of soliton leapfrogging in a model of coupled NLTLs similar to figure (8), but without intraline resistance, has been carried out. Much recently in [134], we extended the study to the context of two LC-type NLTLs coupled by a linear capacitance with a linear resistance in its shunt branch. In this subsection, we shall now explore numerically the influence of the intraline resistance on pulse leapfrogging. To do this, we apply a sixth-order Runge-Kutta scheme [137] on the set of four coupled first-order nonlinear ordinary differential equations (197) to (200).

To start we consider small initial values for  $\lambda_i$  and  $\theta_i$ , and in addition select very close initial values for  $\lambda_1$  and  $\lambda_2$  on the one hand, and  $\theta_1$  and  $\theta_2$  on the other hand, which are relevant conditions for leapfrogging to occur. We will later on look at the effects of increasing the initial phase and amplitude differences, on the leapfrogging motion.

Graphs in figure (19) show the time evolutions of  $\lambda_1$  and  $\lambda_2$  for fixed values of the average amplitude  $\kappa = 2$ , and the capacitive coefficient  $M = 0.2$ , and four distinct values of the resistive coefficient  $N = 0.0, 0.001, 0.01, 0.1$ . According to figure (19), the time evolutions of  $\lambda_1$  and  $\lambda_2$  are harmonic oscillations with amplitudes which are more and more exponentially damped with increase in the resistive coefficient  $N$ .

Graphs in figure (20) show the time evolutions of the amplitude difference  $\Delta\lambda$ , with initial values  $\lambda_1 = 0.25, \lambda_2 = 0.2, \theta_1 = 0.25, \theta_2 = 0.2$ . Also this simulation is carried out for fixed values of the average amplitude  $\kappa = 2$ , and capacitive coefficient  $M = 0.2$ , and four distinct values of the resistive coefficient  $N = 0.0, 0.001, 0.01, 0.1$ . We noticed from figure (20) that the amplitude difference  $\Delta\lambda$  oscillates as well harmonically in time, reflecting leapfrogging of the soliton pair. The amplitude difference oscillations are also damped for higher values of resistive coefficient  $N$ .

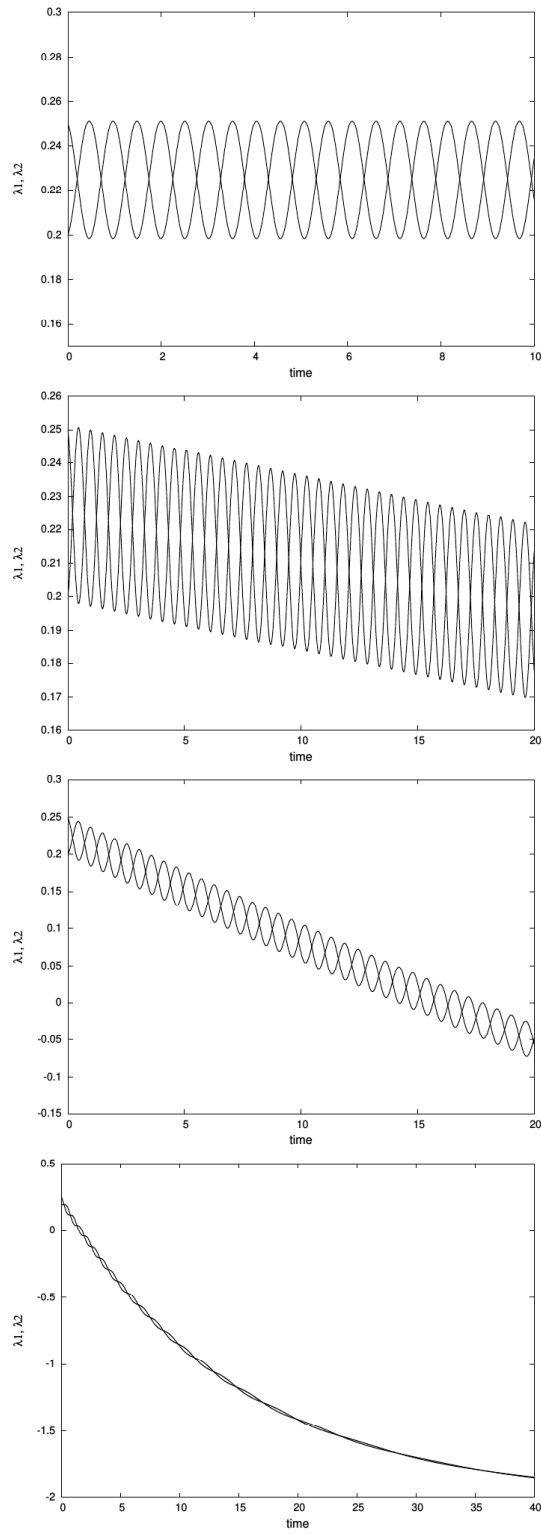


Figure 19: Time variations of  $\lambda_1$ (downward from  $T = 0$ ) and  $\lambda_2$ (upward from  $T = 0$ ) for  $\kappa = 2$ ,  $M = 0.2$  and from top to bottom  $N = 0.0, 0.001, 0.01, 0.1$ .

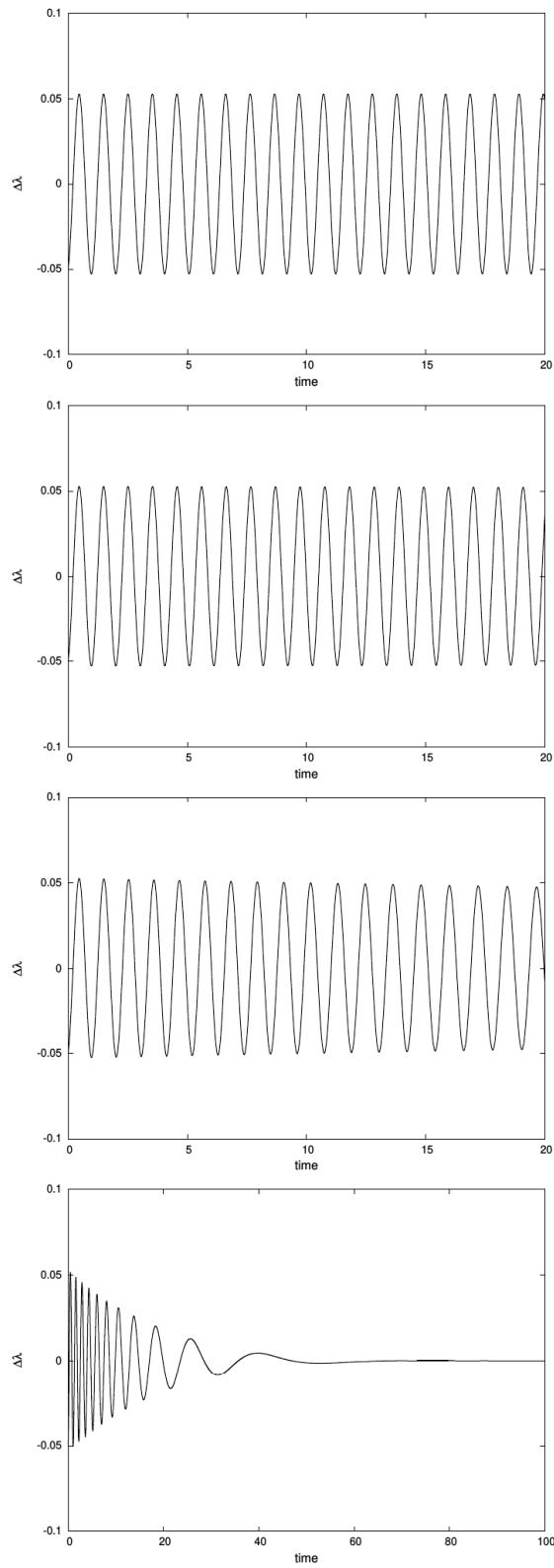


Figure 20: Time variations of amplitude difference  $\Delta\lambda$ , initial values are  $\lambda_1 = 0.25, \lambda_2 = 0.2, \theta_1 = 0.25, \theta_2 = 0.2$ . Also  $\kappa = 2, M = 0.2$  and from top to bottom  $N = 0.0, 0.001, 0.01, 0.1$ .



Figures (21), (22), and (23) are numerical results obtained when the differences of initial values of the two soliton amplitudes and phases are increased. Figure (21) has as initial values  $\lambda_1 = 0.3, \lambda_2 = 0.1, \theta_1 = 0.28, \theta_2 = 0.1, \kappa = 2$  and  $M = 0.2$ . From top to bottom rows:  $N = 0.0, 0.01, 0.1$ .

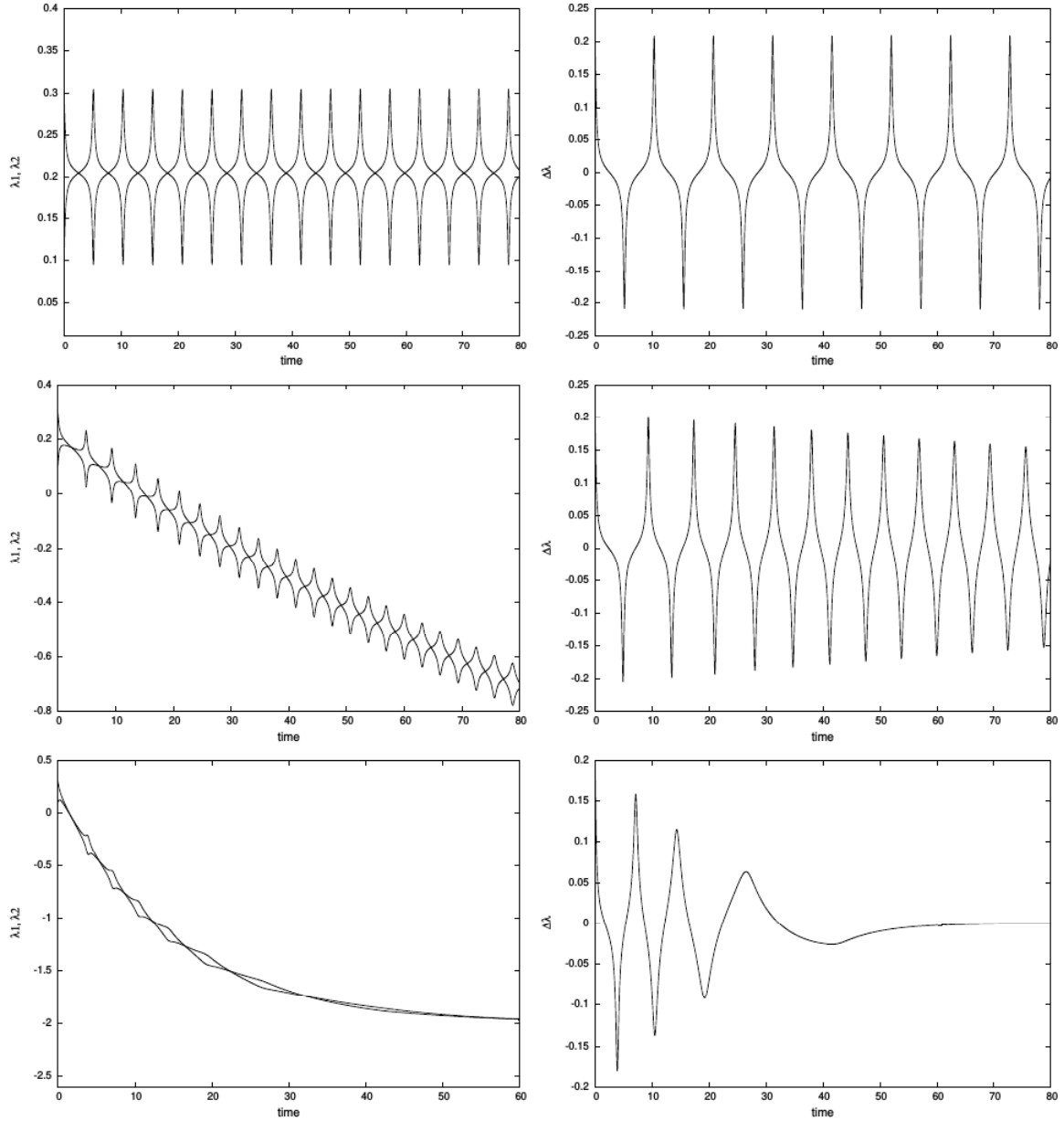


Figure 21: Left column: Time variations of  $\lambda_1$ (downward from  $T = 0$ ) and  $\lambda_2$ (upward from  $T = 0$ ). Right column: Time variations of amplitude difference  $\Delta\lambda$ , initial values are  $\lambda_1 = 0.3, \lambda_2 = 0.1, \theta_1 = 0.28, \theta_2 = 0.1$ . Parameter values are  $\kappa = 2, M = 0.2$ . From top to bottom rows:  $N = 0.0, 0.001, 0.1$ .

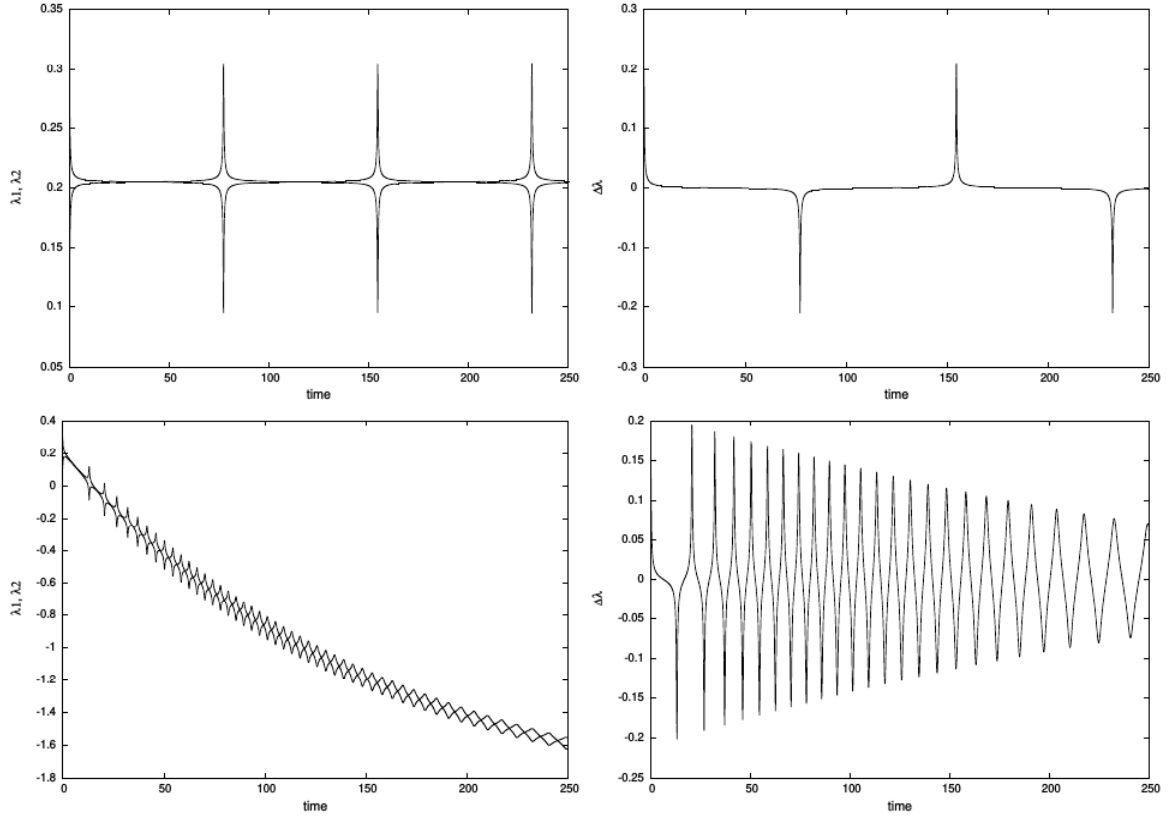


Figure 22: Left column: Time variations of  $\lambda_1$ (downward from  $T = 0$ ) and  $\lambda_2$ (upward from  $T = 0$ ). Right column: Time variations of amplitude difference  $\Delta\lambda$ , initial values are  $\lambda_1 = 0.30076$ ,  $\lambda_2 = 0.1$ ,  $\theta_1 = 0.28$ ,  $\theta_2 = 0.1$ . Parameter values are  $\kappa = 2$ ,  $M = 0.2$ . From top to bottom rows:  $N = 0.0, 0.01$ .

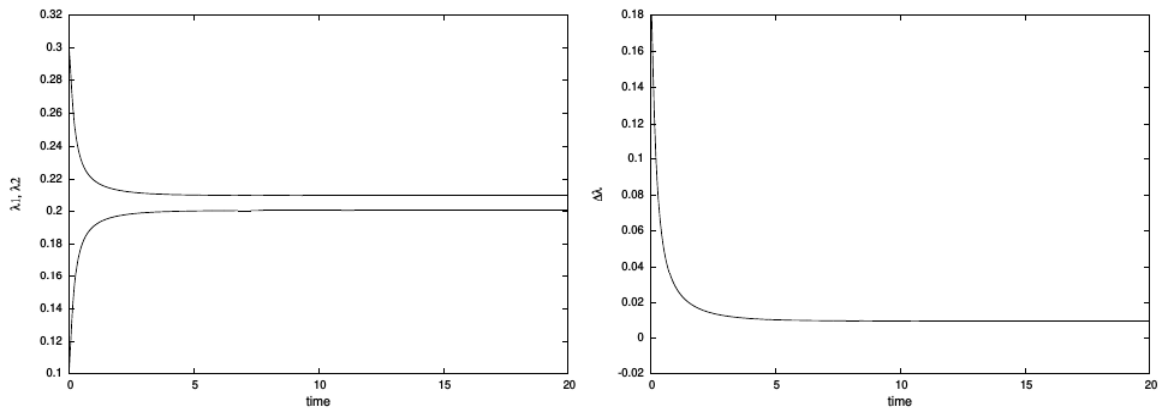


Figure 23: Left column: Time variations of  $\lambda_1$ (downward from  $T = 0$ ) and  $\lambda_2$ (upward from  $T = 0$ ). Right column: Time variations of amplitude difference  $\Delta\lambda$ , initial values are  $\lambda_1 = 0.301$ ,  $\lambda_2 = 0.1$ ,  $\theta_1 = 0.28$ ,  $\theta_2 = 0.1$ . Parameter values are  $\kappa = 2$ ,  $M = 0.2$ ,  $N = 0.0$ .

Figure (22) has as initial values  $\lambda_1 = 0.30076$ ,  $\lambda_2 = 0.1$ ,  $\theta_1 = 0.28$ ,  $\theta_2 = 0.1$ ,  $\kappa = 2$  and  $M = 0.2$ . From top to bottom rows:  $N = 0.0, 0.01$ . Both figures (21) and (22) show that

as the initial values of the amplitudes increases, the effect of the resistive coefficient as a damping factor becomes clearer on the pulse propagation of our soliton signal.

From figures (21) and (22) one sees that when the differences in initial values of these parameters increase, their variations are more and more dominated by anharmonic oscillations.

Figure (23) shows a total suppression of leapfrogging when the differences between the initial amplitudes and phases become relatively large.

### III.3.2 Analysis of Leapfrogging for Coupled LC NLTs with Impurity

#### Adiabatic equations of soliton-pair motion

Within the framework of the adiabatic perturbation theory [19], the temporal evolutions of the amplitudes  $\kappa_i$  and phases  $\theta_i$  ( $i = 1, 2$ ) of the two pulses described by equations (131) and (132) leads to the following set of four coupled first-order ordinary differential equations:

$$\frac{d\kappa_1}{dT} = -\frac{8M_1}{15}\kappa_2^2 \operatorname{sech}^2 A [\tanh A + \tanh^3 A] + N_1\kappa_1^5 [4 \operatorname{sech}^4 y_o - 5 \operatorname{sech}^6 y_o], \quad (215)$$

$$\frac{d\kappa_2}{dT} = \frac{8M_1}{15}\kappa_1^2 \operatorname{sech}^2 A [\tanh A + \tanh^3 A], \quad (216)$$

$$\frac{d\theta_1}{dT} = 4\kappa_1^2 - M_1 - \frac{M_1\kappa_2^3}{\kappa_1^3} \operatorname{sech}^2 A [1 - \frac{17}{9}\tanh^2 A], \quad (217)$$

$$\frac{d\theta_2}{dT} = 4\kappa_2^2 - M_1 - \frac{M_1\kappa_1^3}{\kappa_2^3} \operatorname{sech}^2 A [1 - \frac{17}{9}\tanh^2 A], \quad (218)$$

where  $M_1 = C/\gamma C_o$ ,  $N_1 = 24\beta/\gamma$ , and  $y_o = \kappa_1 u_o$ .

Again we introduce small deviations  $\lambda_i$  from the average amplitude  $\kappa$  of the two solitons as  $\kappa_i = \kappa + \lambda_i$ , and the phase difference  $\Delta\theta = \theta_1 - \theta_2$  which too must be small. using the approximation  $y_2 \approx y_1 + A$ , equations (215) to (218) can be linearized and will yield:

$$\frac{d\lambda_1}{dT} = -\frac{8M_1}{15}\kappa^3 \Delta\theta - N_1(\kappa^5 + 5\kappa^4 \lambda_1) + 7N_1(\kappa^7 + 7\kappa^6 \lambda_1)u_o, \quad (219)$$

$$\frac{d\lambda_2}{dT} = \frac{8M_1}{15}\kappa^3 \Delta\theta, \quad (220)$$

$$\frac{d\theta_1}{dT} = 4(\kappa^2 + 2\kappa\lambda_1) - M_1[2 - 3\kappa^{-1}(\lambda_1 - \lambda_2)], \quad (221)$$

$$\frac{d\theta_2}{dT} = 4(\kappa^2 + 2\kappa\lambda_2) - M_1[2 + 3\kappa^{-1}(\lambda_1 - \lambda_2)]. \quad (222)$$

Equations (221) and (222) suggest that the phase difference  $\Delta\theta$  and the amplitude

difference  $\Delta\lambda$  are related through the differential equation:

$$\frac{d\Delta\theta}{dT} = \left( \frac{8\kappa^2 + 6M_1}{\kappa} \right) \Delta\lambda. \quad (223)$$

Also, equations (219) and (220) lead to the following second-order ordinary differential equation for the amplitude difference:

$$\frac{d^2\Delta\lambda}{dT^2} + \Omega_o^2\Delta\lambda + F(\lambda, u_o) = 0, \quad (224)$$

where

$$\Omega_o^2 = \frac{16M_1}{15} \kappa^2 (8\kappa^2 + 6M_1), \quad (225)$$

$$F(\lambda_1, u_o) = (8\kappa^2 + 6M_1)[(5 - 49\kappa^2 u_o)N_1\kappa^3\lambda_1 + (1 - 7\kappa^2 u_o)N_1\kappa^4]. \quad (226)$$

Equation (224) is nothing else but the equation of motion of an harmonic oscillator with the oscillation frequency  $\Omega_o$ , "driven" by a force  $F(\lambda_1, u_o)$ . This drive leads either to an enhancement or a suppression of  $\Delta\lambda$ .

To be more explicit, the expression of  $F(\lambda_1, u_o)$  given in equation (226) suggests that the amplitude difference will oscillate with increasing amplitude when the defective diode is closer to the input end of the transmission line and the average amplitude  $\kappa$  of the leapfrogging solitons is not too large. When  $\kappa$  is relatively large, the impurity will accelerate the soliton signal on line 1 thus increasing its speed relative to the speed of soliton on line 2.

Concerning the issue of the effects of impurities on soliton propagation in NLTLs, it is instructive to stress that the influence of a localized impurity on soliton propagation in NLTLs has been investigated in some past works. It is therefore well established that a default-type impurity will increase the amplitude of a soliton approaching the impurity, hence causing its acceleration in virtue of the amplitude dependence of the velocity of the KdV soliton. In recent numerical simulations, [139], Pan et al. obtained that the response of a soliton signal to the presence of a localized impurity in an *LC* NLTL is standard:

an excess structural defect will always trap a soliton signal causing its delay, whereas a structural default will accelerate the soliton signal on approaching the impurity, whether the impurity is capacitive or inductive.

### **Numerical Simulations of leagfrogging for coupled $LC$ NLTs with Impurity**

We carried out numerical simulation of the set of coupled first-order nonlinear ordinary differential equations (215)- (218), still with a sixth-order Runge-Kutta algorithm with fixed step. Initial values, as well as values of characteristic parameters of the model, are the same as in section III.3.1 of figures (19) and (20), i.e.:  $\lambda_1 = 0.25$ ,  $\lambda_2 = 0.2$ ,  $\theta_1 = 0.25$ ,  $\theta_2 = 0.2$  and parameter values are  $\kappa = 2$ ,  $M_1 = 0.2$ ,  $u_o = 0.3$ . Results are shown in figure (24) for time evolutions of  $\lambda_1$ (downward from  $T = 0$ ) and  $\lambda_2$ (upward from  $T = 0$ ) for different values of the impurity coefficient  $N_1$ .

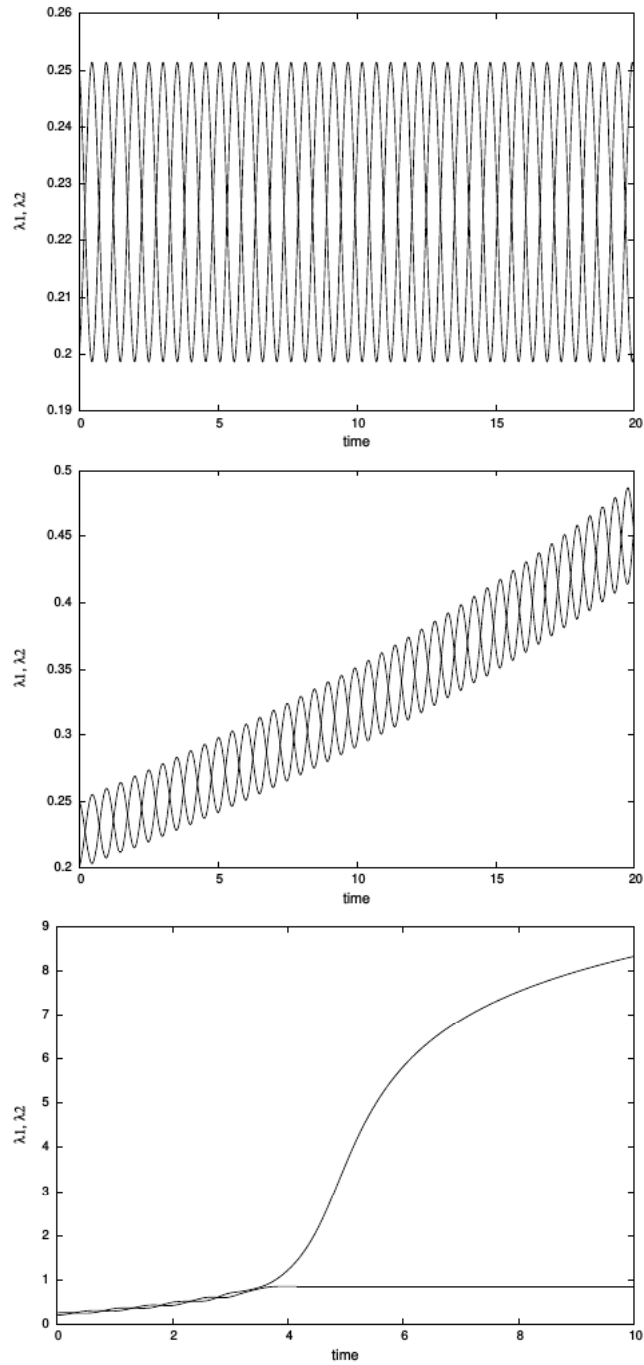


Figure 24: Time variations of  $\lambda_1$ (downward from  $T = 0$ ) and  $\lambda_2$ (upward from  $T = 0$ ) for  $\lambda_1 = 0.25$ ,  $\lambda_2 = 0.2$ ,  $\theta_1 = 0.25$ ,  $\theta_2 = 0.2$  with parameter values  $\kappa = 2$ ,  $M = 0.2$ ,  $u_o = 0.3$  and from top to bottom  $N = 0.0, 0.001, 0.01$ .

Also figure (25) shows the amplitude difference,  $\Delta\lambda$ , for different values of the impurity coefficient  $N$ .

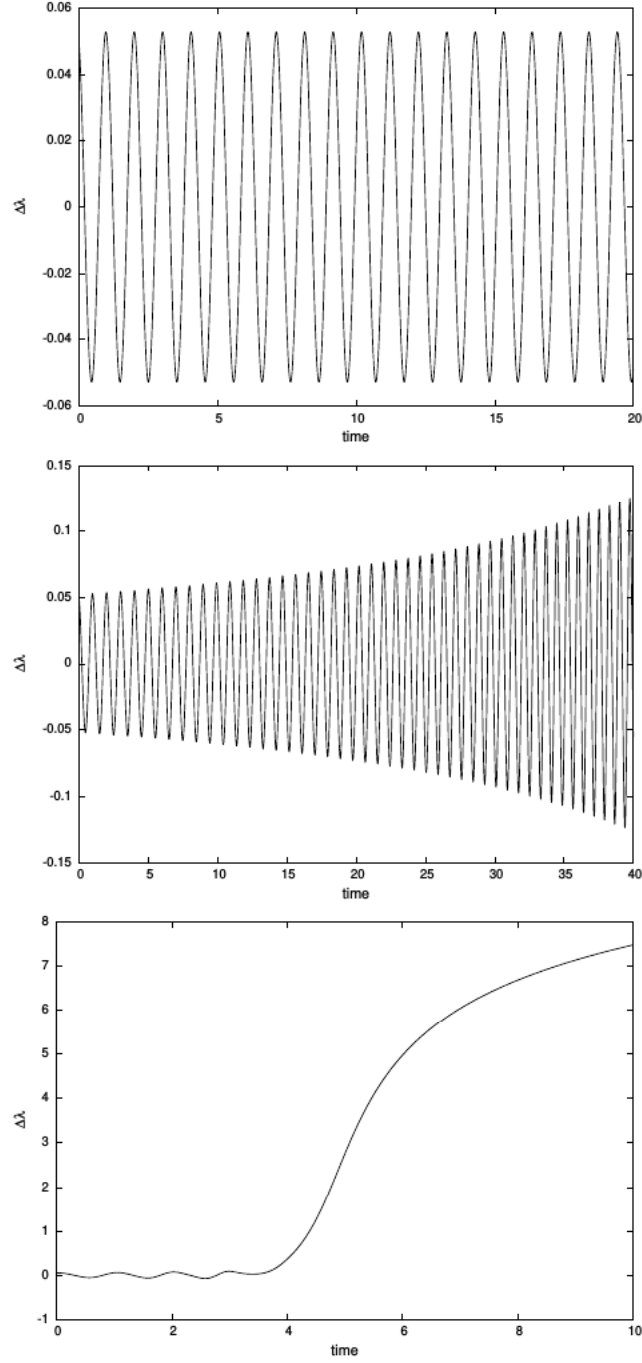


Figure 25: Time variations of  $\Delta\lambda$  for  $\lambda_1 = 0.25, \lambda_2 = 0.2, \theta_1 = 0.25, \theta_2 = 0.2$  with parameter values  $\kappa = 2, M = 0.2, u_o = 0.3$  and from top to bottom  $N = 0.0, 0.001, 0.01$ .

Graphs of figure (24) and (25) show that the soliton leapfrogging is a regular harmonic oscillation with constant maximum amplitudes when there is no impurity. However, as the impurity rate  $\beta$ , and hence the impurity coefficient  $N_1$ , is increased from zero, the amplitude difference  $\Delta\lambda$  oscillates with the maximum oscillation amplitudes increasing



with time. When  $N_1$  attains a critical value, the leapfrogging is suppressed after a short time. A look at the variations of  $\lambda_1$  and  $\lambda_2$  with time on the graphs of figure (24) clearly suggests that  $\lambda_1$  gets amplified after a short propagation time but not  $\lambda_2$ . This implies that there is an acceleration of the soliton signal on line 1 relative to its counterpart on line 2.

We have investigated the leapfrogging dynamics of a pair of KdV solitons in two nonlinear transmission lines, weakly coupled by a linear capacitance. Two different configurations of coupled nonlinear transmission lines were considered: the first model was composed of two *RLC* lines with intraline Schottky varactors while the second model composed of two coupled *LC* lines one of which had a localized capacitive impurity.

In the first model, we obtained that adding the resistive element along with the feedback capacitor on the coupled transmission lines, causes a damping of the soliton amplitudes thus acting against leapfrogging. For leapfrogging to survive the presence of the resistive component, the average amplitude of the two interacting solitons should be large enough and the resistance relatively small, being consistent with the spirit of the adiabatic perturbation theory.

For the second model, we established that a defect in one of the Schottky diodes on line 1 will accelerate the soliton signal on the line, causing a drive of the second soliton with the possibility of their leapfrogging as long as the impurity rate is relatively small. As we increase the impurity rate, the soliton signal in line 1 gains in amplitude and consequently in speed, and hence cannot be followed by the soliton signal in line 2. In this case no leapfrogging can occur.

The effects of a localized impurity on soliton signals in NLTLs have been investigated in several previous works and well established that a localized impurity will always accelerate a soliton approaching the impurity when it is a structural default in the defective electrical component. This response of KdV soliton to the presence of a localized impurity in the NLTL is actually universal, indeed similar behaviors are predicted in many other distinct physical systems such as Josephson-Junction transmission lines [140, 141], Frenkel-Kontorova systems [142, 143], double-well systems [145] and so on.

## III.4 Pulse Amplification and Damping in Lossy Nonlinear Transmission lines with Voltage-Terminals

### III.4.1 Adiabatic equation of soliton motion

Because of the presence of  $P_5(z', \tau')$  in equation (146), the soliton amplitude becomes time dependent and will be denoted  $\kappa$ . Within the framework of the adiabatic perturbation theory [19], the time evolution of  $\kappa$  is determined by the first-order ordinary differential equation:

$$\frac{d\kappa}{d\tau'} = -\frac{1}{4\kappa} \int_{-\infty}^{\infty} dz' P_5(z', \tau') \text{sech}^2 \kappa z'. \quad (227)$$

By substituting  $V$  and  $\phi_1$  given respectively by equations (149) and (153) in equation (146), we obtain:

$$P_5(z', \tau') = 2\alpha\kappa^2 \text{sech}^2 \kappa z' + \alpha\gamma\varphi_0 z' - 4\gamma\kappa^2\varphi_0 z' \text{sech}^2 \kappa z' \tanh \kappa z'. \quad (228)$$

With this last expression, the first-order ordinary differential equation (227) simplifies to:

$$\frac{d\kappa}{d\tau'} = -\frac{2}{3} \left( \alpha - \frac{1}{2} \gamma \varphi_0 \right) \kappa. \quad (229)$$

Integrating equation (229) yields, in the time coordinate  $\tau$ :

$$\kappa(\tau) = \kappa_0 \exp \left[ -\frac{2\eta}{3} \left( \alpha - \frac{1}{2} \gamma \varphi_0 \right) \tau \right]. \quad (230)$$

It turns out that the electrical pulse will be either amplified or damped during propagation, depending on which among the resistance and voltage terminal has the dominant effect on its amplitude. However, expressions of  $\alpha$  and  $\gamma$  in formula (147) and (148) respectively, suggest that  $\gamma$  will be generally smaller than  $\alpha$ . Indeed  $\gamma$  is proportional to  $m$ , a small parameter compared with the quantity  $V_J/RC_0$  determining the magnitude of  $\alpha$ . In the next section we solve the line equations numerically, in order to compare results

of direct numerical simulations with those obtained in this section within the framework of the adiabatic perturbation theory, as concerns the competing effects of the voltage terminal and the resistance on the pulse amplitude.

### III.4.2 Numerical Simulations of Discrete Line Equations

In the previous section we investigated, using the adiabatic perturbation theory, the simultaneous effects of a passive resistance and a voltage terminal on pulse propagation along an LC NLTL. We obtained that the resistance induces a damping whereas the voltage terminal amplifies the electrical pulse, suggesting the possibility to balance the pulse amplification phenomenon predicted in a recent study [135]. However, actually the adiabatic perturbation theory is a variational treatment and as such its results are valid only for very small values of the resistance as well as of the voltage terminal.

To fully appreciate the effects of the presence of a resistance and voltage terminal on characteristic features of the propagating electrical pulse, it is relevant to solve the Kirchhoff equations (136) and (137) numerically. Focusing on the voltage signal  $V_n(t)$ , we applied a sixth-order Runge-Kutta scheme [137] on the following second-order time-differential difference equation, derived from the coupled set (136) and (137) after elimination of current variables i.e.  $I_n(t), I_{n\pm 1}(t)$ :

$$\frac{d^2 Q_n}{dt^2} = \frac{1}{L} (V_{n+1} - 2V_n + V_{n-1}) - \frac{1}{R} \frac{d}{dt} (V_n - \Phi_n). \quad (231)$$

As input profile we opt for a pulse-shaped wave of the form:

$$V_n(t = 0) = A_0 \operatorname{sech}^2(n/\ell_0), \quad (232)$$

where the initial amplitude  $A_0$  and width at half tail  $\ell_0$  of the pulse are two arbitrary real parameters. Throughout simulations they will be fixed as  $A_0 = 1.9$ ,  $\ell_0 = 1.7$  (in units of length of an elementary cell).

Numerical simulations were carried out assuming a NLTL with 500 units cells, with a

propagation time  $0 \leq t \leq 2000$  and a time step of  $10^{-4}$ . Characteristic parameters in the discrete line equation (231) were fixed, except the resistance  $R$  for which different values were considered. Concretely the following values were given to characteristic parameters of the model:  $C_0 = 0.6$ ,  $L = 0.001$ ,  $b = V_J^{-1} = 0.25$ ,  $m = 0.98$ . Also, to check the pulse amplification predicted in [135] and in the analytical development of the previous section, we shall consider  $\Phi_n = \phi_0 n$  where  $\phi_0$  is a constant which will be varied.

Figures (26), (27) and (28) show profiles of the voltage signal  $V(n(t))$  as it propagates, for three distinct values of  $\phi_0$  and different values of the resistance  $R$  in each figure. More precisely figure (26) corresponds to the context where only the resistive component is present in the NLTL, while figures (27) and (28) correspond to  $\phi_0 = 0.5$  and  $\phi_0 = 1.5$ , respectively. In figure (26) the voltage signal  $V_n(t)$  propagates with a manifestly exponentially decreasing amplitude. It is quite noticeable that as the resistance increases the exponential damping sharpens, with a possibility of total disappearance of the pulse due to dissipation by the resistance. Figure (27) and figure (28) show pulse propagation for the same values of the resistance as in figure (26), but now for nonzero values of  $\phi_0$ . Quite remarkably, as  $\phi_0$  is increased the sharp exponential damping observed for  $\phi_0 = 0$  is gradually balanced. Clearly a nonzero value of  $\phi_0$  favors pulse amplification as predicted in [135], and consistent with the analytical result obtained above. Also remarkable on the 3D curves is the behaviour according to which when  $\phi_0$  increases, the pulse desintegrates into two and probably more pulses after a finite propagation time. This behaviour could not be accounted for analytically. From a general standpoint, numerical results suggest that a combination of the resistance with the voltage terminal can enable one control growth of the pulse amplitude or vice-versa, i.e. can prevent pulse from being totally dissipated by a resistive component in the line [144]. For instance a resistance will be needed to maintain a finite-amplitude pulse in a NLTL designed with a voltage terminal. This result is not only interesting, in fact it introduces a novel perspective in various applications such as radar transmissions, microwave and ultra-wideband electronic devices, antenna networks, short-pulse electromagnetics and other contexts where electrical pulse amplifications hold a relevant role [86, 135, 146].

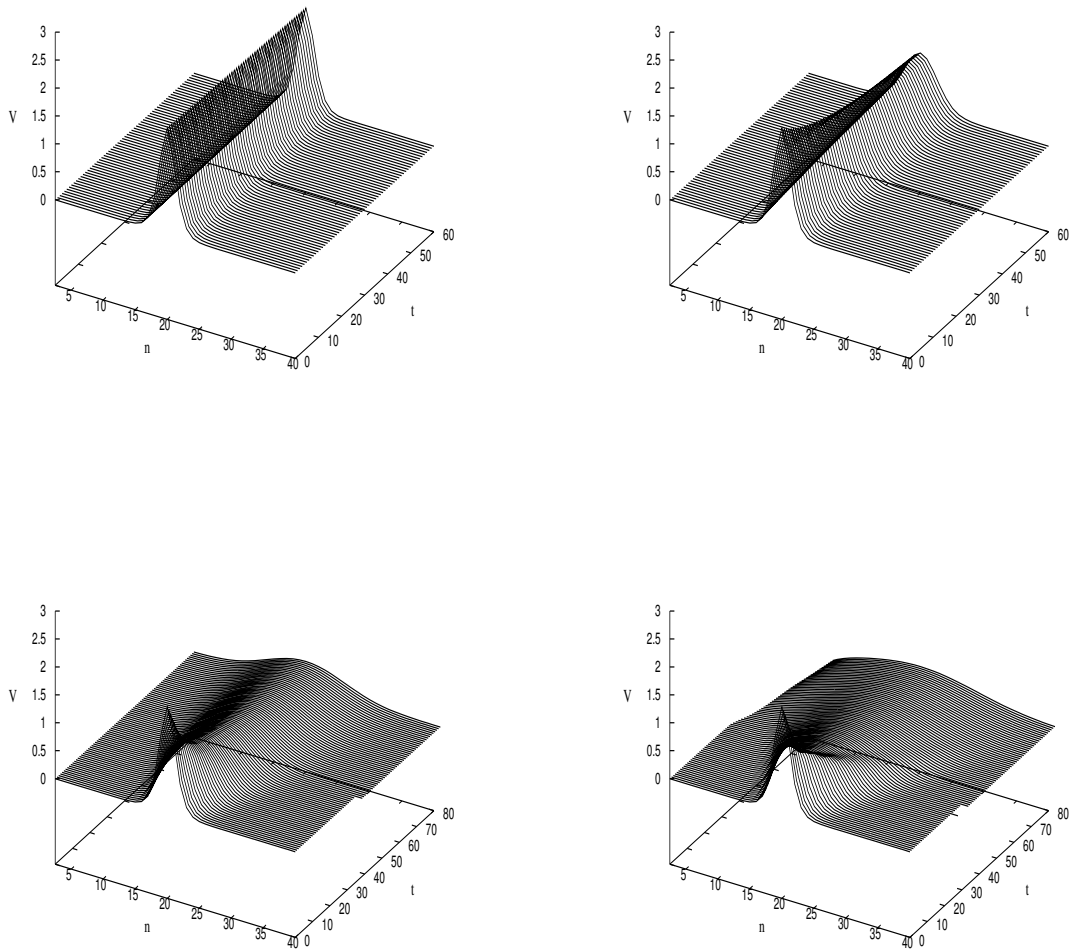


Figure 26: (Color online) space-time evolution of the voltage signal along the NLTL, in the absence of voltage terminal (i.e.  $\phi_0 = 0$ ) and for different values of the resistance  $R$ . Top graphs:  $R = 0.0005$  (left),  $R = 0.01$  (right). Bottom graphs:  $R = 0.05$  (left),  $R = 0.1$  (right).

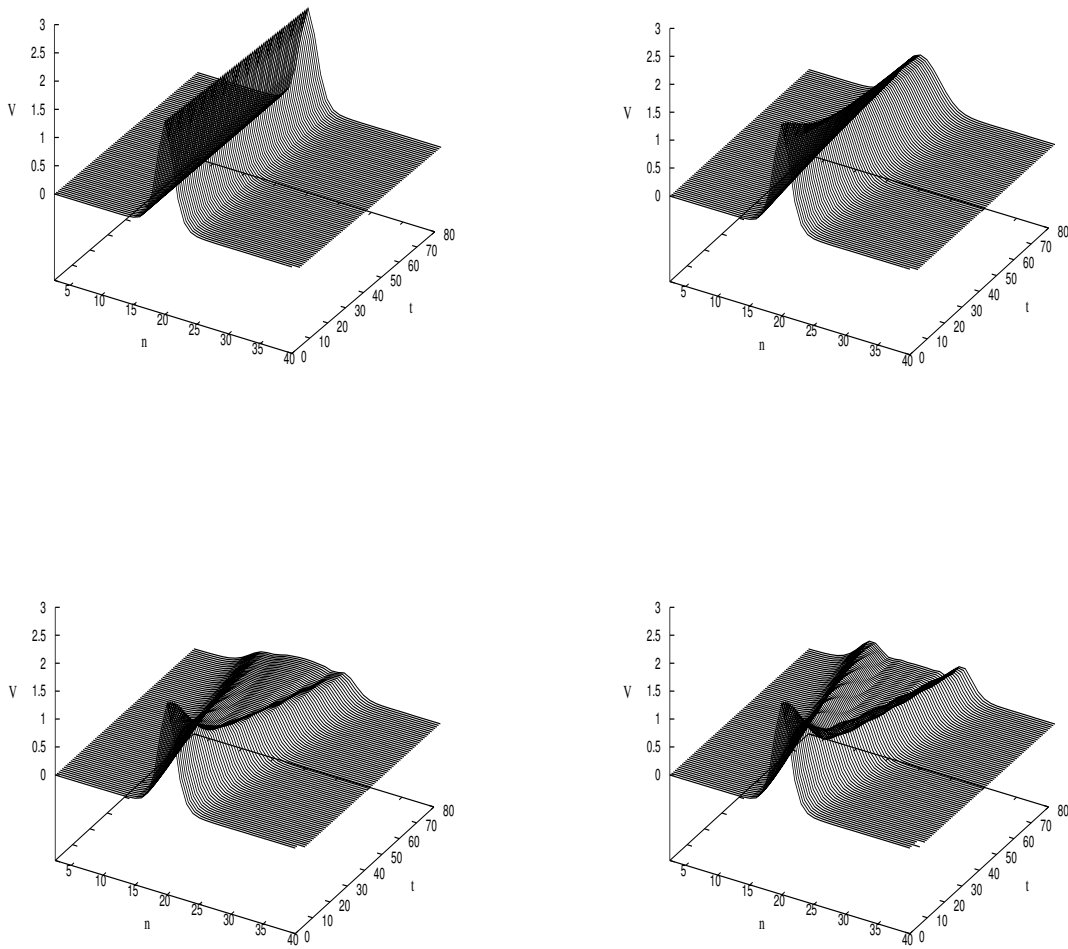


Figure 27: (Color online) space-time evolution of the voltage signal along the NLTL, for  $\phi_0 = 0.5$  and for different values of the resistance  $R$ . Top graphs:  $R = 0.0005$  (left),  $R = 0.01$  (right). Bottom graphs:  $R = 0.05$  (left),  $R = 0.1$  (right).

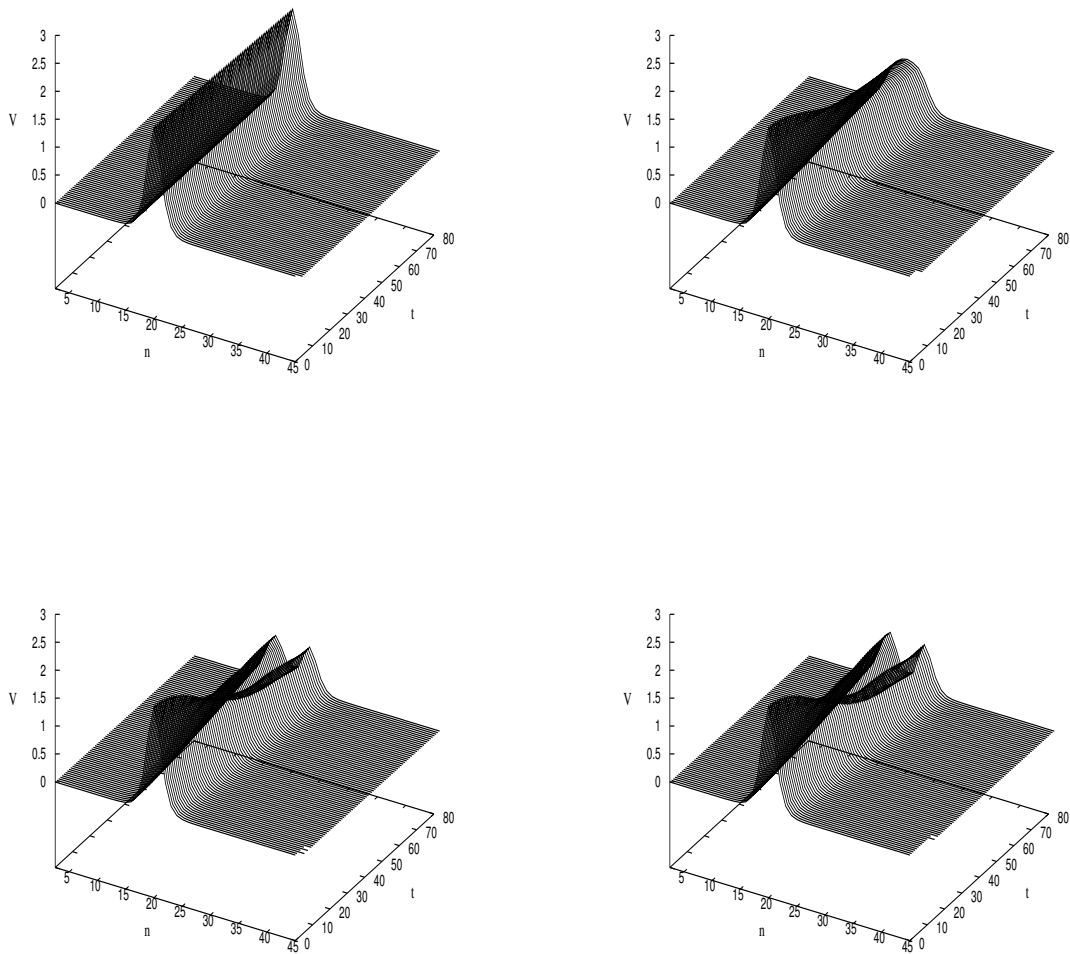


Figure 28: (Color online) space-time evolution of the voltage signal along the NLTL, for  $\phi_0 = 1.5$  and for different values of the resistance  $R$ . Top graphs:  $R = 0.0005$  (left),  $R = 0.01$  (right). Bottom graphs:  $R = 0.05$  (left),  $R = 0.1$  (right).

### III.5 Conclusion

In this chapter we have explored the propagation of signals in NLTLS. In the first case we examined the leapfrogging motion of a pair of solitons along two NLTLS weakly coupled by a linear capacitor shunted by a linear resistor. We established that the resistive coupling caused a decreased in the leapfrogging frequency. This resistive coupling also caused a damping of amplitudes of the signals. Secondly, leapfrogging dynamics was again investigated in two *RLC* lines with intraline Schottky varactors and in two coupled *LC* lines one of which had a localized capacitive impurity. For leapfrogging to survive in the two *RLC* lines, the average amplitude of the two interacting solitons should be large enough and the resistance relatively small. In the coupled lines with a localized capacitive impurity, we established that a defect in one of the varactors will accelerate the soliton signal on the line. Finally pulse amplification and damping was investigated in NLTLS with voltage-terminal modules. Our analytical treatment established that pulse-shaped solitons can propagate through the line while experiencing amplification caused by the voltage-terminal modules and damping due to the resistances.



---

---

# General Conclusion

---

This thesis reports on signal propagation in NLTLs, specifically on the leapfrogging dynamics of electrical pulses propagating in NLTLs and pulse amplification and damping in lossy NLTLs with voltage terminals. The results include a range of background survey on NLTLs, computer simulations, numerical and analytical.

The General Introduction was all about the general overview on NLTLs, review on leapfrogging in nonlinear dynamics and the outline of this thesis. In chapter 1 we discussed the literature review on NLTLs. In this chapter we defined a NLTL as a nonlinear dispersive media where electrical signals can propagate in the form of voltage waves. Also NLTLs are constructed by periodically loading normal transmission lines with nonlinear capacitors and/or inductors. And that the theoretical study of soliton propagation in nonlinear  $LC$  networks has been carried out with much attention devoted to the Toda lattice equation and the KdV equation. Electrical NLTLs are undoubtedly the best platforms for all electrical short pulse generation.

In order to understand soliton propagation in NLTLs, it is necessary to first understand the nature of the medium through which they propagate. Thus its necessary to first of all study the general theory of transmission lines. From this development, a physical understanding for the cause and nature of solitons became clear. Also through this development, some of the basics of the mathematical understanding of solitons became clearer, and the connection between the physical and the mathematical concepts of solitons can be made.

Chapter 1 also described the detail development of transmission lines, theory of NLTLs, soliton systems and the perturbation theory. All these form the mathematical backbone of this thesis. Under transmission lines we defined and described the different

types of transmission lines, i.e., coaxial line, two-wire line, parallel plate, planar and microstrip lines. But most of our discussions were restricted to two parallel conductors with the distance between the two conductors being substantially smaller than the wavelengths of the signals on the line. Next the theory of transmission lines is discussed and its equivalent circuit model was presented. From this circuit model, line equations were derived and some characteristics of transmission lines examined. From an understanding of transmission lines, we then presented the NLTL which comprise of a transmission line periodically loaded with varactors.

In chapter 2, we presented and discussed the materials and methods used in the research work of this thesis. Equivalent circuit models for the coupled NLTLs (lossy and lossless) were presented. Amongst the nonlinear model reduction methods discussed in the chapter, the perturbation method applied to the KdV equation is most importantly treated, since the KdV equation is the main evolution equation of our soliton signal. In addition to this the sixth order Rung-Kutta method used in our numerical analysis was also discussed.

In chapter 3, we presented and discussed the main results of this thesis. In the first section, the dynamics of soliton-pair leapfrogging in two  $RC$  coupled NLTLs is examined. In this section we aimed at investigating the leapfrogging of a pair of electrical pulses propagating each along a nonlinear  $LC$  line, both weakly interacting via a coupling branch composed of a linear capacitor shunted by a linear resistance. We obtained that the leapfrogging was possible provided the two electrical pulses were almost identical and moved at nearly equal speeds. By describing the leapfrogging as oscillations of the phase and amplitude differences between the two interacting solitons, we obtained the leapfrogging frequency and showed that it was a decreasing function of the resistive coupling coefficient. Numerical simulations revealed that as the phase and amplitude differences between the two electrical pulse increase, their separation also increases leading to suppression of the leapfrogging motion over a finite propagation time. The resistance coupled to the capacitive coupling was shown to extend the leapfrogging propagation time, thus the resistive element could be utilize as a control mechanism

for the lifetime of leapfrogging motions of solitons in weakly coupled nonlinear  $LC$  transmission lines.

In real physical contexts it is difficult to design an electrical network with a completely lossless dielectric medium between the conductors. Therefore, understanding how dielectric medium losses influence the leapfrogging dynamics is an important issue for multiplexed signal propagations and energy transfer in transmission line networks. leapfrogging on NLTLs can for instance be used to manage traveling multiple electrical pulses, as well as the transmission of multiplexed signals with minimal energy. A good understanding of the behaviours of leapfrogging pulses on NLTLs could therefore extend the application of NLTLs in ultrafast electronics.

Next in chapter 3, we investigated the leapfrogging motion of a soliton-pair in two distinct physical models. In the first model we considered the case of two  $RLC$  NLTLs coupled via a linear capacitance, and in the second model two capacitively coupled  $LC$  NLTLs one of which contains an imperfect varactor. In both models, we first derived, using KCL and KVL, the discrete set of nonlinear equations for the coupled NLTLs. Because we were seeking for pulse signals, we applied a multiple-scale expansion of solutions in the full continuum limit which enabled us to obtain a set of coupled KdV equations in the relevant scale. These coupled set of KdV equations were then treated analytically within the framework of the adiabatic perturbation theory, by defining appropriate variables for leapfrogging of the two KdV signals as they propagate at nearly equal amplitudes and velocities. We obtained in the first model that adding the resistive element along with the feedback capacitor on the coupled NLTLs, causes a damping of the amplitude of the soliton thus acting against leapfrogging. Therefore for leapfrogging to survive this damping effect of the resistive component, the average amplitude of the two interacting solitons should be large enough and the resistance relatively small. We established in the second model that a defect in one of the varactors in line 1 of the coupled NLTLs, will accelerate the soliton signal on the line, causing a drive of the second soliton with the possibility of their leapfrogging as long as the impurity rate is relatively small. As we increased the impurity rate, the soliton in line 1 gains in amplitude and

consequently in speed, and hence cannot be followed by the soliton signal in line 2. At this point and after, no leapfrogging can occur.

Finally in chapter 3, a model of nonlinear electrical transmission line periodically loaded with Schottky varactors shunted by resistances and connected to voltage terminal modules, was investigated. Following the multiple-scale expansion method, we analytically derived the perturbed KdV equation where the perturbation term groups the effects of the voltage terminal and of the resistance. This analytical study led to a KdV-type pulse whose amplitude is amplified during propagation due to the voltage terminal, and damped due to the resistance. Numerical simulations by means of a sixth-order Runge-Kutta algorithm further provides evidence of a dominant effect of the resistive component over amplification due to voltage terminal. Our simulations also brought out a possible pulse disintegration into two pulses caused by the competition between damping and amplification upon propagation.

This work finds relevant application in energy transfer on transmission line networks, where leapfrogging of simultaneously launched electrical pulses can help manage their characteristic propagation parameters such as their speeds, phases, intensities, widths and so on.

## Perspectives

Numerical analysis is a powerful tool to study evolutions of nonlinear waves in a self-consistent manner. Combination of numerical analysis and analytical solutions can help us to understand nonlinear wave behavior and underline physical processes in a complicated nonlinear system. Numerical aspects, computational methods are always inevitable studies like soliton propagation in coupled NLTLs.

As fruitful extension to the work presented here:

- Despite the fact that the results obtained in the leapfrogging dynamics of interacting solitons in weakly coupled NLTLs reveal a rich dynamics of the system, as a further perspective it would also be interesting to look at the competing effects of the coupling capacitance and resistance on the leapfrogging motion when the coupling parameters are not too small. Given that adiabatic considerations in this context cannot be applied, only a full numerical treatment of the discrete line equations would be consistent. This later study requires a specific context since several characteristic parameters are involved in the model and their contributions need to be well emphasized both quantitatively and qualitatively.

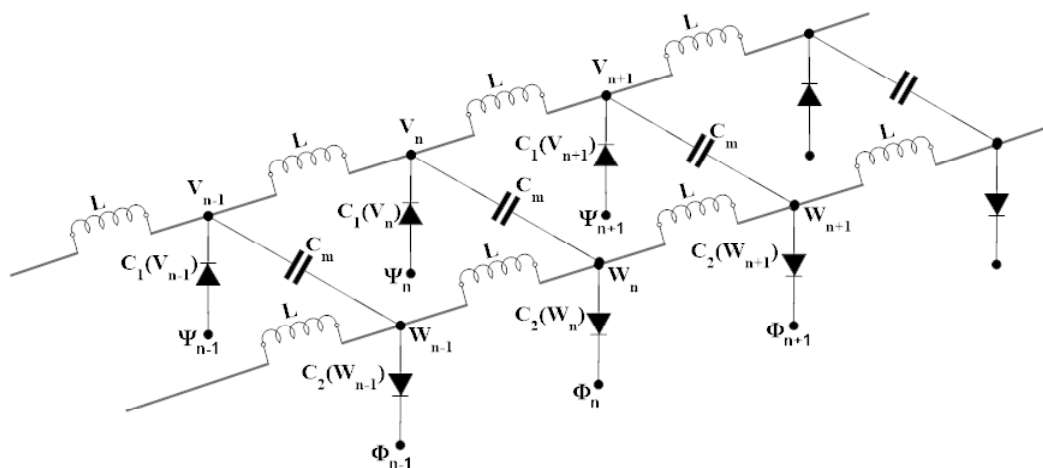


Figure 29: Equivalent circuit model of a coupled NLTLs with voltage terminal modules

- The study of leapfrogging dynamics of solitons in coupled NLTLs can be extended

to a coupled NLTL with voltage terminal modules. The main objective in this line given in figure (29) will be to examine the influence of the step-like voltage on the relative amplitude and phase oscillations of the two interacting solitons.

- Our dynamics of soliton propagation in a single impure NLTL can be extended to study the impure NLTL circuit of figure (30). In this case we consider a model of an electrical circuit, which consist of a primary monoinductance in parallel with a capacitance  $C_1$ , shunted cell to cell by a nonlinear capacitance in parallel with a resistance as shown in figure (30).

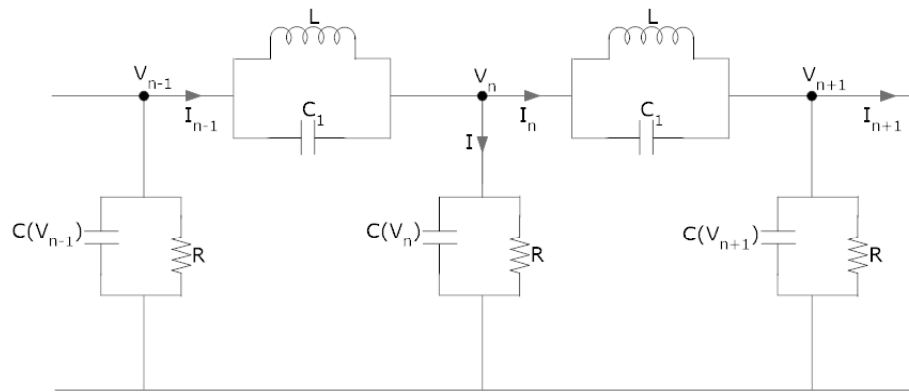


Figure 30: Equivalent circuit model of NLTL with monoinductance in parallel with capacitance  $C_1$ .

- From our understanding of the work on two  $RLC$  or  $LC$  coupled NLTLs, we can extend this to the study of lossy and defective left handed NLTLs.

In this thesis, a conscious effort has been made to approach problems from an analytical point of view, using MMS and perturbation method to derive nonlinear evolution equations which were numerically simulated. We hope that a similar symbiosis of techniques will further advance this study of soliton propagation on NLTLs.

---

# Bibliography

---

- [1] J. Gaudet, E. Schamiloglu, J. O. Rossi, C. J. Buchenauer, and C. Frost, *Nonlinear transmission lines for high power microwave Applications - A survey*, in Proc. IEEE Int. Pulsed Power Conf., pp.131, (2008).
- [2] A. C. Singer and V. Oppenheim, *Circuit implementations of soliton systems* International Journal of Bifurcation and Chaos, **9**, 571, (1999).
- [3] V. Duez, X. Melique, O. Vanbesien, P. Mounaix, F. Mollot, and D. Lippens, *High capacitance ratio with GaAs/InGaAs/AlAs heterostructure quantum well-barrier varactors*, Electron Lett. **34**, 1860, (1998).
- [4] R. Hirota and K. Suzuki, *Studies on lattice solitons by using electrical networks*, J. Phys. Soc. Jpn. **28**, 1366 (1970).
- [5] M. Kintis, L. Xing, F. Flavia, D. Sawdai, L. K. Kwok, and A. Gutierrez, *An MMIC pulse generator using dual nonlinear transmission lines*, Microwave and Wireless Components Lett. **17**, 454 (2008).
- [6] M. J. W. Rodwell, S. T. Allen, R. Y. YU, M. G. Case, U. Bhattacharya, M. Reddy, et al., *Active and Nonlinear wave propagation devices in ultrafast electronics and optoelectronics*, Proc. IEEE **82**, 1037 (1994).
- [7] K. Narahara, *Amplification of short pulses in transmission lines periodically loaded with Schottky varactors*, IEICE Electronics Express **6**, 1199 (2009).
- [8] E. Kengne and R. Vaillancourt, *Propagation of solitary waves on lossy nonlinear transmission lines*. IJMP B.-World Scientific, **23**, 1 (2009).

- [9] E. Carman, M. Case, M. Kamegawa, R. Yu, K. Giboney, and M. J. W. Rodwell, *V-Band and W-Band Broad-Band, Monolithic Distributed Frequency Multipliers*, IEEE Microwave Guid. Wave Lett. **2**, 253, (1992).
- [10] J. R. Thorpe, P. Steenson, and R. Miles, *Non-linear transmission lines for millimeter-wave frequency multiplier applications*, Proceedings of the IEEE Sixth International Conference on Terahertz Electronics, pp. 54, (1998).
- [11] J.-M. Duchamp, P. Ferrari, M. Fernandez, A. Jrad, X. Mélique, J. Tao, S. Arscott, D. Lippens, and R. G. Harrison, *Comparison of fully distributed and periodically loaded nonlinear transmission lines*. IEEE Transactions on Microwave Theory and Techniques, **51**, 1105, (2003).
- [12] D. S. Ricketts, D. Ham, *Electrical solitons: theory, design, and applications*, CRC Press, Taylor and Francis, London, (2011).
- [13] M. Remoissenet, *Waves Called Solitons*, 3th edn., Springer-verlag, Berlin, (1999).
- [14] Y. S. Kivshar, *Intrinsic localized modes as solitons with a compact support*, Phys. Rev. E, **48**, 43 (1993).
- [15] E. Afshari, H. S. Bhat, A. Hajimiri, and J. E. Marsden, *Extremely wideband signal shaping using one- and two-dimensional nonuniform nonlinear line*, J. Appl. Phys. **99**, 054901 (2006).
- [16] K. Narahara and M. Nakamura, *Compensation of polarisation mode dispersion with electrical nonlinear transmission lines*, Jpn. J. Appl. Phys. **42**, 6327 (2003).
- [17] K. Narahara, *Coupled nonlinear transmission lines for doubling repetition rate of incident pulse streams*, Progress in Electromagnetics Research Letters **16**, 69 (2010).
- [18] K. Narahara, *Characterization of partially nonlinear transmission lines for ultrashort-pulse amplification*, Jpn. J. Appl. Phys. **42**, 5508 (2003).



- [19] Y. S. Kivshar and B. A. Malomed, *Dynamics of solitons in nearly integrable systems*, Rev. Mod. Phys., **61**, 763 (1989).
- [20] B. A. Malomed, "Leapfrogging" solitons in a system of coupled KdV equations, Wave Mot. **9**, 401, (1987).
- [21] K. Narahara, *Characterization of leapfrogging solitary waves in coupled nonlinear transmission lines*, Nonlinear Dyn. **81**, 1805 (2015).
- [22] A. K. Liu, T. Kubota and D. R. S. Ko, *Resonant transfer of energy between nonlinear waves in neighbouring pycnoclines*, Stud. Appl. Math. **63**, 25, (1980).
- [23] A. K. Liu, N. R. Pereira and D. R. S. Ko, *Weakly interacting internal solitary waves in neighbouring pycnoclines*, J. Fluid Mech. **122**, 187, (1982).
- [24] P. D. Weidman and M. Johnson, *Experiments on leapfrogging internal solitary waves*, J. Fluid Mech. **122**, 195, (1982).
- [25] J. D. Wright, A. Scheel, *Solitary waves and their linear stability in weakly coupled KdV equations*, Z. Angew. Math. Phys. **58**, 1, (2007).
- [26] M. Nitsche, P. D. Weidman, R. Grimshaw, M. Ghrist and B. Fornberg, *Evolution of solitary waves in a two pycnocline system*, J. Fluid Mech. **642**, 235, (2010).
- [27] B. Z. Essimbi, A. M. Dikandé, T. C. Kofané, and A. A. Zibi, *localized solitary signals on a coupled nonlinear transmission line*, J. Phys. Soc. Jpn. **64**, 2361 (1995).
- [28] K. Narahara, *Asymmetrical solitary waves in coupled nonlinear transmission lines*, Wave Motion **58**, 13 (2015).
- [29] V. K. Madisetti, *The Digital Signal Processing*, 2nd ed., CRC Press, Taylor and Francis, London, (2009).
- [30] W. S. Duan, *Nonlinear waves propagating in the electrical transmission line*, Europhys. Lett. **66**, 192 (2004).

- [31] J. N. Dinkel, C. Setzer, S. Rawal, and K. E. Lonngren, *Soliton propagation and interaction on a two-dimensional nonlinear transmission line*, *Chaos, Solitons & Fractals* **12**, 91 (2001).
- [32] F. Martin and X. Oriols, *Simple model to study wave propagation in periodic-loaded NLTLs*, *Appl. Phys. Lett.* **78**, 2802 (2001).
- [33] D. W. van der Weide, *Delta-doped Schottky diode nonlinear transmission lines for 480-fs, 3.5-V transients*, *Appl. Phys. Lett.* **65**, 7 (1994).
- [34] X. Oriols and F. Martin, *Analytical solitons in NLTLs loaded with HBVs*, *J. Appl. Phys.* **90**, 2595, (2001).
- [35] Désiré Ndjanfang, David Yémélé, Patrick Marquié, T. C. Kofané, *Compact-like pulse signals in a new nonlinear electrical transmission line*, *Progress in Electromagnetics Research B*, EMW Publishing, **52**, 207 (2013).
- [36] B. Z. Essimbi, and I. V. Barashhenkov, *Gap soliton excitations in a Bi-inductance electrical line*, *J. Phys. Soc. Jpn.* **71**, 448 (2002).
- [37] B. Z. Essimbi and A. A. Zibi, *Stationary localized solitary signals in a nonlinear mono-inductance line*, *J. Phys. D* **32**, 3227 (1999).
- [38] B. Z. Essimbi, *Gap soliton excitations in a model of an electric circuit* *Physica Scripta* **67**, 164 (2003).
- [39] K. Narahara, *Traveling-wave retimer with coupled NLTL* *Jpn J. Appl. Phys.* **42**, 1192 (2003).
- [40] K. Narahara, *Characterization of Nonlinear Transmission Lines for Short Pulse Amplification*, *J. Infrared Milli Terahz Waves* **31**, 411 (2010).
- [41] P. D. Green, D. Milovic, A. D. Lott, A. Biswas, *Optical solitons with higher order dispersion by semi-inverse Variational principle*, *Progress in Electromagnetic Research* **102**, 337, (2010).

- [42] G. V. Eleftheriades, A. K. Iyer, and P. C. Kremer, *Planar negative refractive index media using periodically LC loaded transmission lines*, IEEE Trans. Microwave Theory & Tech. **50**, 2397, (2002).
- [43] A. M. Belyantsev and A. B. Kozyrev, *RF oscillation generation in coupled transmission lines with anomalous and normal dispersion*, Technical Physics **46**, 864 (2001).
- [44] A. M. Kozyrev, *The structure of a shock electromagnetic wave synchronous with several waves Propagating in coupled transmission lines with different types of dispersion* Technical Physics **47**, 272 (2002).
- [45] A. M. Belyantsev and A. B. Kozyrev, *Reverse doppler effect under reflection from a shock electromagnetic wave*, Technical Physics vol.**47**, 1477 (2002).
- [46] I. V. Shadrivov, A. A. Sukhorukov, and Y. S. Kivshar, *Nonlinear surface waves in LH materials*, Phys. Rev. E **69**, 01667, (2004).
- [47] B. G. Onana Essama, S. Ndjakomo Essiane, F. Biya Motto, M. Shabat, J. Atangana, *Triangular rogue waves and multi-wave trains generation in a chameleon electrical transmission line*, American Journal of Optics and Photonics, vol.**8**, 61 (2020).
- [48] C. Caloz, H. Okabe, T. Iwai, and T. Itoh, *Transmission line approach of LH materials*, USNC/URSI Nat. Radio Science Meeting, San Antonio, TX, **1**, (2002).
- [49] C. Caloz, I.-H. Lin, and T. Itoh, *Characteristics and potential applications of nonlinear LH transmission line*, Microw. and Opt. Tech. Lett. **40**, 471 (2004).
- [50] A. B. Kozyrev and W. van der Weide, *Nonlinear transmission lines in LH media* IEEE MTT-S Digest, (2004).
- [51] A. Lai, T. Itoh, and C. Caloz, *Composite right/left-handed transmission line metamaterials*, IEEE Microw. Mag. **5**, 34 (2004).

- [52] I. Gil, J. Bonache, J. Garcia-Garcia, and F. Martin, *Tunable metamaterial transmission lines based on varactor-loaded split-ring resonators*, IEEE Trans. Microwave Theory Tech. **54**, 2665 (2006).
- [53] D. Kuylenstierna, A. Vorobiev, P. Linnér, and S. Gevorgian, *Composite right/left handed transmission line phase shifter using ferroelectric varactors*, IEEE Microw. Wirel. Compon. Lett. **16**, 167 (2006).
- [54] A. B. Kozyrev, H. Kim, A. Karbassi, and D.W. van der Weide, *Wave propagation in nonlinear left-handed transmission line media*, Appl. Phys. Lett. **87**, 121109 (2005).
- [55] A. B. Kozyrev and D. W. van der Weide, *Trains of envelope solitons in nonlinear left-handed transmission line media*, Appl. Phys. Lett. **91**, 254111 (2007).
- [56] A. B. Kozyrev and D. W. van der Weide, *Nonlinear left-handed transmission line metamaterials*, J. Phys. D **41**, 173001 (2008).
- [57] A. K. Popov and V. M. Shalaev, *Negative-index metamaterials: Second-harmonic generation, Manley-Rowe relations and parametric amplification*, Appl. Phys. B **84**, 131 (2006).
- [58] David A. Powell, I. V. Shadrivov, and Yuri S. Kivshar, *Asymmetric parametric amplification in nonlinear left-handed transmission lines*, Appl. Phys. Lett. **94**, 084105 (2009).
- [59] F. G. Gharakhili, M. Shahabadi, M. Hakkak, *Bright and dark soliton generation in a LH nonlinear transmission line with series nonlinear capacitance*, Progress in Electromagnetic Research, PIER **96**, 237 (2009).
- [60] G. Bickele Ambassa, F. Biya Motto, B. Essimbi Zobo, T. Crepin Kofane, *Wave solitons in a coupled left-handed nonlinear transmission line: Effect of the coupling parameter*, Chaos, Solitons and Fractals **91**, 400 (2016).
- [61] S. A. Fairlie, *Modulation of the output of an XeCl laser by the generation of electrical solitons*, Optical and Quantum Electronics **26**, 373, (1994).

- [62] S. Ibuka, T. Miyazawa, A. Ishii, *Fast high voltage pulse generator with NLTL for high repetitive operation*, Proc. of 10th IEEE Int. Pulsed Power Conf. **2**, 1365 (1995).
- [63] T. Kuusela, and J. Hietarinta, *Nonlinear electrical transmission line as a burst generator*, Rev. Sci. Instrum. vol. **62**, 2266 (1991).
- [64] N. Seddon, C. R. Spikings, and J. E. Dolan, *RF pulse formation in NLTLs*, Proc. of 16th pulsed power conf. pp.678-681 (2007).
- [65] P. W. Smith, *Transient electronics - pulsed circuit technology*, West Sussex, England: John Wiley and Sons, (2002).
- [66] J. O. Rossi and P. N. Rizzo, *Study of hybrid NLTLs for high power RF generation*, IEEE August (2009).
- [67] G. Gottwald, R. Grimshaw, and B. Malomed, *Parametric envelope solitons in coupled Korteweg-de Vries equations*, Phys. Lett. A **227**, 47 (1997).
- [68] R. Grimshaw and B. Malomed, *New type of gap soliton in a coupled KdV wave system*, Phys. Rev. Lett. **72**, 949 (1994).
- [69] Y. Zhou, M. wang, and Y. Wang, *Periodic wave solutions to a coupled KdV equations with variable coefficients*, Phys. Lett. A **308**, 31 (2003).
- [70] Y. S. Lou, B. Tong, H.-C Hu, and X.-Y. Tang, *Coupled KdV equations derived from two-layer fluids*, J. Phys. A Math. Gen. **39**, 513 (2006).
- [71] H. Triki, A. El Akrmi, and M. K. Rabia, *Soliton solutions in three linearly coupled KdV equations*, Opt. Commun. **201**, 447 (2002).
- [72] R. Guo, Y.-F. Liu, H.-Q. Hao, F.-H. Qi, *Coherently coupled solitons, breathers and rogue waves for polarized optical waves in an isotropic medium*, Nonlinear Dyn. **80**, 1221 (2015).
- [73] W.-S Duan, *Nonlinear Waves Propagating in the Electrical Transmission Line*, Europhys. Lett. **66**, 192 (2004).

- [74] K. Narahara, *Coupled NLTLs for doubling repetition rate of incident pulse streams*, Progress in Electromagnetic Research Letters **16**, 67 (2010).
- [75] A. J. Fairbanks, A. M. Darr, A. L. Garner, *A review of nonlinear transmission line system design*, IEEE Access **8**, 148606 (2020).
- [76] S. M. Jackson, M. Swartz, M. Burton, T. W. Head, *Certified Wireless Design Professional Official Study Guide: Exam PW0 - 250*, John Wiley and Sons (2011).
- [77] V. G. Oklobdzija, R. K. Krishnamurthy, *High performance energy efficient microprocessor design*, Springer, (2006).
- [78] G. B. Singh, H. R. Hiziroglu, *Electromagnetic field theory fundamentals*, 2nd Ed. Cambridge University Press, (2004).
- [79] R. V. Antti, A. Lehto, *Radio Engineering for Wireless Communications and sensor Applications*, Artech House, (2003).
- [80] Jiaping Lu, *Design and characterization of GaAs multilayer CPW components and circuits for advanced MMICs*, Ph.D Thesis, University of Manchester, (2011).
- [81] D. Budimir, I. D. Robertson, A. H. Khalid and A. A. Rezazadeh, *Low loss multilayer coplanar waveguide transmission lines on silicon substrate for MMICs*, in 26th European Microwave Conference, pp. 697, (1996).
- [82] D. Sriram Kumar, A. Srinivas and G. Ratnakar, *Simulation and analysis of coplanar waveguide (CPW) discontinuities*, 200th Microwave International Conference on Recent Advances in Microwave Theory and Applications, pp. 784, (2008).
- [83] M. S. Nikoo and S. M.-A. Hashemi, *New soliton solution of a varactor-loaded nonlinear transmission line*, IEEE Trans. Microw. Theory Techn., **65**, 4084, (2017).
- [84] M. S. Nikoo and S. M.-A. Hashemi, *Analysis of the power transfer to a nonlinear transmission line*, IEEE Trans. Microw. Theory Techn., **65**, 4073, (2017).

- [85] M. S. Nikoo, S. M.-A. Hashemi, and F. Farzaneh, *Theory of terminated nonlinear transmission lines*, IEEE Trans. Microw. Theory Techn., **66**, 91, (2018).
- [86] E. Afshari and A. Hajimiri, *Non-linear transmission lines for pulse shaping in silicon*, IEEE J. Sol. State Cir. **40**, 744, (2005).
- [87] P. Indirayanti, W. Volkaerts, P. Reynaert, and W. Dehaene, *Picosecond pulse generation with nonlinear transmission lines in 90-nm CMOS for mm-wave imaging applications*, Proc. 19th IEEE Int. Conf. Electron., Circuits, Syst. (ICECS), Seville, Spain, 885 (2012).
- [88] S. Hollung, J. Stake, L. Dillner, M. Ingvarson, and E. Kollberg, *A distributed heterostructure barrier varactor frequency tripler*, IEEE Microw. Guided Wave Lett., **10**, 24, (2000).
- [89] F. S. Yamasaki, L. P. S. Neto, J. O. Rossi, and J. J. Barroso, *Soliton generation using nonlinear transmission lines*, IEEE Trans. Plasma Sci., **42**, 3471, (2014).
- [90] N. S. Kuek, A. C. Liew, E. Schamiloglu, and J. O. Rossi, *Pulsed RF oscillations on a nonlinear capacitive transmission line*, IEEE Trans. Dielectr. Electr. Insul., **20**, 1129, (2013).
- [91] J. O. Rossi, L. P. Silva, J. J. Barroso, F. S. Yamasaki, and E. Schamiloglu, *Overview of RF generation using nonlinear transmission lines*, Proc. IEEE Pulsed Power Conf. (PPC), **1**, (2015).
- [92] L. P. S. Neto, J. O. Rossi, J. J. Barroso, and A. R. Silva, *Characterization of ceramic dielectrics for sub-GHz applications in nonlinear transmission lines*, IEEE Trans. Plasma Sci., **42**, 3274, (2014).
- [93] H. Ikezi, J. S. DeGrassie, and J. Drake, *Soliton generation at 10 MW level in the very high frequency band*, Appl. Phys. Lett., **58**, 986, (1991).
- [94] G. Branch and P. W. Smith, *Fast-rise-time electromagnetic shock waves in nonlinear, ceramic dielectrics*, J. Phys. D: Appl. Phys., **29**, 2170, (1996).

- [95] M. P. Brown and P. W. Smith, *High power, pulsed soliton generation at radio and microwave frequencies*, in 11th IEEE Int. Pulsed Power Conf. Dig. Tech. Papers, Baltimore, MD, USA, **1**, 346, (1997).
- [96] J. Darling, *High power pulsed RF generation by soliton type oscillation on nonlinear lumped element transmission lines*, Ph.D. dissertation, Eng. Sci. Dept., Oxford Univ., Oxford, U.K., (2009).
- [97] M. J. W. Rodwell, M. Kamegawa, R. Yu, M. Case, E. Carman, and K. S. Giboney, *GaAs nonlinear transmission lines for picosecond pulse generation and millimeter-wave sampling*, IEEE Trans. Microw. Theory Techn., **39**, 1194, (1991).
- [98] J. Stake, A. Malko, T. Bryllert, and J. Vukusic, *Status and prospects of high-power heterostructure barrier varactor frequency multipliers*, Proc. IEEE, **105**, 1008, (2017).
- [99] H. Shi, W.-M. Zhang, C. W. Domier, N. C. Luhmann, Jr., L. B. Sjogren, and H.-X. L. Liu, *Novel concepts for improved nonlinear transmission line performance*, IEEE Trans. Microw. Theory Techn., **43**, 780, (1995).
- [100] Q. R. Marksteiner, B. Carlsten, and S. Russel, *Numerical calculations of RF efficiency from a soliton generating nonlinear transmission line*, J. Appl. Phys., **106**, 113306, (2009).
- [101] J. M. Elizondo-Decanini et al., *Soliton production with nonlinear homogeneous lines*, IEEE Trans. Plasma Sci., **43**, 4136, (2015).
- [102] M. G. Case, *Nonlinear transmission lines for picosecond pulse, impulse and millimeter-wave harmonic generation*, Ph.D. dissertation, Dept. Elect. Comput. Eng., California Univ., Santa Barbara, CA, USA, (1993).
- [103] A. M. Belyantsev and A. B. Kozyrev, *Influence of local dispersion on transient processes accompanying the generation of RF radiation by an electromagnetic shock wave*, Tech. Phys., **43**, 80, (1998).



- [104] D. M. French and B. W. Hoff, *Spatially dispersive ferrite nonlinear transmission line with axial bias*, IEEE Trans. Plasma Sci., **42**, 3387, (2014).
- [105] V. V. Rostov, N. M. Bykov, D. N. Bykov, A. I. Klimov, O. B. Kovalchuk, and I. V. Romanchenko, *Generation of subgigawatt RF pulses in nonlinear transmission lines*, IEEE Trans. Plasma Sci., **38**, 2681, (2012).
- [106] I. V. Romanchenko, V. V. Rostov, A. V. Gunin, and V. Y. Konev, *Gyromagnetic RF source for interdisciplinary research*, Rev. Sci. Instrum., **88**, 024703, (2017).
- [107] J.-W. B. Bragg, J. C. Dickens, and A. A. Neuber, *Material selection considerations for coaxial, ferrimagnetic-based nonlinear transmission lines*, J. Appl. Phys., **113**, 064904, (2017).
- [108] S. J. F. Chadwick, N. Seddon, and S. Rukin, *A novel solid-state HPM source based on a gyromagnetic NLTL and SOS-based pulse generator*, Proc. IEEE Pulsed Power Conf., Chicago, IL, USA, 178, (2011).
- [109] D. V. Reale, D. Mauch, J. M. Johnson, A. A. Neuber, J. C. Dickens, and J. J. Mankowski, *Radiation from SiC PCSS driven gyromagnetic nonlinear transmission line high power microwave source*, Proc. IEEE Int. Power Modulator High Voltage Conf. (IPMHVC), Santa Fe, NM, USA, Jun. 123, (2014).
- [110] J.-W. B. Bragg, J. Dickens, and A. Neuber, *Investigation into the temperature dependence of ferrimagnetic nonlinear transmission lines*, IEEE Trans. Plasma Sci., **40**, 2457, (2012).
- [111] I. V. Romanchenko, V. V. Rostov, V. P. Gubanov, A. S. Stepchenko, A. V. Gunin, and I. K. Kurkan, *Repetitive sub-gigawatt RF source based on gyromagnetic nonlinear transmission line*, Rev. Sci. Instrum., **83**, 074705, (2012).
- [112] I. V. Romanchenko et al., *Four channel high power RF source with beam steering based on gyromagnetic nonlinear transmission lines*, Rev. Sci. Instrum., **88**, 054703, (2017).

- [113] J. O. Rossi, L. P. S. Neto, F. S. Yamasaki, J. J. Barroso, E. G. L. Rangel, and E. Schamiloglu, *High-voltage soliton generation with nonlinear lumped varactor diode lines*, Proc. 18th Symp. Oper. Appl. Areas Defense, So Jos dos Campos, Brazil, 22, (2016).
- [114] D. M. French, B. W. Hoff, S. Heidger, and D. Shiffler, *Dielectric nonlinear transmission line*, Proc. IEEE Int. Pulsed Power Conf., Chicago, IL, USA, 341, (2011).
- [115] N. A. Benedek and C. J. Fennie, *Why are there so few perovskite ferroelectrics?* J. Phys. Chem. C, 117, 13339, (2013).
- [116] A. T. Mulder, N. A. Benedek, J. M. Rondinelli, and C. J. Fennie, *Turning ABO<sub>3</sub> anti-ferroelectrics into ferroelectrics: Design rules for practical rotation-driven ferroelectricity in double perovskites and A<sub>3</sub>B<sub>2</sub>O<sub>7</sub> RuddlesdenPopper compounds*, Adv. Funct. Mater., 23, 4810, (2013).
- [117] B. Nouri, M. S. Nakhla, and R. Achar, *Efficient simulation of nonlinear transmission lines via model-order reduction*, IEEE Trans. Microw. Theory Techn., 65, 673, (2017).
- [118] J. Chen and S. M. Kang, *An algorithm for automatic model-order reduction of nonlinear mems devices*. In Proceedings of the IEEE international symposium on circuits and systems, 2, 445 (2000).
- [119] Y. Chen and J. White, *A quadratic method for nonlinear model order reduction*. In Proceedings of the international conference on modeling and simulation of microsystems, 447 (2000).
- [120] Yong Chen, *Model order reduction for nonlinear systems*, Ph.D Thesis, Massachusetts Institute of Technology, (1999).
- [121] J. R. Phillips, *Projection frameworks for model reduction of weakly nonlinear systems*, In DAC '00: Proceedings of the 37th conference on design automation, NY USA, ACM Press, 184 (2000).
- [122] D. M. Vasilyev, *Theoretical and practical aspects of linear and nonlinear model order reduction techniques*, Ph.D Thesis, Massachusetts Institute of Technology, (2008).

- [123] U. N. Ghosh, P. Chatterjee, R. Roychoudhury, *The effect of  $q$ -distributed electrons on the head-on collision of ion acoustic solitary waves*, *Physics of Plasma*, **19**, 012113 (2012).
- [124] R. Gogoi, N. Devi, C. G. Das, *Small amplitude solitary waves propagating in a plasma with negative ions*, *Indian Journal of Pure and Applied Physics*, **46**, 621 (2008).
- [125] J. R. Taylor, editor, *Optical solitons : theory and experiment*, Cambridge University Press, (1992).
- [126] R. Hirota and K. Suzuki, *Theoretical and experimental studies of lattice solitons in nonlinear lumped networks*, *Proc. IEEE*, **61**, 1483 (1973).
- [127] M. Tokuyama and H. Ohtagaki, *Chaos in a series circuit with a nonlinear capacitor and a nonlinear inductor*, *Electr. Eng. Jpn.*, **150**, 35 (2005).
- [128] J. C. Butcher, *On Runge-Kutta processes of high order*, *J. Austral. Math. Soc.*, **4**, 179 (1964).
- [129] N. S. Kuek, A. C. Liew, E. Schamiloglu, and J. O. Rossi, *Oscillating pulse generator based on a nonlinear inductive line*, *IEEE Trans. Plasma Sci.*, **41**, 2619 (2013).
- [130] N. S. Kuek, A. C. Liew, E. Schamiloglu, and J. O. Rossi, *RF pulse generator based on a nonlinear hybrid line*, *IEEE Trans. Plasma Sci.*, **42**, 3268 (2014).
- [131] N. S. Kuek, A. C. Liew, E. Schamiloglu, and J. O. Rossi, *Circuit modeling of nonlinear lumped element transmission lines including hybrid lines*, *IEEE Trans. Plasma Sci.*, **40**, 2523 (2012).
- [132] R. Boylestad and L. Nashelsky, *Electronic Devices and Circuit Theory*, 7th Edition, Prentice Hall, USA, (2003).
- [133] H. Jie, Z. Qian, Y. Hao, D. Junrong and Z. Haiying, *Planar Schottky varactor diode and corresponding large signal model for millimeter-wave applications*, *J. Semicond.* **35**, 0540061, (2014).

- [134] **N. A. Akem**, L. A. Ngate, A. M. Dikandé, B. Z. Essimbi, *Leapfrogging dynamics of interacting solitons in weakly coupled nonlinear transmission lines*, SN Applied Sciences, **1**, 552, (2019).
- [135] K. Narahara, *Amplification of Short Pulses in Transmission lines Periodically Loaded with Schottky Varactors*, IEICE Electron. Expr. **6**, 1199, (2009).
- [136] **N. A. Akem**, A. M. Dikandé, B. Z. Essimbi, *Leapfrogging of electrical solitons in coupled nonlinear transmission lines: effect of an imperfect varactor*, SN Applied Sciences, **2**, 21, (2020).
- [137] H. A. Luther, *An explicit six-order Runge-Kutter formula*, Math. Comp. (we used  $v = 1$ ), **22**, 434, (1968).
- [138] Y. S. Kivshar and B. A. Malomed, *Solitons in a system of coupled Korteweg-de Vries equations*, Wave Mot. **11**, 261, (1989).
- [139] J. T. Pan, W. Z. Chen, F. Tao, W. Xu, *Influence of impurities on solitons in the nonlinear LC transmission line*, Phys. Rev. E **83**, 016601, (2011).
- [140] A. Shnirman, E. Ben-Jacob, B. A. Malomed, *Tunneling and resonant tunneling of fluxons in a long Josephson junction*, Phy. Rev. B **55**, 14677, (1997).
- [141] I. O. Starodub, Y. Zolotaryuk, *Scattering of quasi-one-dimensional solitons on impurities in large Josephson junctions*, Phys. Lett. A **376**, 3101, (2012).
- [142] O. M. Braun and Yu. S. Kivshar, *Nonlinear dynamics of the Frenkel-Kontorova model with impurities*, Phys. Rev. B **43**, 1060, (1991).
- [143] B. A. Malomed, *Interaction of a soliton with an impurity in the sine-Gordon model of a commensurate charge-density-wave system*, J. Phy. C **21**, 5163, (1998).
- [144] **N. A. Akem**, A. M. Dikandé, B. Z. Essimbi, *Pulse amplification and damping in Lossy Nonlinear transmission Lines*, Rom. J. Phys., **65**, 123, (2020).

- [145] A. M. Dikandé, and T. C. Kofané, *Oscillatory motions of solitons in finite inhomogeneous structures*, J. Phys: Condense Mat. **6**, 6229, (1994).
- [146] H. L. Bertoni, L. Carin and L. B. Felsen (editors): *Ultra-wideband, Short-Pulse Electromagnetics*, Springer, Berlin, (2012).

---

## List of Publications

---

1. **Nkongho Achere Akem**, L. Akong Ngate, Alain M. Dikandé and B. Z. Essimbi, *Leapfrogging dynamics of interacting solitons in weakly coupled nonlinear transmission lines*, SN Applied Sciences **1**, 552 (2019).
2. **Nkongho Achere Akem**, A. M. Dikandé and B. Z. Essimbi, *Leapfrogging of electrical solitons in coupled nonlinear transmission lines: effect of an imperfect varactor*, SN Applied Sciences **2**, 21 (2020).
3. **Nkongho Achere Akem**, A. M. Dikandé and B. Z. Essimbi, *Pulse amplification and damping in Lossy Nonlinear transmission Lines*, Rom. J. Phys., **65**, 123, (2020).



Research Article

# Leapfrogging dynamics of interacting solitons in weakly coupled nonlinear transmission lines

Nkongho Achere Akem<sup>1,2</sup> · L. Akong Ngate<sup>1</sup> · Alain M. Dikandé<sup>1</sup>  · B. Z. Essimbi<sup>2</sup>

© Springer Nature Switzerland AG 2019

## Abstract

The dynamics of two electrical pulses forming a boundstate, propagating along two nonlinear transmission lines weakly coupled by linear capacitors shunted with linear resistances, is considered from both analytical and numerical standpoints. The study rests on an analysis of time series of the amplitudes and phases of the two interacting electrical pulses, within the framework of the variational theory based on exact one-soliton solution to the Korteweg-de Vries equation. In the regime where the two pulses propagate at nearly equal velocities, their relative amplitude/phase evolutions can result in periodic quasi-harmonic oscillations so-called leapfrogging motion. In this specific regime of motion, it is found that besides the expected damping effect on the soliton amplitudes, the resistance can also sustain their leapfrogging motion. Analytical expression of the leapfrogging frequency is derived, providing a better understanding of the competing effects of the coupling capacitor and the resistive shunt on the leapfrogging motion. Leapfrogging motions of co-propagating pulses in electrical networks can be very useful in high-intensity signal transmissions involving least energy cost for the propagating signals.

**Keywords** Coupled nonlinear transmission lines · Soliton pairs · Leapfrogging · KdV equations · Numerical simulations

## 1 Introduction

Nonlinear transmission lines (NLTs) are dispersive media in which electric signals propagate in form of well-localized pulses [1–13], usually referred to as electrical solitons. Owing to their robustness that is their ability to cover long distances (thousands of kilometers) without change in profiles, electrical solitons have been actively investigated over the past fifty years starting from the pioneer model of Hirota and Suzuki [1, 2, 14–23]. In the microwave domain in particular NLTs have recently been shown [21] to represent the ideal source of stable high-intensity sharp pulses.

Typically a NLT is constructed by periodically loading a linear transmission line with reverse-biased semiconductor diodes (such as Schottky varactors), or by arranging inductors and varactors in a one-dimensional (1D)

lattice. In such structures nonlinearity originates from the varactors whose capacitance is designed to change with applied voltage, while line dispersion stems from the structural periodicity of the loaded elementary circuits composing the ladder transmission line. When nonlinearity and dispersion are balanced, electrical currents and all related physical parameters (such as the voltages) acquire solitonic shape profiles and thus long-lived high-intensity electric signals are generated [15]. In addition to maintaining their shapes during propagation, solitons possess other important properties [15, 24]. Namely they can survive collisions with other solitons or solitary waves, and in electrical transmission lines specifically it was recently established [25–27] that they can retain their profiles upon scatterings with localized as well as distributed structural defects (i.e. impurities) on the lines. Current applications

✉ Alain M. Dikandé, amdikande@gmail.com | <sup>1</sup>Laboratory of Research on Advanced Materials and Nonlinear Science (LaRAMaNS), Department of Physics, Faculty of Sciences, University of Buea, PO Box 63, Buea, Cameroon. <sup>2</sup>Present Address: Laboratory of Electronics and Electrical Systems, Department of Physics, Faculty of Science, University of Yaoundé I, P.O. Box 812, Yaoundé, Cameroon.



SN Applied Sciences (2019) 1:552

| <https://doi.org/10.1007/s42452-019-0555-8>

Received: 2 March 2019 / Accepted: 3 May 2019

Published online: 13 May 2019

SN Applied Sciences  
A SPRINGER NATURE journal

involving NLTs are numerous, under large signal conditions they can serve as impulse compressors and frequency multipliers [21], they are utilized for transportation of electrical energy through overhead high voltage cables, they serve as metal strips on printed circuit boards to carry digital data or control signals, they are utilized as coupled microstrips in microwave filters, as ribbon cables to connect electronic systems and so on. Resistive NLTs are ideal devices for the study of short-pulse amplitude control [20, 28] and reshaping [21].

Nonlinear electrical networks, composed of at least two coupled nonlinear transmission lines, have been considered in the studies of simultaneous propagation of electrical soliton packets obeying coupled Korteweg-de Vries (KdV) equations [18, 29–32]. Theoretical as well as experimental results, in the specific context of two coupled NLTs, have revealed a rather complex dynamics of the interacting pulses as they propagate together. In particular when two electrical pulses propagate along two separate but coupled transmission lines, the strength of their interaction mediated by the coupling will usually depend on their speeds one relative to the other. It was observed experimentally [33] that when the difference in velocities of the two pulses is very small, their interaction is optimized thus favoring a bound state in which electrical energy will be alternately transferred from a leading soliton to a trailing soliton. In this process, when one of the two solitons in the bound state is at its maximum amplitude, it leads the pair motion while the trailing soliton is at its minimum amplitude. As the energy leaves the leading soliton to the trailing soliton, the amplitude of the leading soliton dies down while the amplitude of the trailing soliton grows. Given that the velocity of the KdV soliton increases with amplitude [24], the trailing soliton is expected to speed up and to eventually overtake the leading soliton such that the direction of energy transfer is reversed. Under certain conditions this overtaking will occur repeatedly, giving rise to relative oscillations

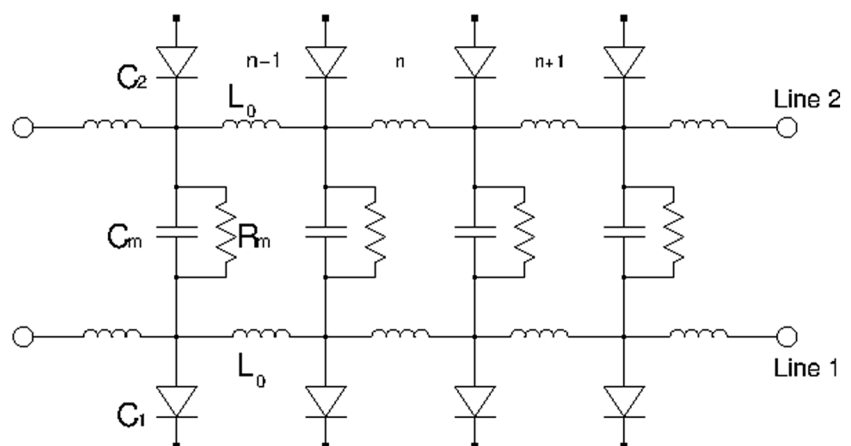
in amplitudes and phases in which the two solitons continuously leap over each other periodically. Such motion, called "leapfrogging", was discussed in ref. [33] in the context of capacitively coupled nonlinear transmission lines. Actually the leapfrogging of solitons is a quite common phenomenon in nature, it has been widely discussed in the past particularly in fluid dynamics [34–40]. The leapfrogging of electrical solitons may offer the possibility to quasi-resonantly transfer energy between coupled ladder lines in distributed electric networks, such process can be of great interest for space and time multiplexed ultrafast electronics.

In this work we are interested in the leapfrogging dynamics of a bound soliton pair propagating in two NLTs, weakly coupled by a capacitive component as considered in Ref. [33] but shunted with a linear resistance. Our main objective is to examine the influence of the resistive component on relative amplitude and phase oscillations of the two interacting solitons. As a matter of fact, if the damping of soliton amplitudes due to resistive components along NLTs is a well established fact, we are anticipating a control role of the resistance in the leapfrogging dynamics of the two interacting electrical pulses.

## 2 Model and coupled KdV equations

The model of two coupled nonlinear transmission lines we are interested in is depicted in Fig. 1. The two lines consist of periodically loaded identical LC elementary circuits, where sections of elementary circuits in line 1 and line 2 are connected by interfacial linear capacitors  $C_m$  shunted by linear resistors  $R_m$ . Dispersion in the system is achieved by the discrete nature of the lines, while nonlinearity is achieved by making use of the conductive nonlinearity of capacitive diodes (i.e. varactors) [41]. In our study we assume the case when the varactors in the two lines are connected with opposite polarities.

**Fig. 1** Equivalent representation of two nonlinear LC transmission lines, coupled by a capacitor  $C_m$  with a resistance  $R_m$  in its shunt branch





Let  $V_n$  and  $I_n$  denote the voltage and current respectively, at the  $n$ th section of line 1, and  $W_n$  and  $J_n$  the voltage and current respectively at the  $n$ th section of line 2. The bias voltages in lines 1 and 2 are  $-V_b$  and  $V_b$  respectively, reflecting the opposite polarities of the varactor diodes on the two lines. For these varactor diodes we assume the following capacitance-voltage characteristics [42]:

$$C_1(x) = C_0 \left(1 - \frac{x}{V_J}\right)^{-m}, \quad C_2(x) = C_0 \left(1 + \frac{x}{V_J}\right)^{-m}, \quad (1)$$

where  $C_0$  is the zero-bias junction capacitance,  $V_J$  is the junction potential and  $m$  (a real number) is a grading index coefficient determined by the doping profile of the varactors [41, 42]. Note that except for the opposite polarities of the varactor diodes the lines are symmetrical, this symmetry turns out to be fundamental for it favors electrical pulses of almost equal velocities to travel on the two lines as a bound state.

Applying Kirchhoff's voltage law on the  $n$ th cell of lines 1 and 2, we obtain:

$$L_0 \frac{dI_n}{dt} = V_{n-1} - V_n, \quad L_0 \frac{dJ_n}{dt} = W_{n-1} - W_n. \quad (2)$$

Kirchhoff's current law on the  $n$ th cell of lines 1 and 2 results in the two coupled transmission line equations:

$$C_1(V_n) \frac{d^2 V_n}{dt^2} + C_m \frac{d^2}{dt^2} (V_n - W_n) + \frac{1}{R_m} \frac{d}{dt} (V_n - W_n) = L_0^{-1} (V_{n+1} - 2V_n + V_{n-1}), \quad (3)$$

$$C_2(W_n) \frac{d^2 W_n}{dt^2} + C_m \frac{d^2}{dt^2} (W_n - V_n) + \frac{1}{R_m} \frac{d}{dt} (W_n - V_n) = L_0^{-1} (W_{n+1} - 2W_n + W_{n-1}). \quad (4)$$

In the long-wavelength limit, we can approximate the discrete position  $n$  by a continuous variable  $x = nh$  where  $h$  is the size of an elementary circuit. In this continuous regime the discrete voltages transform as  $V_n(t) \rightarrow V(x, t)$  and  $W_n(t) \rightarrow W(x, t)$ , such that we can carry out a continuum-limit expansion in powers of  $h$ , for the two quantities  $V_{n\pm 1}(t) = V(x \pm h, t)$  and  $W_{n\pm 1}(t) = W(x \pm h, t)$ . To the fourth order in  $h$  the expansion yields:

$$V_{n\pm 1}(t) = V(x, t) \pm h \frac{\partial V}{\partial x} + \frac{h^2}{2!} \frac{\partial^2 V}{\partial x^2} \pm \frac{h^3}{3!} \frac{\partial^3 V}{\partial x^3} + \frac{h^4}{4!} \frac{\partial^4 V}{\partial x^4} + O(h^5), \quad (5)$$

$$W_{n\pm 1}(t) = W(x, t) \pm h \frac{\partial W}{\partial x} + \frac{h^2}{2!} \frac{\partial^2 W}{\partial x^2} \pm \frac{h^3}{3!} \frac{\partial^3 W}{\partial x^3} + \frac{h^4}{4!} \frac{\partial^4 W}{\partial x^4} + O(h^5). \quad (6)$$

Setting  $h \equiv 1$  for simplicity, Eqs. (3) and (4) become:

$$C_1(V) \frac{\partial^2 V}{\partial t^2} + C_m \frac{\partial^2}{\partial t^2} (V - W) + \frac{1}{R_m} \frac{\partial}{\partial t} (V - W) = L_0^{-1} \left( \frac{\partial^2 V}{\partial x^2} + \frac{1}{12} \frac{\partial^4 V}{\partial x^4} \right), \quad (7)$$

$$C_2(W) \frac{\partial^2 W}{\partial t^2} + C_m \frac{\partial^2}{\partial t^2} (W - V) + \frac{1}{R_m} \frac{\partial}{\partial t} (W - V) = L_0^{-1} \left( \frac{\partial^2 W}{\partial x^2} + \frac{1}{12} \frac{\partial^4 W}{\partial x^4} \right), \quad (8)$$

where  $C_1(V)$  and  $C_2(W)$  are defined in (1).

### 3 Adiabatic equations

As we are interested in electric signals with localized pulse shapes, we shall follow the reductive perturbation theory [35, 43] to obtain the equations governing spatiotemporal evolutions of such localized electric signals. In this respect, we introduce a small parameter  $\varepsilon$  and define the new variables:

$$s = \varepsilon^{1/2}(x - v_0 t), \quad \tau = \varepsilon^{3/2} t, \quad (9)$$

with  $v_0 = 1/\sqrt{L_0 C_b}$ . Next, express the voltages  $V(s, \tau)$  and  $W(s, \tau)$  as series in powers of  $\varepsilon$  i.e.:

$$V(s, \tau) = -V_b + \sum_{i=1}^{\infty} \varepsilon^i v_i(s, \tau), \quad (10)$$

$$W(s, \tau) = V_b + \sum_{i=1}^{\infty} \varepsilon^i w_i(s, \tau). \quad (11)$$

Consistently with the weak-coupling assumption, the coupling capacitance  $C_m$  and coupling resistance  $R_m$  will be taken of the order  $\varepsilon$ . In agreement with this assumption, we can rewrite the two coupling parameters as:

$$C_m = \varepsilon C'_m, \quad (12)$$

$$R_m = \varepsilon^{-3/2} R'_m. \quad (13)$$

Substituting Eqs. (9), (10), (11), (12) and (13) into Eqs. (7) and (8), and keeping only terms of order  $\varepsilon^3$  for which non-linearity balances the dispersion, we obtain the following two coupled KdV equations at the third order in  $\varepsilon$ :

$$v'_{\tau'} - 6v'v'_{s'} + v'_{s's's'} = \eta(v' + w')_{s'} - \eta_1(w' + v'), \quad (14)$$

$$w'_{\tau'} - 6w'w'_{s'} + w'_{s's's'} = \eta(w' + v')_{s'} - \eta_1(v' + w'), \quad (15)$$

where we define:

$$\begin{aligned} \tau' &= \frac{\tau}{\beta_1}, & s' &= \sqrt[3]{12C_0L_0}s, \\ v' &= 6\beta_2\sqrt[3]{12C_0L_0}v_3, & w' &= -6\beta_2\sqrt[3]{12C_0L_0}w_3, \\ \eta &= \frac{C'_m v_0^2 \sqrt[3]{12C_0L_0}}{C_0}, & \eta_1 &= \frac{v_0 r_m}{C_0}, \end{aligned} \tag{16}$$

with  $\beta_1 = 2v_0 - 4\beta_2 v_0 V_b$ ,  $\beta_2 = \frac{m}{V_j}$ , and for convenience we have set  $r_m = R'_m$ . Contributions from terms of order  $\epsilon$  give  $v_1 = 0$  and  $w_1 = 0$ , while contributions of order  $\epsilon^2$  (i.e.  $v_2$  and  $w_2$ ) are determined by the following equations:

$$0 = C_0 v_0^2 \frac{\partial^2 v_2}{\partial s^2} - 2C_0 v_0^2 \alpha_1 v_b \frac{\partial^2 v_2}{\partial s^2} + \frac{1}{12L_0} \frac{\partial^2 v_2}{\partial s^2}, \tag{17}$$

$$0 = C_0 v_0^2 \frac{\partial^2 w_2}{\partial s^2} - 2C_0 v_0^2 \alpha_1 v_b \frac{\partial^2 w_2}{\partial s^2} + \frac{1}{12L_0} \frac{\partial^2 w_2}{\partial s^2}, \tag{18}$$

suggesting that  $v_2$  and  $w_2$  are constants.

The two coupled Eqs. (14) and (15), that provide shape profiles of the nonlinear components of the voltage fields expressed as in series as (10), (11), are not tractable analytically because of the coupling terms in their right-hand side. However, if we assume the two coupling components to be very small, they can readily be treated as perturbations and therefore we can rewrite the set (14) and (15) formally with their right-hand side grouped to give a single perturbation function:

$$\epsilon P(v', w') = \eta(v' + w')_{s'} - \eta_1(w' + v'). \tag{19}$$

In the absence of perturbation, i.e. when  $\epsilon P(v', w') = 0$ , Eqs. (14) and (15) are two independent KdV equations whose exact single-pulse soliton solutions are [35]:

$$v' = -2\kappa_1^2 \text{sech}^2(z_1), \quad w' = -2\kappa_2^2 \text{sech}^2(z_2), \tag{20}$$

where the arguments  $z_1 = \kappa_1(s' - \zeta_1)$  and  $z_2 = \kappa_2(s' - \zeta_2)$  connect the pulse amplitudes  $\kappa_{1,2}$  to their phases  $\zeta_{1,2}$  via:

$$\zeta_1 = 4\kappa_1^3 \tau', \quad \zeta_2 = 4\kappa_2^3 \tau'. \tag{21}$$

It is worthwhile stressing that (20) are just parts of the general solutions to the two line equations, however they are most relevant in that they provide the soliton components in the series representation of these solutions. Hence we shall be mainly interested in the dynamics of these soliton components in the presence of the perturbation  $\epsilon P(v', w') = 0$ . To determine the temporal evolution of characteristic parameters  $\kappa_i$  and  $\zeta_i$  of the two pulse solitons for small  $\epsilon P(v', w')$ , we use the adiabatic perturbation theory [35] which enables us obtain the following set of first-order ordinary differential equations:

$$\frac{d\kappa_i}{d\tau'} = -\frac{\eta}{4\kappa_i} \int_{-\infty}^{\infty} \epsilon P(v', w') \text{sech}^2(z_i) dz_i, \tag{22}$$

$$\begin{aligned} \frac{d\zeta_i}{d\tau'} &= 4\kappa_i^2 - \frac{\eta}{4\kappa_i^3} \int_{-\infty}^{\infty} \epsilon P(v', w') \text{sech}^2(z_i) \\ &\times \left( z_i + \frac{1}{2} \sinh(2z_i) \right) dz_i, \end{aligned} \tag{23}$$

with  $i = 1, 2$ . Note that the interaction between the two solitons will be optimal when their velocities coincide, i.e.  $\zeta_1 = \zeta_2$ . In terms of (20) this can also be formulated in terms of the equality of their amplitudes, i.e.:

$$\kappa_1 = \kappa_2. \tag{24}$$

Let us consider a very small deviation from this optimal state of interaction, due to the soliton velocities not being exactly equal but remaining nevertheless always very close. This can be described by small fluctuations in amplitudes of the two pulses from their unperturbed values  $\kappa_1^0 = \kappa_2^0 = \kappa$ . It follows that since the two lines are identical and symmetric, we can write:

$$\kappa_{1,2} = \kappa + \lambda_{1,2}, \tag{25}$$

where  $\kappa$  is constant and the variables  $\lambda_1$  and  $\lambda_2$  are very small compared to  $\kappa$ . Similarly the phase difference  $\Delta\zeta \equiv \zeta_1 - \zeta_2$  can be assumed so small that we have:

$$z_2 \simeq z_1 + \kappa \Delta\zeta. \tag{26}$$

Substituting Eqs. (20), (25) and (26) in (22) and (23) and integrating, we obtain:

$$\begin{aligned} \frac{d\lambda_1}{d\tau'} &= -\frac{\eta\kappa^3}{15\kappa_1} \text{sech}^2(y) [8\tanh(y) + 8\tanh^3(y)] \\ &- \frac{2\eta_1\kappa_2^2}{3\kappa_1} \text{sech}^2(y) - \frac{2\eta_1\kappa_1}{3}, \end{aligned} \tag{27}$$

$$\begin{aligned} \frac{d\lambda_2}{d\tau'} &= \frac{\eta\kappa^3}{15\kappa_2} \text{sech}^2(y) [8\tanh(y) + 8\tanh^3(y)] \\ &- \frac{2\eta_1\kappa_1^2}{3\kappa_2} \text{sech}^2(y) - \frac{2\eta_1\kappa_2}{3}, \end{aligned} \tag{28}$$

$$\begin{aligned} \frac{d\zeta_1}{d\tau'} &= 4\kappa_1^2 - \eta - \frac{\eta\kappa_2^3}{3\kappa_1^3} \text{sech}^2(y) \left[ 3 - \frac{17}{3} \tanh^2(y) \right] \\ &+ \frac{\eta_1\kappa_2^2}{\kappa_1^3} \text{sech}^2(y) \tanh(y), \end{aligned} \tag{29}$$

$$\begin{aligned} \frac{d\zeta_2}{d\tau'} &= 4\kappa_2^2 - \eta - \frac{\eta\kappa_1^3}{3\kappa_2^3} \text{sech}^2(y) \left[ 3 - \frac{17}{3} \tanh^2(y) \right] \\ &- \frac{\eta_1\kappa_1^2}{\kappa_2^3} \text{sech}^2(y) \tanh(y), \end{aligned} \tag{30}$$

where we have set  $y = \kappa \Delta \zeta$ . Eqs. (27)–(30), that describe the motion of the two weakly interacting electrical solitons in the specific context when their velocities are very close, are solved numerically using a sixth-order Runge-Kutta scheme [44] with fixed step. Numerical results are discussed in the next section.

## 4 Numerical results

To investigate the leapfrogging dynamics of the two electrical solitons we carried out numerical simulations of the four coupled ordinary differential equations Eqs. (27)–(30). Since it is also relevant to see the effects the coupling resistance would have on amplitudes of the individual solitons, in Fig. 2a, b we started with plots of the time series of  $\lambda_1$  and  $\lambda_2$ , for a fixed value of the capacitive coupling  $\eta$  ( $\eta = 0.025$ ), for different values of the resistive coupling parameter i.e.  $\eta_1 = 0.001, 0.005$  and  $0.009$ . One sees that time series of  $\lambda_1$  and  $\lambda_2$  are periodic oscillations, with an exponential decrease of their maxima. It is quite

remarkable that the exponential damping is more and more pronounced as  $\eta_1$  increases.

To highlight the anti-phase oscillations of the two amplitudes, we plot  $\lambda_1$  and  $\lambda_2$  on the same graph for large values of  $\eta_1$  ( $\eta_1 = 0.005$  and  $\eta_1 = 0.009$ ) keeping  $\eta = 0.025$  and  $\kappa = 0.5$ . The leapfrogging motions observed in Fig. 2c, d, occur more exactly when initial values of  $\lambda_1$  and  $\lambda_2$  used in the simulations are very close. Figure 3 illustrates the absence of leapfrogging, when the difference between initial values of the two parameters in the simulations is relatively large. In fact, the signature of leapfrogging is to be observed both in the oscillating phase difference  $\Delta \zeta = \zeta_1 - \zeta_2$ , and in the oscillating amplitude difference  $\Delta \lambda = \lambda_1 - \lambda_2$  of the two solitons. Therefore, to gain a consistent picture of this signature in the two parameters, we solved numerically the amplitude and phase difference equations derived from the coupled set Eqs. (27)–(30), by subtracting Eq. (29) from Eq. (30) on one hand and Eq. (27) from Eq. (28) on the other hand. Figure 4 suggests a dynamics of the soliton pair which we can summarize as follows: initially (i.e. at  $t = 0$ ) the amplitude difference of the two solitons is at some finite initial value, while

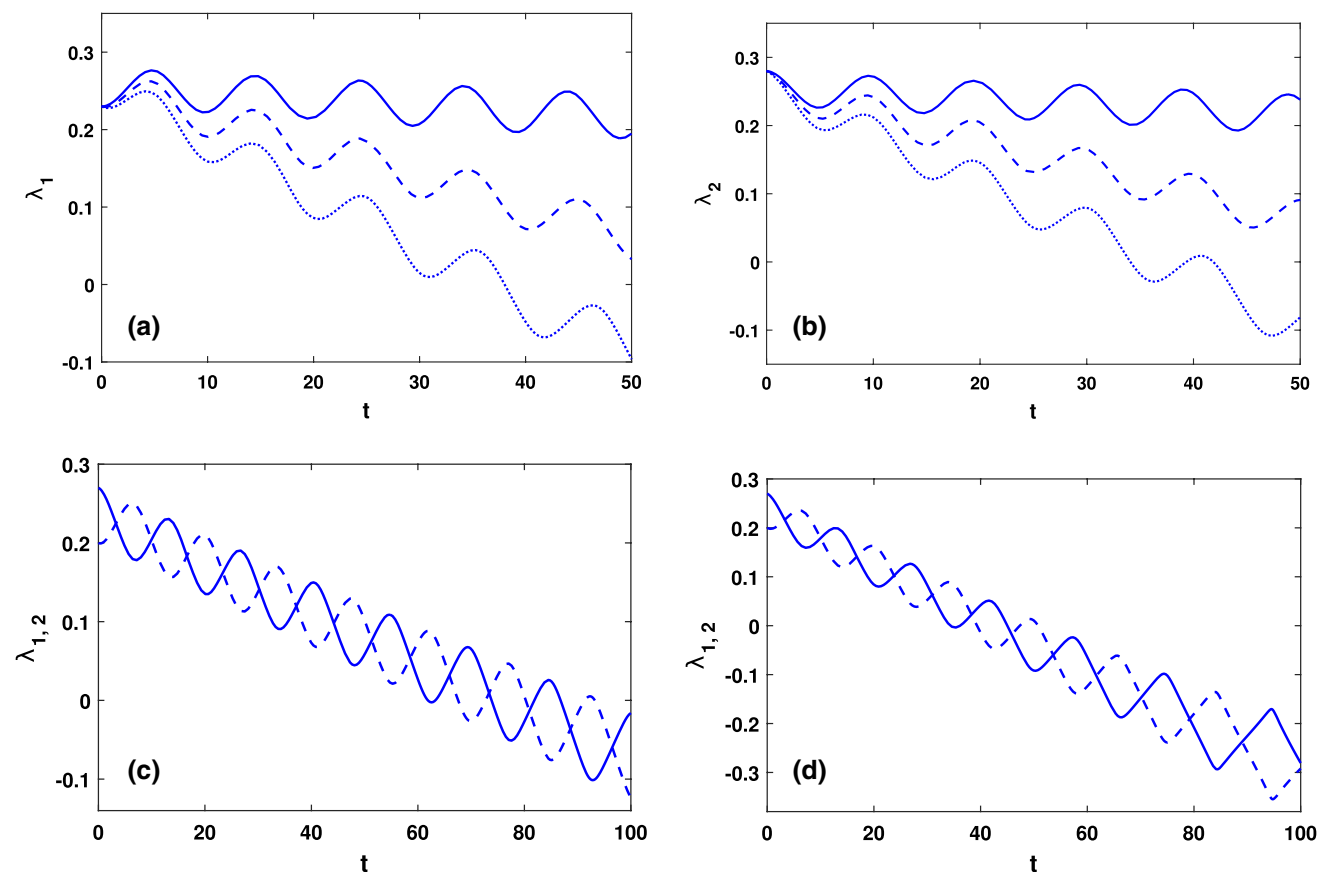


**Fig. 2** (Color online) Top graphs: Temporal evolutions of  $\lambda_1$  (a) and  $\lambda_2$  (b), for  $\eta = 0.23$  and  $\kappa = 0.6$ . The solid, dashed and dotted curves correspond respectively to  $\eta_1 = 0.001, 0.005$  and  $0.009$ . Bottom

graphs: Leapfrogging dynamics of  $\lambda_1$  (solid curve) and  $\lambda_2$  (dashed curve), for  $\eta_1 = 0.005$  (c) and  $\eta_1 = 0.009$  (d)

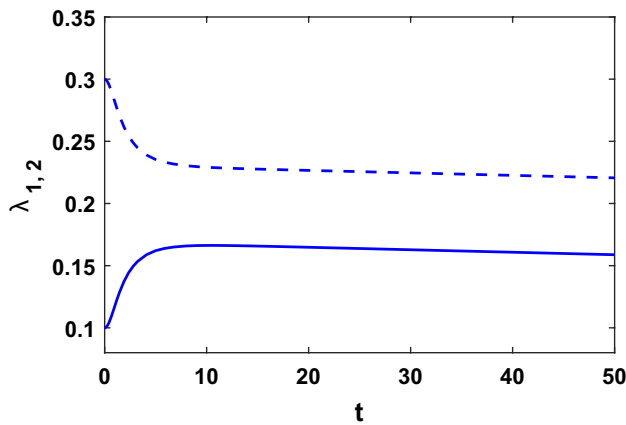


**Fig. 3** (Color online) Suppression of leapfrogging for large initial values of  $\lambda_1$  (i.e. 0.1) and  $\lambda_2$  (i.e. 0.2), with  $\eta = 0.25$ ,  $\eta_1 = 0.0005$  and  $\kappa = 0.5$

their phase difference is zero. As the two solitons propagate they exchange energy, this causes them to slowly approach each other. Their amplitude difference thus decreases gradually to zero at the time when the two electrical pulses coincide and have an equal velocity. After hopping pass each other, their amplitude and phase differences begin to rise again and the cycle continues, for as long as the leapfrogging motion goes on resulting in oscillating amplitude and phase differences.

To further emphasize the effects of the resistance on the leapfrogging dynamics of the bound solitons, we have plotted three sets of curves to illustrate the behaviour of the oscillating amplitude difference and phase difference, with increasing resistance (Fig. 5). Using fairly large values for the resistance, the curves clearly show that as the resistance increases the number of oscillations in  $\Delta\lambda$  and  $\Delta\zeta$  decreases until the leapfrogging motion stops. Since

the oscillating evolutions of the amplitude and phase differences are here assumed to characterize the leapfrogging of the soliton pair, the decrease in the number of oscillations readily indicates a weakening and eventually a relaxation of the leapfrogging motion.

We can understand the origin of the harmonic oscillations observed in numerical solutions to the phase and amplitude difference equations, by remarking that the arguments of the hyperbolic functions in Eqs. (27)–(30) are proportional to  $\Delta\zeta$ . Thus for leapfrogging to occur in numerical simulations, this later parameter should remain very small which justifies our choice of very small initial values for the phase and amplitude differences. Analytically, small amplitude and phase differences imply linearizing Eqs. (27)–(30), which yields:

$$\frac{d\lambda_1}{d\tau'} = -\frac{8}{15}\eta\kappa^2y - \frac{4}{3}\eta_1k - \frac{4}{3}\eta_1\lambda_2, \tag{31}$$

$$\frac{d\lambda_2}{d\tau'} = \frac{8}{15}\eta\kappa^2y - \frac{4}{3}\eta_1k - \frac{4}{3}\eta_1\lambda_1, \tag{32}$$

$$\frac{d\zeta_1}{d\tau'} = 4\kappa_1^2 - \eta - \frac{\eta\kappa_2^3}{4\kappa_1^3} + \frac{\eta_1\kappa_2^2y}{\kappa_1^3}, \tag{33}$$

$$\frac{d\zeta_2}{d\tau'} = 4\kappa_2^2 - \eta - \frac{\eta\kappa_2^3}{4\kappa_1^3} - \frac{\eta_1\kappa_1^2y}{\kappa_2^3}. \tag{34}$$

Subtracting Eq. (34) from (33) and replacing in (31) and (28), we obtain:

$$\frac{d^2\Delta\zeta}{d\tau'^2} = \left( \frac{128}{15}\kappa^4\eta + \frac{96}{15}\kappa^2\eta^2 - 4\eta_1^2 \right) \Delta\zeta. \tag{35}$$

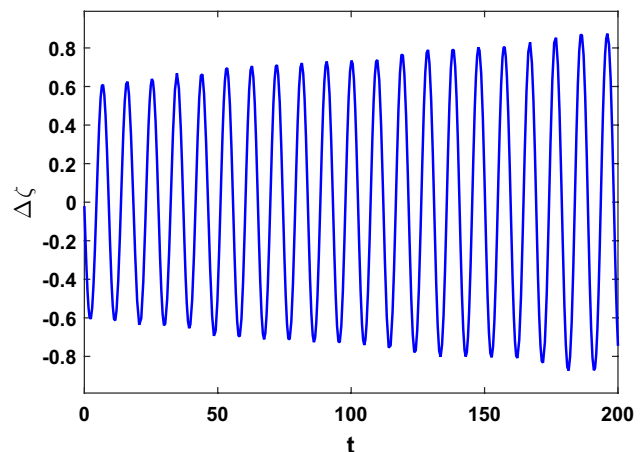
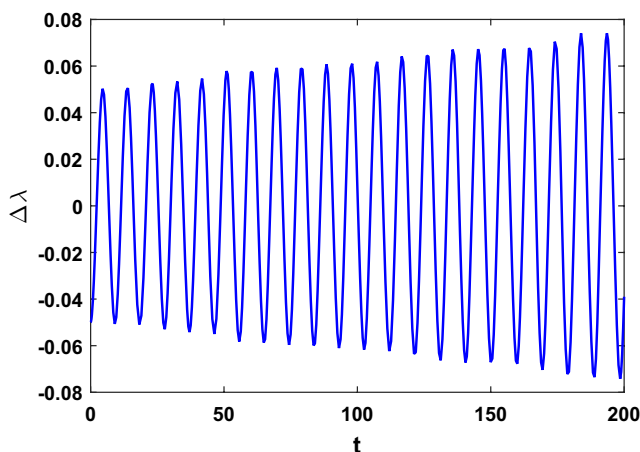
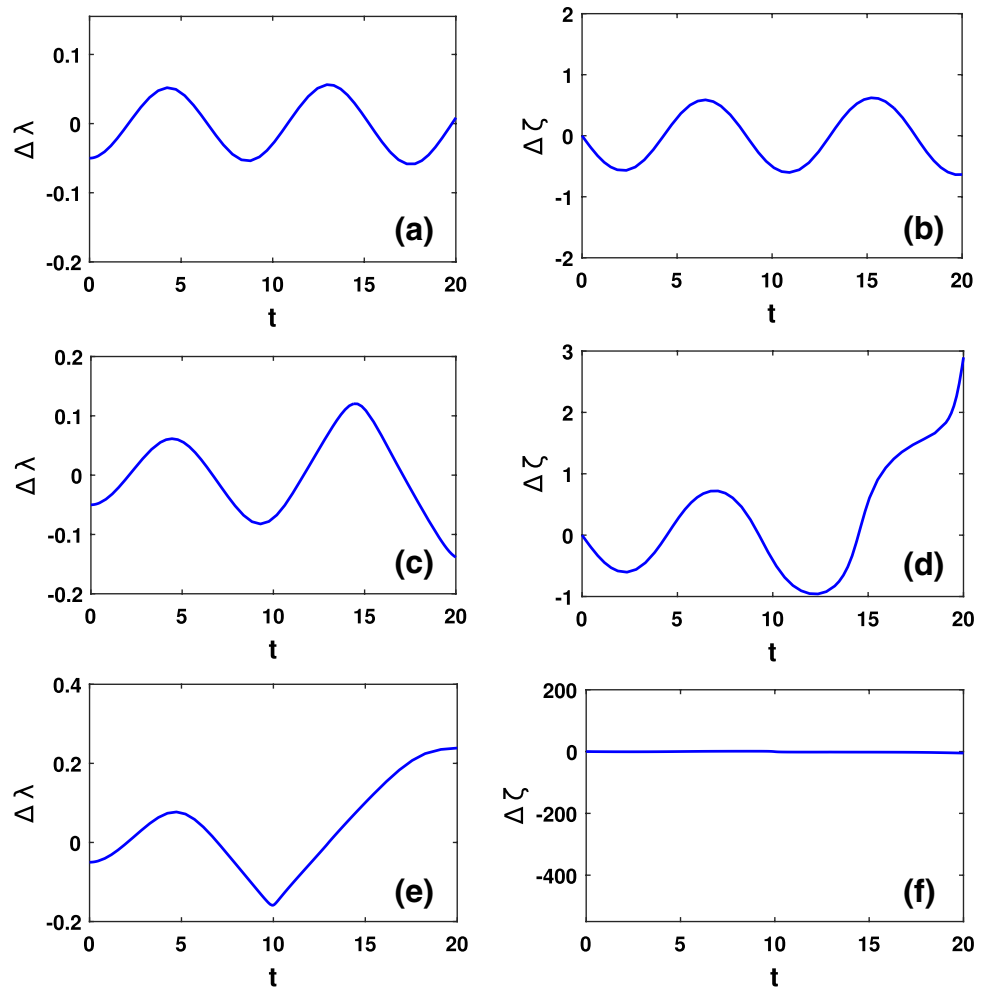


**Fig. 4** (Color online) Temporal oscillations of the amplitude difference  $\Delta\lambda$  and phase difference  $\Delta\zeta$  are shown in the left and right graphs respectively, for  $\eta = 0.25$ ,  $\eta_1 = 0.0005$ , and  $\kappa = 0.63$

**Fig. 5** (Color online) Oscillating amplitude and phase differences for increasing resistance. The top, middle and bottom set of curves are for  $\eta_1 = 0.01, 0.05$  and  $0.09$  respectively. Here  $\eta = 0.25$  and  $\kappa = 0.63$ . Leapfrogging ceases in the last set of curves due to very high value of resistance



This is the equation of motion for an harmonic oscillator, the frequency  $\omega_{lf}$  of which is given by:

$$\omega_{lf}^2 = \left( \frac{128}{15} \kappa^4 \eta + \frac{96}{15} \kappa^2 \eta^2 - 4\eta_1^2 \right). \tag{36}$$

Formula (36) shows that the leapfrogging frequency is decreased by the presence of the resistive element in the coupling branch. From the expression of  $\omega_{lf}$  it is also apparent that as  $\eta_1$  increases the leapfrogging frequency decreases, vanishing at some finite characteristic value of the resistance. This is in agreement with the behaviour observed in Figs. 2a, b, c and 4a, b. In Fig. 6, we plot the leapfrogging frequency against the resistance for different values of  $\kappa$ . The frequency decreases to zero, indicating a decay of the leapfrogging motion as the resistance increases.

In the above analysis it emerged that a choice of small initial values for the amplitude and phase differences was necessary for the observation of leapfrogging in numerical simulations of the coupled set Eqs. (27)–(30). In Fig. 7, we plot the time series of  $\lambda_1$  and  $\lambda_2$  for relatively large values

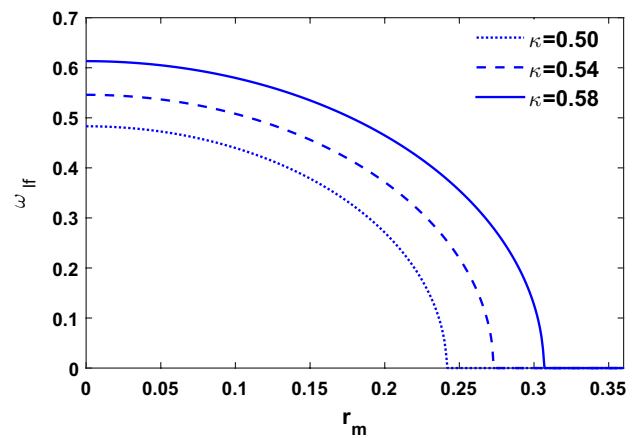


**Fig. 6** (Color online) Influence of the resistance on the leapfrogging frequency for different values of  $\kappa$ .  $\eta = 0.25$

of the initial phase and amplitude differences, considering different values of  $\eta_1$  and  $\kappa = 0.6$ . One sees that the time series of soliton characteristic parameters are now strongly

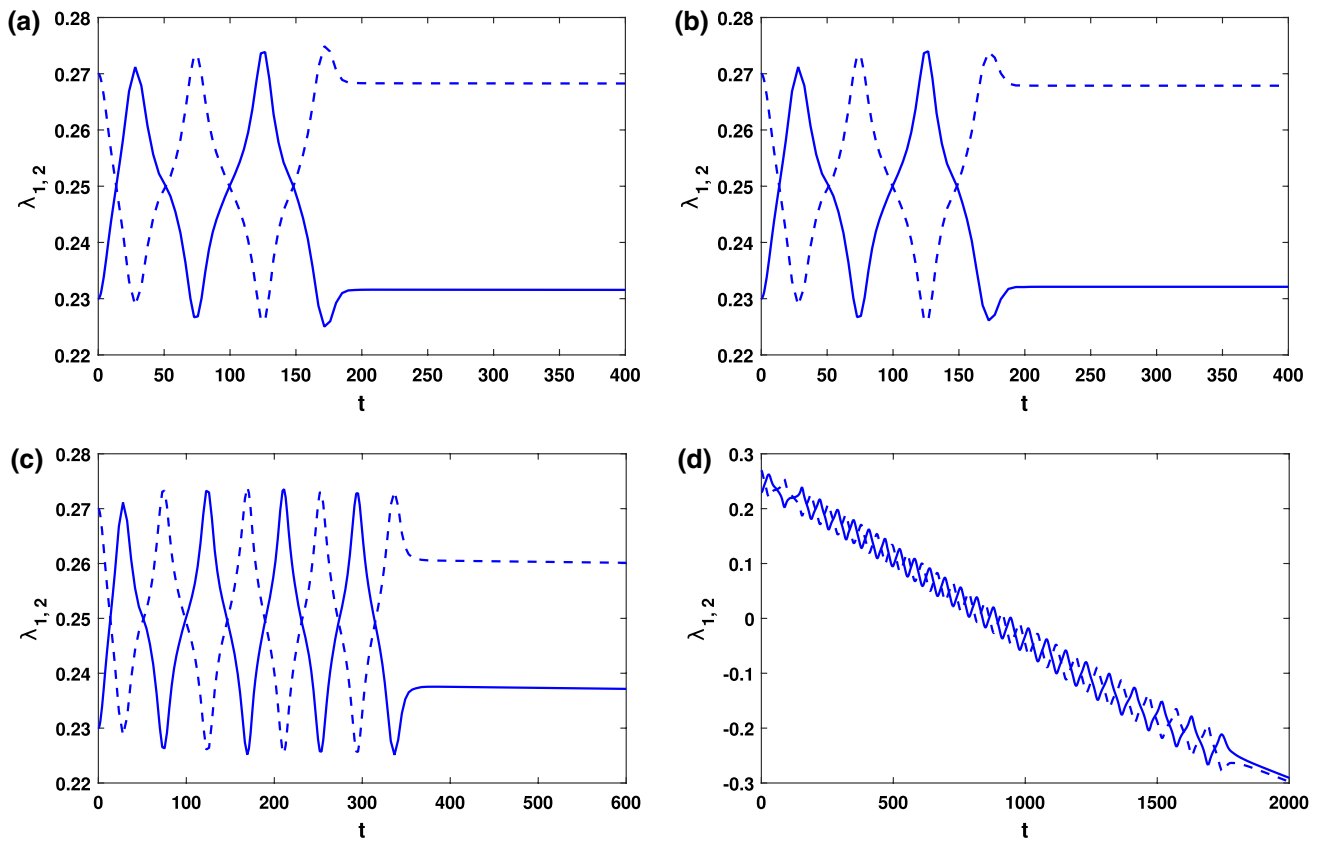


**Fig. 7** (Color online) Anharmonic oscillations of  $\lambda_1$  (solid curves) and  $\lambda_2$  (dashed curves), for large initial values:  $r_m = 5 \times 10^{-10}$  (a),  $r_m = 5 \times 10^{-8}$  (b),  $r_m = 5 \times 10^{-6}$  (c) and  $r_m = 5 \times 10^{-4}$  (d).  $\kappa = 0.6$

anharmonic, and more generally an enhancement of the anharmonicity by relatively large initial values will cause a relaxation of leapfrogging after a finite propagation time. Quite remarkably this later behaviour is valid irrespective of the value of the unperturbed amplitude  $\kappa$ , which indeed remains fix in time. To end, an explicit picture of the leapfrogging dynamics of the two solitons is summarized in the phase-space representation Fig. 8, where  $\lambda_1$  is plotted as a function of  $\lambda_2$ .

### 5 Conclusion

The leapfrogging of soliton pairs was proposed in the past to describe the particular motion of two weakly interacting solitons, characterized by their anti-phase oscillations and oppositely varying amplitudes [34–39, 45]. In fluid dynamics the leapfrogging of co-propagating KdV pulses have been widely discussed, and shown to provide an interesting configuration of the system dynamics in which solitons in the pair oscillate periodically one with respect to the other such as to mutually sustain their propagation at very small velocity [34]. This concept was recently extended to

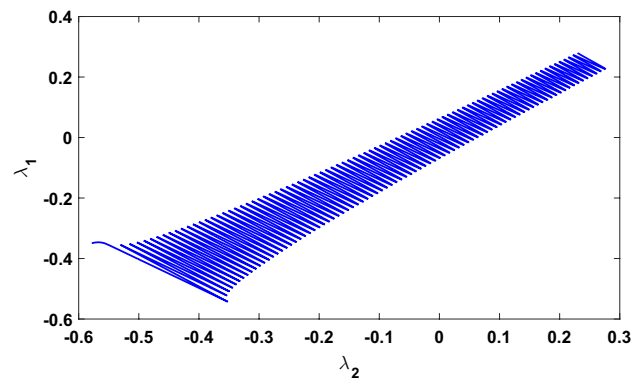


**Fig. 8** (Color online) Phase-space representation of the leapfrogging dynamics. Here,  $\eta_1 = 0.23$ ,  $\eta = 0.001$  and  $\kappa = 0.6$

nonlinear electrical transmission lines by Narahara [33], who considered two capacitively coupled nonlinear transmission lines and determined characteristic properties for the leapfrogging motion of electrical soliton pairs.

In the present work we examined the possible leapfrogging motion of a pair of solitons along two nonlinear LC transmission lines, weakly coupled by a linear

capacitor shunted by a linear resistor. We established the leapfrogging motion by solving numerically the coupled variational equations associated with the two interacting solitons for very small initial values of the amplitude and phase differences, and obtained analytically that the resistive coupling component would cause a decrease in the leapfrogging frequency. Note that numerical curves also suggest a damping of amplitudes of the two solitons, also caused by the resistive coupling.

Although the results obtained in this work reveal a rich dynamics of the system, it would also be interesting to look at the competing effects of the coupling capacitance and resistance on the leapfrogging motion when the coupling parameters are not too small. Given that adiabatic considerations in this context cannot be applied, only a full numerical treatment of the discrete line equations would be consistent. This later study requires a specific context since several characteristic parameters are involved in the model and their contributions need to be well emphasized both quantitatively and qualitatively. This aspect is considered in a separate work.

## Compliance with ethical standards

**Conflict of interest** The authors declare that they have no conflict of interest.

## References

- Hirota R, Suzuki K (1970) Studies on lattice solitons by using electrical networks. *J Phys Soc Jpn* 28:1366
- Hirota R, Suzuki K (1973) Theoretical and experimental studies of lattice solitons in nonlinear lumped networks. *Proc IEEE* 61:1483
- Kuusela T, Hietarinta J, Kokko K, Laiho R (1987) Soliton experiments in a nonlinear electrical transmission line. *Eur J Phys* 8:27
- Kuusela T (1995) Soliton experiments in transmission lines. *Chaos Solitons Fractals* 5:2419
- Mostafa SI (2009) Analytical study for the ability of nonlinear transmission lines to generate solitons. *Chaos Solitons Fractals* 39:2425
- Dinkel JN, Setzer C, Rawal S, Lonngren KE (2001) Soliton propagation and interaction on a two-dimensional nonlinear transmission line. *Chaos Solitons Fractals* 12:91
- Lin MM, Duan WS (2005) Wave packet propagating in an electrical transmission line. *Chaos Solitons Fractals* 24:191
- Koon KT, Marquié P, Dinda PT (2014) Experimental observation of the generation of cutoff solitons in a discrete LC nonlinear electrical line. *Phys Rev A* 41:4534
- Zayed EME, Alurrfi KAE (2015) A new Jacobi elliptic function expansion method for solving a nonlinear PDE describing the nonlinear low-pass electrical lines. *Chaos Solitons Fractals* 78:148
- Kengne E (2004) Ginzburg–Landau system of complex modulation equations for a distributed nonlinear-dispersive transmission line. *J Phys A* 37:6053
- Kengne E, Chui ST, Liu WM (2006) Modulational instability criteria for coupled nonlinear transmission lines with dispersive elements. *Phys Rev E* 74:0366141
- Kengne E, Liu WM (2006) Exact solutions of the derivative nonlinear Schrödinger equation for a nonlinear transmission line. *Phys Rev E* 73:0266031
- Kengne E, Lakhssassi A (2015) Analytical studies of soliton pulses along two-dimensional coupled nonlinear transmission lines. *Chaos Solitons Fractals* 73:191
- Jäger D (1982) Experiments on KdV Solitons. *J Phys Soc Jpn* 51:1686
- Remoissenet M (1999) *Waves called solitons: concepts and experiments*. Springer, New York
- Rodwell MJW et al (1994) Active and nonlinear wave propagation devices in ultrafast electronics and optoelectronics. *Proc IEEE* 82:1037
- Essimbi BZ, Dikandé AM, Kofané TC, Zibi AA (1995) Asymmetric gap solitons in a non-linear LC transmission line. *Phys Scr.* 52:17
- Essimbi BZ, Dikandé AM, Kofané TC, Zibi AA (1995) Gap solitons in nonlinear symmetric electric circuit. *J Phys Soc Jpn* 64:2777
- Singer AC, Oppenheim AV, Wornell GW (1999) Detection and estimation of multiplexed soliton signals. *IEEE Trans Signal Proc* 47:2768
- Narahara K (2010) Characterization of nonlinear transmission lines for short pulse amplification. *J Infrared Millim Terahertz Waves* 31:411
- Afshari E, Hajimiri A (2005) Nonlinear transmission lines for pulse shaping in silicon. *IEEE J Solid-State Circuits* 40:744
- Dikandé AM, Ga-Akeku B (2009) Localized short impulses in a nerve model with self-excitable membrane. *Phys Rev E* 80:041904
- Oriols X, Martin F (2001) Analytical solitons in nonlinear transmission lines loaded with heterostructure barrier varactors. *J Appl Phys* 90:2595
- Drazin PG, Johnson RS (1989) *Solitons: an introduction*. Cambridge University Press, Cambridge
- Sato M, Yasui S, Kimura M, Hikihara T, Sievers AJ (2007) Management of localized energy in discrete nonlinear transmission lines. *Eur Phys Lett* 80:30002
- Tsuboi T, Toyama FM (1991) Computer experiments on solitons in a nonlinear transmission line. I. Formation of stable solitons. *Phys Rev A* 44:2686
- Tsuboi T, Toyama FM (1991) Computer experiments on solitons in a nonlinear transmission line. II. Propagation of solitons in an impurity-doped line. *Phys Rev A* 44:2691
- Gasch A, Berning T, Jäger D (1986) Generation and parametric amplification of solitons in a nonlinear resonator with a Korteweg-de Vries medium. *Phys Rev A* 34:4528
- Yoshinaga T, Kakutani T (1980) Solitary and shock waves on a coupled transmission line. *J Phys Soc Jpn* 49:2072
- Yoshinaga T, Kakutani T (1987) Fast and slow mode solitons on a coupled transmission line. *J Phys Soc Jpn* 56:3447
- Kofané TC, Zebaze M, Zibi AA (1990) Non-linear wave modulation on a coupled transmission line. *J Phys D* 23:764
- Narahara K (2015) Asymmetrical solitary waves in coupled nonlinear transmission lines. *Wave Motion* 58:13
- Narahara K (2015) Characterization of leapfrogging solitary waves in coupled nonlinear transmission lines. *Nonlinear Dyn.* 81:1805
- Malomed BA (1987) Leapfrogging solitons in a system of coupled KdV equations. *Wave Motion* 9:401
- Kivshar YS, Malomed BA (1989) Dynamics of solitons in nearly integrable systems. *Rev Mod Phys* 61:763
- Liu AK, Pereira NR, Ko DRS (1982) Weakly interacting internal solitary waves in neighbouring pycnoclines. *J Fluid Mech* 122:187

37. Weidman PD, Johnson M (1982) Experiments on leapfrogging internal solitary waves. *J Fluid Mech* 122:195
38. Gear JA, Grimshaw R (1984) Weak and strong interactions between internal solitary waves. *Stud Appl Math* 70:235
39. Nitsche M, Weidman PD, Grimshaw R, Ghrist M, Fornberg B (2010) Evolution of solitary waves in a two-pycnocline system. *J Fluid Mech* 642:235
40. Berger MS (1990) *Mathematical structures of nonlinear science: an introduction*. Kluwer, Dordrecht
41. Boylestad R, Nashelsky L (2013) *Electronic devices and circuit theory* (7<sup>th</sup> edition). Prentice Hall, Englewood Cliffs
42. Jie H, Qian Z, Hao Y, Junrong D, Haiying Z (2014) Planar Schottky varactor diode and corresponding large signal model for millimeter-wave applications. *J Semicond* 35:0540061
43. Taniuti T, Wei CC (1968) Reductive perturbation method in nonlinear wave propagation. I. *J Phys Soc Jpn* 24:941
44. Luther HA (1968) An explicit sixth-order Runge–Kutta formula. *Math Comput* 22:434
45. Narahara K (2018) Modulation of pulse train using leapfrogging pulses developed in unbalanced coupled nonlinear transmission lines. *Math Probl Eng*, Article ID 2869731. <https://doi.org/10.1155/2018/2869731>

**Publisher's Note** Springer Nature remains neutral with regard to jurisdictional claims in published maps and institutional affiliations.






## Research Article

# Leapfrogging of electrical solitons in coupled nonlinear transmission lines: effect of an imperfect varactor

Nkongho Achere Akem<sup>1</sup> · Alain M. Dikandé<sup>1,2</sup>  · B. Z. Essimbi<sup>3</sup>

Received: 14 October 2019 / Accepted: 20 November 2019

© The Author(s) 2019 

## Abstract

The leapfrogging dynamics of a pair of electrical solitons is investigated, by considering two capacitively coupled nonlinear transmission lines with and without intraline resistances. We discuss two distinct transmission line set-ups: in the first, we assume two RLC ladder lines with intraline varactors and a coupling linear capacitor, and in the second, we consider two capacitively coupled lossless lines with a varactor carrying impurity (imperfect diode) in one of the two interacting transmission lines. In the first context, we find that the soliton-pair leapfrogging mimics the motion of a damped harmonic oscillator, the frequency and damping coefficient of which are obtained analytically. Numerical simulations predict leapfrogging of the soliton pair when the differences in the initial values of the amplitude and phase are reasonably small, and the resistance is not too large. In the second context, leapfrogging occurs when the impurity rate is small enough and the differences in the initial values of the amplitude as well as phase are also small. As the impurity rate increases, the soliton signal in the imperfect line gets accelerated upon approaching the defective diode, causing only this specific soliton signal to move faster than its counterpart, leading to the suppression of leapfrogging.

**Keywords** Coupled nonlinear transmission lines · Soliton signals · Capacitive impurity · Adiabatic perturbation theory · Numerical simulations

## 1 Introduction

The Hirota circuit [1, 2] is a simple LC ladder circuit with a linear inductance, but an active feedback capacitor embedded within the main branch of the circuit. This circuit has long served as a paradigm for the generation and propagation of nonlinear signals in electrical networks, simulating the so-called Toda lattice [3, 4] and admitting exact soliton solutions [5–9]. In this electrical system, the nonlinearity balancing the dispersion (related to the ladder nature of the line) is introduced by a capacitor, whose capacitance is controlled by the imposed bias voltage, thus acting like a capacitive diode (“varicap” diode or varactor). The nonlinear signal generated in this nonlinear

transmission line (NLTL) is a localized electrical signal with a bell shape, propagating with features of pulse soliton (i.e., translate at constant speed keeping a permanent bell shape) due to the effect of varactors periodically loaded throughout the line. NLTLs are of interest because of their applications in several fields, e.g., under large signal conditions NLTLs can serve as impulse compressors or frequency multipliers [10]. NLTLs have also proved to be of great practical use in extremely wideband focusing and shaping of signals [11]; in the microwave domain, they are ideal sources of highly stable large-amplitude sharp pulses [12].

Several studies have been devoted to modelling, both analytically and numerically, the propagation of nonlinear signals in NLTLs in various physical contexts

✉ Alain M. Dikandé, dikande.alain@ubuea.cm | <sup>1</sup>Laboratory of Research on Advanced Materials and Nonlinear Science (LaRAMaNS), Department of Physics, Faculty of Sciences, University of Buea, PO Box 63, Buea, Cameroon. <sup>2</sup>Present Address: Max Planck Institute for the Physics of Complex Systems (MPIPKS), Nöthnitzer Str. 38, 01187 Dresden, Germany. <sup>3</sup>Laboratory of Electronics and Electrical Systems, Department of Physics, Faculty of Science, University of Yaoundé I, PO Box 812, Yaoundé, Cameroon.



including resistive NLTLS, transmission lines with impurities, networks of coupled NLTLS and so on [13–27]. Two most common theoretical pictures have emerged, namely one in which the nonlinear electrical signals are soliton solutions to the Korteweg–de Vries (KdV) or coupled KdV equations [27–29] and one in which they are looked out as modulated envelope solitons described by the nonlinear Schrödinger or coupled nonlinear Schrödinger equations [10, 12, 18, 19]. Much interesting to us, recent theoretical as well as numerical works [30, 31] have established that under specific conditions, the coupling of two NLTLS can promote novel interesting configurations of soliton bound states in which soliton pairs propagate with opposite phases, but nearly equal velocities. Bound soliton states of this kind, known as leapfrogging solitons, have actually been predicted and observed experimentally in many other physical contexts [32–38] as, for instance, in hydrodynamics and plasma dynamics.

In general, the amplitudes and phases of two leapfrogging pulses depend on their initial positions and initial velocities, such that as they propagate they remain always close one to another with their amplitude and phase differences vanishing periodically with time. In the specific context of coupled NLTLS, leapfrogging propagation of soliton pairs provides means to convey pairs of large-amplitude signals at low energy cost from their interactions. Indeed when the difference in velocities of the two signals is very small, their interaction is optimized, thus favouring a bound state in which the electrical energy will be alternately transferred from the leading soliton signal to the trailing soliton signal. This leads to a periodic change in positions of the two solitons, a leading one becoming a trailing soliton and vice versa. So to say, the leapfrogging motion can be used to manage the transmission of pairs of travelling electrical pulses in electrical networks, putting into play a minimum possible power loss from the individual electrical soliton signals.

In a previous study [31], we investigated the leapfrogging dynamics of soliton pairs propagating along two LC NLTLS, weakly coupled by a linear capacitance shunted with a linear resistance. We obtained that the inclusion of a resistive element in the shunt branch of the coupling capacitance enables to control the amplitude and phase differences of the interacting pulses during their propagation. Instructively, the coupled model considered in this previous study was an extension of the study done in ref. [29] where the author addressed the problem considering only the capacitive coupling. In the present work, we are interested in the leapfrogging motion of a soliton pair in two distinct physical contexts: first, we consider the case of two RLC NLTLS coupled via a linear capacitance and two capacitively coupled LC NLTLS one of which contains a defective varactor. We first derive, using Kirchhoff's voltage

and current rules, the discrete set of nonlinear equations for the coupled NLTLS in the two physical contexts. Next, seeking for pulse signals, a multiple-scale expansion of solutions is applied in the full continuum limit which enables us to obtain a set of coupled KdV equations in the relevant scale. The coupled set of KdV equations is then treated analytically within the framework of the adiabatic perturbation theory [39], by defining appropriate variables for leapfrogging of the two KdV pulses as they propagate at nearly equal amplitudes and velocities. Their leapfrogging are explored numerically by means of a sixth-order Runge–Kutta scheme with fixed steps [40], and conditions for suppression of leapfrogging are determined.

## 2 Analysis of leapfrogging for coupled RLC NLTLS

### 2.1 Model, line equations and coupled dissipative KdV equations

Consider two NLTLS as depicted in Fig. 1, where each elementary section in the line consists of a linear inductor  $L$  in parallel with a nonlinear capacitor of capacitance  $C = C(V)$ . The two lines are coupled by means of linear capacitor  $C_m$  at each mode.

The nonlinear capacitors are varactor diodes, and except for their opposite polarities in our study, we shall use a common type of varactor diode with a Schottky barrier for both lines [30, 31]. Therefore, our Schottky varactors can be represented by the following capacitance–voltage characteristics [41]:

$$C_1(x) = C_0 / \left(1 - \frac{x}{V_j}\right)^m, \quad (1)$$

$$C_2(x) = C_0 / \left(1 + \frac{x}{V_j}\right)^m, \quad (2)$$

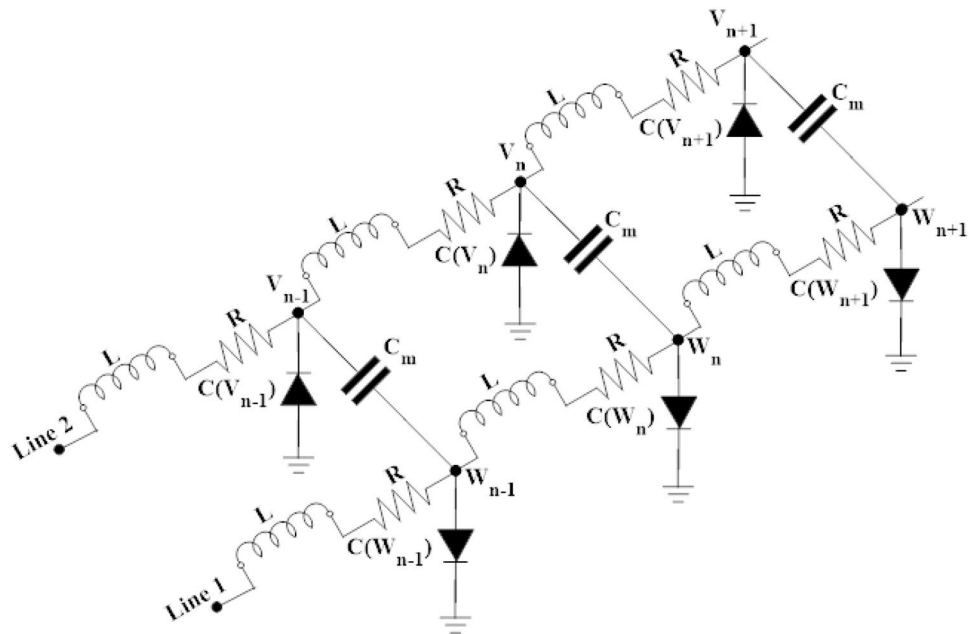
where  $C_0$ ,  $V_j$  and  $m$  are, respectively, the zero-bias capacitance, the junction potential and the grading coefficient [41, 42]. We assume that the bias voltages in lines 1 and 2 are  $-V_b$  and  $V_b$ , respectively, reflecting the opposite polarities of varactor diodes loaded on the two lines. For convenience, we define:

$$C_b \equiv C_0 / \left(1 + \frac{V_b}{V_j}\right)^m, \quad (3)$$

an effective zero-bias capacitance which below turns out to be a relevant characteristic parameter.

Applying Kirchhoff's rules on the two coupled electrical ladder circuits, we obtain the following set of discrete transmission line equations:

**Fig. 1** Equivalent representation of two nonlinear RLC transmission lines with Schottky-type in-line varactors  $C(V)$ , coupled by linear capacitors  $C_m$



$$L \frac{d}{dt}(J_{n-1} - J_n) + R(J_{n-1} - J_n) = W_{n-1} - 2W_n + W_{n+1}, \quad (4)$$

$$L \frac{d}{dt}(I_{n-1} - I_n) + R(I_{n-1} - I_n) = V_{n-1} - 2V_n + V_{n+1}, \quad (5)$$

$$J_{n-1} - J_n = \frac{dQ_n}{dt} + C_m \frac{d}{dt}(W_n - V_n), \quad (6)$$

$$I_{n-1} - I_n = \frac{dq_n}{dt} + C_m \frac{d}{dt}(V_n - W_n). \quad (7)$$

In the above set,  $W_n$  and  $J_n$  are, respectively, the voltage and current of the  $n$ th section in line 1, and  $V_n$  and  $I_n$  are, respectively, the voltage and current of the  $n$ th section in line 2. In the continuum limit, when the size of elementary sections in the circuits is very small compared with the length of the transmission lines, the right-hand side of Eqs. (4) and (5) can readily be approximated with partial derivatives with respect to a continuum variable  $x = nl$ . This, more exactly, corresponds to the long-wavelength approximation which consists in Taylor expanding the discrete variables  $W_{n\pm 1}$  and  $V_{n\pm 1}$ , i.e.,

$$W_{n\pm 1} = V_n \pm \frac{\partial W}{\partial x} + \frac{1}{2} \frac{\partial^2 W}{\partial x^2} \pm \frac{1}{6} \frac{\partial^3 W}{\partial x^3} + \frac{1}{24} \frac{\partial^4 W}{\partial x^4} + \dots, \quad (8)$$

$$V_{n\pm 1} = V_n \pm \frac{\partial V}{\partial x} + \frac{1}{2} \frac{\partial^2 V}{\partial x^2} \pm \frac{1}{6} \frac{\partial^3 V}{\partial x^3} + \frac{1}{24} \frac{\partial^4 V}{\partial x^4} + \dots. \quad (9)$$

Also, from the definition  $dQ_n = C(W_n)dW_n$  and  $dq_n = C(V_n)dV_n$  and setting  $\alpha_0 = m/V_j$ , Eqs. (4)–(7) reduce to:

$$LC_0 \left( \frac{\partial^2 W}{\partial t^2} + \frac{\alpha_0}{2} \frac{\partial^2 W^2}{\partial t^2} \right) + LC_m \frac{\partial^2}{\partial t^2}(W - V) + RC_m \frac{\partial}{\partial t^2}(W - V) + RC_0 \left( \frac{\partial W}{\partial t} + \frac{\alpha_0}{2} \frac{\partial W^2}{\partial t} \right) = \frac{\partial^2 W}{\partial x^2} + \frac{1}{12} \frac{\partial^4 W}{\partial x^4}, \quad (10)$$

$$LC_0 \left( \frac{\partial^2 V}{\partial t^2} - \frac{\alpha_0}{2} \frac{\partial^2 V^2}{\partial t^2} \right) + LC_m \frac{\partial^2}{\partial t^2}(V - W) + RC_m \frac{\partial}{\partial t^2}(V - W) + RC_0 \left( \frac{\partial V}{\partial t} - \frac{\alpha_0}{2} \frac{\partial V^2}{\partial t} \right) = \frac{\partial^2 V}{\partial x^2} + \frac{1}{12} \frac{\partial^4 V}{\partial x^4}. \quad (11)$$

As we are interested in voltage signals with localized wave profile in space and time, it is useful to find appropriate equations reproducing such structures. In this goal, we choose the reductive perturbation method [43], in which the voltage variables  $W$  and  $V$  can be expanded in series according to:

$$W(x, t) = -V_b + \sum_{i=1}^n \epsilon^i W_i(x, t), \quad (12)$$

$$V(x, t) = V_b + \sum_{i=1}^n \epsilon^i V_i(x, t). \quad (13)$$

In addition, we apply the following new transformations on the space and time coordinates, as well as on the resistance coefficient  $R$ :

$$z = \epsilon^{\frac{1}{2}}(x - \eta t), \tau = \epsilon^{\frac{3}{2}}t, R = \epsilon^{\frac{3}{2}}R_1, \tag{14}$$

where  $\eta = (LC_b)^{-1/2}$  with  $C_b$  defined in (3). Furthermore, the coupling capacitance  $C_m$  must be of order  $\epsilon$  [31], i.e., we should define  $C_m = \epsilon C$ . Substituting Eqs. (12) to (14) into Eqs. (10) and (11) and using the above transformation of the coupling capacitance, we obtain the following equations to the order  $O(\epsilon^3)$ :

$$-\frac{2}{\eta} \frac{\partial^2 W_1}{\partial z \partial \tau} + \frac{\alpha_0 C_0}{2C_b} \frac{\partial^2 W_1^2}{\partial z^2} + \frac{C}{C_b} \frac{\partial^2}{\partial z^2} (W_1 - V_1) - R_1 C_b \eta \frac{\partial W_1}{\partial z} = \frac{1}{12} \frac{\partial^4 W_1}{\partial z^4}, \tag{15}$$

$$-\frac{2}{\eta} \frac{\partial^2 V_1}{\partial z \partial \tau} - \frac{\alpha_0 C_0}{2C_b} \frac{\partial^2 V_1^2}{\partial z^2} + \frac{C}{C_b} \frac{\partial^2}{\partial z^2} (V_1 - W_1) - R_1 C_b \eta \frac{\partial V_1}{\partial z} = \frac{1}{12} \frac{\partial^4 V_1}{\partial z^4}. \tag{16}$$

By integration of Eqs. (15) and (16) once with respect to  $z$ , and scaling  $W_1, V_1, \tau$  and  $z$  as  $W_1 = \frac{6\gamma C_b}{\alpha_0 C_0} \psi, V_1 = -\frac{6\gamma C_b}{\alpha_0 C_0} \phi, \tau = \frac{2}{\eta} T$  and  $z = \gamma u$  where  $\gamma = 1/\sqrt[3]{12}$ , we find:

$$\frac{\partial \psi}{\partial T} - 6\psi \frac{\partial \psi}{\partial u} + \frac{\partial^3 \psi}{\partial u^3} = P_1(u, T), \tag{17}$$

$$\frac{\partial \phi}{\partial T} - 6\phi \frac{\partial \phi}{\partial u} + \frac{\partial^3 \phi}{\partial u^3} = P_2(u, T). \tag{18}$$

This last set describes two coupled KdV equations, in which the quantities  $P_i(u, T), i = 1, 2$  grouping the coupling and the resistive terms play roles of perturbations and are defined as:

$$P_1(u, T) = \frac{C}{\gamma C_b} \frac{\partial}{\partial u} (\psi + \phi) - R_1 C_b \eta \psi, \tag{19}$$

$$P_2(u, T) = \frac{C}{\gamma C_b} \frac{\partial}{\partial u} (\phi + \psi) - R_1 C_b \eta \phi. \tag{20}$$

When  $P_i(u, T) = 0$ , the two homogeneous KdV equations  $\partial_T \psi - 6\psi \partial_u \psi + \partial_u^3 \psi = 0$  and  $\partial_T \phi + 6\phi \partial_u \phi + \partial_u^3 \phi = 0$  admit the following one-soliton solutions [5]:

$$\psi = -2\kappa_1^2 \operatorname{sech}^2 y_1, \tag{21}$$

$$\phi = -2\kappa_2^2 \operatorname{sech}^2 y_2, \tag{22}$$

where  $y_1 = \kappa_1(u - \theta_1), \theta_1 = 4\kappa_1^2 T$  and  $y_2 = \kappa_2(u - \theta_2), \theta_2 = 4\kappa_2^2 T$ . In the original coordinates, the above one-soliton solutions can be rewritten as:

$$W(x, t) = -\frac{3(V_J + mV_b)D_1}{\sqrt[3]{12m}} \operatorname{sech}^2 \left( \sqrt{\frac{D_1}{4\gamma^2}} (x - \eta(1 + \frac{1}{2}\gamma D_1)t) \right), \tag{23}$$

$$V(x, t) = \frac{3(V_J + mV_b)D_2}{\sqrt[3]{12m}} \operatorname{sech}^2 \left( \sqrt{\frac{D_2}{4\gamma^2}} (x - \eta(1 + \frac{1}{2}\gamma D_2)t) \right), \tag{24}$$

with  $D_1 = 4\epsilon\kappa_1^2$  and  $D_2 = 4\epsilon\kappa_2^2$ . Within the framework of the adiabatic perturbation theory [39], the temporal evolutions of the amplitudes  $\kappa_i$  and phases  $\theta_i (i = 1, 2)$  of the two pulses are determined by solving the following coupled first-order ordinary differential equations:

$$\frac{d\kappa_i}{dT} = -\frac{1}{4\kappa_i} \int_{-\infty}^{\infty} P_i(y_i, T) \operatorname{sech}^2 y_i dy_i, \tag{25}$$

$$\frac{d\theta_i}{dT} = 4\kappa_i^2 - \frac{1}{4\kappa_i^3} \int_{-\infty}^{\infty} P_i(y_i, T) \left[ y_i + \frac{1}{2} \sinh(2y_i) \right] \operatorname{sech}^2 y_i dy_i. \tag{26}$$

To find explicit forms of these variational equations, we must substitute the pulse solutions (23) and (24) into the perturbation parameters  $P_i(u, T)$ . Doing so, Eqs. (25) and (26) burst into the following four coupled first-order ordinary differential equations:

$$\frac{d\kappa_1}{dT} = -\frac{8M}{15} \kappa_2^2 \operatorname{sech}^2 A [\tanh A + \tanh^3 A] - \frac{2}{3} N \kappa_1, \tag{27}$$

$$\frac{d\kappa_2}{dT} = \frac{8M}{15} \kappa_1^2 \operatorname{sech}^2 A [\tanh A + \tanh^3 A] - \frac{2}{3} N \kappa_2, \tag{28}$$

$$\frac{d\theta_1}{dT} = 4\kappa_1^2 - M - \frac{M\kappa_2^3}{\kappa_1^3} \operatorname{sech}^2 A \left[ 1 - \frac{17}{9} \tanh^2 A \right], \tag{29}$$

$$\frac{d\theta_2}{dT} = 4\kappa_2^2 - M - \frac{M\kappa_1^3}{\kappa_2^3} \operatorname{sech}^2 A \left[ 1 - \frac{17}{9} \tanh^2 A \right], \quad (30)$$

where  $M = \frac{C}{\gamma C_b}$ ,  $N = R_1 C_b \eta$  and  $A = \kappa \Delta\theta$ , with  $\Delta\theta = \theta_1 - \theta_2$  the phase difference. Leapfrogging of the two interacting solitons corresponds to small oscillations of their amplitudes  $\kappa_i$  around a common average value  $\kappa$ . Consequently, we can introduce a small deviation  $\lambda_i$  from the average amplitude  $\kappa$ , in such a way that we can write  $\kappa_i = \kappa + \lambda_i$ . Similarly the phase difference  $\Delta\theta$  must be small. Using the approximation  $y_2 \approx y_1 + A$  and linearizing Eqs. (27)–(30) become:

$$\frac{d\lambda_1}{dT} = -\frac{8M}{15} \kappa^3 \Delta\theta - \frac{2N}{3} (\kappa + \lambda_1), \quad (31)$$

$$\frac{d\lambda_2}{dT} = \frac{8M}{15} \kappa^3 \Delta\theta - \frac{2N}{3} (\kappa + \lambda_2), \quad (32)$$

$$\frac{d\theta_1}{dT} = 4(\kappa^2 + 2\kappa\lambda_1) - M \left[ 2 - \frac{3}{\kappa} \Delta\lambda \right], \quad (33)$$

$$\frac{d\theta_2}{dT} = 4(\kappa^2 + 2\kappa\lambda_2) - M \left[ 2 + \frac{3}{\kappa} \Delta\lambda \right], \quad (34)$$

with  $\Delta\lambda = \lambda_1 - \lambda_2 = \kappa_1 - \kappa_2$ . From these equations, one obtains:

$$\frac{d^2 \Delta\theta}{dT^2} + \gamma_d \frac{d\Delta\theta}{dT} + \omega_0^2 \Delta\theta = 0, \quad (35)$$

$$\Delta\lambda = \frac{\kappa}{(8\kappa^2 + 6M)} \frac{d\Delta\theta}{dT}. \quad (36)$$

Equations (35) and (36) are reminiscent of the motion of a damped harmonic oscillator, where the damping coefficient  $\gamma_d$  and the resonance frequency  $\omega_0$  are defined as:

$$\gamma_d = \frac{2N}{3}, \quad \omega_0^2 = \frac{16}{15} M \kappa^2 (8\kappa^2 + 6M). \quad (37)$$

It is remarkable that the damping coefficient  $\gamma_d$  is a linear function of the intraline resistance  $R_1$ , while the resonance frequency  $\omega_0$  (or the frequency of undamped harmonic oscillations) is proportional to the coupling capacitance  $C$ . It is worth noting that the adiabatic perturbation theory is valid only when  $C_m/C_b \ll V_s/V_b$  where  $V_s = 12\epsilon\kappa^2(V_J + mV_b)/\sqrt[3]{12m}$  is the average voltage amplitude of the incident solitons. Given that the coupling capacitance  $C$  and the intraline resistance  $R_1$  should be very small consistently with the spirit of the adiabatic perturbation theory, the leapfrogging frequency can only be

increased with an increase in the pulse amplitude  $\kappa$ . In the next section, we shall carry out numerical simulations on the variational Eqs. (31)–(34), in order to gain a more rich insight onto parameter values for which leapfrogging of the pulse pair is more likely to be favoured.

## 2.2 Numerical simulations of leapfrogging for the coupled RLC NLTs

In ref. [30], an analysis of soliton leapfrogging in a model of coupled NLTs similar to Fig. 1, but without intraline resistances, has been carried out. Much recently, we have extended the study to the context of two LC-type NLTs coupled by a linear capacitance with a linear resistance in its shunt branch. In the present study, we shall explore numerically the influence of the intraline resistance on pulse leapfrogging. In this last purpose, we applied a sixth-order Runge–Kutta scheme [40] on the set of four coupled first-order nonlinear ordinary differential Eqs. (27)–(30). To start, we considered small initial values for  $\lambda_i$  and  $\theta_i$  and, in addition, selected very close initial values for  $\lambda_1$  and  $\lambda_2$ , on the one hand, and  $\theta_1$  and  $\theta_2$ , on the other hand, which are relevant conditions for leapfrogging to occur. Later on, we shall look at the effects of increasing the initial phase and amplitude differences, on the leapfrogging motion.

Graphs in Fig. 2 show time evolutions of  $\lambda_1$  and  $\lambda_2$  (left column) and of the amplitude difference  $\Delta\lambda$  (right column), for fixed values of the average amplitude  $\kappa$  and the capacitive coefficient  $M$ , but four distinct values of the resistive coefficient  $N$ , listed in the figure caption.

According to Fig. 2, time evolutions of  $\lambda_1$  and  $\lambda_2$  are harmonic oscillations with amplitudes which are more and more exponentially damped with increase in the resistive coefficient  $N$ . The amplitude difference  $\Delta\lambda$  too oscillates harmonically in time, reflecting leapfrogging of the soliton pair. Figures 3, 4 and 5 show the numerical results obtained when the differences in the initial values of the two solitons' amplitudes and phases are increased. One sees that when the differences in the initial values of these parameters increase, their variations are more and more dominated by anharmonic oscillations. Figure 5 shows a total suppression of leapfrogging when the differences between the initial amplitudes and phases become relatively large.

## 3 Analysis of leapfrogging for coupled LC NLTs with impurity

Let us now consider two coupled NLTs without intraline resistance as represented in Fig. 6. This model was studied in ref. [30], with an emphasis on conditions under which soliton leapfrogging is expected.

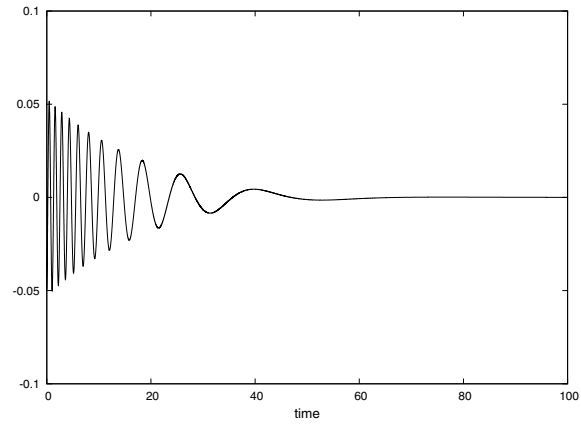
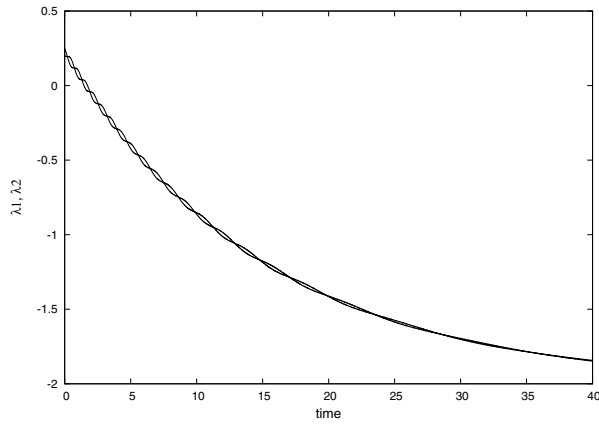
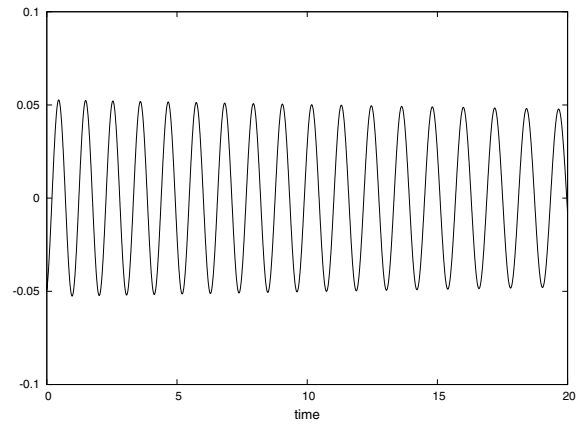
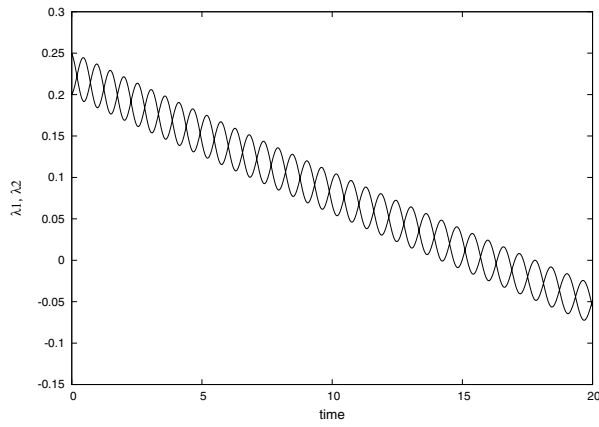
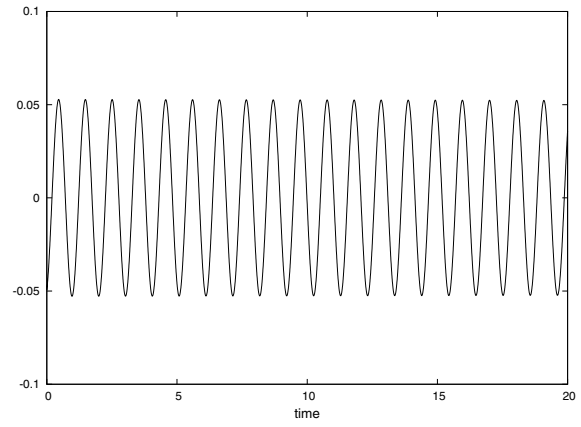
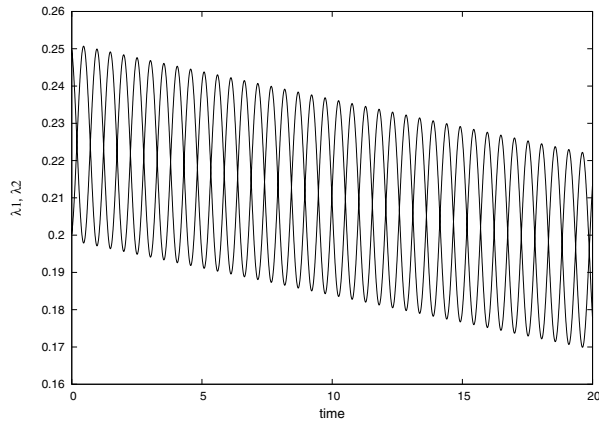
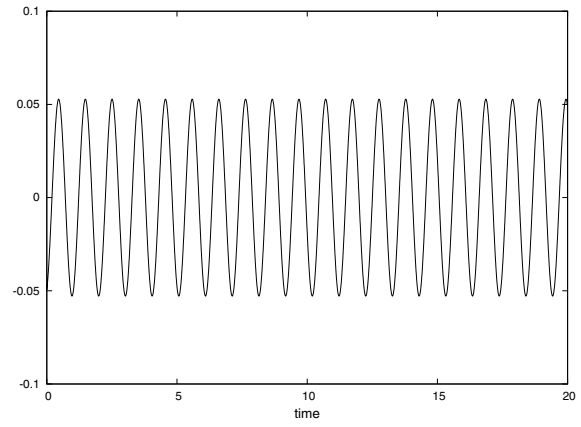
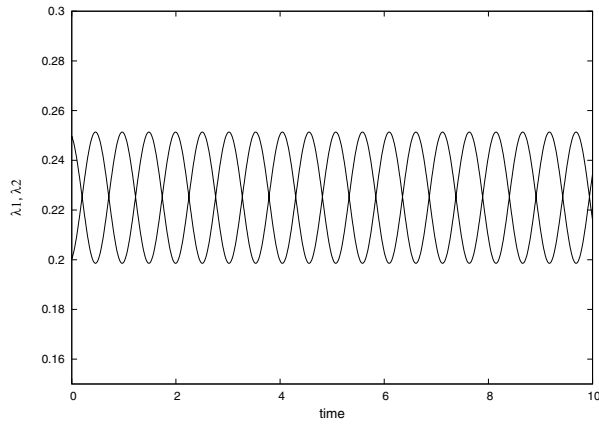


**Fig. 2** Left column: time variations of  $\lambda_1$  (downward from  $T = 0$ ) and  $\lambda_2$  (upward from  $T = 0$ ), right column: time variations of  $\Delta\lambda$ , the initial values are  $\lambda_1 = 0.25, \lambda_2 = 0.2, \theta_1 = 0.25, \theta_2 = 0.2$ . Parameter values are  $\kappa = 2$  and  $M = 0.2$ . From top to bottom rows:  $N = 0, 0.001, 0.01, 0.1$

Here, we are interested in the evolution of leapfrogging solitons in the electrical transmission network in Fig. 6, when one Schottky diode in line 1 is imperfect. Mathematically, we model the imperfection by an impurity in the feedback part of the diode localized at position  $x = x_0$  on the NLTL 1. Using a  $\delta$  function to represent the localized impurity, the capacitances of the two varactors can be expressed:

$$C_1(W) = C_0 / \left[ 1 - \frac{W}{V_j} (1 - \beta \delta(x - x_0)) \right]^m \tag{38}$$

$$C_2(V) = C_0 / \left( 1 + \frac{V}{V_j} \right)^m, \tag{39}$$

where the impurity rate  $\beta$  is assumed positive ( $0 \leq \beta \leq 1$ ). For convenience, we have set the bias voltage  $V_b$  to zero and hence  $C_b = C_0$ . Also let  $\alpha_1 = \frac{\alpha_0}{2} (1 - \beta \delta(x - x_0))$ . The transmission line equations are then given by:

$$L \frac{d}{dt} (J_{n-1} - J_n) = W_{n-1} - 2W_n + W_{n+1}, \tag{40}$$

$$L \frac{d}{dt} (I_{n-1} - I_n) = V_{n-1} - 2V_n + V_{n+1}, \tag{41}$$

$$J_{n-1} - J_n = \frac{dQ_n}{dt} + C_m \frac{d}{dt} (W_n - V_n), \tag{42}$$

$$I_{n-1} - I_n = \frac{dq_n}{dt} + C_m \frac{d}{dt} (V_n - W_n). \tag{43}$$

In the continuum limit, the right-hand side of Eqs. (40) and (41) are approximated with partial derivatives with respect to  $x$ . Again from the definition  $dQ_n = C(W_n)dW_n$  and  $dq_n = C(V_n)dV_n$ , Eqs. (40) to (43) reduce to:

$$\begin{aligned} LC_0 \left( \frac{\partial^2 W}{\partial t^2} + \alpha_1 \frac{\partial^2 W^2}{\partial t^2} \right) + LC_m \frac{\partial^2}{\partial t^2} (W - V) \\ = \frac{\partial^2 W}{\partial x^2} + \frac{1}{12} \frac{\partial^4 W}{\partial x^4}, \end{aligned} \tag{44}$$

$$\begin{aligned} LC_0 \left( \frac{\partial^2 V}{\partial t^2} - \frac{\alpha_0}{2} \frac{\partial^2 V^2}{\partial t^2} \right) + LC_m \frac{\partial^2}{\partial t^2} (V - W) \\ = \frac{\partial^2 V}{\partial x^2} + \frac{1}{12} \frac{\partial^4 V}{\partial x^4}. \end{aligned} \tag{45}$$

We expand the voltage variables  $W$  and  $V$  in series, i.e.,

$$W(x, t) = \sum_{i=1}^n \epsilon^i W_i(x, t), \tag{46}$$

$$V(x, t) = \sum_{i=1}^n \epsilon^i V_i(x, t). \tag{47}$$

In addition to transformations introduced in the previous section, we apply the following transformation on the space coordinate:

$$z = \epsilon^{\frac{1}{2}} (x - \eta_0 t), \tag{48}$$

where  $\eta_0 = (LC_0)^{-1/2}$ . Substituting Eqs. (46) to (48) into Eqs. (44) and (45) and integrating once with respect to  $z$ , we obtain the following equations to the order  $O(\epsilon^3)$ :

$$\begin{aligned} \frac{2}{\eta} \frac{\partial W_1}{\partial \tau} - \alpha_0 W_1 \frac{\partial W_1}{\partial z} + \frac{1}{12} \frac{\partial^3 W_1}{\partial z^3} = \frac{C}{C_0} \frac{\partial}{\partial z} (W_1 - V_1) \\ - \frac{\alpha_0 \beta}{2} \int \delta(z - z_0) \frac{\partial^2 W_1^2}{\partial z^2} dz, \end{aligned} \tag{49}$$

$$\frac{2}{\eta} \frac{\partial V_1}{\partial \tau} + \alpha_0 V_1 \frac{\partial V_1}{\partial z} + \frac{1}{12} \frac{\partial^3 V_1}{\partial z^3} = \frac{C}{C_0} \frac{\partial}{\partial z} (V_1 - W_1). \tag{50}$$

By scaling  $W, V, \tau$  and  $z$  as  $W_1 = \frac{6\gamma}{\alpha_0} \psi, V_1 = -\frac{6\gamma}{\alpha_0} \phi, \tau = \frac{2}{\eta_0} T$  and  $z = \gamma u$  where  $\gamma$  is the same as defined in the previous section (i.e.,  $\gamma = 1/\sqrt[3]{12}$ ), we find:

$$\frac{\partial \psi}{\partial T} - 6\psi \frac{\partial \psi}{\partial u} + \frac{\partial^3 \psi}{\partial u^3} = P_3(u, T), \tag{51}$$

$$\frac{\partial \phi}{\partial T} - 6\phi \frac{\partial \phi}{\partial u} + \frac{\partial^3 \phi}{\partial u^3} = P_4(u, T). \tag{52}$$

The perturbation terms  $P_i(u, T), i = 3, 4$  in the present case are given by:

$$P_3(u, T) = \frac{C}{\gamma C_0} \frac{\partial}{\partial u} (\psi + \phi) - \frac{3\beta}{\gamma} \int \delta(u - u_0) \frac{\partial^2 \psi_1^2}{\partial u^2} du, \tag{53}$$

$$P_4(u, T) = \frac{C}{\gamma C_0} \frac{\partial}{\partial u} (\phi + \psi). \tag{54}$$

In the absence of perturbations, Eqs. (51) and (52) are two independent KdV equations admitting one-soliton solutions similar to (21) and (22). With these solutions, the adiabatic perturbation theory leads to the following set of four coupled first-order ordinary differential equations for the variational parameters  $\kappa_i$  and  $\theta_i (i = 1, 2)$ :

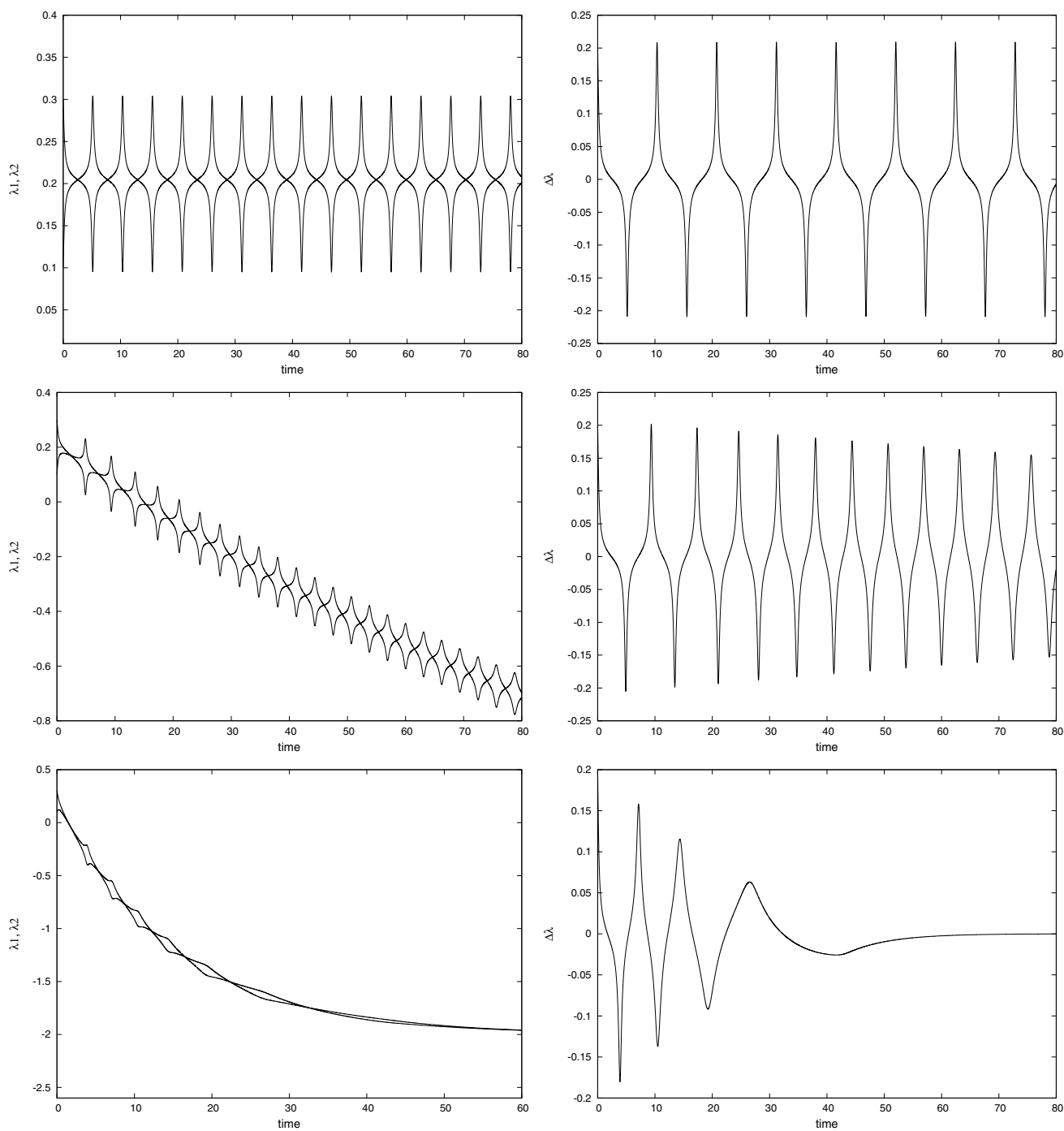


**Fig. 3** Left column: time variations of  $\lambda_1$  (downward from  $T = 0$ ) and  $\lambda_2$  (upward from  $T = 0$ ), right column: time variations of  $\Delta\lambda$ , the initial values are  $\lambda_1 = 0.3, \lambda_2 = 0.1, \theta_1 = 0.28, \theta_2 = 0.1$ . Parameter values are  $\kappa = 2$  and  $M = 0.2$ . From top to bottom rows:  $N = 0, 0.01, 0.1$

$$\frac{d\kappa_1}{dT} = -\frac{8M_1\kappa_2^2}{15} \operatorname{sech}^2 A [\tanh A + \tanh^3 A] + N_1 \kappa_1^5 [4\operatorname{sech}^4 y_0 - 5\operatorname{sech}^6 y_0], \tag{55}$$

$$\frac{d\kappa_2}{dT} = \frac{8M_1\kappa_1^2}{15} \operatorname{sech}^2 A [\tanh A + \tanh^3 A], \tag{56}$$

$$\frac{d\theta_1}{dT} = 4\kappa_1^{-2} - M_1 - \frac{M_1\kappa_2^3}{\kappa_1^3} \operatorname{sech}^2 A \left[ 1 - \frac{17}{9} \tanh^2 A \right], \tag{57}$$



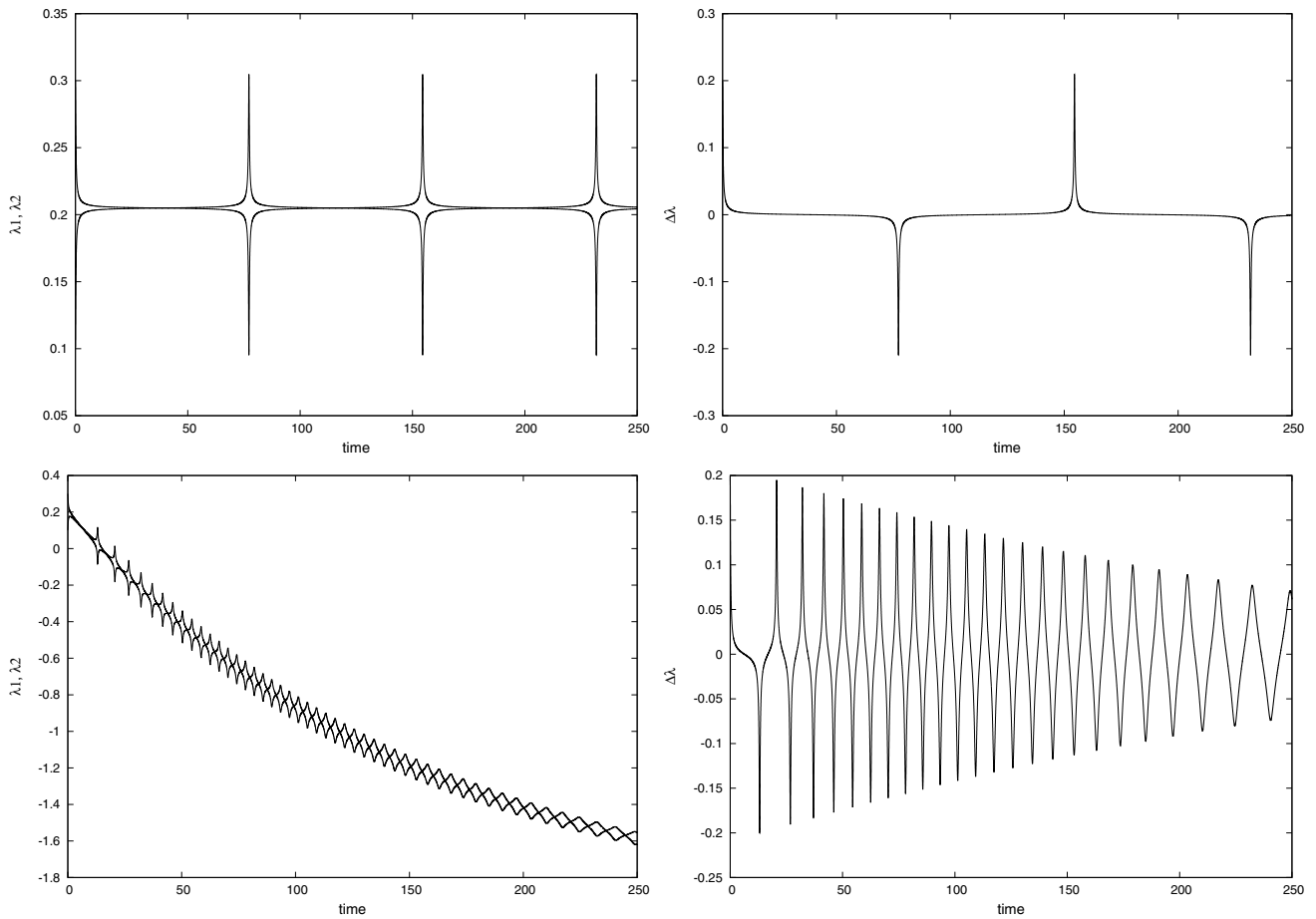


**Fig. 4** Left column: time variations of  $\lambda_1$  (downward from  $T = 0$ ) and  $\lambda_2$  (upward from  $T = 0$ ), right column: time variations of  $\Delta\lambda$ , the initial values are  $\lambda_1 = 0.30076, \lambda_2 = 0.1, \theta_1 = 0.28, \theta_2 = 0.1$ . Parameter values are  $\kappa = 2$  and  $M = 0.2$  From top to bottom rows:  $N = 0, 0.01$

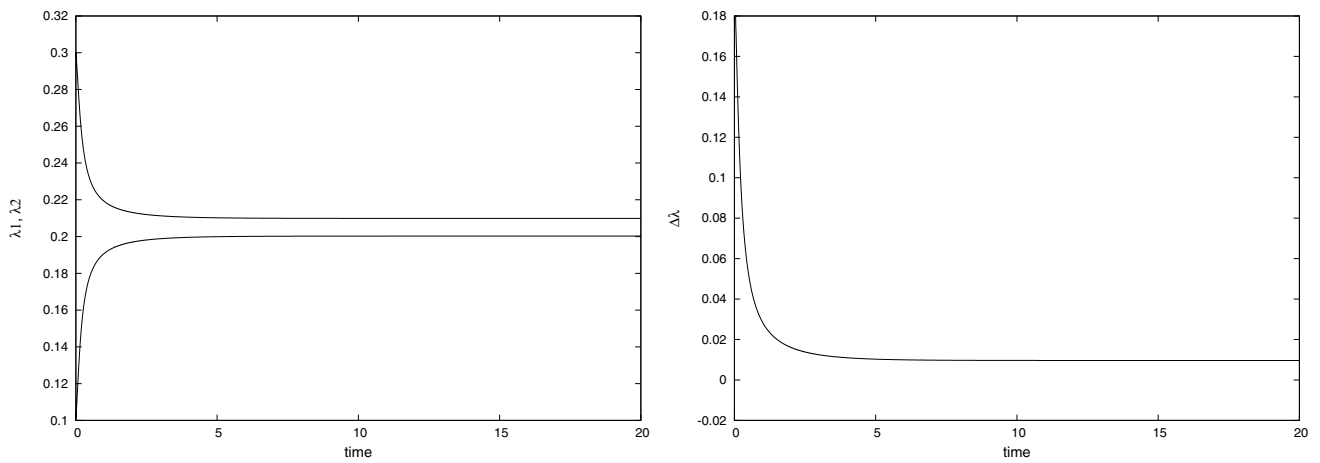
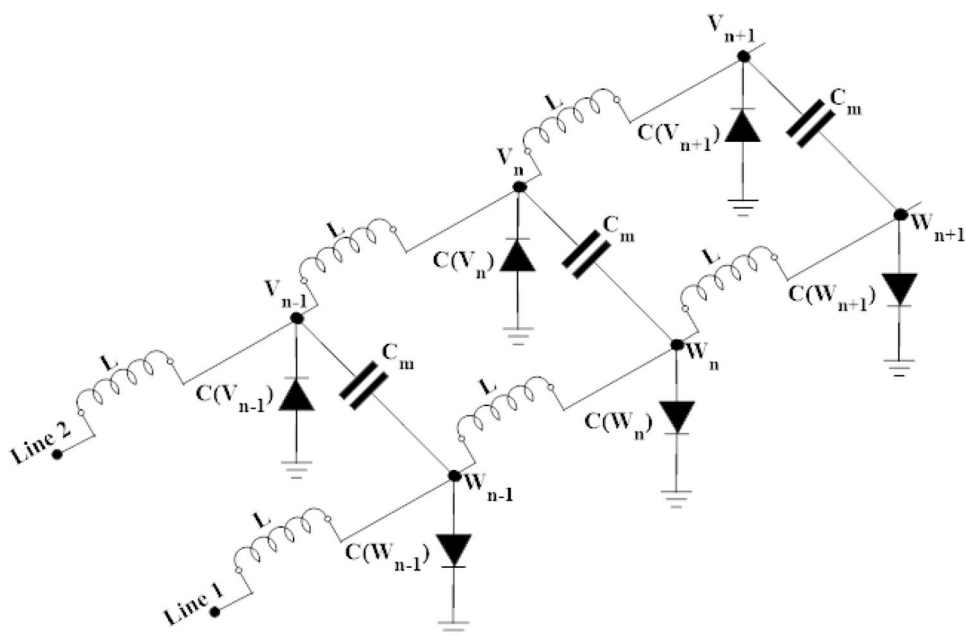


**Fig. 5** Left graph: time variations of  $\lambda_1$  (downward from  $T = 0$ ) and  $\lambda_2$  (upward from  $T = 0$ ), right graph: time variations of  $\Delta\lambda$ , the initial values are  $\lambda_1 = 0.301, \lambda_2 = 0.1, \theta_1 = 0.28, \theta_2 = 0.1$ . Parameter values are  $\kappa = 2, M = 0.2, N = 0$

**Fig. 6** Equivalent circuit model of coupled NLTLs. The capacitance at the  $n$ th cell is given by  $C(V_n)$



$$\frac{d\theta_2}{dT} = 4\kappa_2^2 - M_1 - \frac{M_1\kappa_1^3}{\kappa_2^3} \operatorname{sech}^2 A \left[ 1 - \frac{17}{9} \tanh^2 A \right], \quad (58)$$

where  $M_1 = C/\gamma C_0$ ,  $N_1 = 24\beta/\gamma$  and  $y_0 = \kappa_1 u_0$ . Again we introduce small deviations  $\lambda_i$  from the average amplitude  $\kappa$  of the two solitons as  $\lambda_i$ , as  $\kappa_i = \kappa + \lambda_i$  and the phase difference  $\Delta\theta = \theta_1 - \theta_2$  which too must be small. Using the approximation  $y_2 \approx y_1 + A$ , Eqs. (55) to (58) can be linearized and yield:

$$\frac{d\lambda_1}{dT} = -\frac{8M_1}{15} \kappa^3 \Delta\theta + [(49\kappa^2 u_0 - 5)N_1 \kappa^4] \lambda_1 + (7\kappa^2 u_0 - 1)N_1 \kappa^5, \quad (59)$$

$$\frac{d\lambda_2}{dT} = \frac{8M_1}{15} \kappa^3 \Delta\theta, \quad (60)$$

$$\frac{d\theta_1}{dT} = 4(\kappa^2 + 2\kappa\lambda_1) - M_1[2 - 3\kappa^{-1}(\lambda_1 - \lambda_2)], \quad (61)$$

$$\frac{d\theta_2}{dT} = 4(\kappa^2 + 2\kappa\lambda_2) - M_1[2 + 3\kappa^{-1}(\lambda_1 - \lambda_2)]. \quad (62)$$

The last two equations suggest that the phase difference  $\Delta\theta$  and the amplitude difference  $\Delta\lambda$  are related through the differential equation:

$$\frac{d\Delta\theta}{dT} = \frac{8\kappa^2 + 6M_1}{\kappa} \Delta\lambda. \quad (63)$$

On the other hand, the first two equations lead to the following second-order ordinary differential equation for the amplitude difference:

$$0 = \frac{d^2 \Delta\lambda}{dT^2} + \Omega_0^2 \Delta\lambda + F(\lambda_1, u_0), \quad (64)$$

$$\begin{aligned} \Omega_0^2 &= \frac{16M_1}{15} \kappa^2 (8\kappa^2 + 6M_1), \\ F(\lambda_1, u_0) &= (8\kappa^2 + 6M_1) \\ &\quad [(5 - 49\kappa^2 u_0)N_1 \kappa^3 \lambda_1 + (1 - 7\kappa^2 u_0)N_1 \kappa^4]. \end{aligned} \quad (65)$$

Equation (64) is nothing else, but the equation of motion of an harmonic oscillator with the oscillation frequency  $\Omega_0$ , “driven” by a force  $F(\lambda_1, u_0)$ . This drive leads to either an enhancement or a suppression of  $\Delta\lambda$ .

To be more explicit, the expression of  $F(\lambda_1, u_0)$  given in formula (65) suggests that the amplitude difference will oscillate with increasing amplitude, when the defective diode is closer to the input end of the transmission line and the average amplitude  $\kappa$  of the leapfrogging solitons is not too large. When  $\kappa$  is relatively large, the impurity will accelerate the soliton signal on line 1, thus increasing its speed relative to the speed of soliton on line 2.

Concerning the issue of the effects of impurities on soliton propagation in NLTLs, it is instructive stressing that the influence of a localized impurity on soliton propagation in NLTLs has been investigated in some past works. It is therefore well established that a default-type impurity will increase the amplitude of a soliton approaching the impurity [25, 26], hence causing its acceleration in virtue of the amplitude dependence of the velocity of the KdV soliton. In recent numerical simulations, Pan et al. [26] obtained that the response of a soliton signal to the

presence of a localized impurity in an LC NLTL is standard: an excess structural defect will always trap a soliton signal causing its delay, whereas a structural default will accelerate the soliton signal on approaching the impurity, whether the impurity is capacitive or inductive.

We carried out numerical simulations of the set of coupled first-order nonlinear ordinary differential equation (55)–(58), still with a sixth-order Runge–Kutta algorithm with fixed step. The initial values, as well as values of characteristic parameters of the model, are the same we used for Fig. 2 (see values in the caption of Fig. 7). Results are

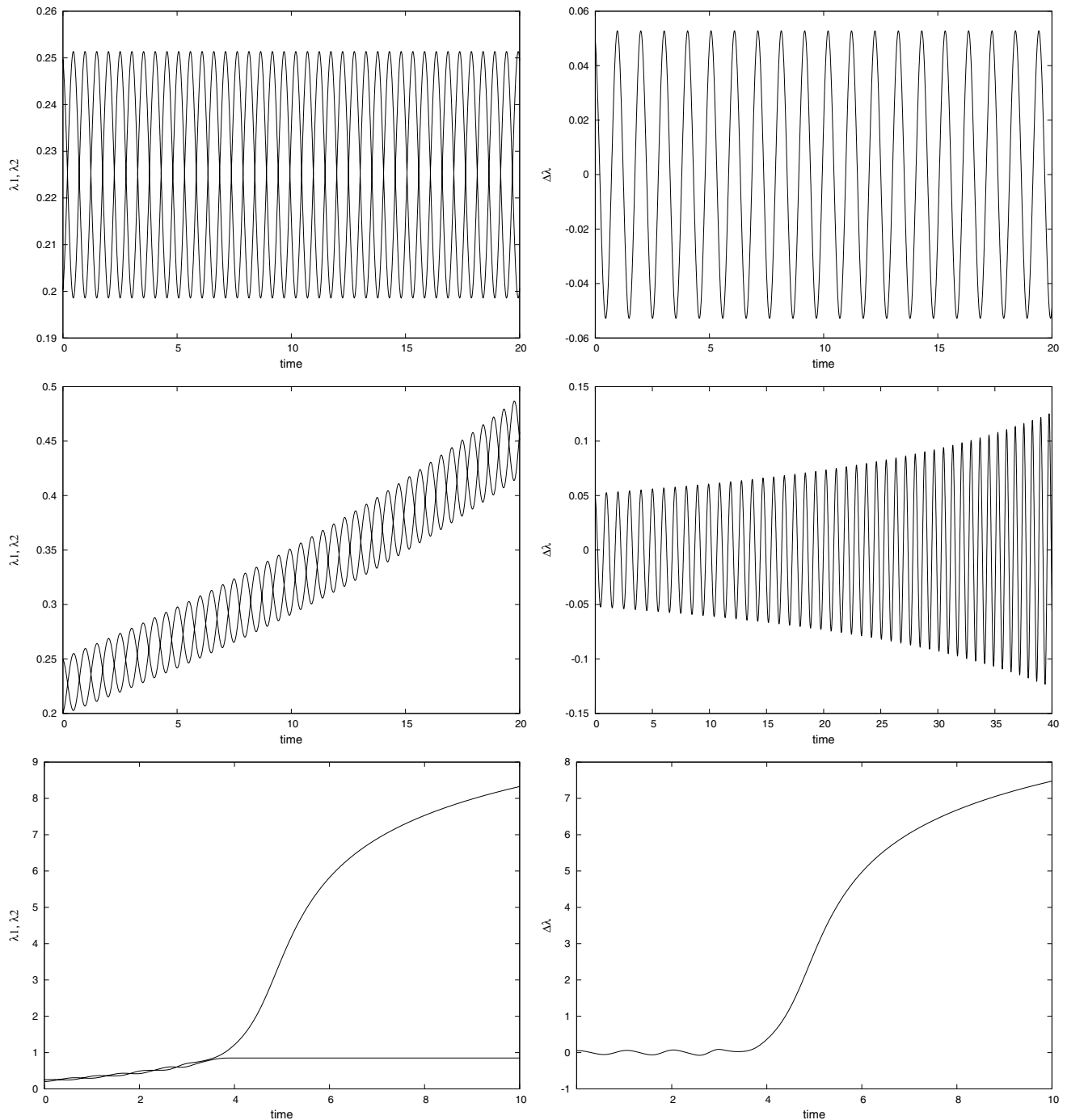


**Fig. 7** Left column: time variations of  $\lambda_1$  (downward from  $T = 0$ ) and  $\lambda_2$  (upward from  $T = 0$ ), right column: time variations of  $\Delta\lambda$ , the initial values are  $\lambda_1 = 0.25$ ,  $\lambda_2 = 0.2$ ,  $\theta_1 = 0.25$ ,  $\theta_2 = 0.2$ . Param-

eter values are  $\kappa = 2$ ,  $M_1 = 0.2$ ,  $u_0 = 0.3$ . From top to bottom rows:  $N_1 = 0, 0.001$  and  $0.01$

shown in Fig. 7, where we plotted  $\lambda_1$  and  $\lambda_2$ , and the amplitude difference, for different values of the impurity coefficient  $N_1$ .

Graphs in Fig. 7 show that the soliton leapfrogging is a regular harmonic oscillation with constant maximum amplitudes when there is no impurity. However, as the impurity rate  $\beta$  (and hence the impurity coefficient  $N_1$ ) is increased from zero, the amplitude difference  $\Delta\lambda$  oscillates with the maximum oscillation amplitudes increasing with time. When  $N_1$  attains a critical value, the leapfrogging is suppressed after a short time. A look at the variations of  $\lambda_1$  and  $\lambda_2$  with time on the left graph clearly suggests that  $\lambda_1$  gets amplified after a short propagation time, but not  $\lambda_2$ , implying an acceleration of the soliton signal on line 1 relative to its counterpart on line 2.

## 4 Conclusion

We have investigated the leapfrogging dynamics of a pair of KdV solitons in two nonlinear transmission lines, weakly coupled by a linear capacitance. Two different physical configurations of coupled nonlinear transmission lines were considered: the first model was two RLC lines with intraline Schottky varactors, and in the second model, we considered two coupled LC lines one of which had a localized capacitive impurity. For the first model, we obtained that adding the resistive element along with the feedback capacitor on the coupled transmission lines causes a damping of the soliton amplitudes, thus acting against leapfrogging. For leapfrogging to survive the presence of the resistive component, the average amplitude of the two interacting solitons should be large enough and the resistance relatively small, consistently with the spirit of the adiabatic perturbation theory. For the second model, we established that a defect in one of the Schottky diodes on line 1 with accelerate the soliton signal on the line, causing a drive of the second soliton with the possibility of their leapfrogging as long as the impurity rate is relatively small. As we increase the impurity rate, the soliton signal in line 1 gains in amplitude and consequently in speed, and hence cannot be followed by the soliton signal in line 2. In this case, no leapfrogging can occur.

The effects of a localized impurity on soliton signals in NLTLs have been investigated in several previous works; it is there well established that a localized impurity will always accelerate a soliton approaching the impurity when it is a structural defect in the defective electrical component [25, 26]. This response of KdV soliton to the presence of a localized impurity in the NLTL is actually universal; indeed, similar behaviours are predicted in many other distinct physical systems such as Josephson junction

transmission lines [44, 45], Frenkel–Kontorova systems [46, 47] and double-well systems [48].

**Acknowledgements** Open access funding provided by Max Planck Society. A. M. Dikandé wishes to acknowledge support from the Alexander von Humboldt foundation. He also thanks Pr. Holger Kantz at MPIPKS Dresden for hosting his visit in the “Nonlinear Time Series Analysis” research group.

## Compliance with ethical standards

**Conflict of interest** The authors declare that they have no conflict of interest.

**Open Access** This article is distributed under the terms of the Creative Commons Attribution 4.0 International License (<http://creativecommons.org/licenses/by/4.0/>), which permits unrestricted use, distribution, and reproduction in any medium, provided you give appropriate credit to the original author(s) and the source, provide a link to the Creative Commons license, and indicate if changes were made.

## References

- Hirota R, Suzuki K (1970) Studies on lattice solitons by using electrical networks. *J Phys Soc Jpn* 28:1366
- Jager D (1985) Characteristics of travelling waves along the nonlinear transmission lines for monolithic integrated circuits: a review. *Int J Electron* 58:649
- Toda M (1967) Vibration of a chain with nonlinear interaction. *J Phys Soc Jpn* 22:431
- Toda M (1989) *Theory of nonlinear lattices*, 2nd edn. Springer, Berlin
- Ablowitz M, Clarkson P (1991) *Solitons, nonlinear evolutions and inverse scattering*. Cambridge University Press, Cambridge
- Drazin PG, Johnson RS (1996) *Solitons: an introduction*. Cambridge University Press, Cambridge
- Filippov AT (2010) *Versatile soliton*. Birkhäuser, Basel
- Ricketts DS, Ham D (2011) *Electrical solitons: theory, designs and applications*. CRC Press, Boca Raton
- Tao T (2009) Why are solitons stable? *Bull AMS* 46:33
- Kengne E, Vaillancourt R (2009) Propagation of solitary waves on lossy nonlinear transmission lines. *Int J Mod Phys B* 23:1
- Afshari E, Hajimiri A (2005) Nonlinear transmission lines for pulse shaping in silicon. *IEEE J Sol State Circuits* 40:744
- Kengne E, Liu WM (2006) Exact solutions of the derivative nonlinear Schrödinger equation for a nonlinear transmission line. *Phys Rev E* 73:0266031
- Ndzana FII, Mohamadou A, Kofané TC, English LQ (2008) Modulated waves and pattern formation in coupled discrete nonlinear LC transmission lines. *Phys Rev E* 78:016606
- Ndzana FII, Mohamadou A, Kofané TC (2008) Modulational instability in a purely nonlinear coupled complex Ginzburg–Landau equations through a nonlinear discrete transmission line. *Chaos* 18:043121
- Narahara K (2003) Traveling-wave retimer with coupled nonlinear transmission line. *Jpn J Appl Phys* 42:1192
- Kuusela T, Hietarinta J, Kokko K, Laiho R (1987) Soliton experiments in a nonlinear electrical transmission line. *Eur J Phys* 8:27
- Kuusela T (1995) Soliton experiments in transmission lines. *Chaos Solitons Fractals* 5:2419

18. Essimbi BZ, Dikandé AM, Kofané TC, Zibi AA (1995) Asymmetric gap solitons in a non-linear LC transmission line. *Phys Scrip* 52:17
19. Essimbi BZ, Dikandé AM, Kofané TC, Zibi AA (1995) Localized solitary signals on a coupled nonlinear transmission line. *J Phys Soc Jpn* 64:2777
20. Singer AC, Oppenheim AV, Wornell GW (1999) Detection and estimation of multiplexed soliton signals. *IEEE Trans Sign Proc* 47:2768
21. Dikandé AM, Ga-Akeku B (2009) Localized short impulses in a nerve model with self-excitable membrane. *Phys Rev E* 80:041904
22. Oriols X, Martin F (2001) Analytical solitons in nonlinear transmission lines loaded with heterostructure barrier varactors. *J Appl Phys* 90:2595
23. Sato M, Yasui S, Kimura M, Hikihara T, Sievers AJ (2007) Management of localized energy in discrete nonlinear transmission lines. *Euro Phys Lett* 80:30002
24. Tsuboi T, Toyama FM (1991) Computer experiments on solitons in a nonlinear transmission line I. Formation of stable solitons. *Phys Rev A* 44:2686
25. Tsuboi T, Toyama FM (1991) Computer experiments on solitons in a nonlinear transmission line II. Propagation of solitons in an impurity-doped line. *Phys Rev A* 44:2691
26. Pan JT, Chen WZ, Tao F, Xu W (2011) Influence of impurities on solitons in the nonlinear LC transmission line. *Phys Rev E* 83:016601
27. Jäger D (1982) Experiments on KdV solitons. *J Phys Soc Jpn* 51:1686
28. Gasch A, Berning T, Jäger D (1986) Generation and parametric amplification of solitons in a nonlinear resonator with a Korteweg–de Vries medium. *Phys Rev A* 34:4528
29. Narahara K (2010) Characterization of nonlinear transmission lines for short pulse amplification. *J Infrared Millim Terahertz Waves* 31:411
30. Narahara K (2015) Characterization of leapfrogging solitary waves in coupled nonlinear transmission lines. *Nonlinear Dyn* 81:1805
31. Nkongho Achere A, Akong Ngate L, Dikandé AM, Essimbi BZ (2019) Leapfrogging dynamics of interacting solitons in weakly coupled nonlinear transmission lines. *SN Appl Sci* 1:552
32. Hietala N, Hänninen R, Salman H, Barenghi CF (2016) Leapfrogging Kelvin waves. *Phys Rev Fluids* 1:084505
33. Lui AK, Kubota T, Ko DRS (1980) Resonant transfer of energy between nonlinear waves in neighbouring pycnoclines. *Stud Appl Math* 63:26
34. Lui AK, Pereira NR, Ko DRS (1982) Weakly interacting internal solitary waves in neighbouring pycnoclines. *J Fluid Mech* 122:187
35. Weidman PD, Johnson M (1982) Experiments on leapfrogging internal solitary waves. *J Fluid Mech* 122:195
36. Gear JA, Grimshaw R (1984) Weak and strong interactions between internal solitary waves. *Stud Appl Math* 70:235
37. Nitsche M, Weidman PD, Grimshaw R, Ghrist M, Fornberg B (2010) Evolution of solitary waves in a two-pycnocline system. *J Fluid Mech* 642:235
38. Malomed BA (1987) Leapfrogging solitons in a system of coupled KdV equations. *Wave Motion* 9:401
39. Kivshar YS, Malomed BA (1989) Dynamics of solitons in nearly integrable systems. *Rev Mod Phys* 61:763
40. Luther HA (1968) An explicit sixth-order Runge–Kutta formula. *Math Comput* 22:434
41. Jie H, Qian Z, Hao Y, Junrong D, Haiying Z (2014) Planar Schottky varactor diode and corresponding large signal model for millimeter-wave applications. *J Semicond* 35:0540061
42. Boylestad R, Nashelsky L (2013) *Electronic devices and circuit theory*, 7th edn. Prentice Hall, Englewood Cliffs
43. Jeffrey A, Kawahara T (1982) *Asymptotic methods in nonlinear wave theory*. Pitman, London
44. Shnirman A, Ben-Jacob E, Malomed BA (1997) Tunneling and resonant tunneling of fluxons in a long Josephson junction. *Phys Rev B* 55:14677
45. Starodub IO, Zolotaryuk Y (2012) Scattering of quasi-one-dimensional solitons on impurities in large Josephson junctions. *Phys Lett A* 376:3101
46. Malomed BA (1988) Interaction of a soliton with an impurity in the sine-Gordon model of a commensurate charge-density-wave system. *J Phys C* 21:5163
47. Braun OM, Kivshar YS (1998) Nonlinear dynamics of the Frenkel–Kontorova model. *Phys Rep* 306:1
48. Dikandé AM, Kofané TC (1994) Oscillatory motions of solitons in finite inhomogeneous structures. *J Phys Condens Matter* 6:6229

**Publisher's Note** Springer Nature remains neutral with regard to jurisdictional claims in published maps and institutional affiliations.

# PULSE AMPLIFICATION AND DAMPING IN LOSSY NONLINEAR TRANSMISSION LINES

A. NKONGHO ACHERE<sup>1,2</sup>, ALAIN M. DIKANDÉ<sup>1,a</sup>, B. Z. ESSIMBI<sup>2</sup>

<sup>1</sup>Laboratory of Research on Advanced Materials and Nonlinear Science (LaRAMaNS), Department of Physics, Faculty of Science, University of Buea, P.O. Box 63 Buea, Cameroon

Corresponding author<sup>a</sup>: amdikande@gmail.com

<sup>2</sup>Laboratory of Electronics and Electrical Systems, Department of Physics, Faculty of Science, University of Yaoundé I, P. O. Box 812 Yaoundé, Cameroon

*Received July 2, 2020*

*Abstract.* A model of nonlinear electrical transmission line, which mimics a ladder circuit periodically loaded with Schottky varactors having a resistance in their shunt branches and connected to voltage-terminal modules, is considered from both analytical and numerical standpoints. Analytical treatment of the problem, following the multiple-scale expansion and the adiabatic perturbation theory involving a perturbed Korteweg-de Vries equation, establishes that pulse-shaped electrical solitons can propagate in the nonlinear transmission line while experiencing amplification due to the voltage terminals, but also a damping caused by the resistance. Direct numerical simulations of the line equations provide evidence of a dominant damping effect due to the resistance, over pulse amplification due to the voltage terminal. Numerical simulations bring out a novel process namely a possible disintegration of the single pulse into two or more pulses upon propagation in the nonlinear transmission line, resulting from the competition between amplification and damping.

*Key words:* Nonlinear transmission lines, Schottky varactors, Linear resistors, Pulse amplification and damping.

## 1. INTRODUCTION

The study of nonlinear phenomena has become very popular due to manifestations of the fascinating features of nonlinearity in a large variety of natural processes, ranging from fluids, plasma and optics to solid-state, biological and chemical systems [1–13]. In electronics nonlinear transmission lines (NLTs) have attracted a great deal of interest [2, 14–21] since the pioneer ladder circuit introduced by Hirota and Suzuki [22]. The Hirota-Suzuki circuit, seen as an electrical equivalent of the well-known Toda lattice [23], is a ladder line consisting of VARICAP diodes (or varactors) and linear inductances periodically loaded along the line to form a one-dimensional ( $1D$ ) propagation medium. In this  $1D$  propagation medium, the nonlinearity is provided by the varactors, while the dispersion is related to the periodic arrangements of elementary circuits. This leads to a system for which the dynamics can be represented by standard nonlinear partial differential equations such as the Korteweg-de

Romanian Journal of Physics **65**, 123 (2020)

Vries (KdV), nonlinear Schrödinger or complex Ginzburg-Landau equations [24], depending on competing conditions between nonlinearity and dispersion (or diffraction, depending on physical contexts [25–31]). A feature common to these equations is the possibility for large-amplitude waves among their solutions, the so-called solitons [1, 2] and resulting from the competition between nonlinearity and dispersion. Concretely, solitons in NLTLs are high-power electric waves related to the propagation of voltage excitations along the lines. NLTLs find widespread applications in wideband and microwave digital signal processings, for instance, they are used in wireless, radar, and sensor array processings [32], etc.

There has been recent interest in the possibility for short-pulse amplification using NLTLs, for possible applications in high-resolution measurements and high-speed communication systems [32]. Thus, considering the Hirota-Suzuki line and envisaging connection of elementary circuits to voltage-terminal modules (or voltage edges), it was shown that the propagation of a KdV pulse could result into pulse amplification by the voltage terminal. Quite remarkably, while the pulse amplification was of a universal exponential law, the amplification rate was dependent on the specific characteristic properties of the Schottky varactor loaded in the line. In the general context of studies of soliton propagation in NLTLs, it is well known that although pulses possess robust shape by virtue of their soliton features, resistive components that are almost always present in the line cause pulse energy to be dissipated as it propagates. Given that within the framework of the adiabatic perturbation theory [24], the amplitude damping in this later case too follows an exponential law, it is useful to examine the competition between the amplification due to voltage terminals and the damping related to a resistive component.

To address the above issue we consider a modified version of the NLTL discussed recently [33], which is just the Hirota-Suzuki line with a voltage terminal in each elementary circuit. In the present study, the Schottky diode will be shunted with a resistive component of a constant resistance  $R$ . We first proceed analytically by deriving, following the multiple-scale expansion method [34], a perturbed KdV equation, where the perturbation term groups the effects of the voltage terminal and of the resistance and is treated *via* the adiabatic perturbation approach [24]. The analytical study leads to a KdV-type pulse, the amplitude of which is enhanced during propagation due to the voltage terminal, and damped due to the resistance. Next, numerical simulations of the discrete line equations by means of a sixth-order Runge-Kutta algorithm [35] will be carried out, providing evidence of a dominant effect of the resistive component over amplification due to the voltage terminal. Simulations also bring out a possible pulse disintegration into two pulses, as a result of the competition between damping and amplification upon propagation.

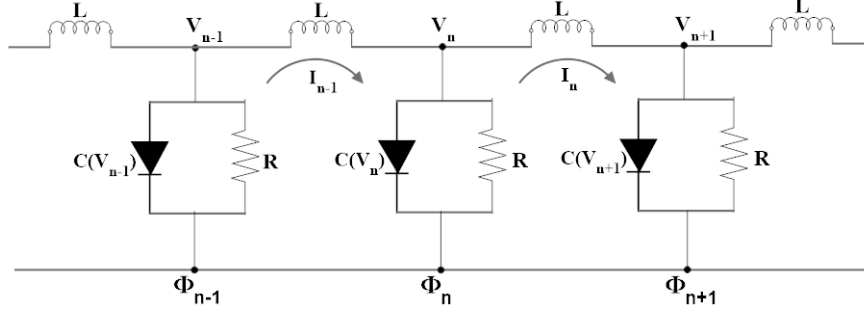


Fig. 1 – Equivalent circuit model of a Schottky-type lossy NLTL, with a voltage terminal connected to each elementary electric cell.

## 2. MODEL AND THEORETICAL ANALYSIS

Consider a NLTL consisting of a homogeneous inductor  $L$ , and a nonlinear capacitor  $C(V)$  shunted by a passive resistance  $R$  in each unit cell as shown in Fig. 1. Each unit cell of the NLTL is individually biased by a voltage terminal such that  $V_n$ ,  $I_n$ , and  $\Phi_n$  are the voltage, current, and bias voltage respectively, in the  $n^{\text{th}}$  cell.

The Schottky varactor is a capacitor of a nonlinear capacitance, with a generic CV characteristics [36, 37]:

$$C(V) = \frac{C_0}{\left(1 - \frac{V}{V_J}\right)^m}, \quad (1)$$

where  $V$  is the line voltage. In the above formula  $C_0$ ,  $V_J$ , and  $m$  are the zero-bias junction capacitance, the characteristic junction voltage, and the grading index, respectively. In the following we shall define a nonlinear coefficient  $b = 1/V_J$ . Also instructive to note, the grading index  $m$  can take distinct values depending on the specific Schottky diode at hand [36, 37]. For most Schottky diodes the grading index will be within the interval  $0 < m \leq 1$  [36, 37].

Applying Kirchhoff's laws in the  $n^{\text{th}}$  unit cell, we obtain the following set of equations for the line voltage  $V_n$  and current  $I_n$ :

$$L \frac{dI_{n-1}}{dt} = V_{n-1} - V_n, \quad (2)$$

$$I_{n-1} - I_n = \frac{dQ_n}{dt} + \frac{V_n - \Phi_n}{R},$$

$$Q_n = C(V_n - \Phi_n) V_n, \quad (3)$$

where  $Q_n$  represents the total charge stored in the Schottky diode embedded within the  $n^{\text{th}}$  unit cell. Since the sizes of unit cells are usually negligible compared with the lengths of the line, the electrical signals propagating along the line are expected



to spread over many cells such that the discrete spatial coordinate  $n$  can be replaced by a continuous one *i.e.*  $x$ . For mathematical simplifications we set the size of unit cells to unity, and a long-wavelength expansion of the voltage variables  $V_{n\pm 1}$  up to the fourth-order term yields:

$$V_{n\pm 1} = V_n \pm \frac{\partial V}{\partial x} + \frac{1}{2} \frac{\partial^2 V}{\partial x^2} \pm \frac{1}{6} \frac{\partial^3 V}{\partial x^3} + \frac{1}{24} \frac{\partial^4 V}{\partial x^4} + \dots \quad (4)$$

Eliminating the current  $I_n$  from equations (2), (3) and applying the long-wavelength approximation, the continuous evolution equation for the line voltage  $V(x, t)$  is obtained as:

$$L \frac{\partial C(V - \Phi)}{\partial V} \left( \frac{\partial V}{\partial t} \right)^2 + LC(V - \Phi) \frac{\partial^2 V}{\partial t^2} + \frac{L}{R} \frac{\partial(V - \Phi)}{\partial t} = \frac{\partial^2 V}{\partial x^2} + \frac{1}{12} \frac{\partial^4 V}{\partial x^4}. \quad (5)$$

We seek for solutions to equation (5) that are nonlinear waves with pulse shape. To this end, we adopt the reductive perturbation approach [34] by which the continuous variables  $V(x, t)$  and  $\Phi(x, t)$  are series expanded in powers of some perturbation coefficient  $\epsilon$ , *i.e.*:

$$V(x, t) = \sum_{i=1}^n \epsilon^i V_i(x, t), \quad (6)$$

$$\Phi(x, t) = V_0 + \sum_{i=1}^n \epsilon^i \phi_i(x, t), \quad (7)$$

where it is assumed that  $\epsilon \ll 1$ . In addition to equations (6) and (7) we equally introduce the new space and time variables:

$$z = \epsilon^{\frac{1}{2}}(x - \eta t), \quad \tau = \epsilon^{\frac{3}{2}} t, \quad (8)$$

and rescale the resistance accordingly, *i.e.* [33, 38]:

$$R = \epsilon^{-\frac{3}{2}} R_1, \quad (9)$$

where  $\eta = (LC_0)^{-1/2}$ . By evaluating equation (5) at each order of  $\epsilon$ , we can extract equations describing contributions from different orders of the perturbation  $\epsilon$ . Namely, the terms of orders  $O(\epsilon)$  and  $O(\epsilon^2)$  give constant contributions [34] whereas the terms of order  $O(\epsilon^3)$ , grouped together, introduce nonlinear excitations governed by the following perturbed KdV equation:

$$\begin{aligned} \frac{\partial V_1}{\partial \tau} - \frac{m}{2\sqrt{LC_0}(V_0 + V_J)} V_1 \frac{\partial V_1}{\partial z} + \frac{1}{24\sqrt{LC_0}} \frac{\partial^3 V_1}{\partial z^3} = \\ - \frac{m}{2\sqrt{LC_0}(V_0 + V_J)} \phi_1 \frac{\partial V_1}{\partial z} - \frac{V_J}{2R_1 C_0 (V_0 + V_J)} (V_1 - \phi_1). \end{aligned} \quad (10)$$

Let us rescale  $V_1$ ,  $\tau$ , and  $z$  as follows:

$$V_1 = \frac{18(V_0 + V_J)}{m}V, \quad \tau = \frac{1}{9\eta}\tau', \quad z = \frac{1}{6}z'. \quad (11)$$

With these new variables, equation (10) reduces to:

$$\begin{aligned} \frac{\partial V}{\partial \tau'} - 6V \frac{\partial V}{\partial z'} + \frac{\partial^3 V}{\partial z'^3} &= P(z', \tau'), \\ P(z', \tau') &= \alpha V - \alpha\gamma\phi_1 - 6\gamma\phi_1 \frac{\partial V}{\partial z'}, \end{aligned} \quad (12)$$

where

$$\alpha = \frac{V_J}{18\eta R_1 C_0 (V_0 + V_J)}, \quad (13)$$

$$\gamma = \frac{m}{18(V_0 + V_J)}. \quad (14)$$

In the absence of perturbation, *i.e.* when  $P(z', \tau') = 0$ , the KdV equation admits the following one-soliton solution [1, 24]:

$$V(z', \tau') = -2\kappa_0^2 \operatorname{sech}^2 y, \quad (15)$$

$$y = \kappa_0(z' - \zeta), \quad \zeta = 4\kappa_0^2 \tau', \quad (16)$$

where  $\kappa_0$  is the soliton amplitude. In the original system of coordinates, *i.e.*  $(x, t)$ , the above one-soliton solution becomes:

$$V(x, t) = -\frac{A(V_0 + V_J)}{m} \operatorname{sech}^2 \left[ \sqrt{A} \left( x - \frac{t}{\sqrt{LC_b}} - \frac{At}{6\sqrt{LC_b}} \right) \right], \quad (17)$$

where  $A = 36\epsilon\kappa_0^2$ . To keep the spirit of Ref. [33] regarding the effects of voltage terminals on pulse propagation in the NLTL, we shall pick:

$$\begin{aligned} \Phi(x, t) &= V_0 + \epsilon^{\frac{3}{2}}\varphi_0(x - \eta t) \\ &= V_0 + \epsilon\varphi_0 z. \end{aligned} \quad (18)$$

Comparing equation (18) and equation (7) we find that:

$$\phi_1 = \varphi_0 \frac{z'}{6}. \quad (19)$$

Because of the presence of  $P(z', \tau')$  in equation (12), the soliton amplitude becomes time dependent and will be denoted  $\kappa$ . Within the framework of the adiabatic perturbation theory [24], the time evolution of  $\kappa$  is determined by the first-order ordinary differential equation:

$$\frac{d\kappa}{d\tau'} = -\frac{1}{4\kappa} \int_{-\infty}^{\infty} dz' P(z', \tau') \operatorname{sech}^2 \kappa z'. \quad (20)$$

By substituting  $V$  and  $\phi_1$  given respectively by (15) and (19) in equation (12), we obtain:

$$P(z', \tau') = 2\alpha\kappa^2 \operatorname{sech}^2 \kappa z' + \alpha\gamma\varphi_0 z' - 4\gamma\kappa^2\varphi_0 z' \operatorname{sech}^2 \kappa z' \tanh \kappa z'. \quad (21)$$

With this last expression, the first-order ordinary differential equation (20) simplifies to:

$$\frac{d\kappa}{d\tau'} = -\frac{2}{3} \left( \alpha - \frac{1}{2}\gamma\varphi_0 \right) \kappa. \quad (22)$$

Integrating equation (22) yields, in the time coordinate  $\tau$ :

$$\kappa(\tau) = \kappa_0 \exp \left[ -\frac{2\eta}{3} \left( \alpha - \frac{1}{2}\gamma\varphi_0 \right) \tau \right]. \quad (23)$$

It turns out that the electrical pulse will be either amplified or damped during propagation, depending on which among the resistance and voltage terminal has the dominant effect on its amplitude. However, expressions of  $\alpha$  and  $\gamma$  in formula (13) and (14) suggest that  $\gamma$  will be generally smaller than  $\alpha$ . Indeed  $\gamma$  is proportional to  $m$ , a small parameter compared with the quantity  $V_J/RC_0$  determining the magnitude of  $\alpha$ .

In the next Section we solve the line equations numerically, in order to compare results of direct numerical simulations with those obtained in this Section within the framework of the adiabatic perturbation theory, as concerns the competing effects of the voltage terminal and the resistance on the pulse amplitude.

### 3. NUMERICAL SIMULATIONS OF DISCRETE LINE EQUATIONS

In the previous Section we have investigated, using the adiabatic perturbation theory, the simultaneous effects of a passive resistance and a voltage terminal on pulse propagation along an LC NLTL. We obtained that the resistance induces a damping whereas the voltage terminal amplifies the electrical pulse, suggesting the possibility to balance the pulse amplification phenomenon predicted in a recent study [33]. However, actually the adiabatic perturbation theory is a variational treatment and as such its results are valid only for very small values of the resistance as well as of the voltage terminal.

To fully appreciate the effects of the presence of a resistance and voltage terminal on characteristic features of the propagating electrical pulse, it is relevant to solve the Kirchhoff equations (2) and (3) numerically. Focusing on the voltage signal  $V_n(t)$ , we have applied a sixth-order Runge-Kutta scheme [35] on the following second-order time-differential difference equation, derived from the coupled set (2) and (3) after elimination of current variables, *i.e.*  $I_n(t)$ ,  $I_{n\pm 1}(t)$ :

$$\frac{d^2 Q_n}{dt^2} = \frac{1}{L} (V_{n+1} - 2V_n + V_{n-1}) - \frac{1}{R} \frac{d}{dt} (V_n - \Phi_n). \quad (24)$$

As input profile we opt for a pulse-shaped wave of the form:

$$V_n(t=0) = A_0 \operatorname{sech}^2\left(n/\ell_0\right), \quad (25)$$

where the initial amplitude  $A_0$  and width at half tail  $\ell_0$  of the pulse are two arbitrary real parameters. Throughout simulations they will be fixed as  $A_0 = 1.9$ ,  $\ell_0 = 1.7$  (in units of length of an elementary cell).

Numerical simulations were carried out assuming a NLTL with 500 units cells, with a propagation time  $0 \leq t \leq 2000$  and a time step of  $10^{-4}$ . The characteristic parameters in the discrete line equation (24) were fixed, except the resistance  $R$  for which different values were considered. Concretely, the following values were given to characteristic parameters of the model:  $C_0 = 0.6$ ,  $L = 0.001$ ,  $b = V_J^{-1} = 0.25$ ,  $m = 0.98$ . Also, to check the pulse amplification predicted in Ref. [33] and in the analytical development of the previous Section, we shall consider  $\Phi_n = \phi_0 n$ , where  $\phi_0$  is a constant, which will be varied.

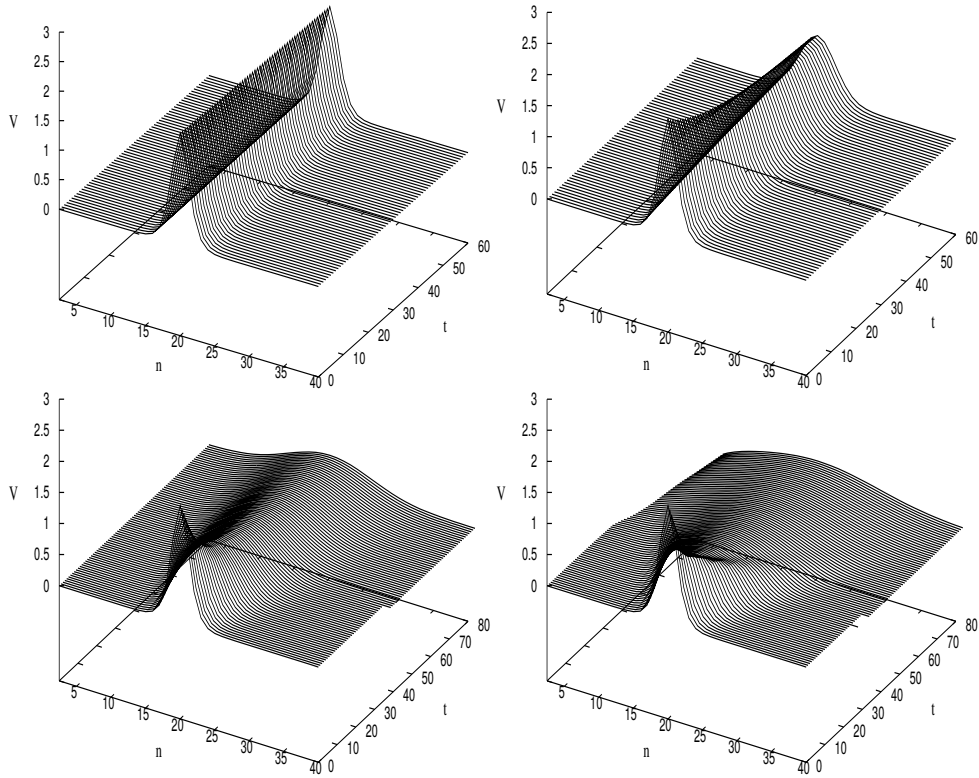


Fig. 2 – Space-time evolution of the voltage signal along the NLTL, in the absence of voltage terminal (*i.e.*  $\phi_0 = 0$ ) and for different values of the resistance  $R$ . Top graphs:  $R = 0.0005$  (left),  $R = 0.01$  (right). Bottom graphs:  $R = 0.05$  (left),  $R = 0.1$  (right).

Figures 2, 3, and 4 show the profiles of the voltage signal  $V_n(t)$  as it propagates, for three distinct values of  $\phi_0$  and different values of the resistance  $R$  in each figure. More precisely Fig. 2 corresponds to the context where only the resistive component is present in the NLTL, while Figs. 3 and 4 correspond to  $\phi_0 = 0.5$  and  $\phi_0 = 1.5$ , respectively.

In Fig. 2 the voltage signal  $V_n(t)$  propagates with a manifestly exponentially decreasing amplitude. It is quite noticeable that as the resistance increases the exponential damping sharpens, with a possibility of total disappearance of the pulse due dissipation by the resistance.

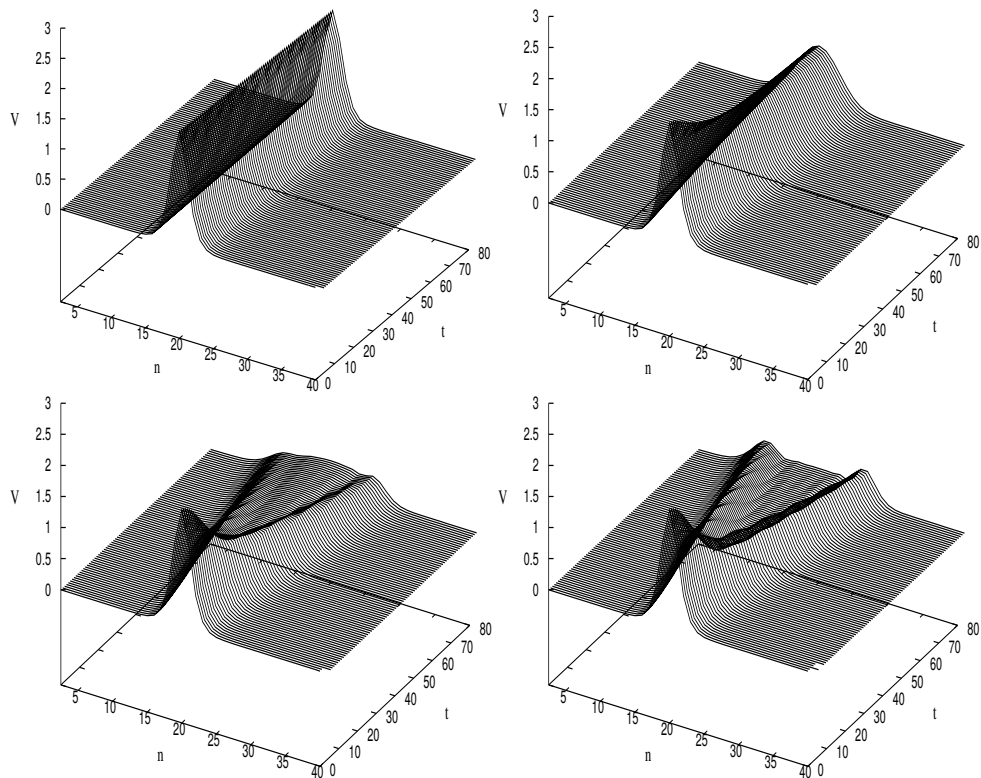


Fig. 3 – Space-time evolution of the voltage signal along the NLTL, for  $\phi_0 = 0.5$  and for different values of the resistance  $R$ . Top graphs:  $R = 0.0005$  (left),  $R = 0.01$  (right). Bottom graphs:  $R = 0.05$  (left),  $R = 0.1$  (right).

Figures 3 and 4 show pulse propagation for the same values of the resistance as in Fig. 2, but now for nonzero values of  $\phi_0$ . Quite remarkably, as  $\phi_0$  is increased the sharp exponential damping observed for  $\phi_0 = 0$  is gradually balanced. Clearly a nonzero value of  $\phi_0$  favors pulse amplification as predicted in Ref. [33], and consistently with the analytical result obtained above. Also remarkable on the 3D curves

is the behaviour according to which when  $\phi_0$  increases, the pulse disintegrates into two and probably more pulses after a finite propagation time. This behaviour could not be accounted for analytically.

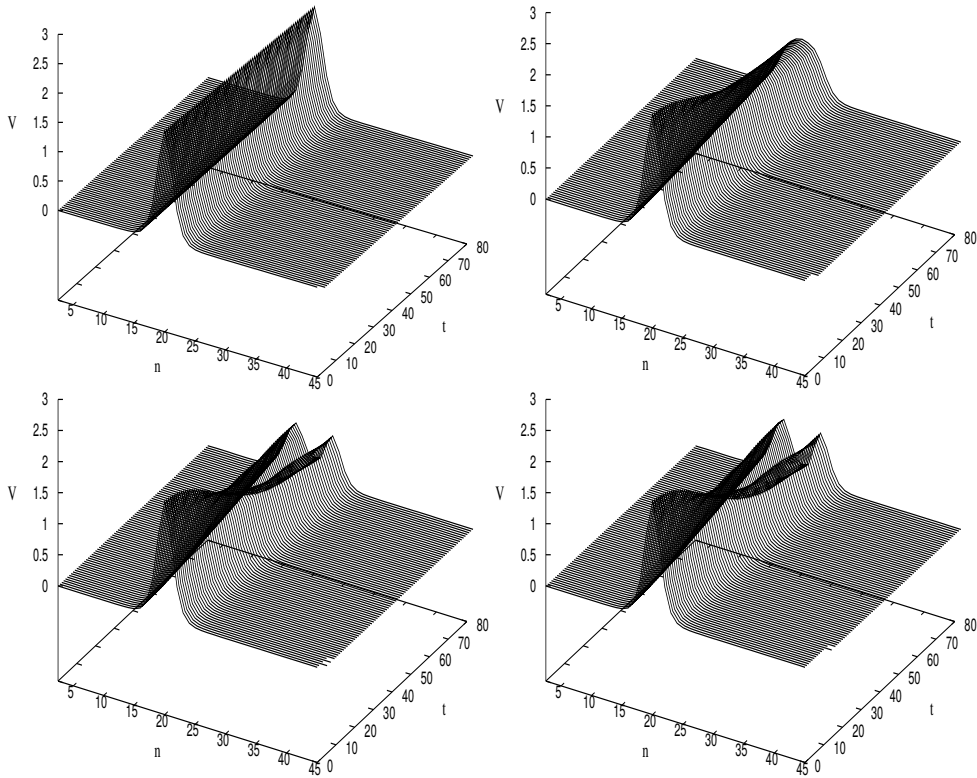


Fig. 4 – Space-time evolution of the voltage signal along the NLTL, for  $\phi_0 = 1.5$  and for different values of the resistance  $R$ . Top graphs:  $R = 0.0005$  (left),  $R = 0.01$  (right). Bottom graphs:  $R = 0.05$  (left),  $R = 0.1$  (right).

From a general standpoint, the numerical results suggest that a combination of the resistance with the voltage terminal can enable one the control growth of the pulse amplitude or *vice-versa*, *i.e.* can prevent pulse from being totally dissipated by a resistive component in the line. For instance, a resistance will be needed to maintain a finite-amplitude pulse in a NLTL designed with a voltage terminal. This result is not only interesting, in fact it introduces a novel perspective in various applications such as radar transmissions, microwave and ultra-wideband electronic devices, antenna networks, short-pulse electromagnetics and other contexts where electrical pulse amplifications hold a relevant role [33, 39, 40].

#### 4. CONCLUSION

Since the pioneering work by Hirota and Suzuki on a model of NLTL mimicking the Toda lattice [2, 22], there has been increasing interest to wave propagations along nonlinear and dispersive transmission lines. These specific electronic devices are ladder structures resulting from periodically arranged elementary circuits composed of an inductance, a resistance, and a capacitive diode (*i.e.* a varactor) introducing nonlinearity in the device. The periodic arrangement of unit circuits along the transmission line introduces dispersion, and the balance of nonlinearity by this dispersion favors high-intensity signals with soliton features in the NLTL.

A NLTL model was introduced in a recent work [33] to account for pulse amplifications in physical contexts where such processes would be required. The NLTL model was a ladder structure with unit circuits made up of a linear inductor in the main branch, and a nonlinear capacitor (*i.e.* a varactor) in derivation connected to a voltage edge (here denoted voltage terminal). By carrying out analytical investigations within the framework of the multiple-scale expansion method, combined with the adiabatic perturbation theory, it was shown that the voltage terminal induces an exponential amplification of the pulse with time. However for practical purposes it is useful that the pulse amplitude should remain finite along the transmission line, which might not be the case when the voltage terminal acts alone. As a control effect we envisaged the combination of the voltage terminal with a resistive component shunting the varactor.

Analytically, we have established that when a resistance is added in the transmission line the exponential amplification due to the voltage terminal is balanced. This observation was confirmed in numerical simulations of the line equations, where the pulse amplitude was clearly seen to decrease exponentially during propagation with a fall-off (or slope) less and less pronounced with increase of the voltage terminal. Also remarkable, we have observed in numerical simulations that when both the resistance and the voltage terminal are relatively large, their competition can favor pulse disintegration into two or more pulses. This last observation, as well as the observed balance of pulse amplification by damping due to the resistance, are quite appealing for they introduce novel perspectives in several contexts of electronic communications and particularly antenna networks, radar transmissions, ultra-wideband electronics, and short-pulse electromagnetics [33, 39, 40].

*Acknowledgements.* The authors thank T. C. Kofané for fruitful discussions. This work has been partially completed at the Abdus Salam International Centre for Theoretical Physics (ICTP), Trieste, Italy (A. M. Dikandé is a “Senior Associate” Scientist at ICTP).

## REFERENCES

1. P. G. Drazin and R. S. Jonhson, *Solitons: an Introduction* (2nd edn., Cambridge University Press, Cambridge, 1989).
2. M. Remoissenet, *Waves Called solitons: Concepts and Experiments* (3rd edn., Springer, Berlin, 1999).
3. Y. V. Kartashov, G. E. Astrakharchik, B. A. Malomed, and L. Torner, *Nature Reviews Physics* **1**, 185 (2019).
4. B. A. Malomed and D. Mihalache, *Rom. J. Phys.* **64**, 106 (2019).
5. D. Mihalache, *Rom. Rep. Phys.* **69**, 403 (2017).
6. S. V. Sazonov, *Rom. Rep. Phys.* **70**, 401 (2018).
7. D. J. Frantzeskakis, H. Leblond, and D. Mihalache, *Rom. J. Phys.* **59**, 767 (2014).
8. H. Leblond and D. Mihalache, *Physics Reports* **523**, 61 (2013).
9. Y. V. Kartashov, B. A. Malomed, and L. Torner, *Rev. Mod. Phys.* **83**, 247 (2011).
10. R. J. M. Issokolo and A. M. Dikandé, *Phys. Fluids* **30**, 054102 (2018).
11. R. D. Dikandé Bitha and A. M. Dikandé, *Phys. Rev. A* **97**, 033813 (2018).
12. A. M. Dikandé, *Phys. Rev. A* **81** 013821 (2010).
13. E. N. Epie, A. M. Dikandé, and T. C. Kofané, *Phys. Lett. A* **372**, 6890 (2008).
14. T. Kuusela, J. Hietarinta, K. Kokko, and R. Laihom, *Eur. J. Phys.* **8**, 27 (1987).
15. T. Kuusela, *Chaos, Solitons Fract.* **5**, 2419 (1995).
16. B. Z. Essimbi, A. M. Dikandé, T. C. Kofané, and A. A. Zibi, *Physica Scripta* **52**, 17 (1995).
17. B. Z. Essimbi, A. M. Dikandé, T. C. Kofané, and A. A. Zibi, *J. Phys. Soc. Jpn.* **64**, 2777 (1995).
18. A. C. Singer, A. V. Oppenheim, and G. W. Wornell, *IEEE Trans. Sign. Proc.* **47**, 2768 (1999).
19. A. M. Dikandé and B. Ga-Akeku, *Phys. Rev. E* **80**, 041904 (2009).
20. T. Tsuboi and F. M. Toyama, *Phys. Rev. A* **44**, 2686 (1991).
21. T. Tsuboi and F. M. Toyama, *Phys. Rev. A* **44**, 2691 (1991).
22. R. Hirota and K. Suzuki, *Proc. IEEE* **61**, 1483 (1973).
23. M. Toda, *J. Phys. Soc. Jpn.* **22**, 431 (1967).
24. Y. S. Kivshar and B. A. Malomed, *Rev. Mod. Phys.* **61**, 763 (1989).
25. E. G. Charalampidis, J. Cuevas-Maraver, D. J. Frantzeskakis, and P. G. Kevrekidis, *Rom. Rep. Phys.* **70**, 504 (2018).
26. C. B. Ward and P. G. Kevrekidis, *Rom. J. Phys.* **64**, 112 (2019).
27. Z. Li, H. Wei, and P. He, *Rom. Rep. Phys.* **71**, 110 (2019).
28. F. Tsitoura, T. P. Horikis, and D. J. Frantzeskakis, *Rom. Rep. Phys.* **71**, 104 (2019).
29. Y. Song, Z. Wang, C. Wang, K. Panajotov, and H. Zhang, *Advanced Photonics* **2**, 024001 (2020).
30. C. Hou, L. Bu, F. Baronio, D. Mihalache, and S. Chen, *Rom. Rep. Phys.* **72**, 405 (2020).
31. H. Lin, J. He, L. Wang, and D. Mihalache, *Nonl. Dynamics* **100**, 2839 (2020).
32. V. K. Madisetti (ed.), *The Digital Signal Processing* (2nd edn., CRC Press, Taylor and Francis, London, 2009).
33. K. Narahara, *IEICE Electron. Expr.* **6**, 1199 (2009).
34. T. Taniuti, *Prog. Theor. Phys. Suppl.* **55**, 1 (1974).
35. Numerical simulations were carried out using a sixth-order Runge-Kutta algorithm adapted from H. A. Luther, *Math. Comp.* **22**, 434 (1968).
36. R. Boylestad and L. Nashelsky, *Electronic Devices and Circuit Theory* (7th edn., Prentice Hall, USA, 2013).
37. H. Jie, Z. Qian, Y. Hao, D. Junrong, and Z. Haiying, *J. Semicond.* **35**, 0540061 (2014).



- 
38. A. A. Nkongho and A. M. Dikandé, Springer Nat. Appl. Sc. (SNAS) **2**, 21 (2020).
  39. E. Afshari and A. Hajimiri, IEEE J. Solid-State Circ. **40**, 744 (2005).
  40. H. L. Bertoni, L. Carin, and L. B. Felsen (eds.), *Ultra-wideband, Short-Pulse Electromagnetics* (Springer, Berlin, 2012).